DEVELOPMENT AND CHARACTERISATION OF NOVEL FLUORAPATITE GLASS-CERAMICS FOR USE IN GLASS IONOMER CEMENTS

Tomas Duminis BSc (Hons)

A thesis submitted in fulfilment of the requirements for the degree of Doctor of Philosophy in the Institute of Dentistry, Queen Mary University of London

Institute of Dentistry
Bart's and the London School of Medicine and Dentistry
Queen Mary University of London
Mile End Road
London
E1 4NS

2018

Statement of Originality

I, Tomas Duminis, confirm that the research included within this thesis is my own work or that where it has been carried out in collaboration with, or supported by others, that this is duly acknowledged below and my contribution indicated. Previously published material is also acknowledged below.

I attest that I have exercised reasonable care to ensure that the work is original, and does not to the best of my knowledge break any UK law, infringe any third party's copyright or other Intellectual Property Right, or contain any confidential material.

I accept that the College has the right to use plagiarism detection software to check the electronic version of the thesis.

I confirm that this thesis has not been previously submitted for the award of a degree by this or any other university.

The copyright of this thesis rests with the author and no quotation from it or information derived from it may be published without the prior written consent of the author.

Signature: Tomas Duminis

Date: 10/06/2018

ABSTRACT

Introduction: Remineralisation potential of GICs can be improved by using apatite additives in the cement. The aesthetics of GICs depends on refractive index match between the different components in the material. The problem arises when the cement with the filler is mixed because apatite particles in the cement paste agglomerate during the mixing process and scatter light at the interfaces as a result of RI mismatch. The RI of the fluoride-containing GICs glasses is also difficult to predict and match to the polysalts/liquid component.

Aims: 1. to modify Appen model so that the refractive indices of bioactive glasses and the fluoride-containing GIC glasses can be calculated to match the refractive index of the liquid component and the polysalts produced during the setting reaction; 2. to develop strontium-containing optically clear FAp glass-ceramics with known refractive indices.

Methods: Refractive indices of ionomer-type and bioactive glasses were measured which were then used to derive Appen factors for the amorphous metal fluorides. Subsequently, using the derived Appen factors, two series of glasses were designed based on the SiO_2-Al_2O_3-P_2O_5-CaO/SrO-CaF_2/SrF_2 components. The developed series were then analysed for their ability to crystallise to apatite phases by DSC, XRD, ATR-FTIR and MAS-NMR solid-state characterisation techniques.

Results: It was found that Appen factors for the metal fluorides are higher than the RI of the corresponding crystal phases. It was also found that the fluoride content and the RI of GIC glasses correlate linearly. It was found that the developed glasses with predicted RIs crystallised to apatite phases on

controlled heat-treatment. More detailed analysis of the developed glass-ceramics revealed this to be in the form of acid-resistant fluorapatite. Increasing strontium content in the developed base glasses was found to promote surface crystallisation and resulted in a linear increase in strontium incorporation into the FAp lattice.

Conclusions: Appen model was successfully modified which can be used to predict refractive indices of fluoride-containing glasses used in dental cements. RI-tailored nanoscale FAp glass-ceramics have been successfully developed for use in aesthetic GICs. Increasing strontium content in the developed compositions was found to promote surface crystallisation of FAp phases. Developed FAp GCs can be incorporated into GICs for improved remineralisation.

Table of Contents

Contents

Acknowledgements

I would like to express my sincere gratitude for my supervisors Prof Robert Hill and Dr Saroash Shahid for their excellent supervision, guidance and mentorship during the project. Likewise, I like to sincerely thank Dr Natalia Karpukhina for her excellent supervision and guidance with new concepts in solid-state chemistry and for encouragement during the project. I want to acknowledge and thank Dr Harold Toms (School of Biological and Chemical Sciences) for his valuable time and for sharing his expertise in the NMR spectroscopy, Dr Nadezda Tarakina and Dr Russell Bailey (Nanovision) for their help with the imaging techniques, and Dr Rory Wilson (X-ray powder diffraction facility) for running the experiments and for helping in the data analysis. I also want to thank my fellow colleagues: Wei-Te Huang, Alessia D'Onofrio, Jamila Al-Mohammadi, Farah Al-Khayyat, Rawan Albeshti and Natheer Al-Eesa for the friendship and for contributing to the very positive environment at the Centre of Oral Bioengineering. I acknowledge and thank Cera Dynamics Limited, the Institute of Dentistry and the Armourers & Brasiers' Company for the financial and in-kind contribution towards my PhD project. I would also like to thank the International Association for Dental Research and the Society of Glass Technology for facilitating and encouraging research communication with an aim to benefit the wider society. And finally, I would like to acknowledge and thank my family and all those that have been very supportive during this challenging journey.

List of Figures

List of Tables

List of Equations

List of Abbreviations

A-M	Apatite-Mullite
A-L	Apatite-Leucite
APS	Amorphous Phase Separation
ART	Atraumatic Restorative Technique
ATR-FTIR	Attenuated Total Reflectance - Fourier Transform Infrared Spectroscopy
A-W	Apatite-Wollastonite
BFS	Biaxial Flexural Strength
ClAp	Chlorapatite
CR	Contrast Ratio
CS	Compressive Strength
DC	Dental Composite
DMTA	Dynamic Mechanical Testing Analysis
DSC	Differential Scanning Calorimetry
EEB	European Environmental Bureau
ESP	Electron Spin Resonance
FAp	Fluorapatite
FID	Free Induction Decay
FS	Flexural Strength
GC	Glass-Ceramic
GIC	Glass Ionomer Cement
LLPS	Liquid-Liquid Phase Separation
NBO	Non-Bridging Oxygen
ND	Neutron Diffraction
NMR	Nuclear Magnetic Resonance
RF	Radio Frequency
RI	Refractive Index
SANS	Small Angle Neutron Scattering
SBF	Simulated Body Fluid
SMR	Scanning Electron Microradiography
T_c	Glass crystallisation temperature
TEM	Transmission Electron Microscopy

TFS	Three-point flexural strength
T_g	Glass transition temperature
T_m	Melting temperature
T_x	Crystallisation window
$T_{c\ onset}$	Crystallisation onset
UN	United Nations
XMT	X-ray microtomography
XRD	X-ray powder diffraction
OR	Ostwald ripening
MAS	Magic angle spinning
HAADF-TEM	High angle annular dark field - transmission electron microscopy

CHAPTER 1:

BACKGROUND STUDY & LITERATURE REVIEW

1 Introduction

1.1 Background

Given the recent legally-binding call for the phasing out of mercury-containing dental amalgam by the United Nations (UN) and by the European Environmental Bureau (EEB), it is expected that the alternative dental restoratives, such as glass ionomer cements (GICs) and dental composites (DCs) will very soon replace dental amalgam. Both organisations have requested member states to focus on minimally invasive dentistry, with an emphasis on atraumatic restorative technique (ART) treatments. The ART technique is a minimally invasive technique where soft caries are excavated using hand instruments and a restoration consisting of a high viscosity glass ionomer cement is placed. GICs are formed by an acid-base reaction, whereby aqueous poly-(acrylic acid) attacks an alumino-silicate glass, which then releases various cations, mainly Al^{3+} and Ca^{2+} that crosslink the polyacid chains and form a strong polycarboxylate cement. In the recent literature, it has been shown that GICs have the potential to re-mineralise hard caries through the diffusion of ions, such as calcium and strontium that form part of the mineral content of the tooth. GIC are also known to release fluoride ions that replace hydroxyl groups in the apatite lattice and henceforth increase mineral density and acid resistance due to the higher lattice energy. GICs are also known to have similar mechanical properties to dentine, such compressive strength and very similar thermal expansion coefficient. On that basis, glass ionomer cements are ideal materials for the ART technique.

It is proposed that the re-mineralisation potential of GIC can be enhanced by the inclusion of apatite within the cement, which will provide nucleation sites for remineralisation. Dispersion of nano-apatite within the GIC matrix may compromise restoration aesthetics, because small particles agglomerate and form larger particles, which then results in light scattering at the apatite-cement interfaces as a result of the refractive index mismatch between apatite (1.63) and the cement matrix (RI ~1.50). Quite a few glasses developed for GICs have been shown to crystallise to fluorapatite (FAp) phases upon controlled heat-treatment. Pre-treating GIC glasses in the furnace to produce nano-sized FAp glass-ceramics will be investigated to overcome the poor GIC aesthetics arising from the agglomeration of the dispersed particles. The hypotheses of this study are that nano-sized fluorapatite phases in the glass-ceramics: 1. will not affect restoration aesthetics; 2. will improve mechanical properties of the GIC; 3. will promote further crystal growth and remineralisation of hard caries by the formation of biomimetic cement-dentine interfaces.

Furthermore, the composition of the GIC glass can determine the rate of ion diffusion from the GIC to the effected caries. It is known that glasses with higher non-bridging oxygen content exhibit more bioactivity because they dissolve in physiological solutions more rapidly. However, fast dissolution of GIC glass may be undesirable because it will predispose GIC restoration to a mechanical failure. The addition of strontium in the GIC glass composition may provide a source of odontoblast-stimulating ions as well as improved radiopacity with the addition of strontium.

Another type of dental material is the dental composite which consists of polymer (matrix) and glass (filler) components. Dental composites set by

polymerisation of resin monomers. If the glass component in the dental composite is bioactive, the material can form apatite and can help to remineralise carious dentine.

1.2 Aims and Objectives

1.2.1 Aims

The aim of this study is to develop and characterise novel strontium-containing FAp glass-ceramics with known refractive indices for use in aesthetic GICs.

1.2.2 Objectives

- To modify the Appen model by experimentally deriving Appen factors for the amorphous fluorides which will then provide a tool for accurate refractive index calculation of the fluoride-containing GIC glasses.
- To use the modified Appen model to develop glass compositions with the desired refractive index and to then subsequently heat-treat these glasses to develop FAp-containing glass-ceramics.
- To characterise developed glasses and glass-ceramics by solid-state characterisation techniques, such as DSC, XRD, ^{31}P MAS-NMR and ^{19}F MAS-NMR and TEM to understand their thermal behaviour and coordination chemistry.

1.1 Glass

1.1.1 Definition of Glass

The glass is defined as "*a hard, usually transparent, substance used, for example, for making windows and bottles*". In the science community, glass

is usually defined as a “super cooled liquid”. However, a more detailed definition of glass by the American Society of Testing and Materials “*an inorganic product of fusion that has cooled to a rigid condition without crystallising*” is also widely accepted (Carter and Norton, 2007). Essentially, glasses can be better defined as amorphous materials that exhibit a glass transition temperature. This last definition distinguishes an amorphous glass from a nano-crystalline solid that can also show amorphous x-ray powder diffraction pattern.

1.1.2 Goldschmidt’s Criterion

The earliest and simplest theory of glass formation was based on the works of Swiss-Norwegian mineralogist, Victor Goldschmid. Goldschmidt is considered to be the founder of modern-day crystal chemistry and he was known for being able to develop empirical rules for glass formation from his studies. Goldschmidt understood the importance of ionic radius of an element and that this would determine whether it can form a glass or not. Goldschmidt proposed that a ratio from 0.2 to 0.4 of radius-of-cation to radius-of-anion is a condition of glass formation (Vogel, 1994). Since the radius ratio between 0.2-0.4 tend to produce tetrahedral coordinated cations, Goldschmidt believed that only tetrahedrally coordinated cations can form glasses during cooling (Shelby, 2005). For example, in the case of silicate glass, the ionic radius of silicon is 0.39Å and the ionic radius of oxygen is 1.4Å, therefore the ratio between the two radii is approximately 0.28, which obeys Goldschmidt’s Criterion and thus can form a glass.

1.1.3 Zachariasen's Random Network Theory

Based on line-broadening from X-ray diffraction patterns obtained from silica-based glasses, Randall *et al.* (1930) postulated that glass structure is comprised of nanocrystals, approximately 15Å in size, estimated from Scherer's equation:

$$(\tau = \frac{K\lambda}{\beta COS\theta})$$ (**Equation 1.1**)

However, Zachariasen (1932) argued that glass densities are too small and as such glasses cannot contain crystallites.

Zachariasen noted that silica, which can readily form a glass instead of re-crystallising after melting and cooling forms a network rather than densely packed crystals. This network is three-dimensional and consists of oxygen tetrahedrally connecting silicon at all four corners, just like in the corresponding crystal; however, it lacks periodicity and symmetry (Shelby, 2005). Thus, Zachariasen proposed that the ability to form such networks is the ultimate condition for glass formation.

Zachariasen also considered structural arrangements of the elements which would produce such networks and developed the following set of rules:

1. An oxygen atom is linked to not more than two atoms A
2. The number of oxygen atoms surrounding atom A must be small, 3 or 4
3. The oxygen polyhedra share corners, not edges or faces
4. For three-dimensional networks, at least three corners must be shared

1.3.3.1 Network Formers

Network formers are oxides which are capable of forming a glass. Zachariasen concluded that B_2O_3, SiO_2, GeO_2, P_2O_5, As_2O_5, P_2O_3, As_2O_3, Sb_2O_5, V_2O_5, Sb_2O_5, Cb_2O_5, Ta_2O_5 may form glasses because these oxides satisfy all four rules on glass formation.

1.3.3.2 Network Modifiers

Network modifiers are oxides which disrupt glass network by creating non-bridging oxygens. Common examples of network modifiers are Na_2O and CaO.

1.3.3.3 Intermediate Oxides

Intermediates are cations which cannot form a glass by themselves but can do so in association with a network former. Aluminium oxide and titanium oxide are examples of intermediate oxides.

1.2 Glass Crystallisation

1.2.1 Nucleation

Crystal growth requires a nucleus on which the crystal will grow. The formation of such a nucleus is termed nucleation. Nucleation can either be homogeneous or heterogeneous. Homogeneous nucleation occurs when nuclei of the crystal phase form spontaneously within the glass melt. Heterogeneous nucleation occurs when nuclei form at pre-existing nucleation sites, such as crucible walls, nucleation agents or impurities within the glass

melt. If no nuclei are present, crystal growth cannot occur and therefore the material will form a glass.

1.2.2. Crystal Growth

Crystal growth is a major process in crystallisation. It can be defined as a process by which a characteristic crystal lattice is built up through the addition of atoms or structural units.

1.3 Apatite Glass-Ceramics

1.3.1 Introduction

Apatite is named after the Greek word *Apátē* which means deceit because in appearance, apatite is often mistaken for a number of other minerals. Apatite has a chemical formula $Ca_5(PO_4)_3(F, Cl, OH)$. Due to an adaptive framework structure of apatite (White *et al*., 2005), apatite lattice can readily accommodate a number of ionic substitutions. Naturally occurring apatites are found in igneous, metamorphic and sedimentary earth rocks and relatively recently, isomorphs of fluor- and hydroxyapatite were found on the surface of the Moon (McCubbin *et al*., 2010). Furthermore, meteorites from the planet Mars, for example, Chassigny, which fell in provincial France in 1815 brought melt inclusions of Martian fluor- and chlor- apatites (McCubbin and Nekvasil, 2008). Apatite is also the major inorganic component naturally found in the hard tissues of vertebrates, therefore it has a profound biological and clinical significance.

Biological apatites have a chemical formula of $Ca_5(PO_4)_3(OH)$, with some degree of CO_3^{2-} substitutions for PO_4^{3-} , F^- for OH^- and Na+ or Mg^{2+} for Ca^{2+} ions. Synthetic hydroxyapatite (HAp) has been used in various forms of

healthcare, such as for bone replacement, dental cements and dental porcelains. However, sintered porous or even dense HAp bone implants often fail due to poor mechanical properties that are inferior to the mechanical properties of the human bone (**Table 1.1**).

Table 1.1: Mechanical properties of the glass-ceramics for orthopaedic applications

Material	Phase	Density g/cm^3	Thermal expansion coefficient (×10^{-6} K^{-1})	Compressive strength (MPa)	Flexural strenght (MPa)	Young's modulus (GPa)	Fracture toughness (MPa $\sqrt{m^2}$)	Source
Cortical bone	Hydroxyapatite +organic matrix	1.9	27.5 ± 3.9*	133-295	35-283	7-20	5-7	An and Draughn (2000) *Ranu (1987)
HA	Hydroxyapatite	3.16	10	120-150	60-120	35-120	0.8-1.2	Orlovskii et al. (2002)
A-W	Fluor/oxyapatite and wollastonite	3.07	8-10	1080	215	118	2	Kokubo (2008)
Bioverit I	Apatite and fluorphlogopite	2.8	8-12	500	140-180	70-88	1.2-2.1	Höland and Beall (2012)
Bioverit II	Apatite and fluorphlogopite	2.5	8-12	450	90-140	70	1.2-1.8	Höland and Beall (2012)
Bioverit III	Fluorapatite and aluminium phosphate	2.7-2.9	14-18	-	60-90	45	0.6	Höland and Beall (2012)
A-M	Fluorapatite and mullite	2.7-3.3	8-10	-	90-330	70-90	1.0-3.3	Ducheyne (2011)

Moreover, sintered blocks of HAp require machining to shape to match the complex contours of the defect using expensive diamond tipped tools. A porous and bioactive 3D material may be highly desirable for bone regeneration because a porous material will allow osteoblasts to proliferate and integrate inside the 3D structure and enable vascularisation of the newly formed bone, provided the porosity of the material is adequate. However, with the introduction of porosity into any bone substitute material or implant, mechanical properties are compromised as discussed by Karageorgiou and Kaplan (2005), rendering many of the porous bone substitute materials inadequate for load-bearing applications. Since the early 1970s', quite a few melt-derived glasses have been developed that crystallise to apatite phases on controlled heat-treatment.

A glass-ceramic material can be cast into complex shapes by the lost wax casting route, which is usually a simple and cost-effective process. For illustration purposes, the reader is presented with an apatite-mullite glass-ceramic chess piece (**Figure 1.1**) produced by casting molten glass to shape by the lost wax method, which shows the complexity of shapes and surface detail that can be attained by this route.

Figure 1.1: Apatite-mullite chess piece cast to shape by the lost wax method (Karpukhina *et al*., 2014)

Machinable glass-ceramics (GCs), such as mica GCs discussed in this review can also be processed by computer aided design/computer aided manufacturing (CAD/CAM).

Apatite-containing GCs are highly biocompatible and can induce bone formation in vivo (Ducheyne *et al*., 2011). Therefore, apatite-based GCs are highly attractive for medical and dental applications. A bioactive material is defined as a material that exhibits a biological response at the interface once in contact with a biological tissue. A bioactive material may induce a biological response through its surface topography or by a controlled release of therapeutic ions. A number of bioactive apatite containing glass-ceramics

have been developed for orthopaedic applications and these can be categorised based on the type of secondary crystal phases present in the material: apatite-wollastonite (A-W), commercially known as Cerabone®; apatite-fluoromica (A-FM), commercially known as Bioverit®; and apatite-mullite (A-M). Several apatite containing GCs have also been developed for restorative dentistry applications for the fabrication of dental inlays, crowns, bridges and veneers. These are namely apatite-leucite (A-L), commercially known as IPS d.SIGN®; and with apatite as the only phase, for example IPS e.max ZirPress® and IPS e.max Ceram®. Fluorapatites are also good host crystals for rare earths and exhibits low phonon energies; therefore, apatite-containing glass-ceramics have also been investigated for potential applications in optoelectronics. They are also particularly attractive in nuclear waste immobilization, such as for the immobilization of chloride and strontium waste, where the apatite-immobilized radioactive elements are readily incorporated into the apatite lattice.

1.3.2 Prior Liquid-Liquid Phase Separation – Precursor to Nucleation and Crystal Growth

Liquid-liquid phase separation (LLPS) also known as amorphous phase separation (APS) can occur in undercooled liquids either at or below the glass liquidus temperature. If LLPS occurs above the glass liquidus temperature, then such phase separation is termed stable immiscibility. On the other hand, if LLPS occurs below the liquidus state, such LLPS is termed as metastable immiscibility. Undercooled liquids can undergo phase

separation through spinodal decomposition or via nucleation and growth processes (binodal decomposition) (**Figure 1.11**).

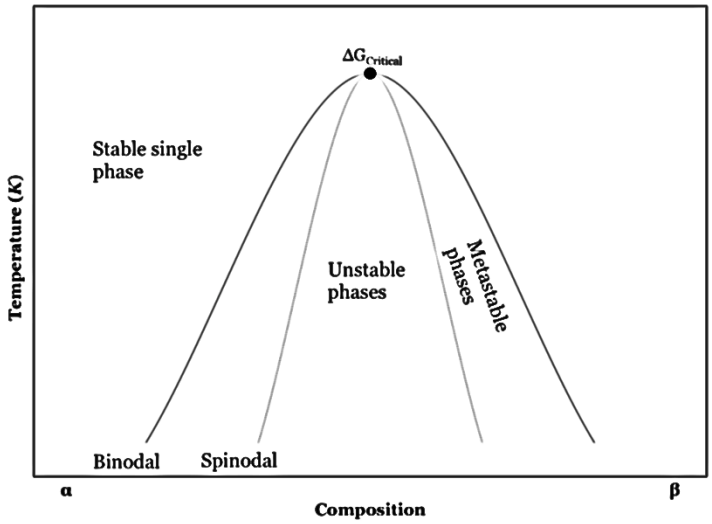

Figure 1.11 Phase diagram of a binary system (adapted from Cahn *et al*., 1969)

Spinodal decomposition is a diffusion driven mechanism with no activation energy barrier. A system that undergoes spinodal decomposition is always unstable. In contrast, phase separation by nucleation and growth (in the binodal region) has a large free energy barrier and it is a metastable process involving an activation energy. Small angle neutron scattering (SANS) techniques can be used to study LLPS in both, spinodally and binodally decomposed glasses. SANS scattering at lower *q* (scattering vector) values correspond to larger phases, which can be attributed to a phase separation under the binodal region of the phase diagram, whereas neutrons scattered at higher *q* values correspond to a finer scale phase separation, which may be attributed to spinodally decomposed structures (Hill *et al*. (2007). Spinodal decomposition, unlike nucleation, generally results in sharp scattering maximum often referred to as a “spinodal ring” particularly during the early stages of phase separation. It is difficult to observe spinodal decomposition by microscopy techniques because of the diffuse interfaces between the

phases. In contrast, nucleated amorphous phases can be readily observed by microscopy. Transmission electron microscopy (TEM) analysis showed (Hill and Wood, 1995) that LLPS via nucleation and growth results in sharp boundaries between the phases as shown in **Figure 1.12**.

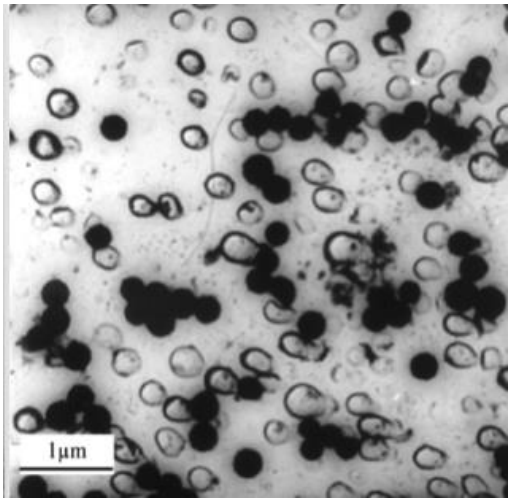

Figure 1.12: Carbon replica TEM of a fluorapatite-mullite glass-ceramic showing evidence of droplet-like amorphous phase separation giving rise to hexagonal fluorapatite crystals (black regions) (Hill and Wood, 1995)

Most of the glass-ceramics discussed in this review undergo a bulk nucleation and crystallisation, which has been attributed to prior liquid-liquid phase separation. Crystal nucleation may be aided by the composition of one of the phases being closer to the crystal phase than the parent glass composition. **Figure 1.12** shows a droplet-like phase (droplets with dark boundaries) which is close to FAp stoichiometry and on heat-treatment crystallises to fluorapatite (FAp) (Hill and Wood, 1995). The A-W GC exhibits surface crystallisation of both phases without the occurrence of prior LLPS (Kokubo, 1982).

There are two main ideas of how prior LLPS can influence the subsequent crystallisation. Vogel and Gerth (1962) proposed that the effect of prior LLPS on glass crystallisation is due to the existence of interfaces in a phase-

separated glass, which provide internal surfaces for heterogeneous nucleation. However, Cahn (1969) and James (1981) suggested that if the composition of the LLPS phase is close to the composition of the subsequent crystal phase, the activation energy is lowered and subsequent homogeneous crystallisation is favoured.

There are few studies on the importance of LLPS in regard to glass-ceramics and it is worth briefly reviewing these studies. Ramsden *et al*. (1984a; 1984b) found that quenched $BaO\text{-}SiO_2$ glasses in which LLPS developed simultaneously with the nucleation of the crystals, the crystal nucleation rate increased with isothermal heat-treatment time. Ramsden *et al*. (1984b) reported that the same system without prior LLPS did not show any increase in the crystal nucleation rates. Thus, Ramsden *et al*. (1984a; 1984b) and later Zanotto *et al*. (1986) concluded that the predominant effect on crystal nucleation arises from the compositional changes brought about by phase separation. Although it has been shown that LLPS has a profound role in the formation of simple glass-ceramics, its effect in complex multicomponent systems, such as those with strong nucleating agents should not be generalised.

Tomozawa *et al*. (1972) reported that lithium silicate glasses showed considerably increased crystal nucleation rates when the glass had undergone LLPS, and proposed that the LLPS droplets consist of silica-depleted diffusion zones at their interfaces, therefore giving rise to sites for heterogeneous nucleation.

The mechanism by which LLPS enhances subsequent crystallisation depends on the composition of the glass and the composition of the crystalline phase. Apatite GC systems developed by Hill *et al*. (2004) bulk

nucleate via prior amorphous separation but can also crystallise through a surface mechanism. In simple glasses such as the lithium silicate glasses, LLPS enhances nucleation rate, by reducing the activation energy for nucleation. Although LLPS can enhance subsequent crystallisation of a glass, based on the classical nucleation theory, the LLPS droplet diameter (D) should be larger than the critical radius (*r**) for crystal nucleation in order for nucleation to take place within the droplet phase. Therefore, fine scale LLPS can potentially suppress nucleation and subsequent crystallisation.

In a study by Clifford *et al*. (2001a) it was found that base glasses in the A-M systems with a molar Ca to P ratio of 1.67 (glass compositions with apatite stoichiometry) crystallise through an internal or bulk mechanism, and that base glasses with Ca to P ratios higher or lower than 1.67 crystallise through a surface mechanism. Interestingly, Clifford *et al*. (2001a) note that compositions with a molar Ca to P ratio above or below 1.67 can crystallise in bulk following an annealing hold for one hour just above the glass transition temperature. Clifford *et al*. (2001a) study provides evidence that LLPS in the apatite-mullite system can be produced below the liquidus by nucleation and growth.

Rafferty *et al*. (2000b; 2003) used high temperature dynamic mechanical thermal analysis (DMTA) to show the presence of two mechanical loss peaks and two reductions in the storage modulus corresponding to two glass transition temperatures (**Figure 1.13**) for many of the A-M glass compositions providing evidence of a prior LLPS. On crystallisation of FAp, only one glass transition temperature (T_g) was observed indicating that one of the two amorphous phases had crystallised to FAp.

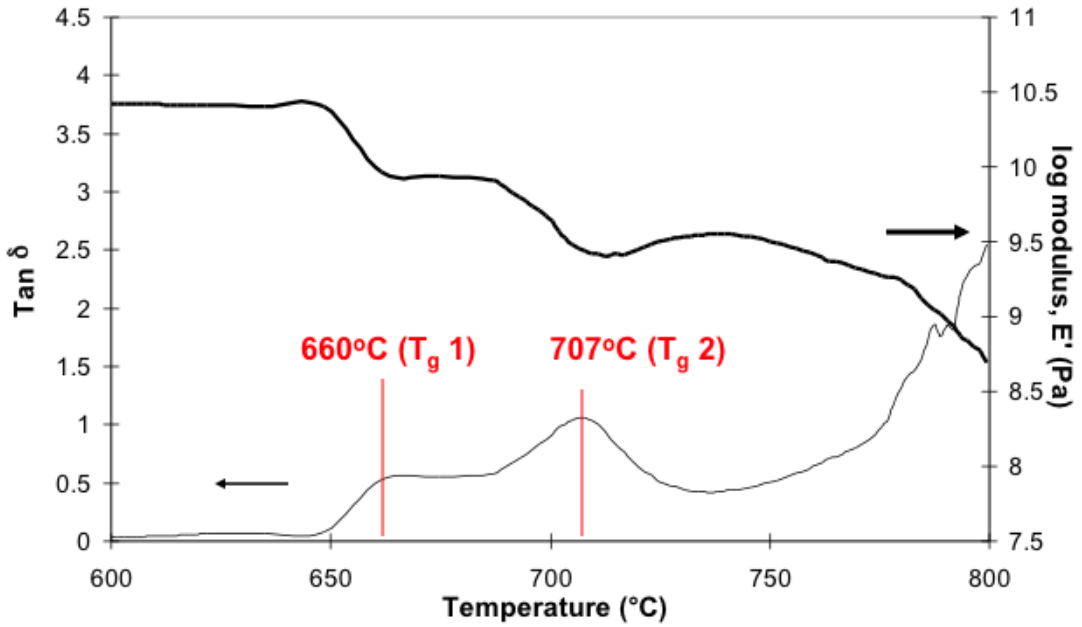

Figure 1.13: Dynamic mechanical testing analysis (DMTA) of an A-M glass-ceramic showing two glass transitions, one at 660°C and second at 707°C and two decreases in modulus (Rafferty *et al.* (2000b) collected at a 5°C/min heating rate in a single frequency mode at 1 Hz
()

Crystals or LLPS droplets in an undercooled liquid can undergo Ostwald ripening (OR) during a heat-treatment. During an OR process crystals or small LLPS droplets can grow beyond the LLPS domain, producing larger LLPS droplets or crystals. Thermodynamically, OR is a favourable process because larger particles have lower surface energy in contrast to smaller particles. Apatite crystal growth through OR process is observed in apatite glass-ceramics, such as reported by Höland *et al*. (2015). One of the key characteristics of an OR process is the reduction in the number of droplets/crystals and an increase in volume fraction as a function of time, pressure or temperature.

FAp is part of the hexagonal group of crystals, therefore it shows a kinetically favoured growth in the crystallographic *c*-direction, which is seen in Höland *et al*. (2015) findings, whereby crystal length as a function of time due to OR process was more pronounced as opposed to crystal expansion at

crystallographic a-direction. OR process can be used to produce a highly homogeneous and mechanically superior microstructure of a GC.

1.3.3 Biomedical Applications of Apatite Glass-Ceramics

1.3.3.1 Orthopaedics

1.3.3.1.1 Fluor/Oxyapatite-Wollastonite Glass-Ceramics

Kokubo *et al*. (1982) developed apatite-wollastonite (*β*-CaSiO3) system based on SiO_2-P_2O_5-CaO-MgO-CaF_2, also known by its commercial name Cerabone®. The *β*-wollastonite phase in the A-W system enhances mechanical performance of the glass-ceramic. Kokubo *et al*. (1987) reported on the A-W GC ability to resist failure by fatigue. It was estimated that the life-time of an A-W GC, under a constant loading of 65 MPa in simulated body fluid is 10 years, compared to a sintered hydroxyapatite, which under the same loading can sustain the loading before fracture for only 1 min. Both, apatite and *β*-wollastonite phases in the A-W system crystallise through a surface mechanism (Kokubo *et al*., 1982). As such, the A-W GC cannot be cast to shape by the lost wax technique and is processed through powder sintering route.

It was often claimed that the apatite phase in the A-W systems is FAp, however Clifford and Hill (1996) noted that the A-W glasses are very deficient in fluoride content with regard to the FAp stoichiometry. Clifford and Hill (1996) further suggested that the apatite formed in A-W systems is therefore more likely to be a mixture of fluor- and oxy-apatite. Based on the pioneering electron spin resonance (ESP) studies of fluor/oxyapatites, it has been long known that O^- can occupy F^- sites (Segall *et al*., 1962; Piper *et al*.,

1965). Nonetheless, at present, the availability of high-resolution solid-state characterisationtechniques such as ^{17}O MAS-NMR coupled with Dynamic Nuclear Polarization (DNP) and high field ^{19}F MAS-NMR could provide fast and accurate elucidation of oxygen and fluoride environments in the A-W GC, however such work is yet to be published.

Calver et al. (2004) reported that modified Kokubo *et al*. (1982) A-W glass with higher metal fluoride content (**Table 1.2, AW3**) resulted in a completely changed apatite crystallisation behaviour. Calver *et al*. (2004) found that the base glass with the highest CaF_2 content favoured volume FAp nucleation and crystallisation.

Table 1.2: Apatite-wollastonite base glass compositions in mole % (Calver *et al*., 2004)

	SiO_2	P_2O_5	MgO	CaO	CaF_2
AW1	35.46	7.15	7.11	50.28	0
AW2	35.46	7.15	7.11	49.88	0.4
AW3	35.46	7.15	7.11	45.51	4.77

Calver *et al*. (2004) also found that A-W systems showed reduced T_g and FAp crystallisation exotherms with increasing calcium fluoride content. Therefore, the low calcium fluoride content in the original A-W system is actually suppressing crystallisation of FAp. Filho *et al*. (1996) suggest that fully crystallised GCs, which are otherwise bioactive, will not exhibit any further bioactivity through the release of ions, such as Ca^{2+} and HPO_4^{2-}, once such ions take up higher energy coordination states in the apatite lattice. Therefore, from a bioactivity point of view, it may not always be desirable to consume therapeutic ions for the formation of apatite within the glass matrix, as opposed to the release of such ions and subsequent formation of apatite on the surfaces of the material, that potentially lead to the formation of a strong and chemically stable implant-bone interface. Furthermore, the molar

Ca to P ratio in a stoichiometric apatite crystal is 10 to 6 (1.67); therefore, GC systems containing a stoichiometric Ca to P ratio, or in other words glass formulations with smaller compositional differences between the glass and the crystal phase preferentially crystallise in bulk, which is unfortunately not the case in the A-W system. On the other hand, the A-W system is inherently aluminium free, thus risks associated with aluminium neurotoxicity, summarized by Kumar and Gill (2009), and reported by Reusche *et al*. (2001) are completely absent.

It could be argued as to why the original A-W system developed by Kokubo *et al*. (1982) contains magnesium and a non-stoichiometric Ca:P:F ratio that could otherwise aid bulk nucleation and crystallisation of apatite phases. There is a considerable and long-standing evidence, for example, as found by X-ray diffraction analysis of precipitated apatites by LeGeros *et al*. (1980), which shows that the presence of Mg^{2+} ions in an aqueous solution cause a strain on the apatite structure causing it to collapse and suppress crystal growth. In view of the biological apatite found in bone as opposed to tooth, Mg^{2+} ions alongside osteocalcine and proteoglycan proteins play a significant role in the development of a nanoscale apatite (Bluementhal *et al*. 1975), providing the bone tissue with a fine microstructure with excellent mechanical properties. Therefore, it could be argued that the A-W system is highly biomimetic in view of the elemental composition of the human bone.

In vivo animal studies on the implanted A-W glass-ceramic provide evidence for excellent osseointegration around the A-W implant and a chemical calcium phosphate based interface (Kitsugi *et al*., 1989; 1990) between the implant and bone, with high bending and compressive strengths of 157 and 1060 MPa, respectively (Nakamura *et al*., 1985). Kokubo *et al*. (1990) found

that A-W GC immersed in tris(hydroxymethyl)aminomethane (TRIS) buffer did not show bioactivity through the formation of apatite and these findings were contradictory to animal studies conducted previously, where the A-W GC was found to form a strong chemical interface with the living bone. Therefore, Kokubo *et al*. (1990) developed a simulated body fluid (SBF), an alternative immersion medium for *in vitro* assessment of bioactivity of the A-W GC. Kokubo *et al*. (1990) argued that TRIS buffer does not mimic the actual body environment because it is completely deficient in ions, such as Ca^{2+} and HPO_4^{2-} naturally found in the body fluids and therefore argued that the lack of apatite formation in TRIS buffer, as opposed to high bioactivity of the A-W GC in SBF, also supports the view that the apatite phase on the surfaces of the A-W GC forms by a chemical reaction between the A-W GC and the ions present in the body fluid. In view of this, it can be further postulated that apatite crystals within the A-W GC act as nuclei on which ions, such as Ca^{2+} and PO_4^{3-} in the solution nucleate and facilitate apatite formation until the eventual fusion between the apatite crystals in the A-W and the apatite in the living bone, whereby a chemical interface is formed.

Kokubo *et al*. (1992) reported that if aluminium is included in the A-W parent glass composition and then subsequently crystallised, the A-W GC does not show any bioactivity in SBF as opposed to the same A-W material without aluminium. The addition of aluminium results in a more chemically stable residual glass phase, which reduces the release of Ca^{2+} and PO_4^{3-} ions which affects apatite formation (Strnad, 1992). Blades *at el*. (1998) conducted *in vivo* animal study on aluminium-containing glass ionomer cements as potential bone cements, where as low as 1 ppm of aluminium released was found to inhibit mineralization of the newly formed osteoid in

rabbit bone. It is important to distinguish that the role of aluminium in Blades *et al*. (1998) study may be attributed to aluminium toxicity to bone-forming cells (Rodriguez *et al*., 1990) and direct inhibition of crystal growth as opposed to reduced bioactivity involving structural parameters of the residual glass phase, as proposed in Strnad's (1992) study.

Good osseointegration as a result of good bioactivity on the implant surfaces (Neo *et al*., 1993) combined with good mechanical properties (Kokubo *et al*., 1985; 1986) perhaps explains why the A-W glass-ceramics have found promising applications in bone and vertebra replacement (Kokubo *et al*., 2008) and it is reported that over 50,000 successful bone implants have been made using the A-W glass-ceramic system (Zanotto, 2010). However, from a manufacturing point of view, a bulk crystallizing A-W material, such as proposed by Calver *et al*. (2004) could provide a more cost-effective material. *In vitro* and *in vivo* bioactivity of the modified A-W system developed by Calver *et al*. (2004) still need to be studied. The original A-W GC is currently manufactured by Nippon Electric Glass Co., Ltd (Japan) (Montazerian and Zanotto, 2016).

1.3.3.1.2 Fluorapatite-Mica Glass-Ceramics

Grossman (1972) of Corning Glass Works, developed the first machinable mica glass-ceramic system, later marketed by Dentsply International under the name Dicor®. Dicor® was seen as a very significant development since the new GC material could be easily machined to shape without a critical failure. Machinability of the mica glass-ceramics is attributed to the eminent cleavage of the mica-type crystals as a result of anisotropic crystal growth.

This facilitates crack propagation in the direction of cutting without causing a critical failure of the material.

Although mica glass-ceramics initially did not contain any apatite phases, Vogel *et al.* (1986) developed two GC systems (**Table 1.3**) with FAp and fluorphlogopite $Mg_3(AlSi_3O_{10}F_2)Na/K$ and $Mg_3(Si_4O_{10}F_2)Na/K$ mica phases and an additional silica-free GC with apatite and aluminium phosphate phases.

Commercially available Bioverit I® and Bioverit II® systems crystallise to FAp and fluorphlogopite in bulk. However, Bioverit II® system crystallises to a smaller fraction of FAp, which can be explained by the very low P_2O_5 content in the nominal composition (**Table 1.3**).

Table 1.3: Examples of Bioverit® base glass compositions in mole % (Vogel and Höland, 2000)

	Bioverit I	**Bioverit II**
SiO_2	29.44	44.12
Al_2O_3	9.04	17.47
P_2O_5	4.66	0.08
CaO	14.89	0.21
MgO	21.29	17.44
Na_2O	2.15	4.23
K_2O	3.57	3.10
TiO_2	-	-
F	14.96	13.17
Cl	-	0.17
ZrO	-	-

Both systems have undergone prior amorphous phase separation into two droplet phases and a glassy matrix phase (Höland and Beall, 2012). One droplet phase is rich in apatite elements whereas the second droplet phase is closer to the fluorphlogopite composition. This may explain why both phases, apatite and fluorophlogopite, crystallise via a homogeneous

mechanism. Bioverit III is a silica-free phosphate glass that crystallises to FAp and an aluminium phosphate ($AlPO_4$) (Höland and Beall, 2012), Bioverit III material exhibits lower mechanical properties (Höland and Beall, 2012) therefore it has not been so extensively studied.

Bioverit II contains a higher fraction of mica crystals. Therefore, Bioverit II GC exhibits better machinability but at the expense of lower mechanical properties than Bioverit I (**Table 1.3**). Based on ^{19}F MAS-NMR experiments of mica ceramics, it was shown that the fluoride ion in mica systems exists mainly in Mg(n)-F type environments, with a chemical shift at about -174 ppm for F-Mg(3) (Fechtelkord *et al*., 2003). As of 2016, apatite-fluoromica GCs, Bioverit I and II are currently manufactured by VITRON Spezialwerkstoffe GmbH (Germany).

1.3.3.1.3 Fluorapatite-Mullite Glass- Ceramics

Mullite is a rare naturally occurring aluminosilicate mineral. Mullite-reinforced matrices exhibit enhanced mechanical properties. FAp phases can act as nucleation and crystal growth sites for new apatite phases between the implant and the living bone. Both crystal phases in the fluorapatite-mullite system show elongated needle-like microstructure and exceptional mechanical properties, particularly flexural strength and fracture toughness of up to 330 MPa and 3.3 MPa $\sqrt{m^2}$ respectively (**Table 1.1**). The A-M GC shows spherulitic crystallisation, which enhances fracture toughness properties of the material (Stanton *et al*., 2010). The system nucleates in bulk; therefore, it is readily castable by the lost wax route.

The first melt-derived castable fluorapatite ($Ca_5(PO_4)_3F$) - mullite ($Al_6Si_2O_{13}$) glass-ceramic was developed by Hill *et al*. (1991) and was based on the SiO_2-Al_2O_3-P_2O_5-CaO-CaF_2 system. Furthermore, Samuneva *et al*. (1998) were also able to produce the A-M glass-ceramic system by a sol-gel route, rather than a melt-quench route.

Hill *et al*. (1991) noted that base glasses with relatively low CaF_2 content (**Table 1.4, A-C)** surface crystallised to apatite and mullite upon heat-treatment, whereas base glasses with metal fluoride content (**Table 1.4, D-E**) bulk crystallised to anorthite with only a small fraction of FAp.

Table 1.4: A-M base glass compositions in mole % (Hill *et al*., 1991)

	SiO_2	Al_2O_3	P_2O_5	CaO	CaF_2
A	37.50	25.00	12.50	25.00	0.00
B	35.29	23.53	11.76	23.53	5.88
C	33.33	22.22	11.11	22.22	11.11
D	31.58	21.05	10.53	21.05	15.79
E	30.00	20.00	10.00	20.00	20.00

The work by Hill *et al*. (1991) and also subsequent work by Hill and Wood (1995), Clifford and Hill (1996), Hill *et al*. (2000), Rafferty *et al*. (2000a), Clifford *et al*. (2001a; 2001b) and later by Stanton and Hill (2005) suggests that metal fluoride as well as phosphorus content in fluoro-phospho-aluminate systems will likely influence prior LLPS and will therefore determine whether the glass crystallises via the homogeneous bulk route (aided by the LLPS composition) or the heterogeneous surface route.

Stanton and Hill (2005) postulated that once crystallisation of FAp crystal has begun, the surrounding glass becomes depleted in F, Ca and P and moves closer to the mullite composition, whereupon it crystallises to mullite by the homogeneous mechanism. Stamboulis *et al*. (2004) explained crystallisation

of FAp and mullite phases in the A-M system in even greater detail by analysing heat-treated A-M samples with Magic Angle Spinning-Nuclear Magnetic Resonance (MAS-NMR) spectroscopy. Spectra from ^{27}Al MAS-NMR in **Figure 1.14(a**) show how aluminium resonance is relatively unchanged until the GC reaches second crystallisation temperature (T_{c2}) whereupon the GC starts to crystallise to mullite. It can be observed from **Figure 1.14(b)**, that a broad peak seen at around 50 ppm, assigned to Al(IV), remains unchanged even after FAp crystallisation (T_{c1}).

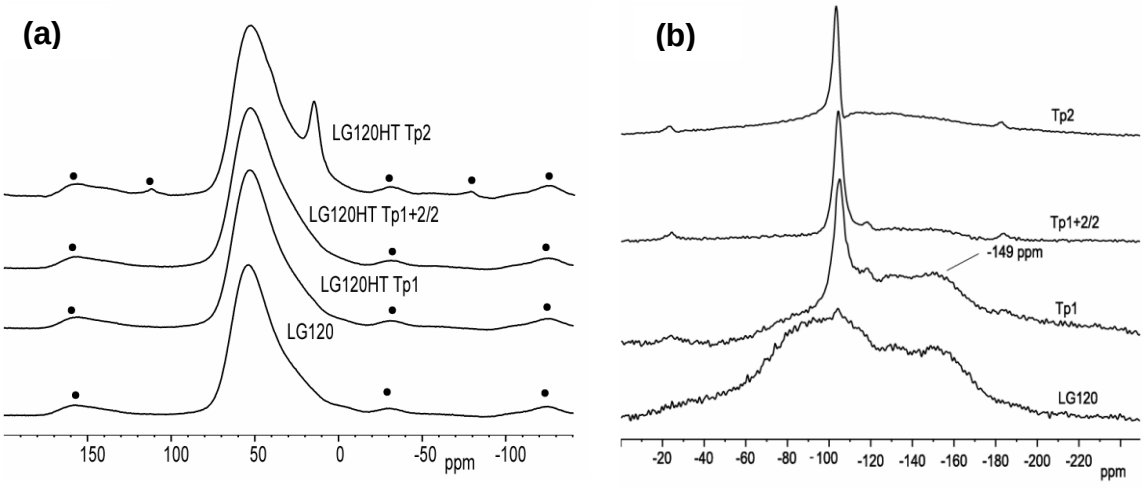

Figure 1.14: ^{27}Al (a) and ^{19}F (b) MAS-NMR spectra of LG120 heat-treated at different temperatures (Stamboulis *et al*., 2004)

During the second phase crystallisation, an additional peak, at around 12 ppm, which is assigned to an Al(VI) in mullite is observed. Stamboulis *et al*. (2004) further explain, that during first and second crystallisation processes, charge balancing cations for maintaining aluminium in a four-fold coordination state, Al(IV) are consumed during FAp formation, therefore, at higher temperatures, the lack of charge balancing cations to keep aluminium in a IV coordination state forces aluminium to take up higher coordination

states, in this case, Al(VI). ^{19}F MAS-NMR spectra as shown in **Figure 1.14** (b) show how the fluoride environment changes with increasing heat-treatment temperature. The lowermost ^{19}F spectrum of the untreated LG120 glass in **Figure 1.14** (b) show two broad peaks at -90 ppm and -150 ppm that can be attributed to the amorphous fluoride environments in the untreated glass, F-M(n) and Al-F-M(n) respectively, (Zang and Stebbins, 2000). However, at T_{C1}, a sharp peak at around -103 ppm develops at the expense of F-Ca(n) peak, which is assigned to fluoride in a F-Ca(3) environment in FAp. At higher temperatures, such as T_{C2}, fluoride from Al-F-M(n) peak is also fully consumed and Stamboulis *et al*. (2004) further proposed that F-M(n) such as F-Ca(n) species preferentially charge balance the non-bridging oxygens in the phosphorus locality. It can be additionally postulated that such preference to balance the non-bridging oxygens in the phosphorus locality reduces kinetic energy barrier to FAp nucleation and crystal growth, because the local environment of Ca, P and F in the glass is similar to that present in fluorapatite.

Relatively recently, Stamboulis *et al*. (2006), Hill *et al*. (2007) and O'Donnell *et al*. (2010) conducted real-time small angle neutron scattering (SANS) and neutron diffraction (ND) experiments on the A-M systems developed in the early 1990s. They postulated that amorphous glasses that form the A-M system may have undergone phase separation by spinodal decomposition during the casting process on a scale of 25-27 nm (Hill *et al*., 2007). Similarly, the same cast A-M system isothermally heat-treated at 740°C and 750°C initially showed neutron scattering at higher *q* which then moved to lower *q* with increasing temperatures where the scale of the LLPS corresponded to about 35 nm. This provides evidence that undercooled

liquids can undergo liquid-liquid phase separation by nucleation and growth, whereupon the chemical system can overcome the thermodynamic and kinetic energy barriers to nucleation and subsequent amorphous phase growth. It is suggested by Hill *et al*. (2007) that the A-M cast glass is initially phase-separated by spinodal decomposition, whereby rapid cooling creates a barrier to nucleation and growth. However, it may be argued, that scattering at lower *q* in the as-cast glasses may be attributed to a finer LLPS by nucleation and growth. SANS experiments by Hill and co-workers provide evidence that finer scale phase separation in the apatite-mullite system increases in size as a function of temperature, which can be either attributed to the fact that the cast A-M system is initially spinodally decomposed and then undergoes LLPS by nucleation and growth or more likely LLPS growth by an Ostwald ripening mechanism.

Further studies of an A-M glass-ceramic analysed by heat-treating an amorphous precursor glass up to 1200°C with in situ TOF-neutron diffraction (O'Donnell *et al*., 2010) explain the crystallisation behaviour of the A-M system in more detail. O'Donnell *et al*., (2010) reported that FAp and mullite crystallised on heating until 1130 °C followed by the partial dissolution of both phases at higher temperatures. It was also found that on the subsequent cooling of the A-M system, recrystallisation occurred and additional new phases were produced, namely berlinite ($AlPO_4$) and cristobalite (SiO_2), which formed at around 1025°C in addition to the FAp and mullite. This indicates that the subsequent cooling of the GC can produce additional crystal phases, which may be undesirable but can be avoided by introducing higher cooling rates to create an energy barrier to nucleation and growth of the undesirable crystal phases.

Stanton and Hill (2005) found that apatite phases in the A-M system grow as dendrites and spherulites. Generally, the microstructure of a GC is strongly influenced by the conditions of the heat-treatment of the parent glass, this namely includes duration, temperature and cooling rate and whether or not the base glass compositions is doped with additional nucleants, for example, such as reported with niobium-doped FAp GCs by Denry *et al*. (2012). Mechanical properties particularly fracture toughness of the A-M GC developed by Hill and co-workers surpass mechanical properties of the alternative glass-ceramic systems discussed in this review (**Table 1.1**).

In vivo animal studies conducted by Freeman *et al*. (2003) show that a fully crystallised A-M glass-ceramic osseointegrates as shown in **Figure 1.15(b)**; however, its amorphous precursor base glass implant does not osseointegrate, which is evident from the fibrous tissue around the glass implant as shown in **Figure 1.15(a)** and the lack of implant-bone interfaces.

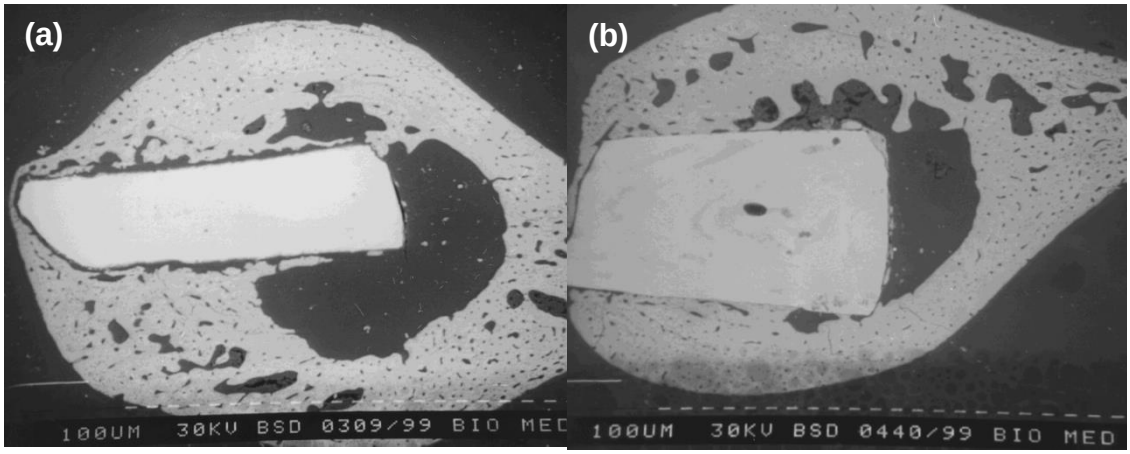

Figure 1.15: Backscattered scanning electron micrographs of implanted LG120 base glass (a) and implanted LG120 glass-ceramic following subsequent crystallisation to fluorapatite and mullite phases (b) (Freeman *et al*., 2003)

Goodridge *et al*. (2007) report on both, *in vitro* and *in vivo* properties of the porous A-M glass ceramic system produced through selective laser sintering (SLS) method, using cast A-M and commercial A-W glass-ceramics as positive controls. In the four weeks study, Goodridge *et al*. (2007) report that

no sign of inflammation or adverse tissue reaction was observed around all the implants. Analyses of the implant-bone interfaces by scanning electron microscopy (SEM) showed evidence for bone ingrowth into the both porous materials, the A-M system produced through SLS method and the A-W sintered glass-ceramic. Although Goodridge *et al*. (2007) report that the laser sintered apatite-mullite system developed by Hill *et al*. (1991) does not form apatite in SBF, previous studies indicate that SBF studies are not adequate in the assessment of bioactivity of aluminium-containing GCs (Strnad, 1992). Stanton *et al*. (2009) assessed the interfacial chemistry between the A-M system and a titanium alloy, for potential applications of the A-M system for orthopaedic implant coatings. Stanton *et al*. (2009) enamelled the A-M glass-ceramic to titanium by heat-treatment and thereafter analysed the interfacial reaction zone between the A-M glass-ceramic and the titanium alloy by high angle annular dark field transmission electron microscopy (HAADF-TEM). Stanton *et al*. (2009) found that titanium diffused into the intermediate layer of the glass-ceramic and postulated that titanium silicides and titanium phosphides were formed based on the elemental analysis of the interfacial zones by energy dispersive X-rays (EDX) that produced characteristic photons for Ti, Si and P atoms but not oxygen atoms. This study shows that the A-M glass-ceramic can chemically bond to titanium. This can be useful in overcoming the problem of coating detachment observed with micromechanical surface retention of plasma sprayed hydroxyapatite coatings (Filiaggi *et al*., 1991). The A-M glass-ceramic coating may enhance osseointegration at the bone-implant interface and may provide long-term stability of the A-M coated implants.

Wood and Hill (1991) produced cements from the A-M glass-ceramic ionomer-type systems with varying degrees of crystallinity for potential application as bone cements. Wood and Hill (1991) found that the degree of crystallinity of the A-M glass-ceramic can influence the properties of the cements, such as working and setting times of the cement pastes and the mechanical properties of the set cements.

1.3.3.1.4 Strontium-Substituted Fluorapatite Glass-Ceramics

Hill *et al*. (2004) developed strontium substituted FAp glass-ceramics for potential orthopaedic applications, in the system SiO_2-Al_2O_3-P_2O_5-CaO/SrO-CaF_2/SrF_2 (**Table 1.5**).

Table 1.5: Strontium-substituted fluorapatite base glass compositions in mole % (Hill *et al*., 2004)

Glass code	SiO_2	Al_2O_3	P_2O_5	CaO	CaF_2	SrO	SrF_2
LG26	32.14	21.43	10.71	21.43	14.29	0.00	0.00
LG119	32.14	21.43	10.71	10.71	14.29	10.71	0.00
LG125	32.14	21.43	10.71	0.00	14.29	21.43	0.00
LG26Sr	32.14	21.43	10.71	0.00	0.00	21.43	14.29

Since strontium has a higher atomic number than calcium, strontium-substituted materials exhibit higher radiopacity, which enables the clinician to distinguish between the implant and bone on a radiograph.

Hill and co-workers (2004) observed that substituting strontium for calcium has little effect on the parent glass structure. However, the crystallisation behaviour of the glasses as a function of strontium content was markedly altered. Base glasses without any strontium exhibited complete bulk crystallisation with the first crystallisation temperature being independent of the particle size, whereas glasses with strontium and no calcium exhibited

predominantly surface nucleation. Glasses with equimolar proportions of calcium and strontium crystallised via bulk and surface. Hill *et al*. (2004) show that increasing strontium substitution hinders bulk crystallisation of apatite, which is reflected in an increase in crystallisation temperature, and promotion of surface nucleation of apatite at the expense of bulk nucleation, as evidenced by particle size dependence on the crystallisation temperature of the FAp phases. Hill *et al*. (2004) also observed that equimolar strontium-calcium composition resulted in a glass with a reduced second exothermic process associated with mullite crystallisation. This can be attributed to an increased mobility of the glass network and a lower glass transition temperature, which produces a more dominant heterogeneous crystallisation effect. Such a reduction in crystallisation temperature would suggest a new crystalline phase, and not simply a reduction in crystallisation temperature (Hill *et al*., 2004).

In another study Hill *et al*. (2006) elucidated Ca and Sr sites in mixed FAp through ^{19}F MAS-NMR. Obtained results showed that the F was present as F-Ca(3) in the all calcium glass and as F-Sr(3) in the all strontium glass. In the mixed glasses fluoride was present as mixed sites: F-Ca(3), F-Ca(2)Sr, F-CaSr(2) and F-Sr(3). Ca had a higher tendency to occupy the F-M(3) sites than Sr which may reflect the higher charge to size ratio of Ca^{2+} relative to Sr^{2+} and its greater affinity for F^- ions.

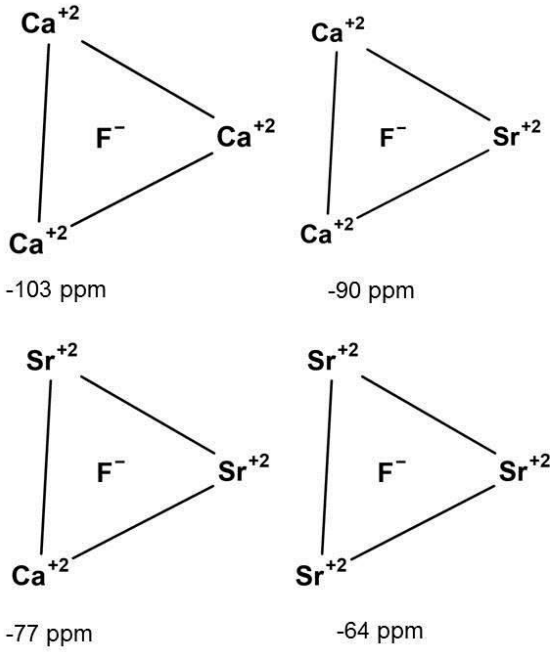

Figure 1.16: ^{19}F MAS-NMR chemical shifts for mixed calcium/strontium apatites, adapted from Hill *et al.* (2006)

An *in vivo* animal study by Sabareeswaran *et al*. (2013) on a glass-ceramic that surface crystallised to a strontium FAp phase and a Sr-celsian phase (feldspar) as identified by XRD was found to be highly ossteoconductive and biocompatible. X-ray microtomography (XMT) analysis of the inorganic-organic interfaces showed highly mineralised newly formed bone adjacent to the synthetic implant surface.

It is known that at low concentrations strontium can promote mineralisation of bone (Verberckmoes and D'Haese, 2003). It is also known that strontium-containing bioactive glasses show increased osteoblast proliferation and alkaline phosphatase activity (Gentleman *et al*., 2010). Therefore, it would be desirable to measure ion release (particularly Sr^{2+}) of the strontium FAp GC developed by Hill *et al*. (2004).

1.3.3.1.5 Fluorapatite and Chlorapatite Glass-Ceramics

Recently, Chen *et al*. (2014a and 2014b) developed novel alkali-free FAp and chlorapatite (ClAp) glass-ceramics from bioactive glasses. Chen *et al*. (2014a) produced a series of bioactive glasses of varying metal fluoride content and found that bioactive glasses with high fluoride content crystallised to FAp and crystalline CaF_2 and SrF_2 on quenching. This shows that metal fluoride content can determine the crystallisation window (T_x) between the glass transition (T_g) and the crystallisation onset ($T_{c\ onset}$). It is desirable to obtain initially amorphous base glass so that the crystallisation of, say FAp phases, can be controlled. Chen *et al*. (2014a) also found that the amorphous base glass powder without any fluoride content crystallised to a wollastonite phase through a surface mechanism. Furthermore, all fluoride containing glasses bulk crystallised to FAp via a homogeneous nucleation mechanism.

Chen *et al*. (2014c) studied novel bioactive chloroapatite glass-ceramics in the system of SiO_2-P_2O_5-CaO-$CaCl_2$. It is known that ClAp completely converts to hydroxyapatite in the presence of water (Elliot and Young, 1967) hence making ClAp glass-ceramics attractive for both, medical and dental applications. Chen *et al*. (2014c) emphasise that ClAp is less stable than FAp. This is attributed to the chloride ion being larger than hydroxyl or fluoride ion. The fluoride ion is small enough to fit in the centre of the Ca(II) triangle in the FAp lattice, whereas larger ions such as hydroxyl and chloride do not fit in the centre of the Ca(II) triangle but are rather displaced above the plane of the Ca(II) triangle. The chloride ion is larger than hydroxyl ion and therefore it is displaced further away from the Ca(II) triangle. This

intrinsic apatite lattice instability brought about by the chloride ion allows the rapid exchange for a smaller ion, such as a hydroxyl ion. On increasing the fluoride or chloride content in the bioactive glass systems, Chen *et al*. (2014b; 2014c) found that there was an increasing tendency of the glasses to crystallise. The halogen-free glass surface crystallised to a pseudowollastonite (α-$CaSiO_3$) and an apatite, presumably an oxyapatite. Pseudowollastonite induces apatite formation in SBF (Siriphannon et al., 2000) and is highly resorbable *in vivo* (de Aza *et al*., 2000). ClAp phases in the Chen et al. (2014b) crystallised via the homogeneous route, which from a material processing point of view is highly desirable. FAp is largely insoluble in vivo so ClAp GCs offer the potential for producing highly resorbable GC implants. Nonetheless, there is a need for further characterisation of these ClAp GCs, including characterisation of the *in vivo* activity and the relationships between the composition, heat-treatment, microstructure and mechanical properties.

1.3.3.2 Dentistry

1.3.3.2.1 Fluorapatite-Leucite Glass-Ceramics

Höland *et al*. (1994) developed FAp-leucite ($KAlSi_2O_6$) (A-L) glass-ceramics in the SiO_2-Al_2O_3-Na_2O-K_2O-P_2O_5-F system, for potential application in restorative dentistry. Research led by Höland led to the development of the commercial apatite-leucite glass-ceramic IPS d.SIGN (Ivoclar Vivadent, Liechtenstein). The needle-like apatite phases in the A-L system crystallised via a homogeneous crystallisation mechanism, which is a likely indication of prior LLPS. Additionally, upon DSC analysis of the A-L system, Höland *et al*.

(2000) observed a unique phenomenon; the A-L system exhibits two endothermic reactions, first at 565°C and second endothermic reaction at 634°C. Previously, the two endothermic reactions were assigned to a phase transformation into two amorphous phases; one glassy, silica-rich phase and a droplet-like phase rich in Ca and P elements. Höland *et al.* (2000) suggests that the second endothermic reaction at 634°C is a transformation to a crystal phase, namely a sodium-calcium orthophosphate ($NaCaPO_4$), which was confirmed by XRD analysis. Furthermore, Höland *et al*. (2000) observed another interesting phenomenon, at higher temperatures (640°C) $NaCaPO_4$ crystals dissolved and recrystallised to a new crystal phase. However, this new crystal phase could not be matched to any known phases when checked against the ICDD (International Centre of Diffraction Data) database. Additionally, Höland *et al*. (2000) found that once the new phase is formed, apatite crystallisation proceeds at 700°C. Heat-treatment of the A-L system at 700°C for 8 hours does not result in a material with needle-like microstructure, it requires additional heat-treatment at 1050°C for 2h for the development of needle-like FAp crystals (Höland *et al*., 2000). This shows that the thermal treatment of the base glass can strongly influence both, the appearance of the material and also the morphology of the GC material.

Höland *et al*. (2000) suggest that the morphology of the needle-like apatite is comparable to that of the apatite in natural teeth. The A-L glass-ceramic exhibits good chemical durability, solubility of the GC being only at 60-70 $\mu g/cm^2$. The translucency of the A-L system varies and is in the range of 5.8-10.4%, depending how the material is processed. The A-L glass-ceramic shows thermal expansion in the range of 14.1-14.8 10^{-6} K^{-1}, which is quite close to that of titanium, therefore the A-L glass-ceramic is highly suitable for

direct sintering on metal abutments. Since 1998, there have been more than 60 million dental restorations performed using commercial IPS d.SIGN® A-L glass-ceramic (Höland and Rheinberger, 2008), making it the most commercially successful glass-ceramic developed to date.

1.3.3.2.2 Strontium-Substituted Apatite-leucite Glass-Ceramics

Höland *et al*. (2015) developed radiopaque strontium FAp (Sr-FAp) containing glass-ceramics (**Table 1.6**) for dental applications where Sr-FAp phase crystallised via the homogeneous mechanisms.

Table 1.6: Strontium fluorapatite based glass compositions (converted to mol % from Höland *et al*. (2015)

Glass code	1	2	3	4	5
SiO_2	58.7	59.4	60.4	61.1	66
Al_2O_3	9	9.1	9	9.1	8.5
Y2O3	3.1	2.2	0.1	0.1	-
La_2O_3	-	-	0.3	-	-
CaO	-	-	-	-	1.8
SrO	5.5	5.5	7.9	5.9	-
ZnO	-	-	-	-	1.3
Na_2O	10.1	10.2	8.4	10	8.9
K_2O	7.5	7.6	2.6	2.7	6.4
P_2O_5	1.8	1.8	1.8	1.7	0.2
F	2.4	2.3	2.6	2.4	3.2
Cs_2O	-	-	4.9	-	-
Rb_2O	-	-	-	4.8	-
ZrO_2	0.5	0.5	0.5	0.6	2.1
TiO_2	0.2	0.2	0.2	0.2	1.2
CeO_2	0.4	0.4	0.4	0.4	0.3
B_2O_3	0.3	0.3	0.4	0.2	0.1
Li_2O	0.5	0.5	0.5	0.8	-
Crystal Phase	$Sr_5(PO_4)_3F$, $KAlSi_2O_6$	$Sr_5(PO_4)_3F$, $KAlSi_2O_6$, $NaSrPO_4$	$Sr_5(PO_4)_3F$, $CsAlSi_2O_6$, $NaSrPO_4$	$Sr_5(PO_4)_3F$, $RbAlSi_2O_6$, $NaSrPO_4$	$Ca_5(PO_4)_3F$

Höland *et al*. (2015) was also able to obtain secondary and tertiary crystal phases, in addition to Sr-FAp, including leucite ($KAlSi_2O_6$), rubidium leucite ($RbSi_2O_6$), caesium pollucite ($CsAl_2Si_2O_6$) and sodium strontium orthophpshate ($NaSrPO_4$). However, both leucite and pollucite phases showed surface crystallisation. Höland *et al*. (2015) found that some of the base glasses that were rapidly quenched into water (to prevent crystallisation) did not avoid crystallisation completely. Based on XRD analysis of all parent glasses Höland *et al.* (2015) found that all glasses, except glass code 5 were nanocrystalline. XRD analyses of the base glasses 1 and 2 showed the presence of nanoscale $Sr_5(PO_4)_3F$, whereas base glasses. 3 and 4 contained nanocrystalline phases of $NaSrPO_4$. Höland *et al*. (2015) also report that only two of the "as-quenched" base glasses were optically clear, namely glass 1 and 5, as opposed to base glasses 2, 3 and 4, which were opalescent in the visible light. Höland *et al*. (2015) showed that Sr-FAp glass-ceramics are radiopaque. Therefore, these glass-ceramics may become more clinically relevant when they are commercially available.

1.3.4 Nanoscale Fluorapatite Glass-Ceramics

Glass-ceramics containing nanoscale phases of crystals are produced by carefully controlling heat-treatments of the parent glasses, in which the nucleation rate is enhanced and the crystal growth rate is low. Crystal growth rates can be suppressed by keeping the crystal growth temperature close to T_g. The T_g of the residual glass phase increases as crystallisation occurs. Crystallisation of fluoride containing phases, such as FAp is particularly

attractive here since a reduction in fluoride content in the residual glass phase results in a large increase in T_g. Alternatively, nanocrystalline phases in GCs can be obtained by developing parent glasses that phase-separate on a nanoscale, whereby subsequent crystal growth is limited by the boundaries of the LLPS domain, provided the glasses cannot overcome kinetic energy barrier to Ostwald ripening. Regardless of the application of the nano-GCs, the size and microstructure of apatite crystals are very important factors that determine whether a glass-ceramic is opaque or transparent after crystallisation. Transparent GCs contain crystals smaller than the wavelength of light. Such nanoscale GCs are used for different applications, ranging from transparent zero thermal expansion coefficient cooking hobs, consumer electronics to laser amplifiers in optoelectronics. Transparency of the GC is highly desirable in these applications because light transmission through a transparent GC is highly efficient due to no or low internal light scattering.

Rare earth elements, such as those in the lanthanide group have special photon absorption and reemission properties. Under near-infrared excitation, rare earth elements can absorb lower energy photons and reemit higher energy photons (anti-Stokes emission). In contrast, quantum dots or organic dyes, on the other hand, are excited by high-energy photons but reemit low energy photons (Stokes emission), which exhibit luminescence in the visible spectrum.

Glasses and glass-ceramics doped with rare earth elements can have some very special optical properties. Such glasses and glass-ceramics are used for applications in solid-state lasers, optical amplifiers and display screens. Glasses doped with rare earth elements usually exhibit broader spectral

bands and smaller absorption and reemission characteristics as compared to glass-ceramics, which are more efficient and show higher absorption and re-emission characteristic in addition to narrower spectral bands (Zhang et al., 2012a; 2013a; 2013b).

Furthermore, fluoride-containing crystals such as FAp are also known to have low phonon energies and low dielectric loss, which is an attractive property in optoelectronics. Despite the commercial use of single crystal lasers based on apatites and the fact that apatite lattices are also very attractive for accommodating rare earth ions there are limited number of publications on nano-crystalline apatite glass-ceramics since the first patent publication by Pinckney and Dajneka (1998).

Tulyaganov (2000) developed FAp ($Ca_5(PO4)_3F$)–anorthite ($CaAl_2Si_2O_8$)-diopside ($CaMgSi_2O_6$) glass-ceramics in the system of SiO_2-Al_2O_3-P_2O_5-CaO-CaF_2-MgO (**Table 1.7**) for potential applications in optical amplifiers. In the above system, FAp crystallisation was through a homogeneous mechanism, whereas anorthite and diopside phases crystallised via a surface mechanism.

Table 1.7: Fluorapatite-anorthite-diopside base glass composition in mol % (Tulyaganov, 2000)

%	SiO_2	Al_2O_3	P_2O_5	CaO	CaF_2	MgO
Mole	34.7	11.1	5.4	37.2	1.8	9.7

Hill *et al*. (2010) found evidence that FAp crystallisation in the Tulyagnov (2000) system was nano-scaled and self-limiting. Hill *et al*. (2010) provide evidence that FAp crystallisation is self-limiting because the system exhibits LLPS on a nano-scale i.e. the size of the phase-separated domain restricts subsequent crystal growth such that it cannot grow easily beyond the bounds of the LLPS. Hill *et al*. (2010) also argued that if the crystallisation of the

fluoride containing crystal phase occurs close to the glass transition temperature and the crystallisation process results in a significant increase in the glass transition temperature and as a result the surrounding “glassy” phase will limit further crystal growth. Hill *et al*. (2010) proposed that metal fluoride content at or below the stoichiometry of the FAp crystal is one of the factors needed to obtain nano-scale phases of FAp in the GC studied. These results are explained in terms of an approach, which views glasses as being inorganic polymers where the presence of fluoride disrupts the glass network, and thereby reduces the energy barrier to homogeneous nucleation and crystallisation of the FAp phases. Notably, Hill *et al*. (2010) also found some evidence that Mg can occupy Ca(II) sites of the FAp lattice, which was previously unknown in GCs. It is known that Mg^{2+} cations limit apatite crystal growth by blocking surface sites on the FAp crystal (LeGeros *et al*., 1980).

Single FAp crystals doped with rare earths have been considered for applications in lasers (Ohlmann *et al*., 1968; Deloach *et al*., 1993; 1994). However, their poor thermomechanical properties (Hopkins *et al*. 1971; Payne *et al*., 1994) can result in beam distortion due to thermal distortion that produces refractive index variations within the crystal. Furthermore, production of single crystals of FAp is not only expensive but unlike a glass-ceramic route cannot be processed into fibres and complex shapes. Polycrystalline apatites generally result in an opaque material, which is undesirable for optoelectronics unless the crystals are nanoscale and the dimensions of the crystals are less than the wavelength of light. Consequently, nanocrystalline FAp GCs are of particular interest.

Zhang *et al*. (2012; 2013a; 2013b) developed Nd and Eu doped visually transparent FAp glass-ceramics (**Table 1.8**) for potential applications in

optical amplifiers. Nd and Eu ions are f-block elements and can exhibit high degree of up-conversion in appropriate crystal lattices; therefore they are highly attractive dopants in rare-earth accommodating lattices, such as the apatite. Zhang *et al*. (2012; 2013a; 2013b) systems crystallise to FAp and mullite, therefore careful control of the heat-treatment is crucial to avoid the crystallisation of the mullite phase.

The ZH1 Nd doped glass (**Table 1.8**), as compared to its un-doped version, showed a markedly reduced FAp crystallisation temperature, in contrast, ZH3, strontium version of the same parent glass did not show a reduction in crystallisation temperature but rather a less pronounced area under the exotherm assigned to FAp. Furthermore, although Zhang *et al*. (2013b) compositions contain strong nucleants, such as P_2O_5, comparing DSC traces of the doped and the undoped ZH3 glasses, less pronounced FAp exotherms observed with the Nd-doped GC may be attributed to enhanced heterogeneous nucleation mechanism, as opposed to reduced overall crystallisation, however, such explanation would have to be confirmed by analysing particle size dependence on the crystallisation temperature.

Table 1.8: Compositions (in mol%) of Nd and Eu doped fluorapatite nano-scale glass-ceramics (Zheng *et al*., 2012a; 2012b; 2013)

	SiO_2	Al_2O_3	P_2O_5	$CaCO_3$	$SrCO_3$	CaF_2	SrF_2	La_2O_3	$LiCO_3$	B_2O_3	ZrO_2	Nd_2O_3	Eu_2O_3
$Ca_5(PO_4)_3F:Nd^{3+}$ (ZH1)	29.4	18	12	20	0	18	0	0.3	0.5	0.3	0.5	1	0
$Ca_5(PO_4)3F:Eu^{3+}$ (ZH2)	29.4	18	12	20	0	18	0	0.3	0.5	0.3	0.5	0	1
$Sr_5(PO_4)_3F:Nd$ (ZH3)	29.4	18	12	0	20	0	18	0.3	0.5	0.3	0.5	1	0

Notably, Zhang *et al*. (2012) system (ZH1, **Table 1.8**) could remain optically clear after 24 hour heat-treatment at 790°C. This indicates that Zhang *et al*. (2012) system has undergone LLPS on a nanoscale, which therefore

restricts FAp growth beyond the LLPS domain. Additionally, the kinetic barrier to Ostwald ripening during heat-treatment is therefore not overcome in Zhang *et al*. (2012; 2013a; 2013b) systems, which prevents crystal growth into the light scattering dimensions.

Furthermore, SrFAp (Zhang *et al*., 2013b) as opposed to CaFAp (Zhang *et al*., 2012) glass-ceramic was found to have a markedly reduced visible spectrum transmittance, which authors attributed to a lower volume fraction of SrFAp crystals (12±2 %) as opposed to the volume fraction of CaFAp (19±6%) in the alternative calcium-containing glass-ceramic. Additionally, Zhang *et al*. (2012) found that Nd doped calcium FAp GC showed better absorption and emission properties as compared to a strontium FAp GC (Zhang *et al*., 2013b) and argued that better absorption and emission properties of a calcium FAp GC may be attributed to a higher fraction of Nd^{3+} ions being incorporated into the former crystal lattice. Therefore, Nd^{3+} doped calcium FAp GCs likely have an advantage over Nd^{3+} doped strontium FAp GCs.

Nonetheless, Zhang *et al*. (2012; 2013a; 2013b) were able to closely match the refractive index between the glass matrix and the crystal phases for smooth photon transitions across the medium. Additionally, the crystals in the GCs are smaller than the excitation and emission wavelengths and therefore such crystals are outside of the light scattering dimensions that in turn produce an energy-efficient material for luminescence application.

1.3.5 Nuclear Waste Immobilisation

Currently, high-level radioactive waste (HLW) from nuclear fission products are fused at high temperatures (~1250°C) with a borosilicate glass and subsequently stored in repositories. However, due to long half-life of α-emitting radioactive elements, these HLW can potentially only be stored for up to three hundred years in these glass matrices. GC, on the other hand, can provide a useful alternative for nuclear waste immobilization because they will provide two barriers of containment: one being the host crystal phase(s) and second the amorphous glass matrix. Additionally, a devitrified material is more resistant to water due to higher network connectivity of the residual glassy phase.

Weber *et al*. (1979; 1993) synthesised Cm-doped silicates with the apatite structure but found them to be poor nuclear waste hosts because they completely transformed into an amorphous state when exposed to nuclear material. This resulted in a volume expansion and micro-fracturing of the material.

It is quite important to point out that phosphate apatite, as opposed to other apatitic phases show better resistance to amorphisation (due to nuclear decay) and better chemical stability. Soulet *et al*. (2001) showed that phosphosilicate FAp ceramics exhibit increasing resistance to amorphisation when SiO_4 is substituted by PO_4. Fang *et al*. (2014) also found that phosphate apatites show superior chemical stability (under an acetic acid challenge) when the atomic proportion of phosphorus replaced by silicon and sulphur did not exceed one third.

At the Atomic Weapons Establishment (UK), Donald *et al*. (2007) developed novel calcium phosphate-based halogen-containing calcium apatite ceramics for a universal actinide- and halide-containing waste immobilization. In the preliminary study, Donald *et al.* (2007) produced four types of experimental halide-containing nuclear waste streams, in addition to a series of mainly sodium aluminium phosphate (NaAlP) glasses for subsequent encapsulation of the waste-hosting calcium phosphate ceramics. However, it is important to underline that apatite ceramics developed by Donald *et al*. (2007) require additional encapsulation in a durable glass matrix. Therefore, it may be argued that ceramics developed by Donald *et al*. (2007) are not traditional GCs. Nonetheless, research led by Donald *et al*. (2007) is still ongoing. From a manufacturing point of view, developing a traditional apatite GC could possibly provide a more cost-effective alternative. Apatite-containing glass-ceramics are potentially excellent candidates as nuclear waste hosts, which is evident from studies on the apatite ceramic materials.

1.4 Glass Ionomer Cement

1.4.1 Glass Component

1.4.1.1 Glass Composition and Structure

Acid-degradable glasses used for glass-poly(alkenoate) (ionomer) cements (GICs) are usually made in the alumino-silicate system of $SiO_2 \cdot Al_2O_3 \cdot P_2O_5 \cdot CaO \cdot CaF_2$ (example shown in **Table 1.90**). In addition to these components, commercial GIC glasses may contain sodium, zinc, strontium and barium components (**Table 1.91**), either as an oxide or a

fluoride. Glass is usually produced by melting glass components in high temperature (1150-1550^{o}C) furnace for a specified period of time, depending on the glass composition. Glasses containing volatile elements are usually produced in cold-top furnace to prevent volatilisation of volatile elements, for example, fluorine.

Table 1.90: Model GIC compositions in mol % (Rafferty *et al*., 2004)

Code	SiO_2	Al_2O_3	P_2O_5	CaO	CaF_2	F
LG99	32.14	21.43	10.71	14.29	21.43	30.00
LG95	32.14	21.43	10.71	20.00	15.71	23.91
LG26	32.14	21.43	10.71	21.43	14.29	21.55
LG115	32.14	21.43	10.71	28.57	7.14	12.50

Table 1.91: Commercial glass compositions in mol % (based on XRF analysis, converted to mol %)

Trade name	SiO_2	Al_2O_3	P_2O_5	CaO	SrO	Na_2O	BaO	ZnO	La_2O_3	K_2O	F
Amalgomer	33.9	14.94	1.31	9.06	0	6.09	0	0	0	0	34.7
Chemfil Rock	28.1	16.83	8.31	7.37	9.29	0.78	0.26	12.89	0	0	16.17
Chemfil Superior	24.13	15.63	3.47	9.57	0.02	8.11	0	0	0	0	39.08
Fuji IX Fast	30.61	17.14	2.23	0.07	14.91	1.33	0.08	0	0	0	33.62
Ionofil	36.13	16.21	2.17	0.25	14.26	1.49	0.04	0	0	1.17	28.28
Ketac Fil	28.84	16.06	2.6	0.09	12.87	3.59	0.04	0	1.23	0	34.68
Ketac Molar	24.89	13.09	1.85	16.17	0	2.69	0	0	3.76	0	37.55
Riva	34.95	17.94	2.08	0.19	14.46	2.37	0.07	0	0	0	27.93
Zero Glass	42.56	13.76	2.01	4.75	1.16	2.93	5.01	0	0	0	27.82

Based on ^{29}Si MAS-NMR experiments, both, laboratory-synthesised and commercial GIC glass compositions show Q^4-(4Al) and Q^4(3Al)(1Si) silicate network structures (Stamboulis *et al*., 2003) and (Stamboulis *et al*., 2004). Glass-poly(alkenoate) cement properties are highly dependent on the ion leachable glass composition and thus require an in-depth understanding of the composition-property relationship. In the two studies, Griffin and Hill (1999) and De Barra and Hill (2000) have concluded that aluminium,

phosphate and metal fluoride content in the GIC glass can influence cement properties in more complex, multi-component fluoro-alumino-silicate glass compositions. Silica is the network former in the glass ionomer glasses where it provides bonding sites for the intermediate and modifying oxides. The crosslinking of the poly-(acrylic acid) (PAA) chains depend on the basicity of the GIC glass. If the glass does not contain sufficient amount of network modifying cations it will not form cement i.e. PAA chains will not be cross-linked. Thus, the GIC glass should have a net positive charge, which is provided by the addition of various metal oxides (Wilson *et al.,* 1980).

Alumina is an intermediate oxide and therefore takes part in the silicate network as an intermediate oxide between the network former and the network modifier. Based on Lowenstein Rules on Glass Formation, alumina can also be classified as a conditional network former because it does not form glass on its own but can do so in association with sufficient amount of a glass forming oxides (Paul, 1982). Aluminium can form Al-O-P (**Figure 1.17**) and Al-O-Si linkages in the silicate network (Griffin and Hill, 1999).

There is a strong association between aluminium coordination number in the GIC glass and the mechanical properties of the cement (Zainuddin *et al*., 2009). Based on solid-state MAS-NMR studies, aluminium in GIC glasses predominantly exists in a four-coordinate state. In addition to four-coordinate aluminium, it can also exist in 5 and 6-coordination states (Stamboulis *et al*., 2004 and Zainuddin *et al*., 2009).

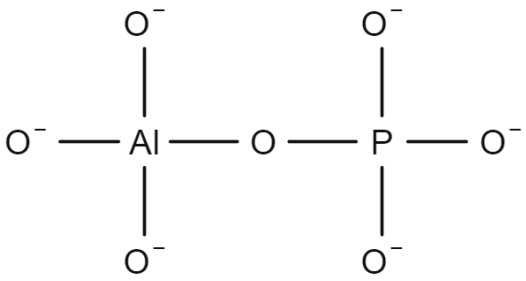

Figure 1.17: Local charge-balancing of aluminium by phosphorus

The phosphate content in the modern GIC glass comprises a significant fraction. Therefore, it is important to understand and localise phosphate species/coordination states in the phosphate-containing GIC glasses. Dupree *et al*., (1989) showed that phosphate in alumino-silicates systems exists as $AlPO_7$ species (**Figure 1.17**).

It was believed by Griffin and Hill (1999) that phosphate content in fluoro-alumino-silicate glasses will influence GIC setting properties because P^{5+} competes with Al^{3+} and Ca^{2+} for COO^- groups. However, it is now understood that Al-O-P linkages within the network are not hydrolysable, and as such aluminium charge balanced by phosphorus does not take part in the GIC setting reaction. Griffin and Hill (1999) found that low phosphate content is beneficial in that it extends working and setting times of the cements, authors also observed small improvements in compressive strength with low phosphate glasses. Griffin and Hill (1999) also concluded that glasses higher in phosphate excessively disrupt the crosslinking process in the cement by competing with metal ions for carboxylate groups and also observed significant reduction of compressive strength and Young's moduli and increase in working and setting times of the cement pastes. Although, Griffin and Hill (1999) have correlated phosphate content with the rheology and the mechanical properties of the cements correctly, their attempt to define the underlying mechanism was unsuccessful until much later.

High phosphate content may give rise to more metastable Al-O-P linkages within the glass network, which makes Al(IV) unavailable for PAA crosslinking (Zainuddin *et al.,* 2012), which as mentioned earlier, is in opposition to the earlier opinions of Griffin and Hill (1999).

Metal oxides, such as calcium oxide modify the alumino-silicate network by linking silicon tetrahedra (**Figure 1.18**).

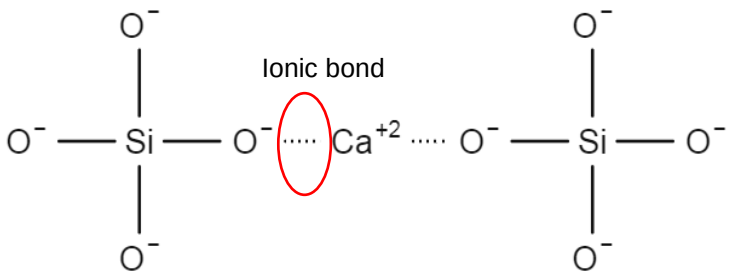

Figure 1.18: Calcium ion bridging two oxygens in the silicate network

Calcium ion can also locally charge balance aluminium. Some commercial GIC glasses contain strontium oxide, either fully or partially substituted for the calcium oxide. Strontium has a slightly larger ionic radius (1.13Å) as compared to calcium (0.99Å), thus glasses containing strontium show decreased glass transition temperatures (Fujikura *et al.,* 2012) and (Fredholm *et al.,* 2010), increased glass density but decreased oxygen densities (Feldhom *et al.,* 2010) explained by a more expanded glass network. Because of the higher atomic number of strontium, strontium-containing GICs provide diagnostic radiopacity (Shahid *et al.,* 2014). It is also notable that, although strontium has a larger atomic radius than calcium, strontium substituted glasses do not have any significant effect in terms of the cement aesthetics compared to unsubstituted glasses (Shahid *et al*., 2014).

Most modern GIC glasses contain a relatively high proportion of fluoride. The fluoride components are attractive additives in GIC glasses because of the anti-cariogenic properties of the fluoride ion and the ability to lower the refractive index of oxide glasses. Fluoride reduces glass transition temperature (Griffin and Hill, 2000), it also reduces melt viscosity and increases glass degradability. Therefore, structural role of the fluoride ion in alumino-silicate glasses is highly interesting and important. During the early studies of the GIC glasses by Wilson and Hill (1988) it was proposed that the fluoride ion, such as from metal fluorite components (CaF_2 and SrF_2), replaces non-bridging oxygens (NBO) with non-bridging fluoride atoms in the silicate network. However, more recent solid-state MAS-NMR studies by Kohn *et al.* (1991), Zeng and Stebbins (2000), Stamboulis *et al*. (2004) and also by Hill *et al*. (2005) suggest that fluoride in the GIC glass system of $SiO_2{\cdot}Al_2O_3{\cdot}P_2O_5{\cdot}CaO{\cdot}CaF_2$ exists as Al-F-M(n) and F-M(n) species, rather than SiO_3F as proposed in the early studies by Wilson *et al*. (1980) and later reported again by Wilson and Hill (1988). Based on more recent MAS-NMR experiments, it is known that fluoride in GIC glasses preferentially exists in Al-F-M(n) and then F-M(n) species (Stamboulis *et al*., 2004). Fluoride species of F-M(n) reduces the average number of NBOs per silicon as it ionically bridges two NBOs, which is observed from ^{29}Si MAS-NMR peak shifting upfield with increasing F-M(n) species (Stamboulis *et al*., 2004). Griffin and Hill (2000) showed that increasing the fluoride content in GIC glasses will reduce working and setting times of the cements. Fluoride is also a powerful glass network disrupter and as such, it increases the availability of hydrolysable bonds for the PAA crosslinking, which explains reduced working and setting times of the cements, observed by Griffin and Hill (2000).

Furthermore, the fluoride ion can also form insoluble complexes with Al^{3+} once Al-O-Si bonds are hydrolysed (Potin-Gautier *et al*., 1997).

1.4.1.2 Glass Processing

Industrially manufactured glass is dried, ground to a fine powder and then usually also sieved using a micron-scale mesh. Glass powder can be pre-treated with an acid, for example, washing the glass with an aqueous solution of acetic acid will reduce the reactivity of the glass. Acid-washing is required when the glass is too reactive. Acid-washing leaves an ion depleted silica layer and prolongs the working and setting times of the subsequently made cements (Billington *et al.,* 2006). Annealing the GIC glasses at temperatures above the T_g is also known to reduce the reactivity of the glasses because this relieves the glass structure from internal stresses and puts the glass into a higher equilibrium. However, manufacturers do not routinely disclose such treatments.

The glass reactivity, clinical aesthetics and mechanical properties of GICs are also influenced by the powder particle size distribution. Smaller particle size distribution in the GIC powder has been shown to increase glass reactivity, compressive strength and Young's modulus (De Caluwé *et al.,* 2014) and (Prentice *et al.,* 2005).

1.4.2 Liquid Component

The first GIC (ASPA-I) liquid was composed solely of aqueous poly-(acrylic acid) solution (Crisp *et al.,* 1975). However, ASPA-I had poor working and setting characteristics and had a poor shelf life due to formation of intermolecular hydrogen bonds between the polymer chains (Crisp *et al.,* 1975). To improve the setting characteristics of the ASPA-I cement, Crisp *et al*. (1975) found that the addition of small amount (originally 5% by mass) of another carboxylic acid, namely tartaric acid, accelerated the working and setting characteristics of the cement. However, only the natural form of L-(+)-tartaric acid could improve the rheology of ASPA-I (Crisp *et al.,* 1975).

Shelf-life and gelation of the developed PAA liquid was still an issue until 1977 when Crisp *et al*. filed a patent claiming unsaturated carboxylic acids of maleate and itaconate to reduce intermolecular hydrogen bonding and thus prevent gelation of the PAA. The rationale behind this invention was that maleic and itaconic polyacids are less stereo regular than PAA and thus the addition of such acids to the PAA solution would prevent PAA chain gelation. However, at the time it was not considered that stereo regularity is determined by the mode of polymerisation of monomers. It still remains unknown if completely atactic PAA would be resistant to gelation.

Molecular weight as well as concentration of PAA can significantly influence mechanical properties of the cement. Crisp *et al.* (1977) found that both the compressive strength and flexural strength properties of the set cement increased linearly over the range of polyacid concentrations studied. The work suggests that it is desirable to use a solution of highly concentrated PAA. Additionally, Fennell and Hill (2001) found that both, increasing molar

mass and concentration of polymer resulted in a nearly linear increase in compressive strength. However, Fennell and Hill (2001) also note that the compressive strength of GICs is as dependent on polymer molar mass and concentration as it is on glass volume fraction. Volume fraction is derived from glass density:

$$\varphi_i = \frac{Mass}{Density} \quad \textbf{(Equation 1.2)}$$

Denser glasses have a smaller volume fraction and less surface area, therefore the availability of cations for PAA crosslinking is in short supply. For better mechanical properties, powder to liquid ratio should be adjusted to the volume fraction of the glass component.

1.4.3 Setting Reaction

The GIC setting reaction is an exothermic acid-base neutralisation reaction. The mechanism of short-term setting reaction of the GICs has been relatively well understood since the development of the first GIC in late 1960 (Crisp and Wilson, 1974). Once the glass powder is mixed with an aqueous solution of PAA, bonds in the glass network are broken down by hydrolysis. It is known that Al^{3+}, Ca^{2+} or Sr^{2+} (in strontium-containing glasses) leach out and ionically bond to COO^- groups found on the PAA chains (**Figure 1.19**). Cations such as Al^{3+} can crosslink up to three neighbouring polyacid chains, however, Munhoz *et al*. (2010) found that the majority of Al^{3+} cations do not form tricarboxylates in a commercial GIC (Fuji IX) but are rather coordinated with one or two carboxylic groups and other negative ions such as the

fluoride ion. Munhoz *et al.* (2010) also identified a second octahedral aluminium species in the ^{27}Al spectra and postulated that it may be assigned to aluminium tartrate.

Based on numerous ^{27}Al solid state MAS-NMR experiments, tetrahedral aluminium converts to octahedral aluminium as the cement sets, which is assigned to hydrated Al^{3+} (Stamboulis *et al*., 2006), (Zainuddin *et al.,* 2009) and (Munhuz *et al*., 2010).

Recently, solid-state NMR experiments provided more insight in the acid-base neutralisation reaction. Stamboulis *et al*. (2006) analysed the setting reaction of model GICs by ^{13}C Cross Polarisation MAS-NMR experiment as well as ^{27}Al, ^{19}F, ^{29}Si and ^{31}P . Stamboulis *et al*. (2006) showed through ^{13}C Cross Polarisation MAS-NMR experiment that peaks assigned to carbonyl groups along the polyacid chains shift downfield (carbon in COOH is deshielded) as a function of cement setting time, which is indicative of proton dissociation from the carbonyl group. It is likely that this is the only experiment of its kind to date that provides clear evidence of an acid-base reaction during the GIC setting process.

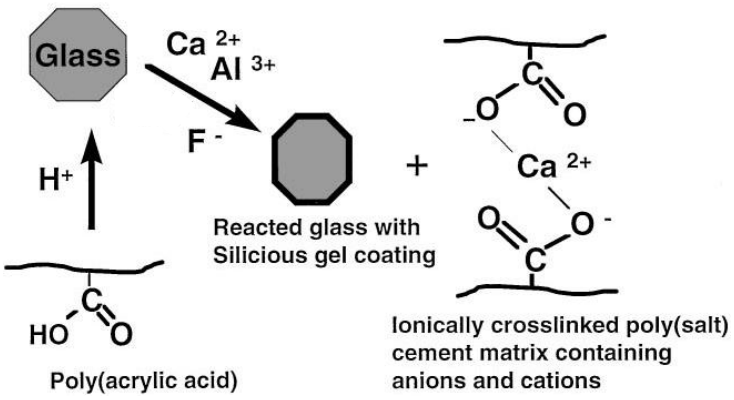

Figure 1.19: Setting reaction of the GIC (Adapted from Griffin and Hill, 1999)

Mechanical properties of GICs improve with time, which shows the presence of an ongoing setting reaction. In early studies, it was postulated that mechanical properties of GICs improve with time because of the continued crosslinking between the metal ions and the polyacid. However, later studies proposed that, in addition to the formation of crosslinks with the polyacid, leached ions are also involved in the formation of a hydrated inorganic silicate network (Wasson and Nicholson, 1993). Although with caution, Matsuya *et al.* (1996) also postulated that increasing mechanical properties of GIC with time is a result of hardening of the hydrated silicate network.

However, more recent work suggests that phosphorus-free glasses do not mature which is indicative that the maturation of GICs is a complex process involving several glass components (Shahid *et al.,* 2008).

Furthermore, it is agreed that the ratio of bound to unbound water increases with ageing of the cements (Bordallo *et al.,* 2006). Therefore, it is reasonable to say that water plays an important role in the setting reaction and in the formation of a hydrated inorganic network.

1.5 Mechanical Properties

1.5.1 Compressive Strength

Compressive Strength (CS) is the maximum stress a material can withstand under a constant load over an area. CS can be expressed by:

$$\sigma = \frac{F}{A} \quad \textbf{(Equation 1.3)}$$

where *F* is the applied load in unit newton and *A* is the area in metres squared. CS is the only strength test specified by the International Organisation for Standardisation standard for a water-based cement for use in Dentistry (ISO 9917-1: 2003). The ISO standard defines compressive strength, relative to the mode of measurement, as

$$c = \frac{4F}{\pi d^2}$$ (**Equation 1.4**)

where *F* is the maximum compressive force applied in unit newton; and *d* is the measured sample diameter in millimetres.

Compared to other mechanical strength tests, CS is a relatively simple procedure with a fast turnaround. However, the use of this test in the assessment of GIC mechanical failure has been criticised since 1990s (McCabe *et al.,* 1990). McCabe *et al.* (1990) found that CS test is unreliable because of the statistically unacceptable variation between the test results. McCabe *et al.* (1990) proposed that "*standards should place less emphasis on the mean value of relatively small number of test specimens and the use of a simple form of probability theory in which, say, 80 per cent of specimens are required to achieve a certain pass level*" proposing that some standards may need to increase the number of test specimens to achieve meaningful results.

Kendall (1978), Darvell (1990), Fennel and Hill (2001) and Baig *et al.* (2015) are of the opinion that stress at failure calculation does not take into account the failure mechanism operating during CS testing, whereby cylindrical specimens fail by '*some unresolved combination of tension and shear*' stresses.

The minimum compressive strength value for water based restorative cements is 100MPa, whereas for water-based lining cements the specified value is 50 MPa (ISO 9917-1: 2003). However, some commercial GICs, such as Amalgomer® show compressive strength of around 400 MPa (Woodfine *et al*., 2006).

1.5.2 Flexural Strength

An alternative approach to understanding the mechanical properties of cements is the assessment of their flexural strength (FS). FS is defined as

$$\sigma = \frac{F}{bd} \quad \textbf{(Equation 1.5)}$$

where *F* is the axial load applied at the fracture point; *b* is the width of the sample; and *d* is the thickness of the sample.

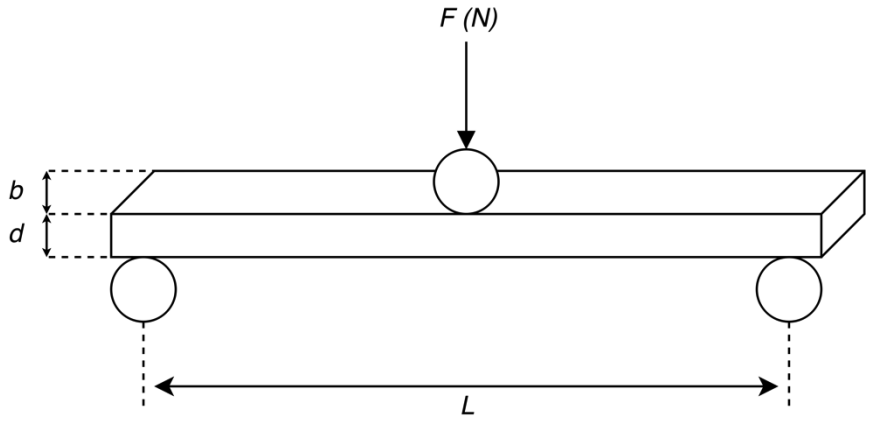

Figure 1.2: Schematic representation of the three-point flexural bend test

For 3-point bend measurement purposes (**Figure 1.2**), FS can be defined by

$$\sigma = \frac{3FL}{2bd^2}$$ (**Equation 1.6**)

where *F* is the axial load force applied, in unit newton; *L* is the length of the sample support span; *b* is the width of the sample; and *d* is the thickness of the sample. In FS experiment, the fracture occurs at midpoint under tension.

As mentioned earlier, a study by Fennel and Hill (2001) concluded that dominant parameters influencing the flexural strength of GICs are the PAA molar mass (**Figure 1.21**) and PAA concentration (**Figure 1.22**).

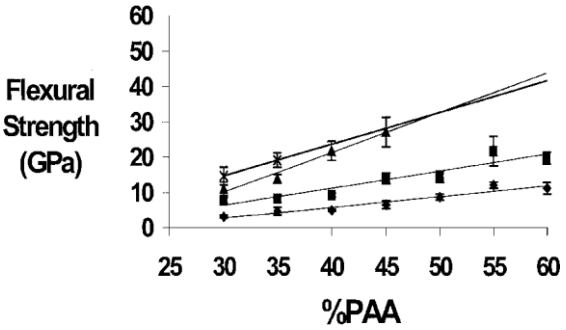

Figure 1.21: Flexural Strength vs PAA concentration (Fennel and Hill, 2001)

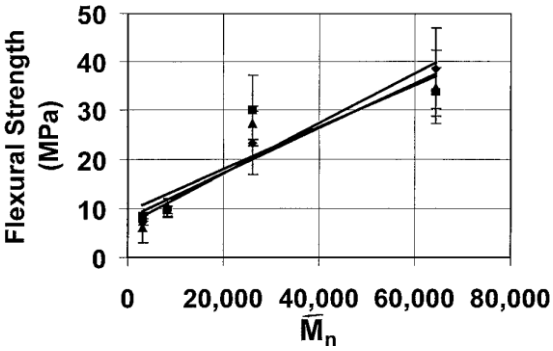

Figure 1.22: Flexural Strength vs PAA molar mass (Fennel and Hill, 2001)

In a study by Dowling *et al.* (2012) compressive strength, three-point flexural strength (TFS) and biaxial flexural strength (BFS) data from three commercial GICs were statistically compared for reproducibility ($p=0.05$). Based on one-way analysis of variance, Dowling *et al.* (2012) found that TFS and BFS were reproducible, however obtained compressive strength values were found to vary significantly and as such authors concluded that compressive strength measurement is not a statistically valid measurement. Authors could not show any statistical difference between TFS and BFS. Authors further suggest that specimen fabrication for BFS is relatively simple

and less operator-dependent compared to specimen fabrication for TFS (Dowling *et al.,* 2012).

1.5.3 Fracture Toughness and Toughness

Abrasive wear resistance of materials is often related to their fracture toughness and hardness (Wilson *et al.,* 1989). Therefore, the measurement of fracture toughness and toughness is another means to assess the mechanical failure of GICs. Toughness is a property of a material to resist fracture when stressed, whereas Fracture Toughness is a property of materials containing a crack to resist fracture when stressed. Tensile Toughness can be defined by:

$$U_T = \sigma \times \varepsilon \quad \textbf{(Equation 1.7)}$$

where ***σ=stress*** and ***ε=strain***; and can be obtained by stress-strain curve integration. Fracture toughness can be defined by:

$$K_{1c} = \sigma_c \sqrt{(\pi a)} \quad \textbf{(Equation 1.8)}$$

where σ_c is critical stress value; π is 3.14… and *a* is area.

1.6 Aesthetics

The aim of clinically aesthetic dentistry is to emulate natural colour and translucency of dentition. This can be achieved by using materials which have similar light absorption and light scattering characteristics. Tooth-coloured materials are produced by the incorporation of inorganic pigments or organic dyes in the material matrix. Inorganic pigments are often preferred to organic dyes because they are insoluble and therefore more durable.

The development of glass ionomer cement in 1968 can be considered a breakthrough in aesthetic dentistry because the new cement was translucent. Since the development of the first GICs aesthetics of modern cements have improved, mainly as a result of better understanding of the glass structure and structure-property relationships.

Translucent cements are produced by matching the refractive index (RI) of the in the material to avoid light scattering at the interfaces. Factors such as the polyalkenoic acid concentration and glass particle size can also influence the aesthetics as well as a number of other physical properties of dental cements.

Most commercial and model laboratory GIC glass compositions contain a significant amount of fluoride (**Table 1.9** and **1.91**). Fluoride ion is a powerful glass network disruptor and it is also known to lower the RI of glasses used in optoelectronics. Therefore, fluoride components may be added to glass compositions to lower the RI of the glasses for a better refractive index match.

For accurate RI calculation it is essential to know the RI of all GIC components, including the RI of the ion leachable glass. RIs of glasses can

be measured, for example by the *Abbé* refractometer or the Becke line technique. The *Abbé* refractometer can only be used if the glass of interest can be readily cast into a monolith with defined dimensions without crystallising or losing fluoride. GIC glasses are known to crystallise to fluorapatite, mullite and anorthite thus they have to be rapidly quenched to prevent crystallisation. Therefore, casting such glasses will result in slow quenching and this may result in crystallisation and any subsequent RI measurements will be practically impossible. In the Becke line technique RI of a glass can be determined on glass particles. Example of the mineral oil liquids used in the Becke Line technique shown is shown in **Figure 1.23**.

Figure 1.23: Mineral oils used in the Becke line test (Cargille, USA)

RI of glass in this technique is measured by immersing and dispersing coarse glass particles into a liquid with a known RI, preferably on a microscope slide and observed under a microscope. The sample is illuminated by a standard wavelength light, usually at 589 nm. If the RI of glass matches the RI of mineral oil it will be indicated by white Becke lines around the dispersed glass particles, which is a sign of low or no light scattering at the interfaces and therefore matching refractive indices. Furthermore, glass particles that are clearly visible and appear opaque indicate high light scattering at the interfaces and thus shows that refractive

indices are mismatching. In such cases, glass particles are then dispersed into a liquid with either a higher or a lower RI until a match is found.

Several models have been proposed that allow mathematical estimation of RI of glasses. Based on recent literature (Priven and Mazurin, 2003), the Appen model was found to estimate refractive indices of glasses with the lowest calculation error compared to other calculation methods. Appen Model uses a set of factors for glass oxides (**Table 1.92**) which are used in the Appen equation (**Equation 1.9**) that allow the estimation of RI of glass if the glass composition is known.

$$n_d = \frac{\sum^{n}{}_{i=1} n_{d,i} c_i}{100} \quad \textbf{(Equation 1.9)}$$

Each component in a glass has an oxide-specific Appen factor $n_{d,i}$, which is multiplied by its mole fraction C_i. The summation of the factors multiplied by their respective mol fractions is equal to the estimated refractive index of the glass, n_d.

Table 1.92: Appen factors for the glass oxides (Appen, 1974)

Oxide	Appen Factor
SiO_2	1.4585
Al_2O_3	1.52
P_2O_5	1.31
Na_2O	1.575
ZnO	1.71
K_2O	1.575
CaO	1.73
SrO	1.775

Glasses used in dentistry usually contain a significant amount of fluoride however, there are no Appen factors published to date for the amorphous metal fluorides.

Aesthetics of GICs are highly important in modern day dentistry; however scientific literature is limited on this aspect to a handful of publications. Translucency of GICs as well as other dental materials can be measured by either absolute translucency or relative translucency (contrast ratio). Spink *et al*. (2013) showed that contrast ratio or relative translucency measurements are not suitable for materials that transmit light at 50% or less.

Contrast ratio (CR) is a measurement of relative translucency. CR can be measured with any spectrophotometric instrument capable of detecting radiation intensity provided standards of known radiation intensities are used. CR is defined as:

$$CR = \frac{L_B}{L_W}$$ (**Equation 1.91**)

Whereby L_B is defined as luminance on a black background and L_W is luminance on a white background.

The contrast ratio was adapted as a measure of translucency or opacity in dental research from the American Society for Testing Materials standard used to measure opacity in papers (Spink *et al.,* 2013), which was then adapted by the American Dental Association in 1977.

Crisp *et al*. (1979), one of the developers of the GIC, provided further methodological improvement in CR measurement. Crisp *et al*. (1979) measured CR of ASPA cements using a goniophotometer. Crisp *et al*. (1979) noted that the standard requires a white background having a reflectance of

$C_{0,70}$ however, at that time, most available white backgrounds had a reflectance value of $C_{0,80}$. Crisp *et al*. (1979) also found that opacities of the first ASPA GICs decreased with time and that powder to liquid ratio did not have a significant effect on the opacities of the cements. Nonetheless, Crisp *et al.* (1979) also found that cements with higher pigmentation were more opaque, compared to identical cements with lower colour pigmentation. Later study by Assmusen (1983), once improved commercial GICs were developed, found that newer GICs were more translucent than the first generation of the cement. Assmusen (1983) also notes that newer GICs still had higher opacities than resin composite materials. Assmusen (1983) found that early water contact with GICs results in a considerable increase in opacity.

1.7 Magic Angle Spinning - Nuclear Magnetic Resonance Spectroscopy

1.7.1 Introduction

Chemical elements that contain an odd number of protons or neutrons have an intrinsic nuclear angular momentum (spin) and a magnetic moment, which are carried by the intrinsic magnetism of the elementary particles, quarks and gluons.

Magnetic moment is related to the spin number of the nucleus (I_i) and the magnetogyric ratio of the nucleus (γ). Magnetic moment can be defined by:

$$\mu_i = \gamma I_i \quad \textbf{(Equation 1.92)}$$

The angular momentum and the magnetic moment are in inverse relationship, i.e. spin is created by a magnetic moment and a magnetic moment creates a spin, explained by Einstein-de-Hass effect and Barnett effect respectively. When a magnetic field is applied to a system with an angular momentum, it exerts a torque and the system can either align itself with the magnetic field or against the magnetic field.

When a magnetic field is applied to nuclei with an intrinsic angular momentum they can either absorb electromagnetic energy and go into a higher energy state or release it and go into a lower energy state. When a specific magnetic field is applied to a magnetisation vector, for example a nucleus, it will precess about this field at a defined frequency, known as the Larmor frequency. Larmor frequency can be defined by:

$$\omega_0 = -\gamma B_0 \quad \textbf{(Equation 1.93)}$$

where ω_0 is the Larmor frequency in hertz, γ is the magnetogyric ratio, a constant for a given nucleus, and B_0 is the applied magnetic field in teslas.

In the nuclear magnetic resonance (NMR) experiment, a static magnetic field is applied to nuclei to align them with and against the applied magnetic field (**Figure 1.24**).

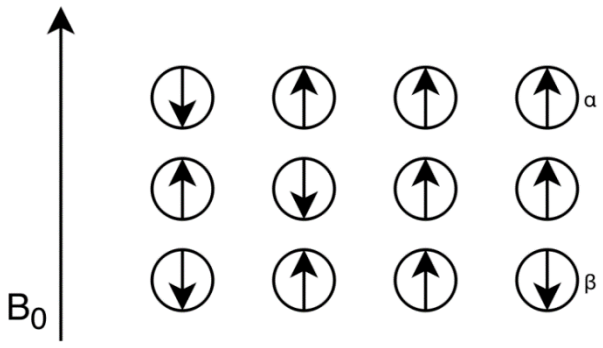

Figure 1.24: Effect of magnetic field on a population of nuclei

A radiofrequency (RF) wave is then applied at the aligned nuclei. RF wave is arranged in the NMR experiment so that its magnetic field oscillates along a direction perpendicular to the static magnetic field (**Figure 1.25**), termed B_0. Once the RF wave is emitted, a nucleus aligned with the magnetic field will flip its magnetic moment i.e. the nucleus will align itself against the magnetic field (**Figure 1.25**).

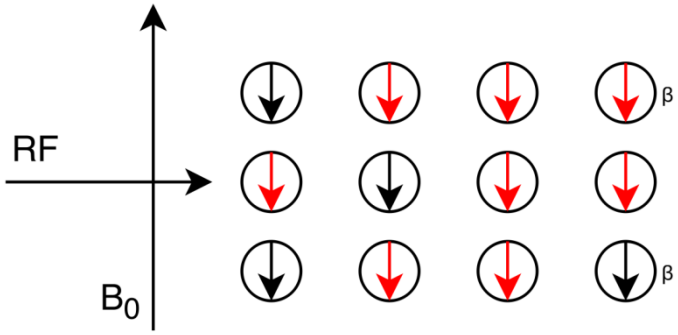

Figure 1.25: Effect of a radio wave on nuclei in a magnetic field

If the RF wave is removed, the nucleus will *resonate* i.e. emit energy and return to its low energy state. It is this resonance energy which is measured and amplified by the NMR spectrometer. The energy emitted by a nucleus is then Fourier-transformed into chemical shift.

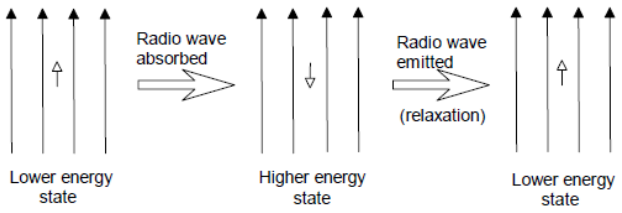

Figure 1.26: The NMR principle (Royal Society of Chemistry, available at http://www.rsc.org/learn-chemistry/wiki/index.php?title=File:NMRworkshopFig01.png&filetimestamp=20111014062217)

1.7.2 Nuclear Spin Interactions

1.7.2.1 Zeeman Effect

Zeeman Effect is the effect of splitting a spectral line into several spectral lines in the presence of a static magnetic field. It can be observed from a population of NMR active nuclei, which in the presence of a magnetic field split into different energy levels.

1.7.2.2 Shielding and Chemical Shift

In the presence of a magnetic field, electrons that surround a nucleus will produce a secondary opposing field. This secondary field generated by the electrons will affect the total field experienced by the nucleus and hence this field can change the resonance frequency of the nucleus. This is known as the shielding interaction. This interaction will cause a frequency shift in the NMR spectrum which is known as the chemical shift.

The shielding of a nucleus is due to electrons that circulate around the applied magnetic field. This produces a secondary field which opposes the applied magnetic field which shields the nucleus. This is known as the diamagnetic contribution to the nuclear shielding.

The de-shielding of a nucleus is due to the distortion in the electron distribution as a result of external magnetic field. This creates a field which supports the applied magnetic field and tends to de-shield the nucleus. This is also known as the paramagnetic contribution to the nuclear shielding.

1.7.2.3 J-couplings (Indirect Dipolar Coupling)

J-couplings are indirect low energy couplings of the nuclear dipoles mediated by local bonding electrons.

1.7.2.3 Dipolar Coupling (Direct Dipolar Coupling)

Dipolar couplings are nuclear interactions through space. Each spin creates a local magnetic field, which affects the spin of surrounding nuclei. In a solution state NMR, the dipole-dipole interaction is averaged to its isotropic value, zero, by molecular tumbling. The strength of dipole-dipole interaction depends on molecular orientation of nuclei. The closer nuclei are to each other the stronger is the dipolar interaction. Dipolar interaction is the major cause of line broadening in solid-state NMR. To cancel anisotropies from dipolar couplings, solid state NMR samples are spun at the magic angle.

1.7.2.4 Quadrupolar Coupling

Most NMR active nuclei have a spin greater than ½ and are termed quadrupolar nuclei. Spins greater than ½ arise from local charge distribution in the nucleus. Quadrupolar nuclei have a non-spherical positive charge distribution compared to ½ nuclei, which have a spherical positive charge distribution. The strength of the quadrupolar interaction depends on the magnitude of the nuclear quadrupole moment and the strength of the electric field gradients in the respective molecule. External magnetic field does not directly affect magnetic quadrupole but rather indirectly determine the orientation of it.

1.7.2.5 Magic Angle Spinning

Solid samples, such as fine powder samples contain molecules with random orientation as opposed to solution samples where molecular orientation is averaged as a result of rapid molecular tumbling in a solution. As such, all nuclear interactions observed in solid-state samples depend on the molecular orientation and are said to be anisotropic. As a result of this, solid samples analysed by the NMR spectroscopy contain broad lines also called powder patterns because nuclei in different molecular orientations present in the sample give rise to different resonance frequencies. When solid state samples contain different nuclear sites, powder patterns may overlap and therefore it may be impossible to distinguish between different nuclear sites.

High resolution solid-state NMR spectra are achieved by spinning solid state samples at the Magic Angle, 54.74. Magic Angle Spinning (MAS) primarily removes the effects of chemical shift anisotropy and dipolar coupling effects.

In solution state NMR, isotropic tumbling of molecules is fast enough to average molecular orientation dependence of the transition frequencies to zero relative to the magnitude of chemical shift anisotropy coupled with other NMR interactions.

Magic Angle Spinning averages molecular orientation dependence of the transition frequencies to zero in solid-state NMR. This is because if the sample is spun about an axis inclined at an angle θ_R (the magic angle) to the applied field, then θ (the angle between B_0 and the principal z-axis of the interaction tensor) will vary with time as the molecule rotates with the sample, which will remove molecular orientation dependence, provided that the spinning rate is fast enough so that θ is averaged rapidly compared with the anisotropy of the interaction being spun out.

If the solid-state sample is not being spun fast enough, spinning sidebands will be produced. Spinning side bands are sharp lines in the MAS-NMR spectra, set apart by the spinning rate and appear on either side of the isotropic chemical shift.

Although, spinning side bands may be very useful for determining anisotropies and asymmetries of nuclear spin interactions, they can obscure isotropic signals and therefore they are usually removed by spinning the sample faster.

1.7.3 Sample preparation for solid-state NMR

Samples such as glass, are usually ground to fine powder and packed in a precisely designed rotor (**Figure 1.27**).

Figure 1.27: Example of a rotor used in solid-state NMR (Bruker, accessed from https://store.bruker-biospin.com/shop/CZ/product/HZ09244A/)

Once sample is packed, the rotor is tightly closed with a drive cap (**Figure 1.28**).

Figure 1.28: Example of a drive cap used in solid-state NMR (Bruker, accessed from https://store.bruker-biospin.com/shop/CZ/product/HZ07306A/)

1.7.4 Tuning and Matching the Probe

Once the rotor with the sample is inside the probe, the probe is tuned and matched to the Larmour frequency of the nucleus being inspected. Most advanced spectrometers use probes that have two channels: ^{1}H (highband) which observes $^{1}H/^{19}F$ resonance and $^{13}C/^{31}P$ (lowband) which observes the resonance of ^{31}P, ^{15}N, ^{13}C etc nuclei. Depending on the type of nucleus being analysed, one of the channels has to be tuned to the appropriate Larmor frequency. This is done by adjusting tuning and matching knobs that extend from the probe. This adjusts two capacitors connecting to the coil. These combined form the resonant circuit of the probe.

1.7.5 Free Induction Decay and Fourier Transformation

In the NMR experiment, energy emitted by a resonant nucleus is received and observed as free induction decay (FID). FID is a time-voltage (x-y) plane. FID is then transformed into NMR spectrum. The Fourier algorithm transforms function of time to signal intensities in the NMR spectrum.

1.7.6 MAS-NMR in Materials Science

The MAS-NMR technique can be used to study the structure of both amorphous and crystalline materials. The energy emitted by a resonant nucleus is characteristic to the various magnetic interactions experience by the nucleus. The strength of these interactions depends on the field strength and the distances of the nearest neighbouring atoms. The amount of energy emitted by a resonant nucleus can be correlated to the atomic arrangement around the nucleus. The atomic arrangement, or in other words, coordination

number of a nucleus can be then linked the various properties of the material.

1.8 Attenuated Total Reflection – Fourier-Transformed Infrared Spectroscopy Technique

Fourier-Transformed Infrared Spectroscopy (FTIR) is a qualitative and semi-quantitative physiochemical technique used to detect bond vibrations in functional groups in solid and liquid matter as a result of applied electro-magnetic radiation. Almost all functional groups can be excited by electro-magnetic radiation in the mid-infrared region. Mid-infrared generally means electro-magnetic radiation in the region from 2.5 µm to 25 µm. This region includes the frequencies corresponding to the phosphate groups found in the apatite. The spectral lines are usually narrow and distinct making it possible to identify and monitor a group corresponding to a specific structure.

Attenuated total reflection (ATR) technique (**Figure 1.29**) is a signal-enhanced FTIR technique which is particularly suitable for characterisation of thick and optically dense materials and requires minimal sample preparation.

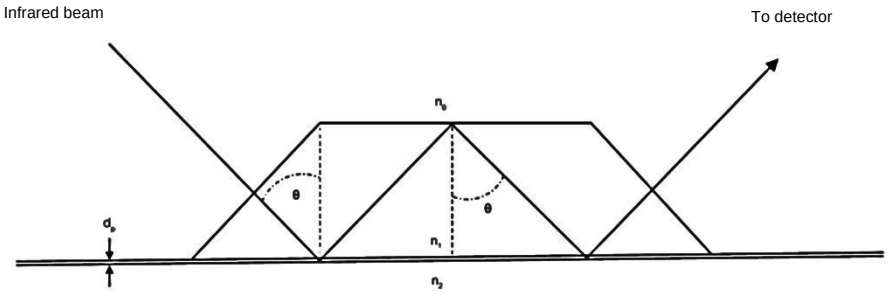

Figure 1.29: Attenuated total reflectance measurement geometry in which a trapezoidal element with a refractive index n_1 is in contact with a sample having a lower refractive index, n_2. In spectral regions where the sample is absorbing, infrared radiation will penetrate into the sample a distance represented by d_p. Figure adapted from Doyle (1992).

In this technique infrared radiation is passed through an infrared transmitting crystal (typically a diamond) with a higher refractive index than the sample. The infrared beam, which consists of a range of frequencies, passes through the crystal undergoes multiple internal reflections. Total internal reflection is a phenomenon which is observed when light passes through materials with different refractive indices. This results in an evanescent wave effect where a portion of the radiation penetrates into the sample and results in stretching and bending of the bonds where characteristic frequencies are absorbed. When the beam leaves the crystal, the signal is measured by a detector. The instrument then generates a transmission or absorption spectrum characteristic to what has been scattered off the surface of the sample.

CHAPTER 2: MATERIALS AND METHODS

2.1 Predicting Refractive Index of Fluoride-Containing Glasses for Aesthetic Dental Restorations

2.1.1 Glass Synthesis

Two series of bioactive glasses containing fluoride components were previously produced by Mneimne *et al*. (2011) and Lynch *et al*. (2012), details of the synthesis are provided in the perspective papers. The compositions of these bioactive glasses are given in **Table 2.1** and **Table 2.2**.

Table 2.1: Compositions of laboratory bioactive alkali phospho-silicate glasses (mol %) (Mneimne *et al*., 2011)

	SiO_2	P_2O_5	CaO	CaF_2	Na_2O
B2	36.41	6.04	24.74	4.53	28.28
C2	34.60	5.74	23.51	9.28	26.87
D2	32.95	5.47	22.38	13.62	25.59
E2	31.37	5.21	21.31	17.76	24.36
F2	28.40	4.71	19.29	25.54	22.06

Table 2.2: Compositions of multicomponent bioactive glasses in mol% (Lynch *et al*., 2012)

	SiO_2	P_2O_5	CaO	CaF_2	SrO	SrF_2	Na_2O	K_2O	ZnO	$CaF_2 + SrF_2$
F0	44	5	15	0	15	0	10	10	1	0
F4	41.91	4.76	14.29	2.38	14.29	2.38	9.53	9.53	0.95	4.76
F13	38.01	4.32	12.96	6.81	12.96	6.81	8.64	8.64	0.86	13.62
F17	36.19	4.11	12.34	8.88	12.34	8.88	8.22	8.22	0.82	17.76
F25	32.76	3.72	11.17	12.77	11.17	12.77	7.45	7.45	0.74	25.54
F32	29.61	3.36	10.09	16.36	10.09	16.36	6.73	6.73	0.67	32.72

The bioactivity of these two series of bioactive glasses was previously studied by Mneimne *et al*. (2011) and Lynch *et al.* (2012) respectively. In these glasses the metal fluorides were added to the composition rather than substituted for the metal oxide. All glasses were melted in platinum/rhodium 80/20 crucibles. Details of the synthesis conditions are given in the

respective papers (Mneimne *et al*., 2011) and (Lynch *et al*., 2012). The first series of ionomer-type glasses (**Table 2.3**) were in the 4.5 SiO_2-3 Al_2O_3-1.5 P_2O_5(5-X)-CaO-X-CaF_2 system.

Table 2.3: Compositions of model laboratory ionomer-type glasses (mol %) (Rafferty *et al*., 2000b)

	SiO_2	Al_2O_3	P_2O_5	CaO	CaF_2
LG99	32.14	21.43	10.71	14.29	21.43
LG95	32.14	21.43	10.71	20.00	15.71
LG134	32.14	21.43	10.71	25.00	10.71
LG115	32.14	21.43	10.71	28.57	7.14
LG116	32.14	21.43	10.71	35.71	0.00

In this series of ion-leachable glasses CaO is substituted for CaF_2 on a molar basis. These glasses were synthesised using a method described earlier by Stanton and Hill (2000). A second series of the high-fluoride ionomer-type glasses (**Table 2.4**) were synthesised and provided by Cera Dynamics Limited (Stoke-on-Trent, UK).

Table 2.4: Compositions of high fluoride ionomer-type glasses produced by Cera Dynamics Limited (mol %)

	SiO_2	Al_2O_3	P_2O_5	Na_2O	CaO	SrO	F
PF124	20.00	14.47	1.87	5.15	0.13	8.47	49.90
PF125	28.71	17.48	2.12	1.67	0.09	15.63	34.30
PF126	23.35	13.30	2.05	5.32	0.12	8.86	47.00
PF127	29.16	15.88	2.56	1.66	0.08	15.51	35.15
PF128	25.03	15.90	7.44	1.67	23.61	0.46	25.89
PF129	25.73	17.34	8.37	1.32	26.98	0.08	20.18
PF130	27.85	18.14	4.34	1.55	27.80	0.02	20.30
PF131	26.17	17.73	4.21	1.48	12.59	16.01	21.81

These high fluoride glass samples were produced in a custom-built cold-top furnace to prevent fluoride volatilisation as silicon tetrafluoride. Full chemical analysis of the industrially manufactured glasses was carried out by X-ray

fluorescence. These glasses have much higher fluoride contents than the laboratory synthesised ionomer glasses whose compositions were designed to prevent fluorine loss as volatile silicon tetrafluoride (Hill *et al*., 1999).

2.1.2 Measurement of Refractive Indices

Fluoride-containing glasses are prone to rapid crystallisation (Stanton and Hill, 2000) and fluorine loss on casting therefore as opposed to using *Abbé* refractometer refractive indices of the samples were measured by the Becke line test (Saylor, 1995). The refractive indices all fluoride-containing amorphous powdered glass samples were measured using polarised light microscopy by mounting the amorphous glass samples in immersion liquids with different refractive indices (Cargille, USA) and making observations of the Becke line. The immersion liquids have known refractive index values ranging from 1.45 to 1.70 with 0.01 intervals. Refractive index measurements were performed at room temperature using the sodium D-line. The microscope was calibrated prior to each measurement using a known RI glass sample. Digital images of the glass samples were captured using a digital camera (Q Imaging, Canada) affixed to the microscope and digitised by manufacturer's software.

2.1.3 Development of Appen Factors

The Appen equation (**Eq. 1.6**) was used to pre-calculate RIs of all glass samples. Because no Appen factors are available for the metal fluorides, the metal fluoride component contribution to the actual RI was underestimated. To compensate for the underestimated RI as a result of the metal fluoride

addition multiple factors were tried for the respective metal fluoride (CaF_2/SrF_2) component until the calculated RI value matched to experimentally derived RI value.

2.2 Effect of Increasing Strontium Substitution on the Structure and Crystallisation Behaviour in SiO_2-Al_2O_3-P_2O_5-CaO/SrO-CaF_2 Glasses

2.2.1 Design Rationale

The glasses were designed based on a well-studied glass composition termed LG99, nominal compositions of the glasses are given in **Table 2.5.** The nominal glass composition was modified by substituting CaO for SrO.

2.2.2 Glass Synthesis

Glasses of defined chemical composition shown in **Table 2.5** were synthesised for this study by the melt-quench technique.

Table 2.5: Nominal glass compositions in the system SiO_2-Al_2O_3-P_2O_5-CaO/SrO-CaF_2

Glass Code	SiO_2	Al_2O_3	P_2O_5	CaO	SrO	CaF_2
LG99	4.5	3	1.5	2	0	3
QMTD1	4.5	3	1.5	1.5	0.5	3
QMTD2	4.5	3	1.5	1	1	3
QMTD3	4.5	3	1.5	0.5	1.5	3
QMTD4	4.5	3	1.5	0	2	3

The glasses were synthesised by melting the following reagents: SiO_2 (Prince Minerals Ltd., Stoke-on-Trent, UK), Al_2O_3, P_2O_5, $CaCO_3$, $SrCO_3$ and CaF_2 (>99.99% purity, Sigma-Aldrich, Gillingham, UK) in platinum/rhodium crucibles at 1450°C for one hour. The resulting melts were rapidly quenched into water to prevent phase separation and crystallisation. Produced glass was then dried for 24 hours. Subsequently, dried glass samples were used for DSC analysis and crystallisation experiments.

2.2.3 Heat-Treatment Protocol

Heat-treatment procedures were developed based on the thermal information derived from the DSC analysis. Heat treatment temperatures are shown in **Table 2.6**.

Table 2.6 Heat-treatment temperatures and T_{C1} (FAp) for the synthesised glasses

Glass	T_g	T_g+50°C	T_g+100°C	T_g+150°C	T_{C1}
LG99	577	627	677	727	732
QMTD1	572	622	672	722	729
QMTD2	567	617	667	717	760
QMTD3	565	615	665	715	781
QMTD4	559	609	659	709	848

Subsequently, five grams of each sample in bulk form were heat-treated at temperatures specified in **Table 2.6** in CeramPress (NEY Dental Inc, Yucaipa, USA) bench-top furnace for 1 hour at a heating rate of 20°C min^{-1}. Heat-treated glass frit was then processed into powder for structural analysis.

2.3 Effect of Metal Oxide for Metal Fluoride Substitution on the Structure and Crystallisation Behaviour of SiO_2-Al_2O_3-P_2O_5-CaF_2/SrF_2-NaF Glasses

2.3.1 Design Rationale

The glasses were designed based on the glass described in Chapter III however in order to reduce refractive indices of the glasses (to match the RI of the liquid component and the polysalts) calcium and strontium oxide components were replaced by calcium and strontium fluoride components. In order to facilitate electric melting a small amount of NaF (0.5 mol) was added to each composition.

2.3.2 Glass Synthesis

Table 2.7 shows the designed composition in moles. These compositions were designed using the Appen factors (discussed in Chapter II) and then synthesised by Cera Dynamics Limited (Stoke-on-Trent, UK) in a cold-top furnace.

Table 2.7: Nominal compositions of the synthesised high-phosphorus high-fluoride glasses in moles

	SiO_2	Al_2O_3	P_2O_5	CaF_2	SrF_2	NaF
QMTD7	4.5	3	1.5	5	0	0.5
QMTD8	4.5	3	1.5	2.5	2.5	0.5
QMTD9	4.5	3	1.5	0	5	0.5

2.4 Solid-State Characterisation of the Developed Glasses and Glass-Ceramics

2.4.1 Differential Scanning Calorimetry

Synthesised amorphous glasses were analysed by differential scanning calorimetry using a Stanton Redcroft DSC 1500 (Rheometric Scientific, Epsom, UK). The crucibles used were matched pairs made of platinum-rhodium alloy. Alumina was used as the reference inert material. DSC analysis was performed in oxygen depleted (N_2) environment at a heating rate of 20 °C min^{-1}.

2.4.2 ATR-FTIR Spectroscopy

Attenuated Total Reflectance–Fourier Transform Infrared Spectroscopy (Spectrum GX, Perkin-Elmer, USA) was also used to analyse heat-treated treated and non-treated glasses. The absorbance data were collected from 500 to 1500cm^{-1} at a resolution of 4 cm^{-1}. Each spectrum presented is a sum of 10 scans.

2.4.3 X-ray Powder Diffraction

In order to identify FAp phases in the developed glass-ceramics, X-ray powder diffraction (XRD) analyses were carried out. Glass-ceramic powders were analysed using X'Pert-PRO diffractometer (PANalytical D.V., Almelo, The Netherlands). Diffraction patterns were collected from 5° to 75° two-theta. The Cu Kα X-ray frequency was λ_1=1.54059 Å.

2.4.4 ^{27}Al MAS-NMR Spectroscopy

^{27}Al MAS-NMR spectroscopy measurements were conducted at a resonance frequency of 156.3 MHz using a higher magnetic field (14.1T) on a Bruker FTNMR 600. The recycle time was 1.0 s and spinning rate of 12 kHz. The ^{27}Al chemical shift scale was calibrated 0 ppm value for 1 M $Al(NO_3)_3$) solution.

2.4.5 ^{31}P MAS-NMR Spectroscopy

Solid-state ^{31}P MAS–NMR experiments were carried out on Bruker Avance 600 MHz NMR instrument. A 30º pulse (the basic one-pulse program) with relaxation delays of 60 s were used to acquire ^{31}P 1D spectra. Samples were contained in a 4 mm or 2.5 mm diameter zirconia rotor at spinning speeds of 12 kHz and 15 kHz to acquire 32 scans for each experiment. ^{31}P spectra were referenced to 85% orthophosphoric acid solution at zero ppm.

2.4.6 ^{29}Si MAS-NMR Spectroscopy

Solid-state ^{29}Si MAS–NMR experiments were carried out on Bruker Avance 600 MHz NMR instrument. A 30º pulse (the basic one-pulse program) with relaxation delays of 120s were used to acquire 512 spectra. Samples were

contained in a 4 mm diameter zirconia rotor. The spinning rate was approximately 12 kHz.

2.4.7 ^{19}F MAS-NMR Spectroscopy

Solid-state ^{19}F MAS–NMR experiments were carried out on Bruker Avance 600 MHz NMR instrument. A 30º pulse (the basic one-pulse program) with relaxation delays of 60s were used to acquire ^{19}F 1D spectra. Samples were contained in a 2.5 mm diameter zirconia rotor at spinning rate of 25 KHz to acquire 80 ^{19}F spectra. All spectra were referenced to 1 M sodium fluoride solution at -120 ppm.

2.4.8 Transmission Electron Microscopy

For the transmission electron microscopy (TEM) analysis one of the optically clear samples (QMTD3, heat-treated at 615ºC) containing FAp phases (based on ^{19}F MAS-NMR analysis) was crushed in ethanol. A drop of this dispersion was put on a copper grid covered with a holey carbon film. The image was captured using a Philips CM30 electron microscope operated at 200 kV.

2.4.9 Compressive Strength

2.4.9.1 Specimen Preparation

Glasses were ground to a fine powder and sieved. Subsequently, fine powder was mixed with an aqueous solution of 50% polyacrylic acid made using deionised water and 80kDa polyacrylic acid powder (Advanced Healthcare Ltd, Tonbridge, UK). Stainless steel moulds, 6mm x 4mm were filled with the cement paste and stored in an incubator at 37ºC for 1 hour to

set. Thereafter, the moulds were disengaged and produced cylindrical cement specimens were stored in individual test tubes filled with 10mL deionised water and transferred to an incubator at 37ºC±1 for further 23 hours.

2.4.9.2 Compressive Strength Analysis

After the 24-hour period the length and width of each specimen was measured. Subsequently, the compressive strength of each specimen was analysed using universal testing machine (Instron model 5567, High Wycombe, England). The compressive load was applied vertically at a loading rate of 1 mm/min.

CHAPTER 3:

PREDICTING REFRACTIVE INDEX OF FLUORIDE-CONTAINING GLASSES FOR AESTHETIC DENTAL RESTORATIONS

3 Introduction

The aesthetics is an important feature of dental restorations in modern day dentistry. In order to develop a translucent glass ionomer cement (GIC) or a dental composite (DC) it is important to match the refractive index of the glass to the polymer or the polysalt cement matrix to avoid light scattering at the interfaces. Light scattering at the interfaces results in an opaque material. In DCs, light scattering because of a RI mismatch between the resin and the glass filler causes light attenuation and strongly influences the depth of cure of the composite material (Shortall *et al*., 2008). Furthermore, in photoactive resin-based composites RI mismatch between the resin and the filler increases light scattering, however the RI of the resin changes dynamically during the curing process (Hadis *et al*., 2010). This can either increase or decrease light scattering depending on the refractive index match, i.e. if the RI of the filler matches the RI of the uncured resin, then light scattering will increase as the material polymerizes and if the RI of the resin is lower, then as the material polymerizes, light scattering will decrease and so will the opacity and light transmission through the material. Optimum RI matching and careful design of the DCs may produce DC materials with considerably improved optical properties. The only alternative way to obtain a highly translucent cement is to have well dispersed nano-sized particles where the dimensions of the particles are smaller than the wavelength of the visible light. Such fine scale powder particles are particularly difficult to manufacture as they have a high tendency to aggregate once mixed essentially forming larger clusters to reduce their high surface energy. Furthermore, it is difficult

and costly to produce such nano-sized particles particularly from melt-derived glasses. It is notable that translucent glass-ceramics are also produced by matching the refractive index between the different components in these multiphasic materials i.e. crystal phase/s and the residual glassy phase.

In the case of fluoride-free glasses the RI of the glass can be calculated to within about 0.01 using the Appen factors (Appen, 1974), which are experimentally derived factors calculated on the basis of previous measurements of RIs of oxide glasses. Appen factors have been successfully used to calculate not only the RI of glass but also thermal expansion coefficients (O'Donnell *et al*., 2010). The RI of an oxide glass can be calculated using the Appen equation (**Eq. 1.6**).

Appen factors for the metal fluorides are not available. Consequently, the refractive index of the fluoride-containing glasses cannot be predicted. Fluoride components are used to reduce the refractive indices of glasses used in optoelectronics (Gan *et al*., 1995). Fluoride-containing glasses are attractive components for dental composites and particularly for glass ionomer cements. The anticariogenic effects of fluoride have been long known (Featherstone *et al*., 1999). Based on Scanning Electron Microradiography (SMR) *in vitro* studies, optimum fluoride concentrations under acidic conditions have also been proposed by Mohammed *et al*. (2014). However, despite the importance of RI it has rarely been measured for fluoride containing dental glasses there is only one peer reviewed article published in the literature. The results presented in this chapter shows how increasing CaF_2 content in bioactive glasses allows design of dental composite materials with improved optical properties, such as improved

depth of cure and reduced light transmission (Hadis *et al*., 2016). Improved depth of cure of the DC will also result in increased longevity of the tooth restoration due to minimized shrinkage and increased polymerisation. The ability to model the role of metal fluorides on the RI of multicomponent glasses also allows the prediction of RI of fluoride-containing glass-ceramics (GCs) used in restorative dentistry, particularly GCs based on fluorapatite and fluoromica phases. The translucency is required for optimal aesthetics, therefore it is important to match the RI of the crystal phase to the residual glass phase. In the fluoromica glass-ceramics, relatively large interlocking crystals are required to provide optimum strength and fracture toughness, as well as machinability in the case of mica glass-ceramics (Höland and Beall, 2012). GCs containing nano-sized crystal phases can also provide the desired aesthetics, however nanoscale mica ceramics will result in a material with poor mechanical properties and poor machinability. Therefore, in summary, it is necessary to develop a model by which refractive indices of fluoride-containing glasses and glass-ceramics can be predicted.

The objectives of this part of the thesis are to:

i) Measure the RI of two types of the fluoride-containing glasses used in glass (ionomer) cement formulations and two types of bioactive glasses, which can be used as remineralising additives in dental composites.

ii) To develop Appen Factors for fluoride-containing glasses so that RIs of these glasses may be calculated which will allow the design of restoratives with improved translucency.

3.1 Results

3.1.1 Refractive Index and Fluoride Content

All glasses used in the study were found to be amorphous by X-ray powder diffraction analysis. **Figures 3.1(a-c)** shows the RI as a function of CaF_2, SrF_2 and F content for phospho-silicate bioactive glasses and alumino-silicate ionomer-type glasses. There is a linear decrease in RI with metal fluoride/elemental fluoride content.

A comparison of the experimental and calculated refractive index values for Mneimne *et al*. (2011) series of bioactive glasses shows a good correlation between the two (**Figure 3.1(a)**).

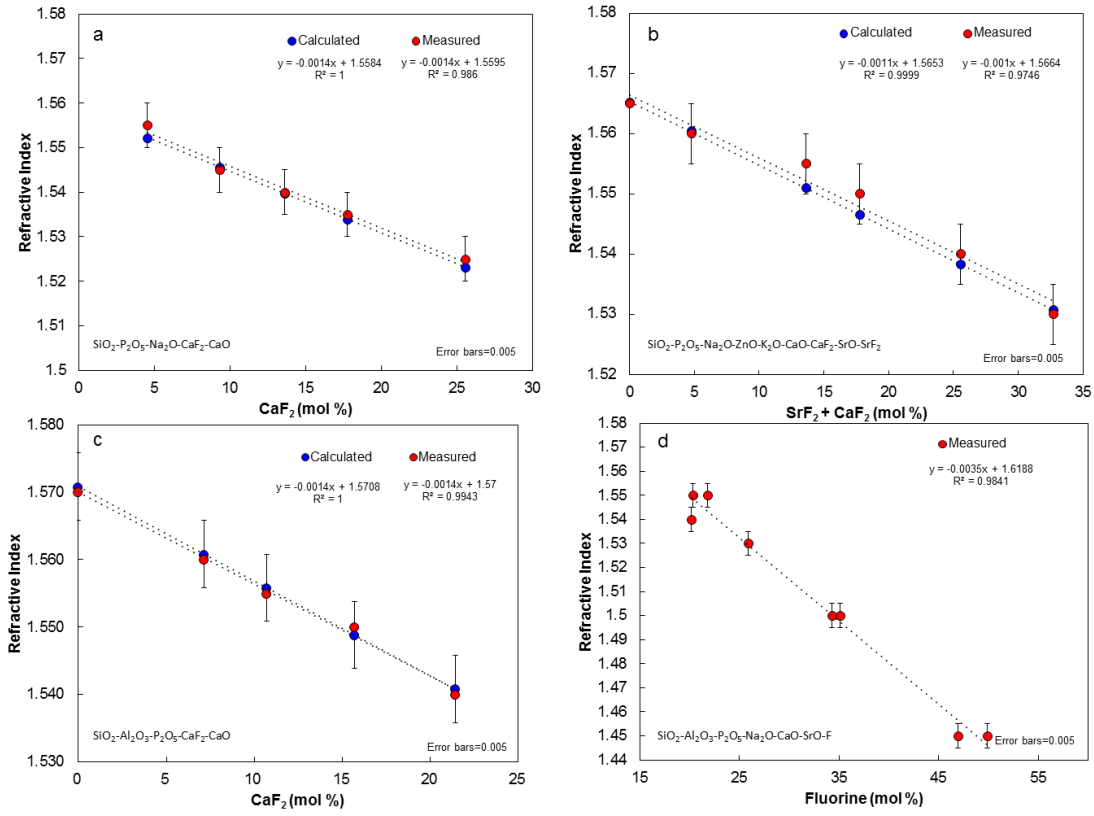

Figure 3.1: Refractive index and fluoride content (a – bioactive glasses described in (Mneimne *et al*., 2011); b – bioactive glasses described in (Lynch *et al*., 2012); c – laboratory synthesised ionomer-type glasses; d – industrially synthesised ionomer-type glasses.

However, for more complex F series of bioactive glasses containing additional oxide components it can be observed that there is a slight deviation between the experimental and calculated RI values with Ca/SrF_2 contents (**Figure 3.1(b)**). **Figure 3.1(c)** shows the RI for a series of ionomer glasses based on $4.5SiO_2$-$3Al_2O_3$-$1.5P_2O_5$(5-X)CaO-$XCaF_2$. The calculated RIs using Appen factors matches the experimentally determined RIs to within 0.005.

Figure 3.1(d) shows the RI as a function of F content for the industrially manufactured high fluoride (PF) series (**Table 2.4**) of glasses. In summary, there is a clear linear relationship between fluoride content (both, elemental fluoride or in the form of metal fluoride) and refractive index of the glasses studied. **Table 3.1** shows series-specific Appen factors derived from this study.

Table 3.1: Empirically derived Appen factors for different series of glasses

	CaF_2	**SrF_2**	**P_2O_5**
(Mneimne *et al*., 2011)	1.42	-	-
(Lynch *et al*., 2012)	1.45	1.47	-
LG	1.59	-	1.48

3.2 Discussion

Based on the experimentally derived RIs of the fluoride-containing glass samples, a linear (R^2=0.98) correlation between elemental fluoride/metal fluoride content and the refractive index of glasses is clearly observed. Generally, fluoride containing glasses have larger atomic spacings and therefore more disrupted structure. Larger spacing in the glass network

results in the reduction in glass density and thus is attributed to lower refractive index. It has been long known that there is a linear correlation between density and refractive index in glasses (Bannister, 1931). However, many materials other than glasses do not exhibit this phenomenon.

It may not be surprising that incorporation of fluoride lowers the dielectric constant of the glasses which is observed in other dielectric materials (Yang *et al*., 2014) and results in reduced polarizability and henceforth a reduction in refractive index.

For the first series of bioactive glasses developed by Mneimne *et al*. (2011) calculated and measured RI values are matching within 0.005. In this series, it was found that CaF_2 contributes to the RI by a factor of 1.42, which is quite close to the RI of crystalline CaF_2, which at room temperature is 1.4338 (Malitson, 1963). It is notable that solid-state ^{19}F MAS-NMR studies of related glasses by Brauer *et al*. (2009) have shown the fluoride ion to be present as F-M(n) species where M is largely Ca with a small fraction of Na and n is close to four. Molecular dynamic simulations by Christie *et al*. (2011) predict the formation of F-Ca(n) species. Thus, in these glasses the fluoride ion exists in a fluorite like F-Ca(4) environment and it is therefore not surprising that the RI can be predicted based on a model assuming the presence of a fluorite-like environment. Furthermore, Brauer *et al*. (2011) measured the density of CaF_2 containing bioactive glasses and showed the density could be predicted based on the assumption of fluoride existing in a CaF_2 like environment and using a density factor for crystalline CaF_2. It is worth noting that in the present glasses, as well as the ones studied by Brauer *et al*. (2011), the CaF_2 was added to the glass rather than being substituted for CaO and in these glasses there is no change in the non-

bridging oxygen content and the *Q* speciation of the silicon remains constant. In the original studies of Hench *et al*. (1998) and more recently by Lusvardi *et al*. (2008) CaF_2 was substituted for CaO which results in changes in the non-bridging oxygen content of the glass and the silicon speciation as well as potential loss of fluoride as silicon tetrafluoride during melting.

The calculations for the second series of bioactive glasses (**Table 2.2**) (Lynch *et al*., 2012), with strontium and potassium components have also been performed by assuming the nominal proportions of CaF_2 and SrF_2 incorporated in the original glass composition. It was found that metal fluorides contribute to the RI by a factor of 1.45 (CaF_2) and 1.47 (SrF_2), which is higher than the factor for the first series. In the final melted glass composition the fluoride might be expected to form more F-Ca(n) species than F-Sr(n) species since Ca^{2+} has a slightly smaller ionic size than Sr^{2+} and this might be expected to favour F-Ca(n) speciation. In addition there is likely to be mixed F-Ca/Sr(n) and F-Na(n) sites where Na and Ca is more prevalent than Sr and this may an effect on the RI and hence may explain why the Appen factor for the metal fluoride component in this series is higher.

Appen factor for CaF_2 for the first series of alumino-silicate glasses (**Table 2.3**) was found to be 1.59, which is much higher when compared to the RI of crystalline CaF_2. In addition, it was also found that Appen factor for P_2O_5 is different from that published by Appen (1974) and is around 1.48 for this series of glasses. This may be due to different phosphorus speciation in glass compositions containing aluminium and can be linked to several structural aspects (Stamboulis *et al*., 2004).

Characterisation by ^{19}F, ^{31}P, ^{29}Si and ^{27}Al MAS-NMR (Zainuddin *et al*., 2012) indicate that the structure of ionomer type glasses is much more complex than the fluoride-containing bioactive glasses.

The fluoride can exist as Al-F-Ca(n), as well as F-Ca(n) and the proportion of these two species changes with the glass composition (Zainuddin *et al*., 2012). The assumption of the glass consisting of a CaF_2 free glass plus CaF_2 like species in the calculation of the RI is only partially valid and neglects the presence of Al-F-Ca(n) species. In addition substituting CaF_2 for CaO may also reduce the non-bridging oxygen content of the glass, which will also influence the RI. In addition increasing fluoride content can cause the Al to move from Al(IV) to higher coordination states of V and VI.

Due to the complexity of the second series of high-fluoride ionomer-type glasses (**Table 2.4**) the data is expressed as measured RI as a function of elemental fluoride content. These compositions contain excessive amounts of fluoride and further structural characterisationis ongoing. However, RIs that all within the compositional domain of this series of glasses can also be predicted based on the amount of elemental fluoride in mol % using the equation for straight line expressed in **Figure 3.1(d)**. Most commercial ionomer glasses also contain small amounts of sodium whereby it forms Al-F-Na(n) species in the glass in addition to Al-F-Ca(n) and F-Ca(n) species. Furthermore, many commercial glasses also contain strontium (Stamboulis, 2004), which can result in Al-F-Sr(n) and F-Sr(n) speciation in addition to mixed species if calcium is included in the composition. In general, the amount of sodium in ionomer glass compositions is typically less than 1% so the formation of Al-F-Na(n) species is not likely to have a large influence on the RI of ionomer-type glasses.

In regard to glass ionomer cements, it is important that the RI of glass matches the RI of the polysalt matrix. This can be quite well facilitated in cement compositions where the initial difference between refractive index of the glass and the refractive index of the liquid component is lower.

3.3 Conclusions

The RI of fluoride containing bioactive glasses correlates linearly with metal fluoride content and the RI can also be predicted readily using Appen factors close to that of fluoride-containing crystalline phases, such as CaF_2 as proposed in the study. The RIs of the more complex ionomer glasses also show a linear relationship with fluoride content. Nonetheless, the study discussed in this chapter proposes a modified Appen Model with new composition-specific Appen factors for the metal fluorides for the development of highly translucent dental materials and improved depth of cure of dental composites. The present study also provides a very useful tool for the design of highly advanced restorative materials which can exhibit bioactivity alongside improved aesthetics and increased restoration longevity.

CHAPTER 4:

EFFECT OF INCREASING STRONTIUM SUBSTITUTION ON THE STRUCUTRE AND CRYSTALLISATION BEHAVIOUR IN SiO_2-Al_2O_3-P_2O_5-CaO/SrO-CaF_2 GLASSES

4 Introduction

Glass ionomer cements have seen significant developments in recent years since they were first described by Wilson and Kent (1971). The more detailed understanding of the structure-property relationship has led to the development of highly advanced glass ionomer cements with improved mechanical properties, setting/working properties and bioaesthetics. This is mainly attributed to the several extensive nuclear magnetic resonance (NMR) studies by Hill and co-workers (Stamboulis *et al*., 2004); (Zainnudin *et al*., 2009) and (Kusumoto *et al*., 2016) that show a clear relationship between short-range order of the GICs glasses and the various properties of the reacted cement, such as glass degradation, setting characteristics of the cements and the mechanical properties of the set cements.

It is known that GICs have the potential to remineralise demineralised dentine *in vivo* through fluoride and strontium diffusion into carious dentine (Ngo *et al*., 2006). Quite a few research groups have also incorporated remineralising additives into glass ionomer cements recently to enhance remineralisation and a number of other properties. Remineralising additives, such as bioactive glasses (De Caluwe *et al*., 2017), synthetic apatite (van Duinen *et al*., 2004) and organic components (Mazzaoui *et al*., 2003) and (Al Zreikat *et al*., 2011) have been shown to promote remineralisation and provide protection during acid challenge. These developments have created a new approach in the way dental caries is managed and treated. Glass ionomer cements are also particularly useful in countries with limited access

to adequate dental care facilities. The advantages of atraumatic restorative treatment (ART) technique were first described by Francken *et al*. (1996). The ART technique is a minimally invasive technique whereby soft caries are hand excavated and the cavity is subsequently filled with a high viscosity GIC. The ART technique does not require a dental drill meaning the tooth can be restored atraumatically without extensive dental equipment. Glass ionomer cements also have a sustained release of fluoride. It is also known that sustained release of fluoride can prevent the development of caries (Featherstone *et al*., 1999). It has also been shown in one of the earlier studies that GICs can uptake and re-release fluoride when exposed to fluoride solutions (Creanor *et al*., 1994).

Strontium components, such as SrO and SrF_2 are widely used in GIC compositions because strontium-substituted materials exhibit more clinically adequate radiopacity (Shahid *et al*., 2014). It is known that strontium-substituted apatite can facilitate more rapid nucleation and growth of apatite phases in SBF (Pan *et al*., 2009). It has also been shown that strontium-releasing biomaterials have the potential to promote bone regeneration (Gentleman *et al*., 2010) and tooth regeneration (Huang *et al*., 2016). Glass-ceramics containing apatite phases have been used for various healthcare applications, for example as bone implant materials, dental crowns and ceramic cements as discussed in more detail in Chapter 1. Wood and Hill (1991) synthesised reactive glasses for glass ionomer cements, which can be developed into FAp glass-ceramics of different crystallinity and can also form cements once mixed with an aqueous solution of poly-(acrylic acid).

The authors showed that the degree of crystallinity can influence the properties of GICs, such as the setting and working times as well as the

mechanical properties of the set cements. Additionally, as discussed in Chapter 1, FAp glass-ceramics developed by Wood and Hill (1991) are highly biocompatible *in vivo* when used as a bone replacement material (Freeman *et al*., 2003) and (Goodridge *et al*., 2007). Drawing from the works by Hill and co-workers the present study aims to exploit the advantages of strontium-substituted compositions and reactive glass-ceramics for the development of a completely new class of nanoscale GICs with improved remineralisation potential.

The objective of this part of thesis is to:

I. Develop optically clear strontium-containing nanoscale apatite glass-ceramics from well-studied model glass ionomer-type compositions and characterise these by solid-state characterisation techniques.

4.1 Results

4.1.1 Differential Scanning Calorimetry Analysis

Figure 4.1 shows DSC traces of the laboratory-synthesised glasses (LG99-QMTD4). It can be observed from **Figure 4.1** that glass compositions increasing in strontium content show reduced bulk crystallisation of the two phases associated with the two observable exothermic reactions.

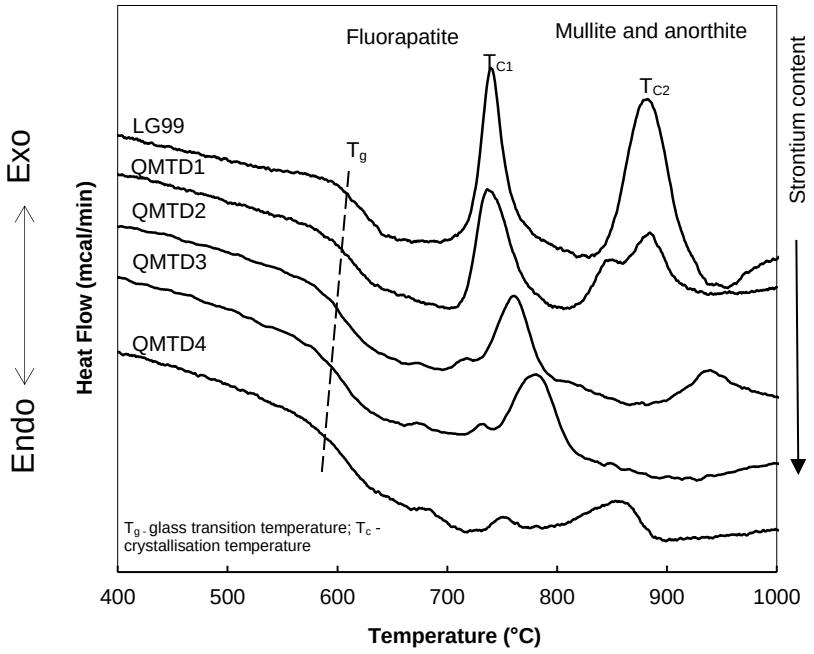

Figure 4.1: DSC traces of the synthesised glasses

Table 4.1: T_g and crystallisation temperatures derived from DSC analysis

Glass code	T_g onset	T_g midpoint	T_{c1}
LG99	577	600	740
QMTD1	572	590	740
QMTD2	567	580	760
QMTD3	565	575	780
QMTD4	559	565	845

Table 4.1 shows the glass transition temperatures against SrO content (moles). Increasing strontium content in the nominal compositions results in a linear reduction in T_g (R^2=0.98) (**Figure 4.2**).

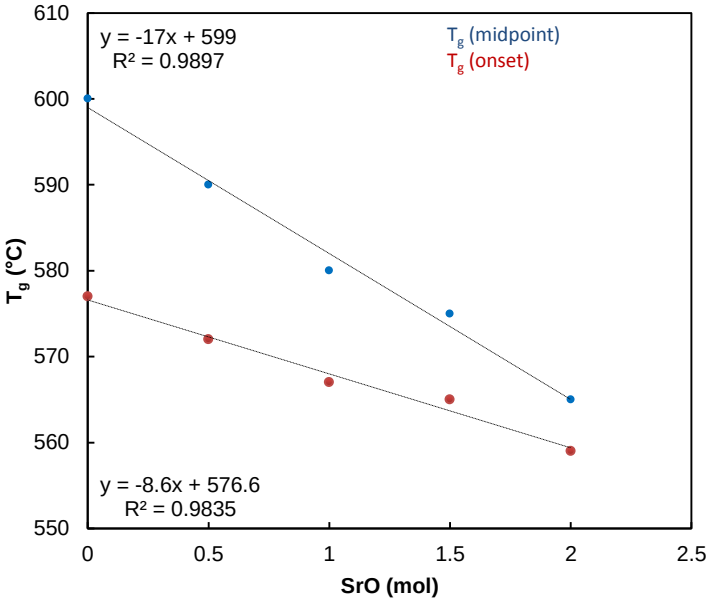

Figure 4.2: T_g as a function of SrO content (mol)

4.1.2 ^{27}Al MAS-NMR Analysis of the Untreated Glasses

Figure 4.3 shows ^{27}Al MAS-NMR spectra of the untreated glasses. All glasses have three observable aluminium environments: Al(IV) seen at around 52.0 ppm, Al(V) seen at around 22.0 ppm and Al(VI) seen at around -3.0 ppm.

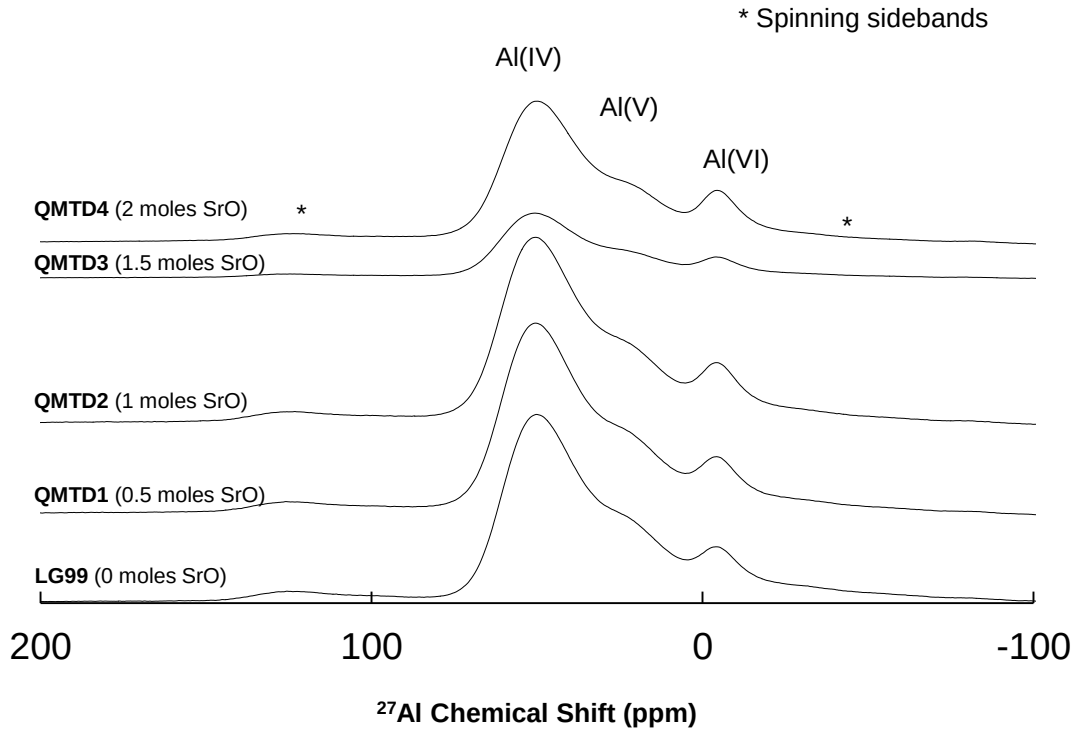

Figure 4.3: ^{27}Al MAS-NMR Spectra of the synthesised glasses showing three aluminium environments, from right to left: Al(IV), Al(V) and Al(VI)

4.1.3 ATR-FTIR Analysis of the Developed Glass-Ceramics

Figures 4.4 to **4.6** shows ATR-FTIR spectra for the developed glass-ceramics. Increasing heat-treatment temperature results in the development of apatitic PO_4^{3-} bands: ν_1 and ν_3 at approximately 1095 and 1035 cm^{-1} and two ν_4 at approximately 600 cm^{-1} and 565 cm^{-1} (Rehman and Bonfield, 1997). All developed glasses also show Si-O-Si and Si-O-NBO signals assigned to symmetric stretch vibration Si-O-Si (Q^4) in the range 1000-1100 cm^{-1} and Si-O-NBO (Q^3) stretching vibration at around 950 cm^{-1} (Sanders *at el*., 1974). The phosphate bands attributed to apatite broaden with increasing SrO content (**Figure 4.6(b)**).

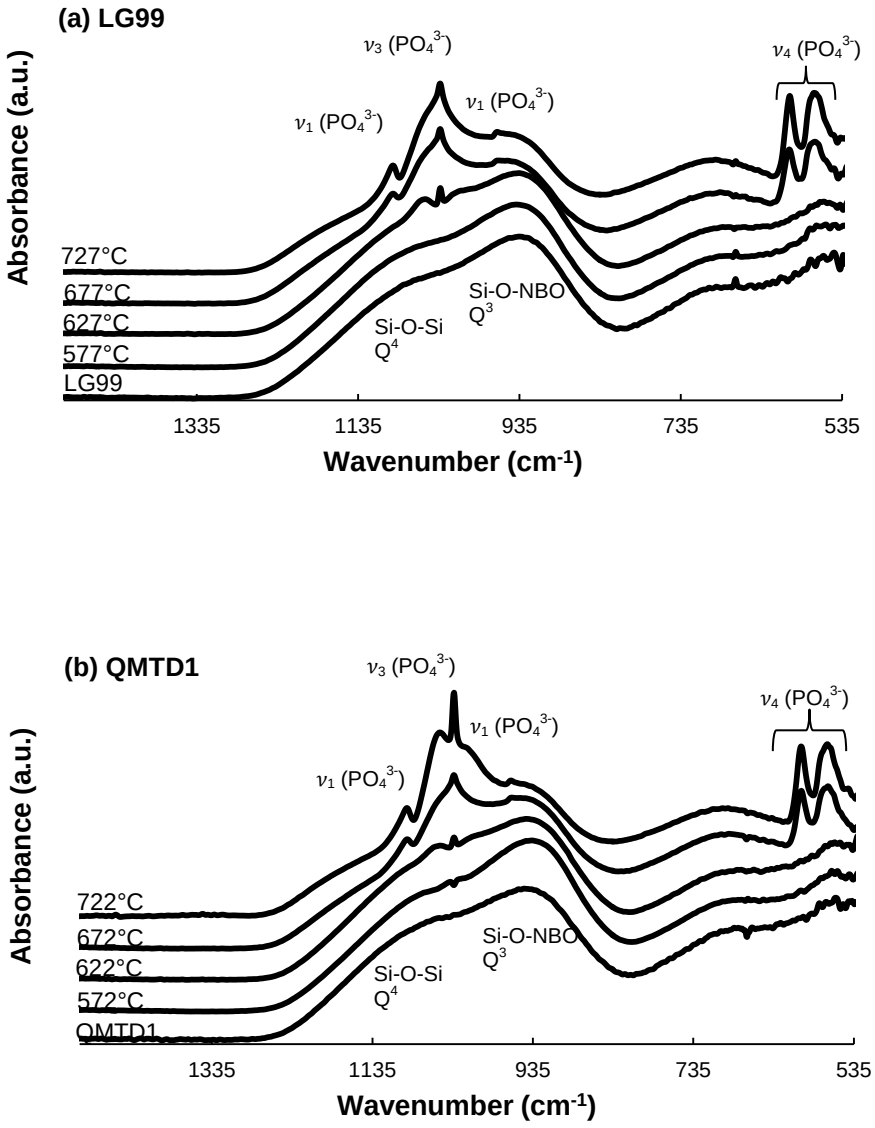

Figure 4.4: (a) ATR-FTIR spectra of the unsubstituted FAp glass-ceramics (LG99); (b) ATR-FTIR spectra of the 0.5 mol SrO FAp glass-ceramics (QMTD1)

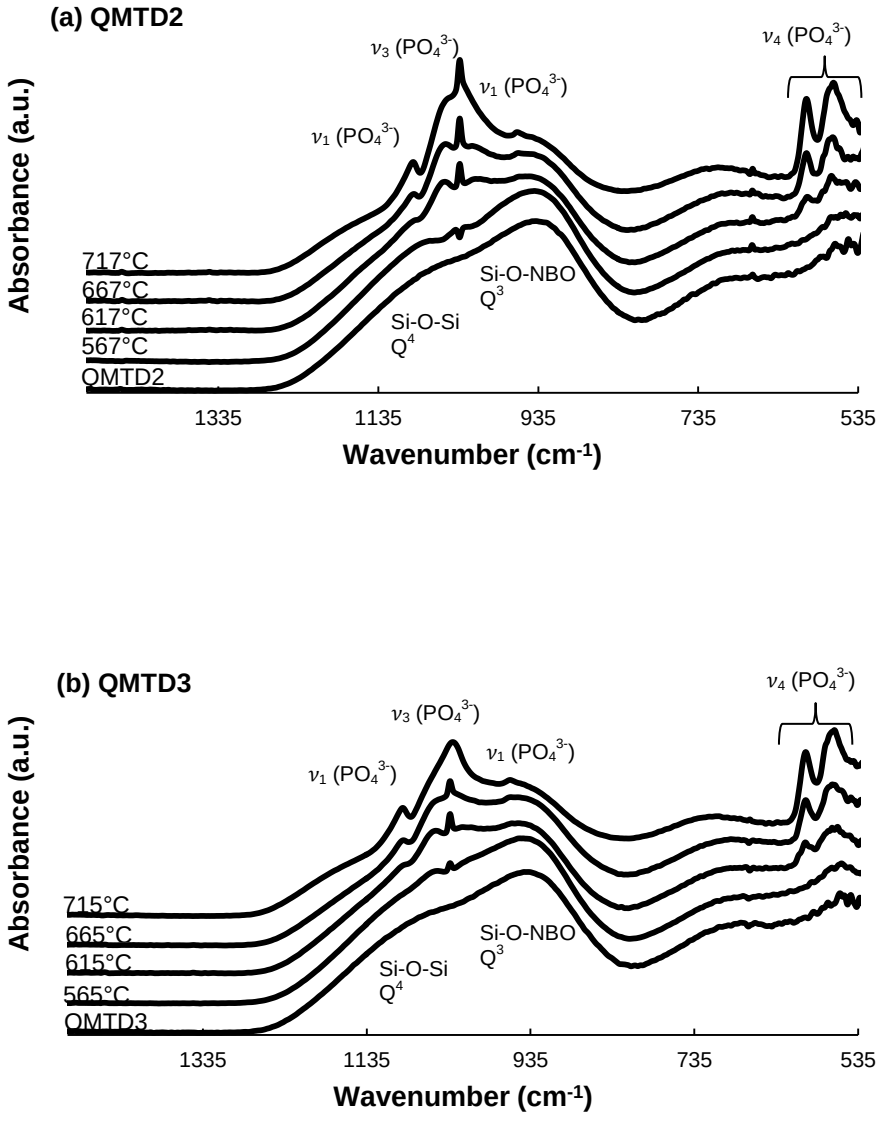

Figure 4.5: (a) ATR-FTIR spectra of the 1 mol SrO FAp glass-ceramics (QMTD2); (b) ATR-FTIR spectra of the 1.5 mol SrO FAp glass-ceramics (QMTD3)

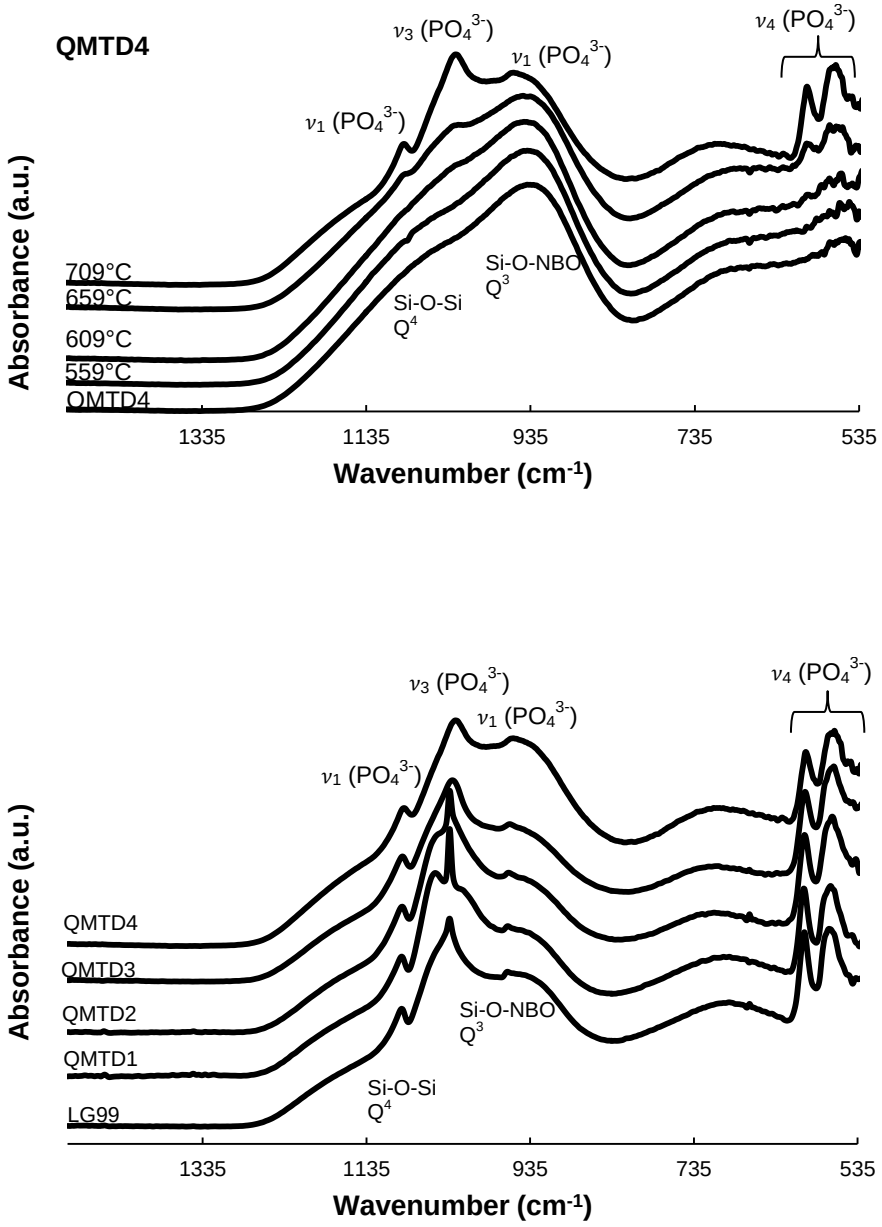

Figure 4.6: (a) ATR-FTIR spectra of the 2 mol SrO FAp glass-ceramic (QMTD4); (b) Changes to ATR-FTIR apatite spectra with increasing strontium content (samples heat-treated at T_g+150ºC)

4.1.4 XRD Analysis of the Developed Glass-Ceramics

X-ray diffraction results shown in **Figure 4.7(a)** show that all synthesised glasses were amorphous. This is evident from the absence of sharp Bragg reflection associated with polycrystalline materials.

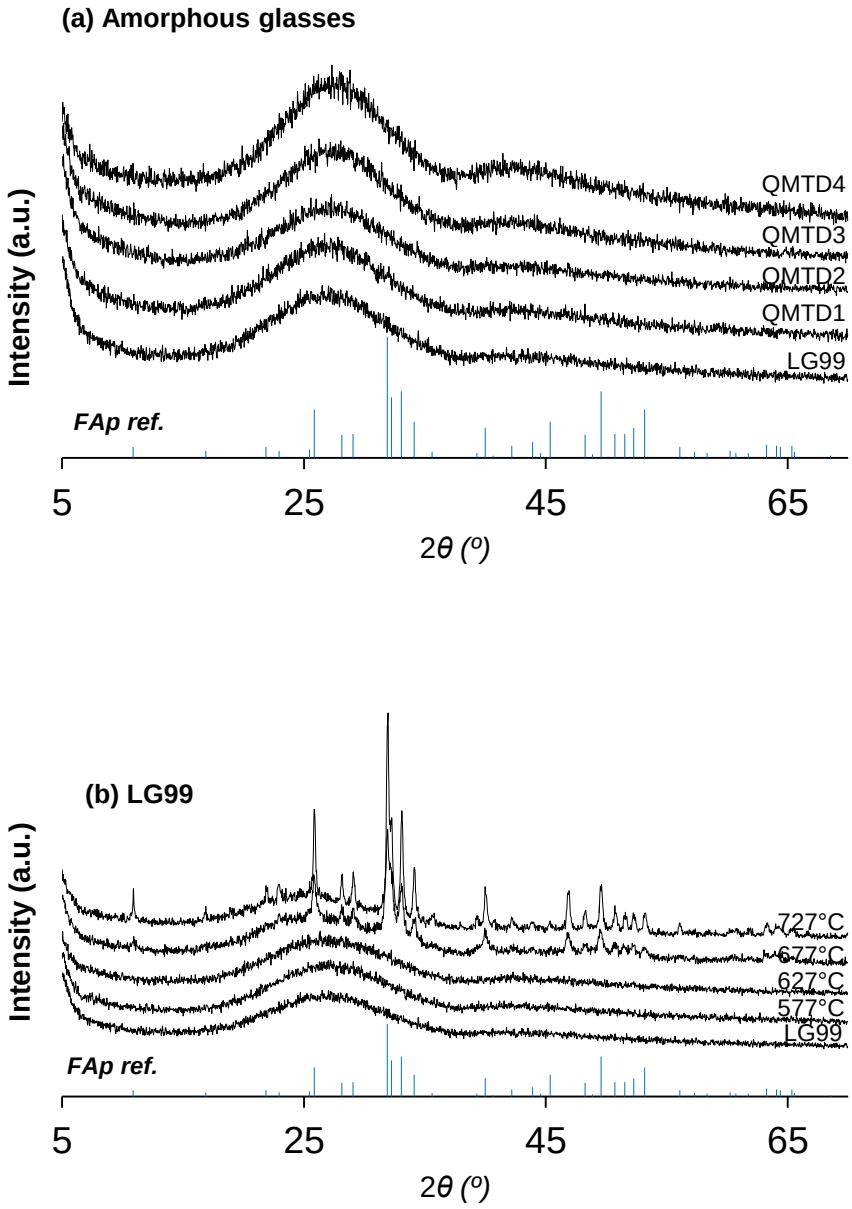

Figure 4.7(a) XRD patterns of the as-synthesised glasses with FAp reference at the bottom (b) XRD patterns of the unsubstituted FAp glass-ceramics (LG99) with FAp reference at the bottom

Figures 4.8(a) to **Figure 4.9(b)** show the development of sharp Bragg reflections corresponding to FAp phases (reference used: ICDD 00-034-0011). Increasing heat-treatment temperature results in increased crystallisation of fluorapatite.

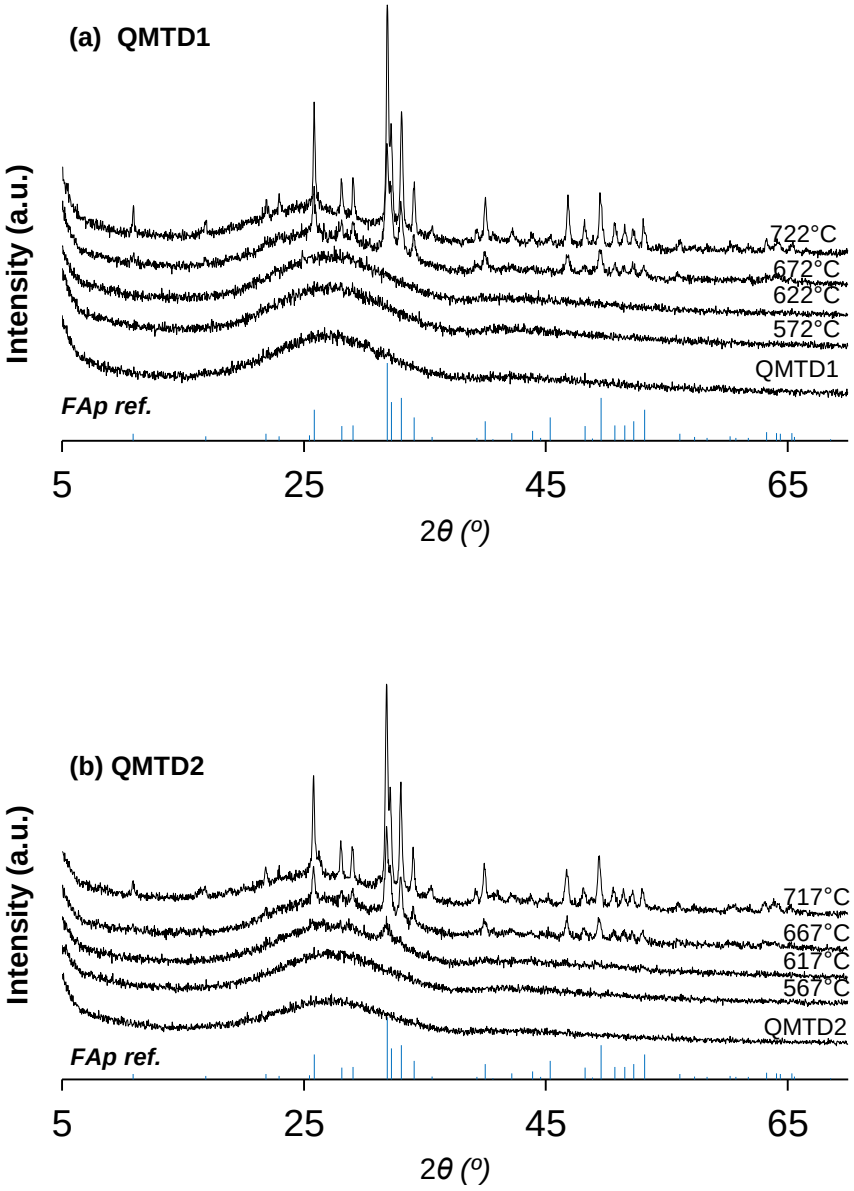

Figure 4.8: (a) XRD patterns of the 0.5 mol SrO FAp glass-ceramics (QMTD1) with FAp reference at the bottom (b) XRD patterns of the developed 1 mol SrO FAp glass-ceramics (QMTD2) with FAp reference at the bottom

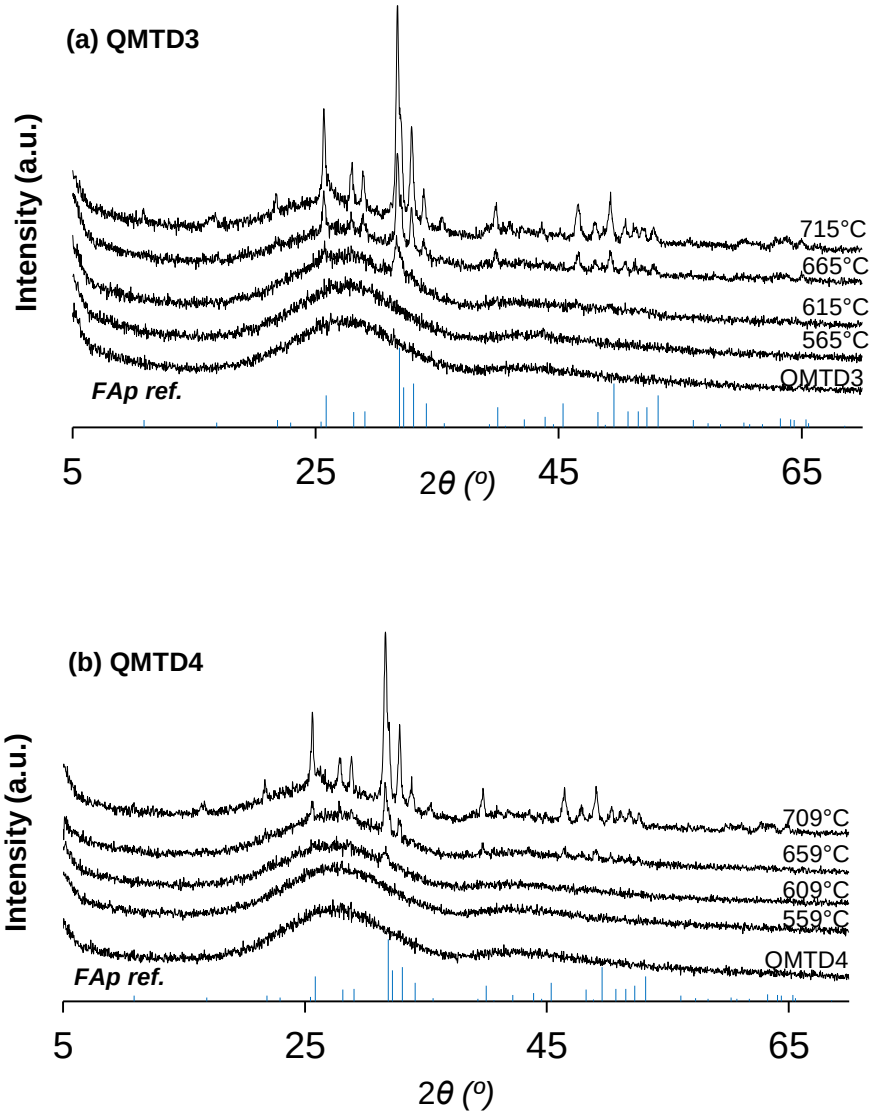

Figure 4.9: (a) XRD patterns of the 1.5 mol SrO FAp glass-ceramics (QMTD3) with FAp reference at the bottom (b) XRD patterns of the developed 2 mol SrO FAp glass-ceramics (QMTD4) with FAp reference at the bottom

4.1.5 Reducing X-ray Diffraction Angles with Increasing Strontium Content

Figure 4.91 shows that X-ray reflection 2-theta angles associated with FAp phases reduce linearly (R^2=0.98). The corresponding d-spacings calculated from 2-theta values for the (211) reflection increase with increasing strontium content. This validates that strontium ion is being incorporated into the crystal lattice upon heat-treatment with increasing strontium content in the nominal glass composition.

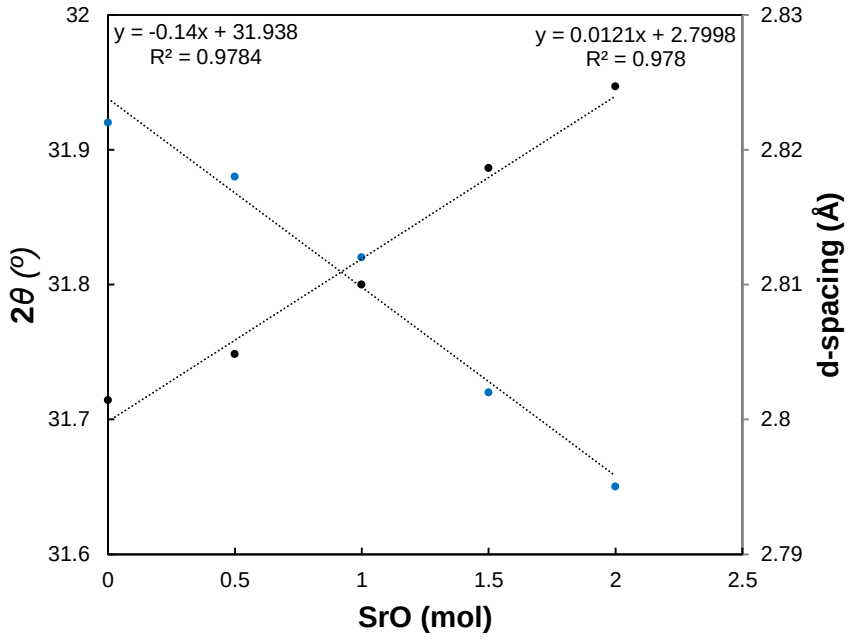

Figure 4.91: Effect of increasing SrO content on FAp reflection at (211) crystallographic plane and the corresponding d-spacing

4.1.6 ^{31}P MAS-NMR Analysis of the Developed Glass-Ceramics

Figure 4.92(a) shows ^{31}P MAS-NMR spectra of the as-synthesised glasses. All glasses show one distinctly observable phosphorus environment at

approximately -6 ppm, which corresponds to a pyrophosphate (Q^1) environment. Figures **4.92(b)** to **4.94(b)** show the development of apatite (at around 2.9 ppm) with increasing heat-treatment temperature. **Figure 4.95** shows chemical shifts (tabulated in **Table 4.2**) for apatite against SrO content in the nominal glass composition in moles. There is a linear (R^2=0.99) relationship between the SrO content and the chemical shift for apatite phases until SrO content reaches 2 moles.

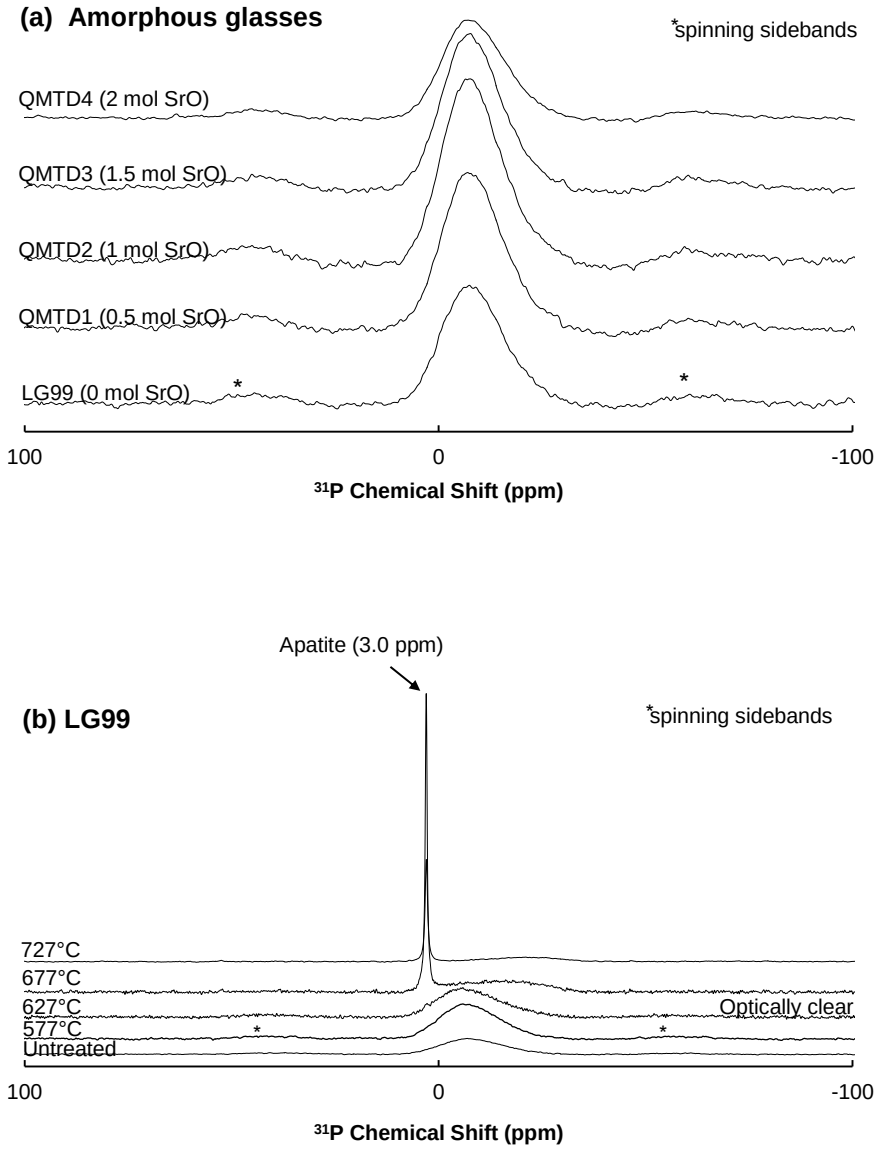

Figure 4.92: (a) ^{31}P MAS-NMR spectra of the as-synthesised glasses (b) ^{31}P MAS-NMR spectra of the unsubstituted FAp glass-ceramics (LG99, no SrO)

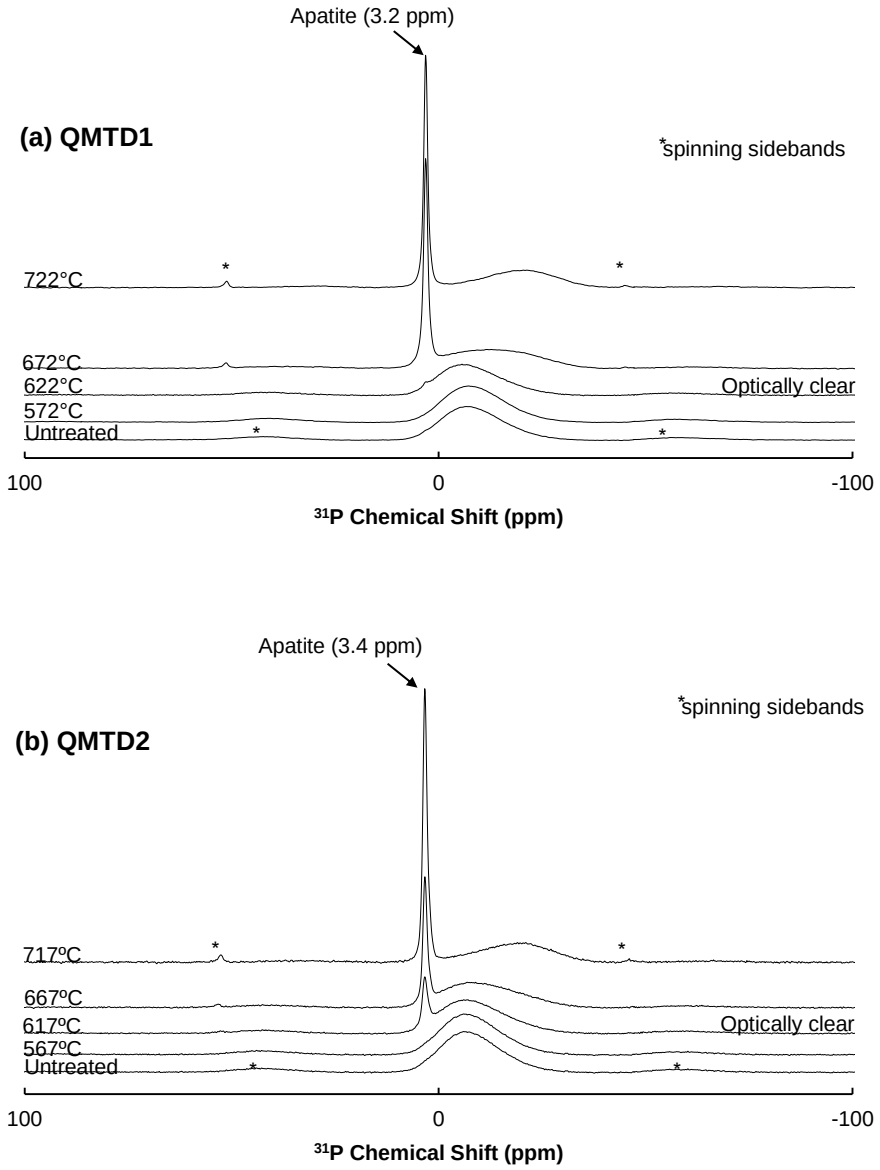

Figure 4.93: (a) ^{31}P MAS-NMR spectra of the strontium-substituted glass-ceramics (QMTD1, 0.5 mol SrO); (b) ^{31}P MAS-NMR spectra of the strontium-substituted glass-ceramics (QMTD2, 1 mol SrO)

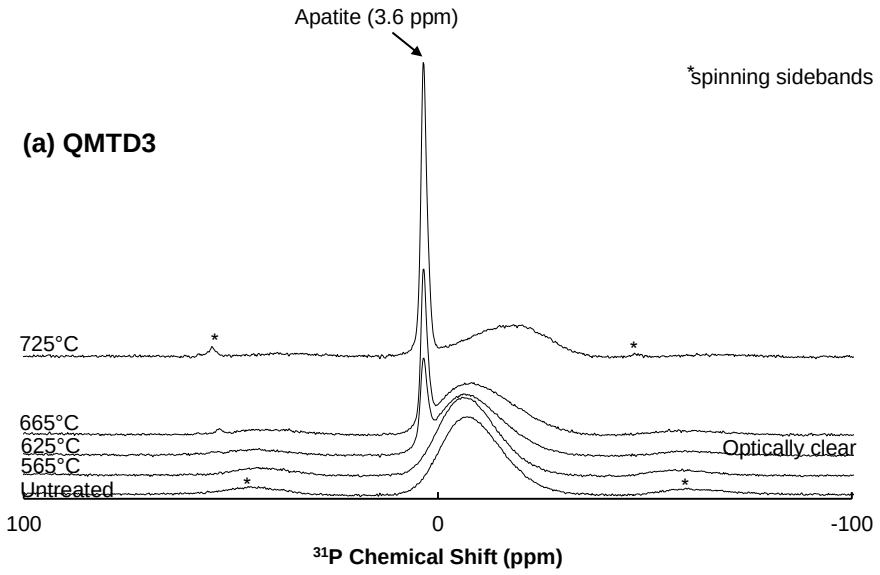

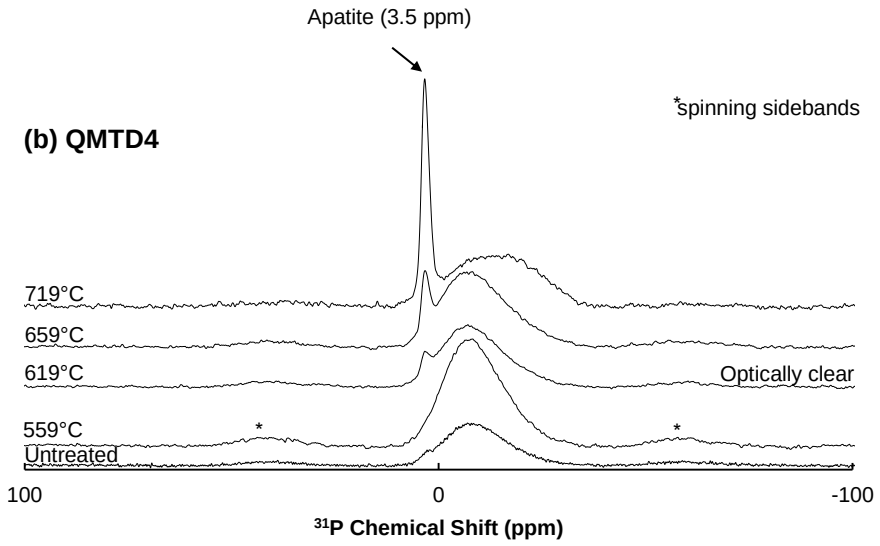

Figure 4.94: (a) ^{31}P MAS-NMR spectra of the strontium-substituted glass-ceramics (QMTD3, 1.5 mol SrO); (b) ^{31}P MAS-NMR spectra of the strontium-substituted glass-ceramics (QMTD4, 2 mol SrO)

Table 4.2: ^{31}P MAS-NMR chemical shift for FAp phases in the developed glass-ceramics

Glass Code	^{31}P MAS-NMR Chemical Shift (ppm)	Expected local environment	SrO Substitution (%)	SrO (moles)
LG99	2.98	P-Ca(4)	0	0
QMTD1	3.23	P-Ca(2)Sr(2)	25	0.5
QMTD2	3.43	P-CaSr(3)	50	1
QMTD3	3.59	P-Sr(4)	75	1.5
QMTD4	3.49	P-CaSr(3), P-Sr(4)	100	2
Synthetic FAp (Rothwell *et al*., 1980)	*2.8 ±0.2*			

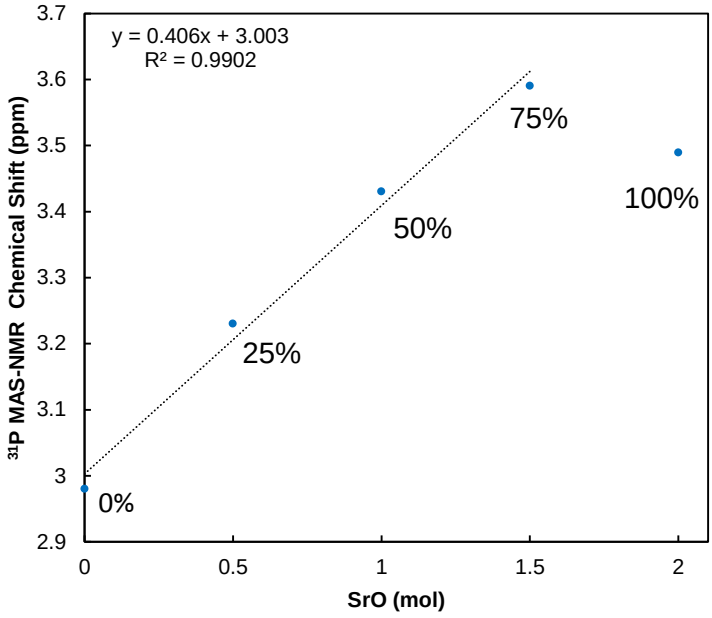

Figure 4.95: Effect of strontium content on ^{31}P MAS-NMR chemical shift in ppm assigned to apatite phases

4.1.7 ^{19}F MAS-NMR Analysis of the Amorphous Base Glasses and Developed Glass-Ceramics

Figure 4.96(a) shows ^{19}F MAS-NMR spectra of the as-synthesised glasses. All glasses show three broad peaks which can be assigned to three amorphous fluoride environments: first peak at around -90 ppm, second at around -125 ppm and third at around -150 ppm. The first peak seen at around -90 ppm can be assigned to F-Ca(n) (Zeng and Stebbins, 2000), the second peak seen at around 125 ppm may be assigned to Si-F-Ca(n) environment (Kiczenski and Stebbins, 2002) and the third peak seen at around -150 ppm can be assigned to Al-F-M(n) environment (Zeng and Stebbins, 2000). The proportion of these changes with increasing strontium content and it appears that increasing strontium content results in increased Si-F-M(n) speciation relative to F-M(n) and Al-F-M(n). **Figure 4.96(b)** shows ^{19}F MAS-NMR spectra of the LG99 developed glass-ceramics. It can be observed from **Figure 4.96(b)** that a peak at around -104 ppm which is assigned to FAp develops at T_g+100ºC and increases in intensity with increasing HT temperature. **Figure 4.97(a)** shows ^{19}F MAS-NMR spectra of the developed glass-ceramics with the lowest strontium substitution. It can be observed from **Figure 4.97(b)** that a peak at around -90 ppm, which is attributed to F-Ca(2)Sr in strontium-substituted FAp develops at T_g+100ºC in addition to F-Ca(3) at -104 ppm in FAp. The signals at -104 ppm and -90 ppm assigned to the fluoride ion in F-Ca(3) and F-Ca(2)Sr in FAp develop at T_g+100°C and increase in intensity with increasing heat-treatment temperature. **Figure 4.97(b)** shows ^{19}F MAS-NMR spectra of the developed QMTD2 (1 mol SrO) glass-ceramics. Two resonant peaks, one at around -

103 ppm and one at around -90 ppm assigned to fluoride ion in F-Ca(3) and F-Ca(2)Sr in FAp develop at T_g+100°C and increase in intensity with increasing temperature. In addition to this, a peak which can be assigned to crystalline Al-F-Ca(2) (Kiczenski and Stebbins, 2002) is also observed at around -147 ppm. **Figure 4.98(a)** shows ^{19}F MAS-NMR spectra of QMTD3 (1.5 mol SrO). Three fluoride environments are observable, one at -104 ppm and the other at -90 ppm assigned to fluoride in F-Ca(3) and F-Ca(2)Sr in FAp begins to develop at 659°C and increase in intensity. **Figure 4.98(b)** shows ^{19}F MAS-NMR spectra of QMTD4 (2 mol SrO). Four resonant peaks, one at -104 ppm, one at -90 ppm, one at around -70 ppm and -60 ppm and can be assigned to the fluoride ion in F-Ca(3), F-Ca(2)Sr, F-Sr(2)Ca and F-Sr(3) in FAp develop at 659°C and increase in intensity with increasing temperature.

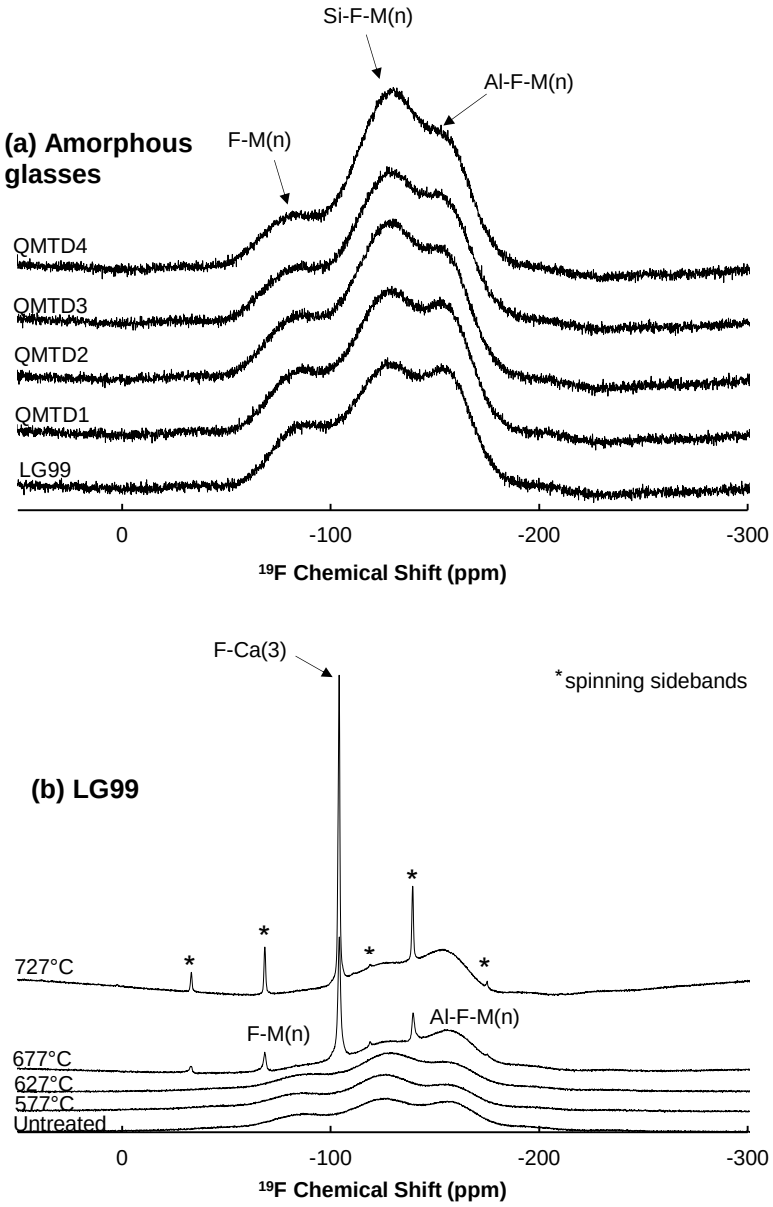

Figure 4.96: (a) ^{19}F MAS-NMR spectra of the as-synthesised untreated glasses (b) ^{19}F MAS-NMR spectra of the developed FAp glass-ceramics (0 mol SrO)

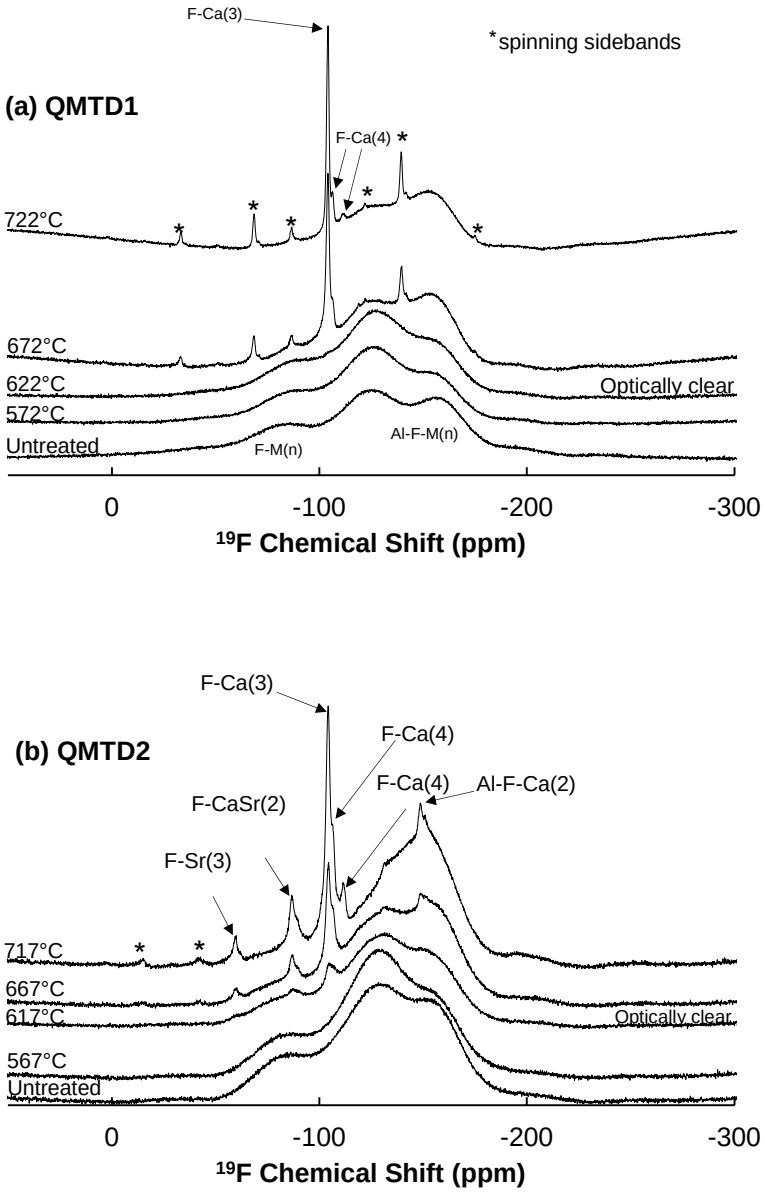

Figure 4.97: (a) ^{19}F MAS-NMR spectra of the developed FAp glass-ceramics (0.5 mol SrO (b) ^{19}F MAS-NMR spectra of the developed FAp glass-ceramics (1 mol SrO)

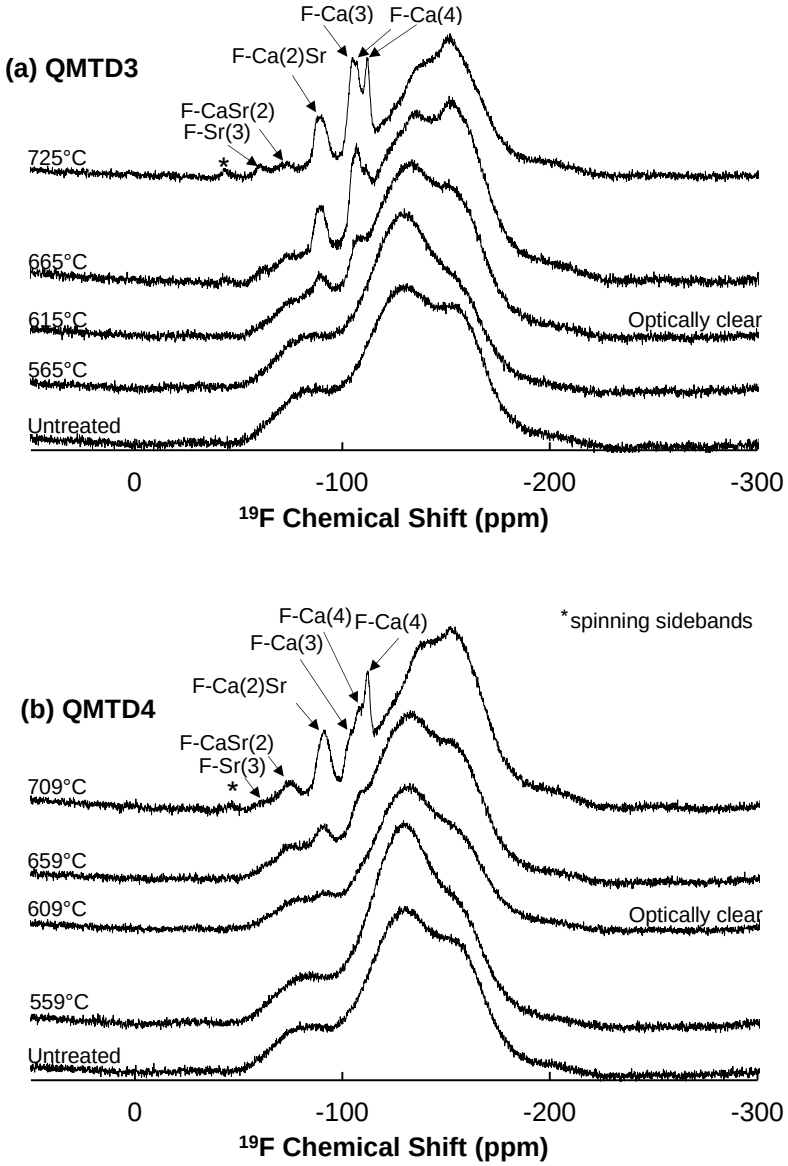

Figure 4.98: (a) ^{19}F MAS-NMR spectra of the developed FAp glass-ceramics (1.5 mol SrO) (b) ^{19}F MAS-NMR spectra of the developed FAp glass-ceramics (2 mol SrO)

4.1.8 TEM Analysis of the Developed Glass-Ceramics

Figure 4.99 shows one of the developed nanoscale glass-ceramics (QMTD3, heat-treated at 615ºC for 1h) which contains strontium-substituted FAp phases. TEM shows a fraction of the glass particle with dark needle-like crystallites within the amorphous glass matrix (dark gray).

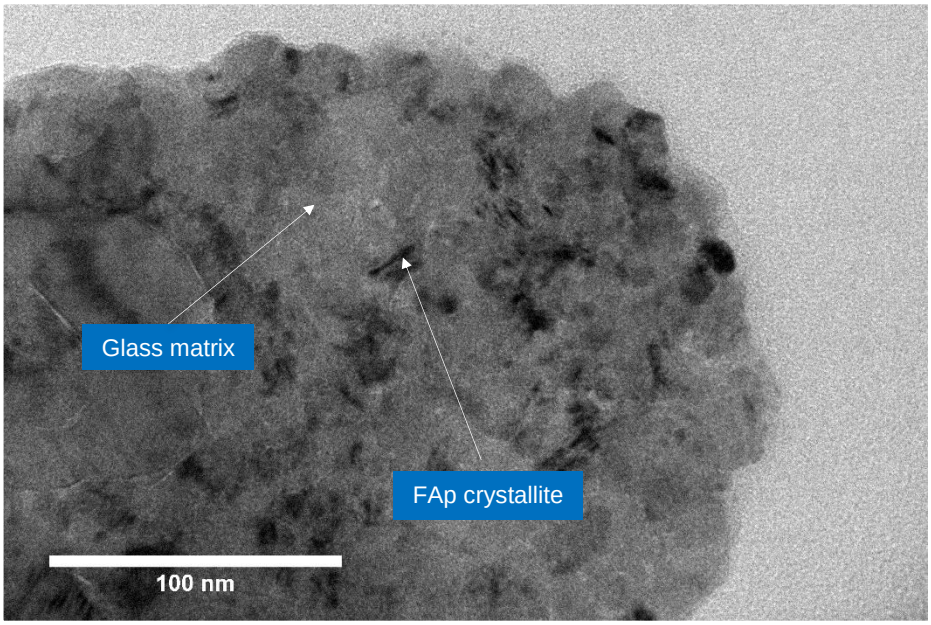

Figure 4.99: Transmission electron micrograph of a crushed glass particle showing need-like strontium-containing fluorapatite crystallites within the amorphous glass matrix

4.2 Discussion

All synthesised glasses were found to be amorphous by XRD (**Figure 4.7(a)**). **Figure 4.2** shows a linear (R^2=0.98) relationship between the T_g and strontium content. It is widely known that strontium-substituted glasses have properties, such as reduced glass transition temperature, more rapid dissolution and much higher reactivity which can be attributed to network expansion as a result of larger Sr^{2+} cation as compared to Ca^{2+}. This phenomenon is also observed in bioactive glasses, such as those studied by O'Donnell *et al*. (2010). Hill *et al*. (2004) and Hill *et al*. (2006) also showed that increasing strontium content substitution in GIC glasses does not result in any significant structural changes in fluoride speciation. Hill *et al*. (2004) showed that increasing strontium in glasses has an effect on crystallisation of FAp phases. It was reported by Hill *et al*. (2004) that increasing strontium content facilitates surface nucleation of apatite phases during the heat-treatment process, which may be attributed to lower lattice energy of $Sr_{10}(PO_4)_6F_2$ as compared to $Ca_{10}(PO_4)_6F_2$ (Flora *et al*. 2004) and suppressed amorphous phase separation as discussed in more detail in Chapter 1. Generally, the fluoride ion tends to preferentially bond to higher field strength cations, such as Ca^{2+} to form F-Ca(n) as opposed to F-Sr(n) species. It is notable that in the present study, FAp phases crystallise at the expense of F-M(n) species. It could be argued that F-M(n) species are present in the phase separated domains which thermodynamically favour bulk FAp crystallisation. Therefore, increasing strontium content may be suppressing the development of the domains that give rise to bulk crystallisation of FAp phases during the heat-treatment. Strontium-

substituted glasses may not phase separate into APS domains or phase separate into domains that are not close to FAp stoichiometry. XRD analysis shown in **Figure 4.91** shows that increasing strontium content results in increased strontium incorporation into the apatite lattice, which is consistent with a crystallography study conducted by O'Donnell *et al*. (2008) where it was showed through XRD analysis that apatite crystal lattice parameters, unit cell volume and density decreased linearly with increasing strontium content in the glasses studied. ^{31}P MAS-NMR results (**Figures 4.92(b)** to **4.94**) show that increasing heat-treatment temperature results in increased apatite crystallisation. **Figure 4.95** shows that ^{31}P resonance from the MAS-NMR experiment is increasing with increasing strontium content, which shows that strontium is being incorporated into the apatite lattice linearly until the substitution reaches 2 moles. At this point the chemical shift no longer exhibits a linear relationship with SrO content. This can be possibly explained by higher degree of disorder in the crystal lattice and Sr^{+2} preference to occupy Ca(I) sites instead of Ca(II) sites at high concentrations as previously suggested by Hill *et al*. (2006). This may result in the development of mixed P-CaSr(3) and P-Sr(4) local environments. All developed FAp glass-ceramics heat-treated at 50°C above the T_g were optically clear. Such fine scale apatite phases can also provide surfaces for apatite growth which is from a clinical perspective highly attractive because apatite-containing GCs in GICs can provide nucleation sites for the development of dentine-cement interfaces. It is known that GCs containing apatite facilitate development of apatite-based biological implant-bone interfaces. Kitsugi *et al*. (1989) showed that an apatite containing glass-ceramic can bond to bone. Similar finding were reported on the apatite-

mullite glass-ceramic by Freeman *et al*. (2003) and Goodrige *et al*. (2007). The ATR-FTIR results (**Figures 4.4-4.6**) are consistent with ^{31}P MAS-NMR results. The phosphate groups assigned to apatite increase in intensity with increasing heat-treatment temperature and broaden (**Figure 4.6(b)**) with increasing strontium content as a result of signal originating from mixed sites. ^{19}F MAS-NMR results from **Figures 4.95(b)** to **Figure 4.97** show the development of mixed apatite phases with increasing strontium content. Hill *at al*. (2006) and more recently Cho *et al*. (2008) showed that increasing strontium substitution in base glasses results in the development of mixed apatites during crystallisation: F-Ca(2)Sr, F-Sr(2)Ca and F-Sr(3) (Hill *et al*., 2006). Pan *et al*. (2009) reported that increasing strontium content in the apatite lattice can facilitate faster apatite nucleation and increased bioactivity of the material. FAp glass-ceramics developed in the present study also show mixed F-Ca(2)Sr and F-Sr(2)Ca phases. It is also notable that ^{19}F MAS-NMR peaks assigned to mixed Ca-Sr and Sr-only apatite species are quite broad as compared to F-Ca(3) species seen at around -103 ppm. Generally, broader peaks indicate a more disordered apatite structure. ^{19}F MAS-NMR analysis of the synthesised glasses shows that all glasses have three distinctly observable amorphous fluoride environments (**Figure 4.95(a)**). The first can be seen at around -87 ppm can be assigned to amorphous F-M(n) (Zeng and Stebbins, 2000) and the second seen at around -152.7 ppm can be assigned to amorphous Al-F-M(n) environment (Zeng and Stebbins, 2000). Kiczenski and Stebbins (2002) reported that the resonance signal seen at around -129.3 ppm in (ppm given in the original article −123.4; −128.7 and −134.5) is in Si-F-Ca(n)-type environment.

It is also notable that the peak seen at around -129.3 ppm (**Figure 4.95(a)**) in the present glasses increases in intensity with increasing strontium content relative to the intensities of F-M(n) and Al-F-M(n). On that basis, it could be assumed that the fluoride environment at -129.3 ppm is strongly influenced by increasing strontium content and it most likely corresponds to an increasing Si-F-Sr(n) environment. The peak at -129.3 ppm could also be F-M(n) and Al-F-M(n) with different n numbers or F-Al-O-P as proposed by Karpukhina *et al*. (manuscript in preparation). Karpukhina *et al*. (manuscript in preparation) report that in compositionally similar glasses reducing calcium content and increasing phosphorus content resulted in an increase in Al-F-Ca(n) and F-Al-O-P species. This is probably due to the lack of charge balancing cations to keep the fluoride ion in F-Ca(4) environment.

Samples treated at temperatures close to T_g have been observed to be optically clear and contain apatite phases. In 2012, Zainuddin *et al*. showed through MAS-NMR experiments that hydroxyapatite/fluorapatite additives in the Glass Carbomer® product are partially consumed during the setting reaction. This may result in reduced long-term bioactivity. Pure FAp phases are more acid resistant and less susceptible to acid consumption by PAA. Heat-treatments of the glasses just above the T_g known as glass annealing can reduce reactivity of the glasses and help to control setting characteristics as discussed by Wood and Hill (1991). Furthermore, strontium-substituted glasses tend to be more reactive due to a more disrupted network, therefore pre-treatment of strontium containing glasses may prolong working and setting times of the cement pastes.

4.3 Summary

The study shows that synthesised ionomer-type glasses with cement-forming ability can be developed into optically clear nanoscale FAp glass-ceramics. The study also provides evidence that increasing strontium content in the developed compositions results in reduced homogeneous crystallisation of FAp phases. It is possible to obtain mixed apatite phases when strontium is included in the nominal composition. Increasing strontium content in the nominal compositions resulted in a linear incorporation of strontium into the apatite lattice during the crystallisation step.

CHAPTER 5:

EFFECT OF METAL OXIDE FOR METAL FLUORIDE SUBSTITUTION ON THE STRUCTURE AND CRYSTALLISATION BEHAVIOUR OF SiO_2-Al_2O_3-P_2O_5-CaF_2/SrF_2-NaF GLASSES

5 Introduction

Fluoride is a very essential component in dental materials primarily due to its anticariogenic effect as a result of the sustained release. Sustained release of fluoride results in the formation of acid-resistant fluorapatite where OH^- ions found in the Ca(II) triangle are replaced by F^- ions which increase the apatite lattice energy and make the crystal less soluble and more acid-resistant. Fluoride is a powerful glass network disruptor and can influence several glass properties, such as glass solubility (Fathi *et al*., 2005a), glass transition temperature (Fathi *et al*., 2005b), crystallisation behaviour (Stanton and Hill, 2004) and optical properties (Gan *et al*., 1995). Solid-state ^{19}F MAS-NMR analysis of the fluoride-containing amorphous aluminosilicate glasses show that they can be highly complex and that the fluoride can exist in at least three different chemical environments (Zeng and Stebbins, 2000).

From an atomic perspective, fluoride as compared to oxygen has a higher nuclear charge and a smaller atomic radius which makes it the most reactive element in the periodic table. Furthermore, fluoride compared to oxygen only requires one electron to complete its outermost shell which from a structural point of view can increase interatomic spacings in the glass matrix provided the fluoride ions are acting as non-bringing oxygens. From an aesthetics perspective, fluoride components in glass compositions are also highly attractive because they can be used to lower the refractive index of the glasses used in dental GICs and reduce light scattering at the glass-polysalt interfaces once the cement is set. However, it is particularly difficult to synthesise glasses containing very high concentrations of fluoride due to fluoride volatilisation during melting as SiF_4 (Hill *et al*., 1999). To retain the maximum amount of fluoride in glass compositions containing high levels of

fluoride, such as those used in optical fibres and dental cements they are usually manufactured in a cold-top furnace. Any volatile species produced during the melting process quench once in contact with the cold-top and fall back into the molten glass.

The present study investigates the structural properties in compositions with significantly higher fluoride content and apatite crystallisation behaviour of three glasses of varying strontium content in the SiO_2-Al_2O_3-P_2O_5-CaF_2/SrF_2-NaF system manufactured in a cold-top furnace. In order to reduce the refractive index of the glasses, all CaO and SrO components were replaced by the respective fluoride components.

Objective of this part of thesis:

I. To synthesise and characterise glasses where CaO and SrO are substituted by the respective fluoride components.

5.1 Results

5.1.1 Differential Scanning Calorimetry

Figure 5.1(a) shows DSC traces of two particle sizes (frit<1 mm and powder <45 µm) for QMTD7 glass samples. The DSC trace for <45 µm powder shows increased area under the peak with a major exothermic reaction seen at around 788°C as compared to the frit sample of the same glass. **Figure 5.1(b)** shows DSC traces of two particle sizes (frit<1mm and powder <45µm) for QMTD8 glass samples. The DSC trace for <45µm powder shows an exothermic peak at around 735°C. Following two exothermic processes, another observable endothermic process takes place at around 861°C. **Figure 5.1(c)** shows DSC traces of two particle sizes (frit <1mm and powder

<45µm) for QMTD9 glass samples. The DSC trace for <45µm powder shows two observable exothermic processes, one at around 671°C and second at 739°C. Following two exothermic processes, an observable endothermic process takes place at around 857°C. The trace for the frit sample does not show any pronounced exothermic events compared to <45µm powder sample.

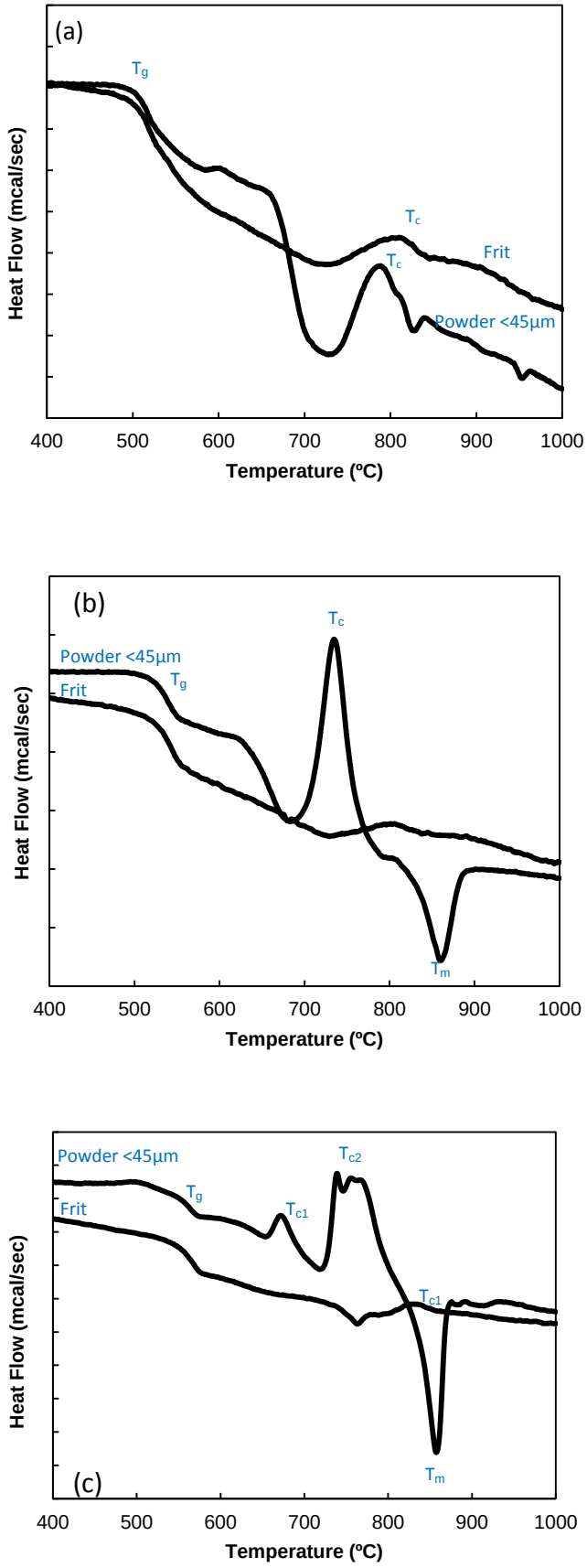

Figure 5.1: DSC traces of the manufactured glasses: (a) QMTD7: frit and powder <45µm (b) QMTD8: frit and powder <45µm and (c) QMTD9: frit and powder <45µm

Figure 5.2 shows glass the glass transition temperature as a percentage of strontium substitution in the nominal compositions. Quite surprisingly, there is a linear increase in T_g with increasing strontium content.

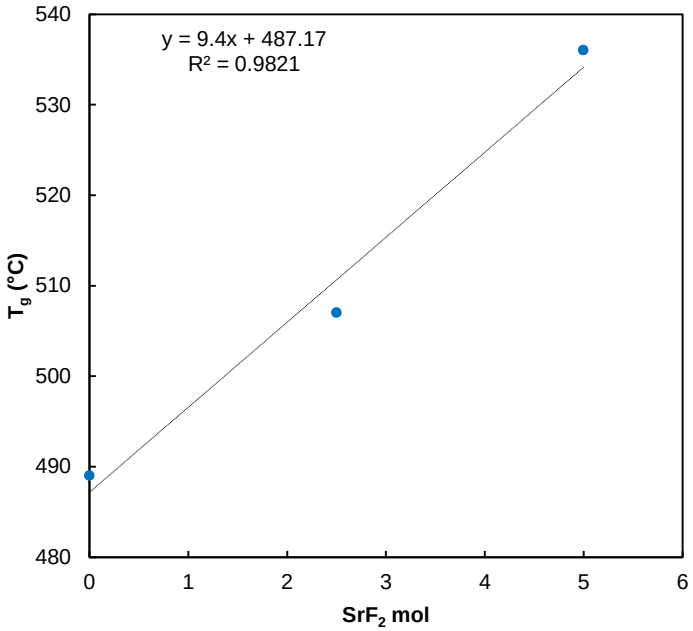

Figure 5.2: SrF_2 nominal strontium content (mol) and glass transition temperature (T_g)

Table 5.1 shows glass transition and glass crystallisation temperatures derived from the DSC traces.

Table 5.1 Glass transition temperatures (T_g) and crystallisation temperatures (T_{C1} and T_{C2}) extracted from the DSC traces

Glass Frit	T_{G1}	T_{C1}	T_{C2}	T_M
QMTD7	489	804	-	-
QMTD8	507	798	-	-
QMTD9	536	778	829	-

5.1.2 ^{27}Al MAS-NMR Analysis of the Manufactured Glasses

Figure 5.3 shows ^{27}Al spectra of the three base glasses. All glasses show three observable aluminium environments: Al-O(4) between 46-49 ppm, a broad shoulder peak at approximately 24 ppm, which corresponds to Al-O(5) and Al-O(6) at approximately -5 ppm.

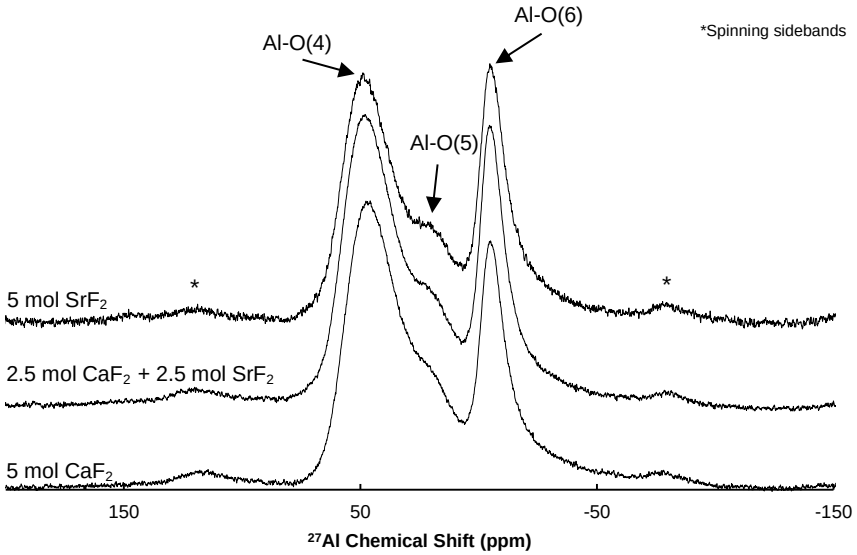

Figure 5.3: ^{27}Al MAS-NMR spectra of the high-phosphorus high-fluoride **glasses**

5.1.3 ^{31}P MAS-NMR Analysis of the Manufactured Glasses

Figure 5.4 shows ^{31}P MAS-NMR spectra of the industrially synthesised glasses. **Figure 5.4(a)** shows ^{31}P MAS-NMR spectra of clear and opaque fractions of the sample. The clear fraction of the all calcium glass shows two observable phosphorus environments, one at around -6.2 ppm and one at around -23 ppm which are both attributed to a pyrophosphate environment (Kirkpatrick and Brow, 1995; Fletcher *et al*., 1993). The opaque fraction of the same batch of glass shows an additional sharp peak at around 2.9 ppm which is attributed to apatite.

Figure 5.4(b) shows ^{31}P MAS-NMR spectra of clear and opaque fractions of the sample. The clear fraction of the equimolar calcium-strontium composition shows one well pronounced phosphorus environment at around -6.6 ppm and another hump at around -23 ppm which is also attributed to a pyrophosphate environment. The spectrum of the opaque fraction of the same sample shows a sharp peak at around 3.3 ppm which is attributed to strontium-substituted apatite. The pyrophosphate environment in the opaque fraction of the same sample is slightly moved to the negative side at around -7.9 ppm.

Figure 5.4(c) shows ^{31}P MAS-NMR spectra of clear and opaque fractions of the sample. The clear fraction of the all strontium composition shows one observable phosphorus environment at around -7.2 ppm. The pyrophosphate environment in the cloudy fraction of the same sample is slightly moved to a more negative side at around -7.9 ppm.

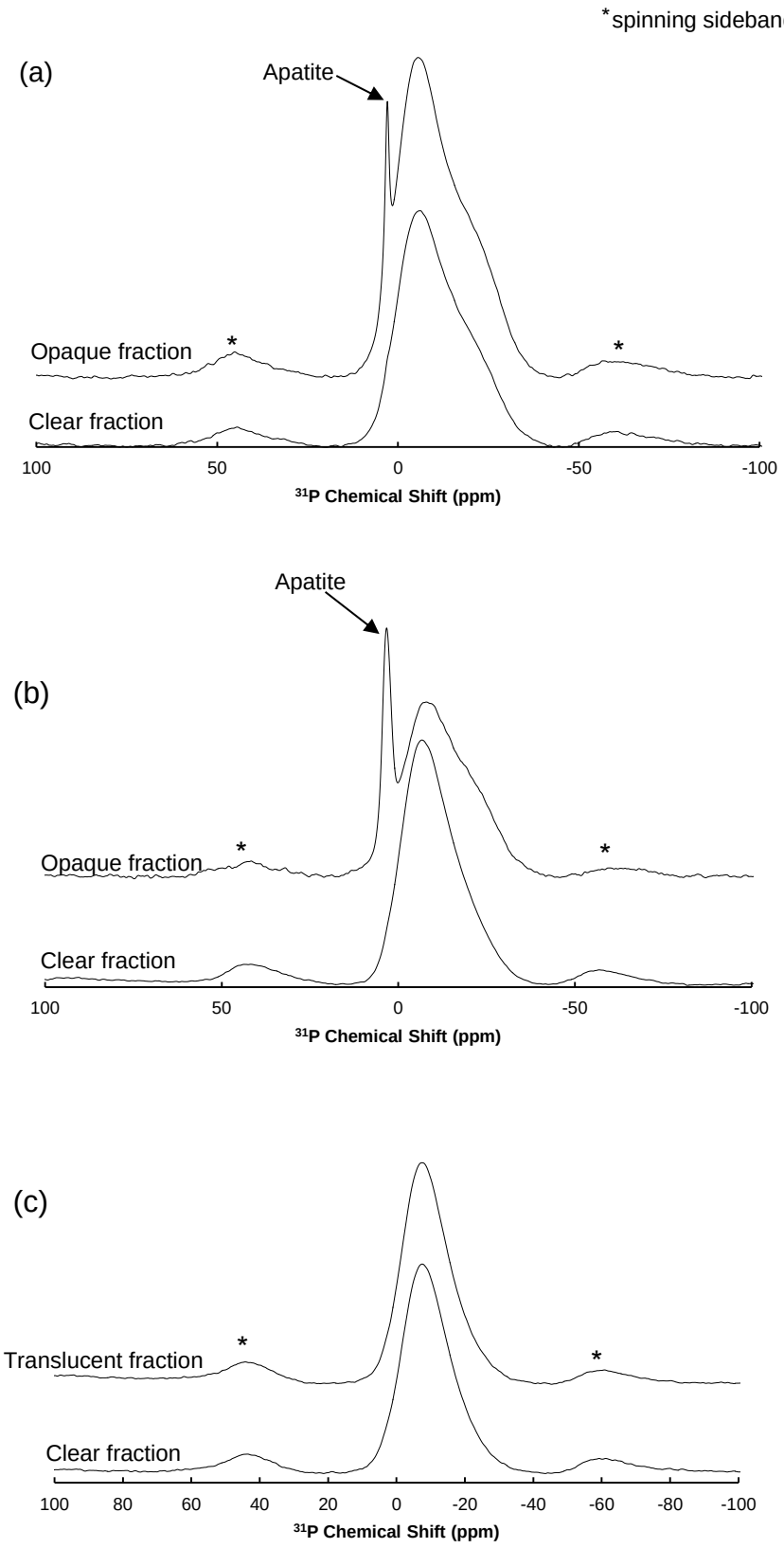

Figure 5.4: ^{31}P MAS-NMR spectra of (a) QMTD7 (Ca): clear fraction and opaque fraction; (b) QMTD8 (Ca-Sr): clear fraction and opaque fraction; (c) QMTD9 (Sr): clear fraction and cloudy fraction

5.1.4 ^{29}Si MAS-NMR Analysis of the Manufactured Glasses

Figure 5.5 shows ^{29}Si MAS-NMR spectra for the amorphous glasses in the high-phosphorus high-fluoride SiO_2-Al_2O_3-CaF_2/SrF_2-NaF system. All spectra show a single resolved peak at around -92 ppm which corresponds to a Q^4 silicate network with either 2 or 3 nearest neighbour 4-coordinate aluminium atoms with the exception of the composition fully substituted with SrF_2 where the chemical shift is slightly shifted towards the Q^3 environment.

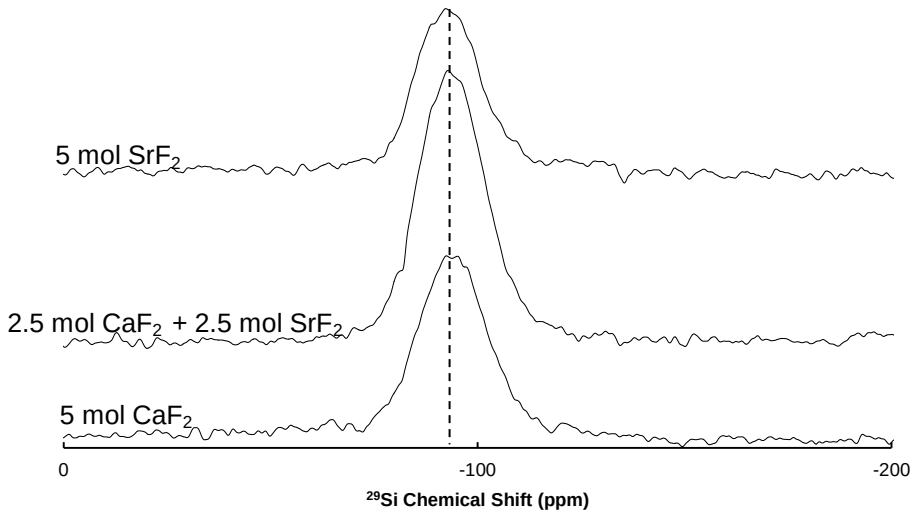

Figure 5.5: ^{29}Si MAS-NMR spectra of the glassed where CaO and SrO are fully substituted by the respective fluoride components

5.1.5 ^{19}F MAS-NMR Analysis of the Industrially Synthesised Glasses

Figure 5.6(a) shows ^{19}F MAS-NMR spectra for the full calcium composition: clear fraction and opaque fraction. Both, clear and opaque fractions show three district fluoride environments: F-Ca(n) at around -90 ppm, Al-F-Ca(n) at around -139 ppm (which may be overlapping with Si-F-Ca(n)) and Al-F-Na at around -187 ppm. Additionally, the opaque fraction of the all calcium

composition contains a relatively low intensity peak at -103 ppm which can be assigned to the fluoride ion in the F-Ca(3) environment in FAp. **Figure 5.6(b)** shows ^{19}F MAS-NMR spectra for the equimolar calcium-strontium glass composition: clear fraction and opaque fraction. Both, clear and opaque fractions show three observable fluoride environments: F-Ca(n) at around -90 ppm, Al-F-Ca(n) at around -138 ppm (which may be overlapping with Si-F-M(n)) and Al-F-Na(n) at around -189 ppm. Additionally, the opaque fraction of QMTD8 sample contains a relatively low intensity peaks at -75 ppm which can be assigned to fluoride ion in F-CaSr(2) environment in strontium-substituted FAp and a peak at around -91 ppm, which can be attributed to F-Ca(2)Sr environment in strontium substituted FAp. **Figure 5.6(c)** shows ^{19}F MAS-NMR spectra for the full strontium composition: clear fraction and opaque fraction. Both, clear and opaque fractions show three observable fluoride environments: F-Sr(n) at around -82 ppm, Al-F-Sr(n) at around -134 ppm (which may be overlapping with Si-F-Sr(n)) and Al-F-Na at around -187 ppm. ^{19}F MAS-NMR of cloudy fraction sample of the same glass does not how any significant differences.

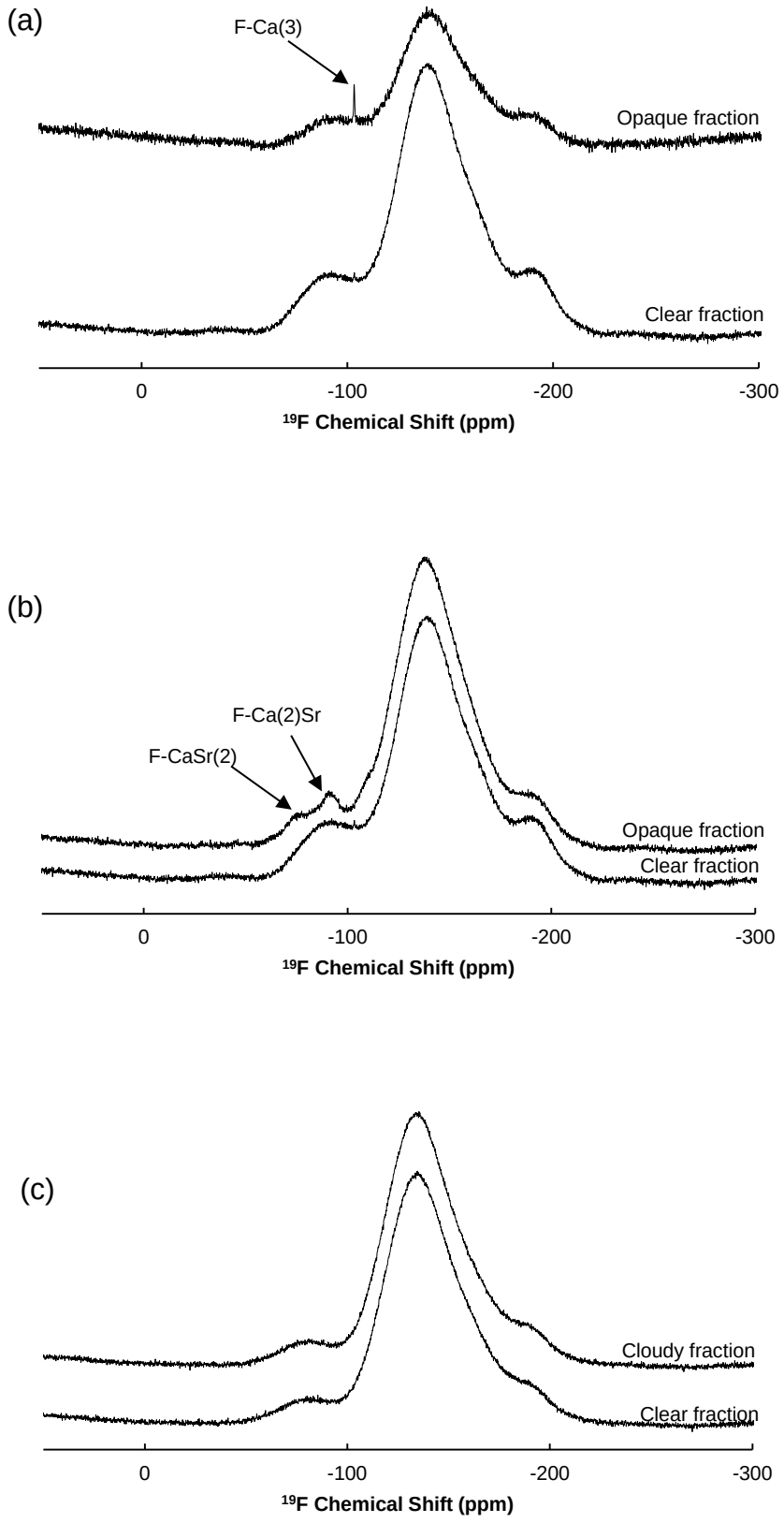

Figure 5.6: ^{19}F MAS-NMR spectra of (a) QMTD7 (Ca): clear fraction and opaque fraction; (b) QMTD8 (Ca-Sr): clear fraction and opaque fraction; (c) QMTD9 (Sr): clear fraction and cloudy fraction

5.1.6 XRD Analysis of the Manufactured Glasses

Figure 5.7(a) shows X-ray powder diffraction patterns of the full calcium glass composition: showing both, clear fraction and opaque fraction. X-ray diffraction pattern for both samples shows broad peaks with maximum intensity at around 27º 2θ corresponding to X-ray scattering from an amorphous material. X-ray diffraction pattern for the opaque fraction sample of the same glass shows XRD patterns which match to FAp. **Figure 5.7(b)** shows X-ray powder diffraction patterns of the equimolar calcium-strontium composition of both clear fraction and opaque fractions. XRD diffraction patterns for both samples shows broad peaks with a maximum intensity at around 27º 2θ corresponding to X-ray scattering from an amorphous material. X-ray diffraction pattern for the opaque fraction sample of the same glass shows characteristic XRD patterns for FAp. **Figure 5.7(c)** shows X-ray powder diffraction patterns of the fully strontium-substituted composition: showing spectra for both, the clear fraction and the opaque fraction of the same sample. X-ray diffraction patterns for both samples shows diffuse scattering which is a typical sign that the material is amorphous. X-ray diffraction pattern for the cloudy fraction sample is quite similar to the clear fraction pattern and does not show sharp peaks associated with crystalline phases.

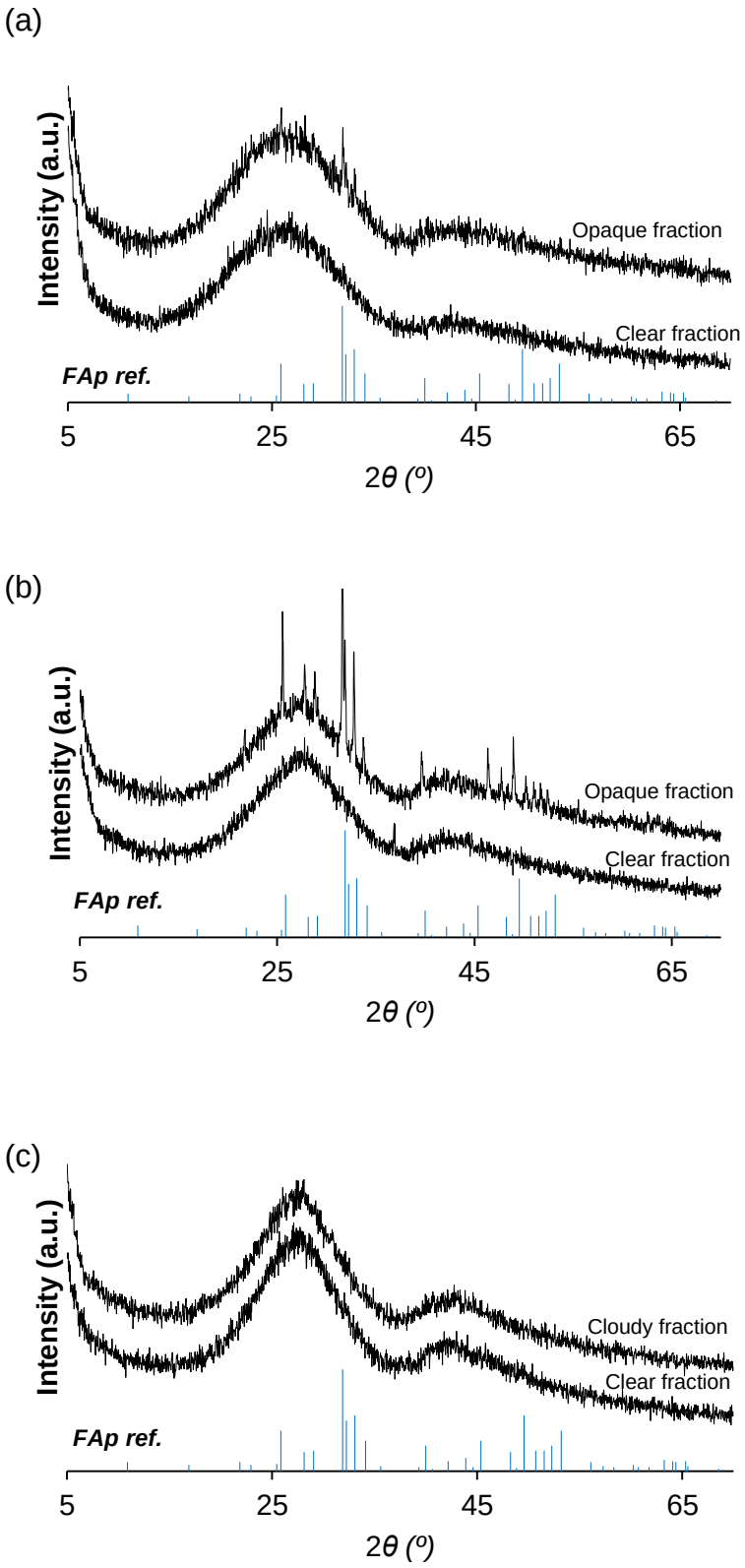

Figure 5.7: XRD patterns of (a) QMTD7: clear fraction and opaque fraction; (b) QMTD8: clear fraction and opaque fraction; (c) QMTD9: clear fraction and cloudy fraction

5.2 Discussion

It was found that a small fraction (approximately 15-20%) of the manufactured glass were either opaque or cloudy, which shows that all synthesised glasses require faster quenching rates to suppress crystallisation. It is essential to obtain initially amorphous glasses so that the subsequent crystallisation process can be controlled.

DSC analysis of the clear fraction of the synthesised glass samples shows an exothermic process at temperatures close to FAp crystallisation temperature. Split T_{C2} peaks observed in **Figure 5.1(c)** show crystallisation of phases at slightly different temperatures which may be due to broader particle size distribution or due to possible epitaxial crystal growth i.e. one crystal phase providing a nucleating surface for the crystallisation of the second phase. The FAp crystallisation temperature in the studied glasses is particle size dependent (**Figures 5.1(a)-5.1(c)**) which is typical of a system crystallising via surfaces. It can be seen from **Figure 5.2** that T_g is increasing with increasing strontium substitution in the nominal composition. This is quite contrary to the compositionally similar glasses discussed in Chapter III. This has never been reported in the literature and may be linked to structural aspects. Zainuddin (2009) showed some evidence that increasing strontium content in the fluoride-containing ionomer-type aluminosilicate glasses may result in an increase in Al-F-M(n) relative to F-M(n) species.

It is also notable that in the previous series of glasses discussed in Chapter III increasing strontium content results in an increased tendency of the

fluoride ion to coordinate in Si-F-M(n) environment which may also influence the T_g.

^{31}P MAS-NMR analysis of the opaque fraction of the manufactured glasses shows that glasses can readily crystallise to apatite phases. The ^{31}P MAS-NMR spectra shown in **Figure 5.4** show that all industrially manufactured glasses have a phosphorus environment at around -6.0 ppm which corresponds to a pyrophosphate environment (Kirkpatrick and Brow, 1995). In aluminium containing glasses phosphate charge balances aluminium and results in the formation of Q^1 pyrophosphate environment with Al-O-P linkages. The PO_4^{3-} cation has a higher overall electrostatic field strength as compared to SiO_4^{4-} therefore Al-O-P bonds are not as hydrolysable as bonds in the Al-O-Si structural unit. This may have some implications in the setting and the mechanical properties of the cements (discussed in Chapter 1). The formation of Al(VI) species can also be possibly avoided by faster quenching. Both calcium and calcium-strontium compositions show an observable shoulder peak at approximately -23.0 ppm which is close to Q^2 environment (Fletcher *et al*., 1993) and is not observable in the composition where CaF_2 is fully substituted by SrF_2. This can mean that phosphorus in the pyrophosphate region at around -23.0 ppm is probably charge balanced by a calcium cation. This amorphous environment is slightly more pronounced in the opaque fraction of the studied glass batches.

^{29}Si MAS-NMR analysis show that silicon in all three glasses is 4-coordinate with either 2 or 3 nearest neighbour 4-coordinate aluminium, which is consistent with compositionally similar Fuji II glasses studied by Pires *et al*. (2004). ^{27}Al MAS-NMR analysis of the amorphous glasses shows three observable aluminium environments: Al(IV), Al(V) and Al(VI). It is known that

Al^{3+} is released from Al(IV) species by hydrolysis. Recent studies have shown that Al^{3+} is consumed by the COO^- during the setting reaction and changes coordination to Al(VI) (Zainuddin *et al*., 2009). The glasses investigated in this study contain a large proportion of Al(IV) species which is a very good indication that the glasses can easily form cements. The ratio of Al(IV) to Al(VI) is considerably lower in the present glasses as compared to those used in commercial cement formulations, such as in Fuji IX studied by Munhoz *et al*. (2010) but can be potentially increased by introducing higher quenching rates during the glass manufacturing process.

X-ray powder diffraction analysis of the glasses (**Figure 5.7**) shows that a fraction of all calcium and mixed calcium-strontium compositions crystallised to apatites (reference used: ICDD 00-034-0011) on quenching with no evidence for other phases. ^{19}F MAS-NMR analysis confirmed this to be in the form of fluorapatite. This is consistent with a study by Hill *et al*. (2006) where investigators also found evidence for mixed calcium/strontium fluorapatites.

5.3 Summary

A fraction of the manufactured glasses crystallised to fluorapatite on quenching, which shows that the developed glasses can be easily developed into fluorapatite glass-ceramics, however they may require faster quenching to prevent crystallisation. Structural analysis of the manufactured glasses by multinuclear solid-state MAS-NMR revealed that they are structurally similar to the glassed used in commercial GICs. The all calcium compositions crystallised to calcium FAp and mixed Ca-Sr composition crystallised to strontium-substituted FAp.

CHAPTER 6: GENERAL DISCUSSION AND CONCLUSIONS

6.1 Predicting Refractive Index of Fluoride-Containing Glasses

The refractive index of the fluoride-containing bioactive glasses correlates linearly (R^2=0.99) with the metal fluoride content. The refractive index can also be predicted using the experimentally derived Appen factors for the metal fluoride components, which are quite close to the refractive indices of the fluoride-containing crystalline phases, such as CaF_2. Refractive indices of the more complex glasses used in dental glass ionomer cements, which contain alumina also show a linear relationship (R^2=0.98) with increasing fluoride content. The Appen factors for the ionomer glasses are somewhat different from fluoride-containing bioactive glasses and this probably reflects the more complex fluoride environment and the presence of species, such as Al-F-M(n). There is a considerable interest in remineralising dental materials and melt-derived bioactive glasses are particularly attractive for this application. Melt-derived bioactive glasses are relatively cheap to manufacture and are relatively simple to synthesize. The most common reason for dental restoration replacement is secondary caries (Lai and Li, 2012). To overcome this clinical problem research scientists have considered using bioactive glass fillers (Khvostenko *et al*., 2013) which can inhibit bacterial growth and also to help in remineralisation of demineralised dentine. White spot lesions is also a significant problem associated orthodontic treatments, which can be prevented by using orthodontic adhesives with a bioactive glass filler, such as those recently developed by Al-Eesa *et al*. (2018). Refractive indices of light-curable dental polymers are known (Fujita *et al*., 2005); however, refractive indices of bioactive glasses have not been studied until now. Results presented in Chapter 2 provide a

very useful tool which can be used to design multicomponent bioactive glass fillers with a refractive index tailored to match the refractive index of the polymer component. This is not only advantageous in terms of the aesthetics but also in terms of the depth of cure of the material (Fujita *et al*., 2005; Shorthall *et al*., 2008). Materials with low light scattering at the interfaces cure more efficiently. Poor depth of cure of the light-curable dental composites is quite often associated with a restoration failure. The dental glass ionomer cement, which has been in the clinical use for almost half a century is of even greater interest in dentistry because of the intrinsic ability to chemically bond to both organic and inorganic components of the tooth and clinically suitable mechanical properties. Therefore, from an engineering point of view being able to predict refractive index of the glasses used in GICs is quite empowering and provides a means by which highly aesthetic GICs and DCs can be developed.

6.2 Effect of Increasing Strontium Substitution on the Structure and Crystallisation Behaviour Behaviour of SiO_2-Al_2O_3-P_2O_5-CaO/SrO-CaF_2 Glasses

From a structural perspective, the developed glasses show a highly interesting tendency of the fluoride ion to preferentially coordinate in an environment at approximately -129.3 ppm with increasing strontium content. Kiczenski and Stebbins (2002) showed that the resonance signal in the as-synthesised amorphous glasses seen at around -129.3 ppm shown in **Figure 4.95(a)** may be attributed to Si-F-Ca(n) (ppm given in the original article −123.4; −128.7 and −134.5). Increasing intensities of the peak assigned to Si-F-Ca(n) as a function of strontium content indicates that in the presence of strontium, the fluoride ion preferentially forms the species which can be

assigned to Si-F-M(n) at around -129.3 as opposed to the Al-F-M(n) species. The results presented in Chapter 3 show that synthesised ionomer-type glasses can be developed into optically clear nanoscale FAp glass-ceramics by pre-treating the glasses at temperatures close to the glass transition temperature. The DSC analysis of the glasses shows that increasing strontium content in the developed compositions results in reduced homogeneous crystallisation of FAp phases, which is quite consistent with a study by Hill *et al*. (2004). Strontium is an essential component in GICs because strontium-substituted GICs exhibit clinically suitable radiopacity (Shahid *et al*., 2014) and there is some evidence that Sr^{2+} can also stimulate dentine regeneration. Therefore, glasses and glass-ceramics developed in this series could provide both, radiopactiy as well as bioactivity. Increasing strontium content in the nominal compositions resulted in a linear incorporation of Sr into the apatite lattice during the crystallisation step. This shows that apart from the changes in FAp crystallisation mechanism, strontium-substituted ionomer-type glasses can be developed into strontium-substituted FAp glass-ceramics.

6.3 Effect of Metal Oxide for Metal Fluoride Substitution on the Structure and Crystallisation Behaviour of SiO_2-Al_2O_3-P_2O_5-CaF_2/SrF_2-NaF Glasses

The refractive index of the glasses developed in the series discussed in Chapter 4 was successfully lowered by increasing the fluoride content, which validates the results presented in Chapter 2. A fraction of the manufactured glasses crystallised to FAp on quenching, which shows that formulated glasses rapidly crystallise and may require faster quenching. Structural

analysis of the manufactured glasses by multinuclear solid-state MAS-NMR revealed that they are structurally similar to the glasses discussed in Chapter 3 and those used in commercially available GICs, however contain a higher proportion of Al(VI), which can possibly be avoided by faster quenching. The full calcium composition crystallised to pure calcium FAp and equimolar Ca-Sr composition crystallised to a strontium-substituted FAp on quenching. The second series of the ionomer-type glasses shows a much lower T_g and refractive index, which is consistent with the higher metal fluoride content in the nominal glass compositions. All three glasses in the second series crystallised through surfaces, which can either be attributed to the fact that all glasses have higher network connectivity (due to lower non-bridging oxygen content) as compared to the glasses studied in Chapter 3 or that increasing strontium substitution may be supressing APS which was previously suggested by Hill *et al*. (2004) or a mixture of both.

6.4 Future Work

1. It would be interesting to measure the density of the glasses studied in Chapter II and see the influence of fluoride content.
2. Optimise cement properties (**Figure 6.1**), i.e. pre-treat one of the developed strontium-containing compositions close to T_g to produce nano FAp glass-ceramic, process pre-treated material into powder and use this to make a cement or use the pre-treated processed material as a remineralising cement component and then assess and optimise mechanical properties of the cements.

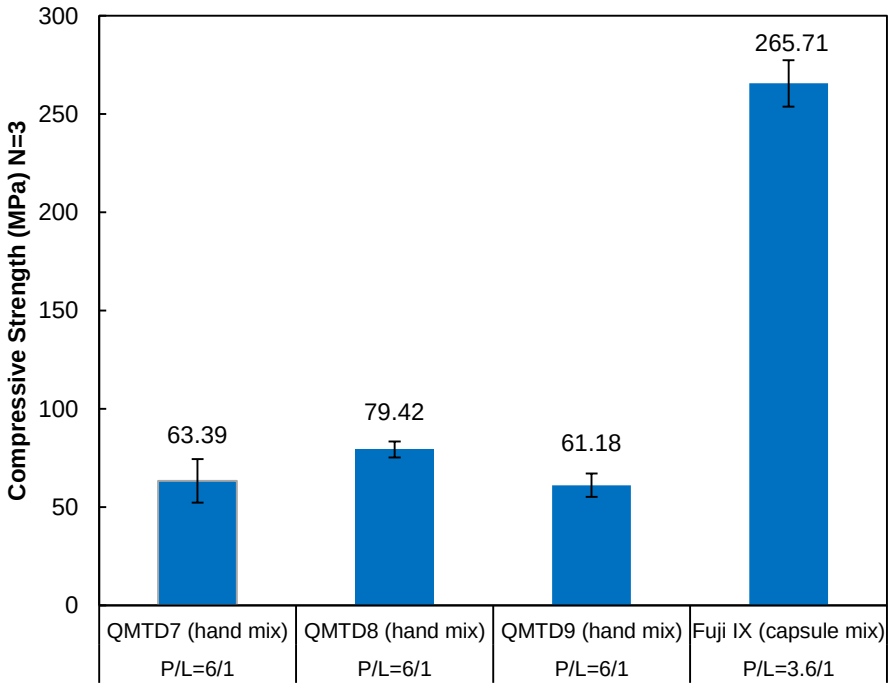

Figure 6.1: Preliminary results on the mechanical properties of the cements made using the untreated glasses discussed in Chapter IV with commercial Fuji IX used as a reference material

3. There is quite a lot of evidence in the scientific literature that FAp containing glass-ceramics can form apatite when exposed to physiological media such as artificial saliva and simulated body fluid, therefore performing apatite formation studies in this media might reveal whether the material is bioactive.
4. Reduction is bulk crystallisation with increasing strontium content may be a sign that glasses containing strontium do not phase separate into APS domains with FAp stoichiometry. It would be desirable to study amorphous phase separation of the synthesised glasses by neutron scattering in order to understand if there is a reduction in the size of the APS domains with increasing strontium content.

5. It would be also interesting to see if there are significant changes in silicon coordination with increasing strontium content which can be analysed by ^{29}Si MAS-NMR.
6. The identified Si-F-M(n) environment discussed in Chapter 3 could also be Al-F-M(n) and F-M(n) with different n numbers or F-Al-O-P species. ^{19}F-^{29}Si cross-polarisation MAS-NMR analysis on the synthesised glasses could further help to understand the environment at -129.3 ppm.

7.0 References

Al-Eesa, N. A., Johal, A., Hill, R.G. and Wong, F.S.L. (2018). "Fluoride containing bioactive glass composite for orthodontic adhesives - Apatite formation properties". Dental Materials, 34(8):1127-1133.

An, Y. H. and Draughn, R.A. (edts) (2000). Mechanical testing of bone and the bone-implant interface. Boca Raton, Florida, CRC Press.

Appen, A. A. (1974). Khimiia stekla. Khimiia, Leningrad. Leningradskoe Otdnie, p. 310-310.

Asmussen, E. (1983). "Opacity of glass-ionomer cements". Acta Odontologica Scandinavica, 41(3):155-157.

Bach, H. and Neuroth, N. (1998). The properties of optical glass, 2nd correction. Print edition. Berlin; New York: Springer.

Baig, M. S. and Fleming, G. J. (2015). "Conventional glass-ionomer materials: A review of the developments in glass powder, polyacid liquid and the strategies of reinforcement". Journal of Dentistry, 43(8):897-912.

Bannister, F. A. A. (1931). "Relation between the density and refractive index of silicate glasses, with application to the determination of imitation gemstones", Mineral Magazine, 22:136-154.

Benetti, A. R., Jacobsen, J., Lehnhoff, B., Momsen, N. C., Okhrimenko, D. V., Telling, M. T., Kardjilov, N., Strobl, M., Seydel, T., Manke, I. and Bordallo, H. N. (2015). "How mobile are protons in the structure of dental glass ionomer cements?". Scientific Reports, 5:8972.

Billington, R. W., Williams, J. A. and Pearson, G. J. (2006) Ion processes in glass ionomer cements. Journal of Dentistry, 34(8), 544-55.

Lynch, E., Brauer, D.S., Karpukhina, N., Gillam, D.G., Hill, R.G. (2012). "Multicomponent bioactive glasses of varying fluoride content for treating dentin hypersensitivity". Dental Materials, 28(2):168-178.

Blades, M., Moore D., P. Revell, P. and Hill R.G. (1998). "*In vivo* skeletal response and biomechanical assessment of two novel polyalkenoate cements following femoral implantation in the female New Zealand White rabbit". Journal of Materials Science: Materials in Medicine, 9(12): 701-706.

Blumenthal, N. C., Betts, F. and Posner, A.S. (1975). "Effect of carbonate and biological macromolecules on formation and properties of hydroxyapatite". Calcified Tissue Research 18(2): 81-90.

Bordallo, H., Aldridge, L., Fouquet, P., Pardo, L., Unruh, T., Wuttke, J. and Yokaichiya, F. (2009) "Hindered Water Motions in Hardened Cement Pastes Investigated over Broad Time and Length Scales. American Chemical Society, Applied Materials and Interfaces, 1(10), 2154-2162.

Brauer D., Al-Noaman, A., Hill, R.G. and Doweidar, H. (2011). “Density-structure correlations in fluoride-containing bioactive glasses”. Materials Chemistry and Physics 2011;130(1-2): 121-125.

Brauer D., Karpukhina N, Law R, and Hill, R.G. (2009) “Structure of fluoride-containing bioactive glasses”. Journal of Materials Chemistry, 19(31):5629-5636.

Cahn, J. W. (1969). "The Metastable Liquidus and Its Effect on Crystallisation Crystallisation of Glass”. Journal of the American Ceramic Society, 52(3):4.

Calver, A., R. G. Hill and A. Stamboulis (2004). "Influence of fluoride content on the crystallisation behavior of apatite-wollastonite glass-ceramics”. Journal of Materials Science, 39(7):2601-2603.

Carter, C. B. and Norton, M. G. (2007). Ceramic Materials: Science and Engineering. New York; London: Springer.

Chen, X., Brauer, D.S., Wilson, R.M., Hill, R.G. and Karpukhina, N. (2014a). "Bioactivity of sodium free fluoride containing glasses and glass-ceramics”. Materials, 7(8):5470-5487.

Chen, X., Brauer, D.S., Wilson R.M., Hill, R.G. and Karpukhina, N. (2014b). "Novel alkali free bioactive fluorapatite glass ceramics”. Journal of Non-Crystalline Solids, 402:172-177.

Chen, X., Hill R.G. and Karpukhina, N. (2014c). "Chlorapatite Glass-Ceramics”. International Journal of Applied Glass Science, 5(3):207-216.

Christie J., Pedone A., Menziani, M. and Tilocca A. (2012) Fluoride Environment in Bioactive Glasses: ab Initio Molecular Dynamics Simulations. Journal of Physical Chemistry, B115(9):2038-2045.

Clifford, A. and Hill, R.G. (1996). "Apatite-mullite glass-ceramics”. Journal of Non-Crystalline Solids, 196:346-351.

Clifford, A., Hill, R.G., Rafferty, A., Mooney, P., Wood, D., Samuneva, B. and Matsuya, S. (2001b). "The influence of calcium to phosphate ratio on the nucleation and crystallisation of apatite glass-ceramics”. Journal of Materials Science: Materials in Medicine, 12(5):461-469.

Clifford, A., Hill, R.G., Towler, M., and Wood, D. (2001a). "The crystallisation of glasses from the ternary CaF_2-$CaAl_2Si_2O_8$-P_2O_5 system”. Journal of Materials Science, 36(16):3955-3961.

Creanor, S., Carruthers, L., Saunders, L., Strang, R., and Foye, R. (1994). "Fluoride update and release characteristic of glass ionomer cements”. Caries Research, 28(5):322-328.

Crisp, S. and Wilson, A. (1974a). “Reactions in glass ionomer cements. 1. Decomposition of powder”. Journal of Dental Research, 53(6):1408-1413.

Crisp, S. and Wilson, A. (1974b). “Reactions in glass ionomer cements. 3. Precipitation reaction”. Journal of Dental Research, 53(6):1420-1424.

Crisp, S., Abel, G. and Wilson, A. (1979) Quantitative measurement of the opacity of aesthetic dental filling materials. Journal of Dental Research, 58(6):1585-1596.

Crisp, S., Ferner, A. J., Lewis, B. G. and Wilson, A. D. (1975a) Properties of improved glass-ionomer cement formulations. Journal of Dentistry, 3(3):125-30.

Crisp, S., Lewis, B. G. and Wilson, A. D. (1975b). “Conductometric titration of aqueous solutions of polyacrylic acid and its copolymers”. Journal of Dental Research, 54(6):1238.

Crisp, S., Lewis, B. G. and Wilson, A. D. (1975c). “Gelation of polyacrylic acid aqueous solutions and the measurement of viscosity”. Journal of Dental Research, 54(6):1173-1175.

Crisp, S., Pringuer, M., Wardlewo, D. and Wilson, A. (1974). “Reactions in glass ionomer cements. 2. Infrared spectroscopic study”. Journal of Dental Research, 53(6):1414-1419.

Darvell, B. (1990). “Uniaxial compression tests and the validity of indirect tensile-strength”. Journal of Materials Science, 25(2a):757-780.

De Aza, P.N., Luklinska, Z.B., Martinez, A., Anseau, M.R., Guitian, F. and De Aza., S. (2000). "Morphological and structural study of pseudowollastonite implants in bone”. Journal of Microscopy, 197(1):60-67.

De Barra, E. & Hill, R. G. (2000). “Influence of glass composition on the properties of glass polyalkenoate cements. Part III: influence of fluorite content”. Biomaterials, 21(6):563-9.

De Caluwe, T., C. Vercruysse, I. Ladik, R. Convents, H. Declercq, L. Martens and R. Verbeeck (2017). "Addition of bioactive glass to glass ionomer cements: Effect on the physico-chemical properties and biocompatibility”. Dental Materials 33(4):E186-E203.

De Caluwé, T., Vercruysse, C. W., Fraeyman, S. and Verbeeck, R. M. (2014). ”The influence of particle size and fluoride content of aluminosilicate glass on the glass ionomer cement properties”. Dental Materials, 30(9):1029-38.

Deloach, L., Payne, S., Chase, L., Smith, L., Kway, W., and Krupke, W. (1993). "Evaluation of absorption and emission properties of Yb^{3+} doped crystals for laser applications". Journal of Quantum Electronics, 29(4):1179-1191.

Deloach, L., Payne, S., L. Smith, Kway, W. and W. Krupke (1994). "Laser and spectroscopic properties of $Sr_5(PO_4)(_3)F$-Yb”. Journal of the Optical Society of America B-Optical Physics, 11(2): 269-276.

Denry, I., Holloway J. and Gupta, P. (2012). "Effect of crystallisation heat treatment on the microstructure of niobium-doped fluorapatite glass-ceramics". Journal of Biomedical Materials Research Part B-Applied Biomaterials, 100B(5):1198-1205.

Donald, I., Metcalfe, B., Fong, S., Gerrard, L., Strachan, D. and Scheele, R. (2007). "A glass-encapsulated calcium phosphate waste form for the immobilization of actinide-, fluoride-, and chloride-containing radioactive wastes from the pyrochemical reprocessing of plutonium metal". Journal of Nuclear Materials, 361(1):78-93.

Doyle, W. M. (1992). Principles and Applications of Fourier Transform Infrared (FTIR) Process Analysis, Technical Note AN–906 Rev.

Dowling, A. H. & Fleming, G. J. (2011). "Can poly(acrylic) acid molecular weight mixtures improve the compressive fracture strength and elastic modulus of a glass-ionomer restorative?". Dental Materials, 27(11):1170-9.

Dowling, A., Fleming, G., McGinley, E. and Addison, O. (2012a). "Improving the standard of the standard for glass ionomers: An alternative to the compressive fracture strength test for consideration?". Journal of Dentistry, 40(3):189-201.

Dowling, A., Fleming, G., McGinley, E. & Addison, O. (2012b). "Improving the standard of the standard for glass ionomers: An alternative to the compressive fracture strength test for consideration?". Journal of Dentistry, 40(3):189-201.

Ducheyne, P., Healy, K.E., Grainger, D.W., Hutmacher, D.W. and Kirkpatrick, C.J. (2011). Comprehensive biomaterials, Elsevier.

Duer, M. J. (2004) Introduction to solid-state NMR spectroscopy. Oxford: Blackwell.

Dupree, R., Holland, D., Mortuza, M., Collins, J. and Lockyer, M. (1989). "Magic angle spinning nmr of alkali phospho alumino silicate-glasses". Journal of Non-crystalline solids, 112(1-3):111-119.

Elliott, J. C. and R. A. Young (1967). "Conversion of Single Crystals of Chlorapatite into Single Crystals of Hydroxyapatite". Nature Letters, 214(5091):904-906.

Fang, Y., Ritter, C. and T. White (2014). "Crystal chemical characteristics of ellestadite-type apatite: implications for toxic metal immobilization". Dalton Transactions, 43(42):16031-16043.

Fathi, H., Johnson, A., van Noort, R. and Ward, J.M. (2005). "The influence of calcium fluoride (CaF_2) on biaxial flexural strength of apatite-mullite glass-ceramic materials". Dental Materials, 21(9):846-851.

Fathi, H., A. Johnson, R. van Noort, J. M. Ward and I. M. Brook (2005). "The effect of calcium fluoride (CaF_2) on the chemical solubility of an apatite-mullite glass-ceramic material". Dental Materials, 21(6):551-556.

Featherstone, J. (1999). "Prevention and reversal of dental caries: role of low level fluoride". Community Dentistry and Oral Epidemiology, 27(1):31-40.

Fechtelkord, M., Behrens, H., Holtz, F., Fyfe, C., Groat, L. and Raudsepp, M. (2003). "Influence of F content on the composition of Al-rich synthetic

phlogopite: Part 1. New information on structure and phase-formation from ^{29}Si, ^{1}H, and ^{19}F MAS NMR spectroscopies". American Mineralogist, 88(1):47-53.

Fennell, B. and Hill, R.G. (2001a). "The influence of poly(acrylic acid) molar mass and concentration on the properties of polyalkenoate cements – Part II Young's modulus and flexural strength". Journal of Materials Science, 36(21):5177-5183.

Fennell, B. and Hill, R.G. (2001b). "The influence of poly(acrylic acid) molar mass and concentration on the properties of polyalkenoate cements – Part III – Fracture toughness and toughness". Journal of Materials Science, 36(21):5185-5192.

Fennell, B. & Hill, R. (2001c) The influence of poly(acrylic acid) molar mass and concentration on the properties of polyalkenoate cements Part I – Compressive strength. Journal of Materials Science, 36(21):5193-5202.

Filho, O. P., Latorre, G.P. and Hench L.L. (1996). "Effect of crystallisation on apatite-layer formation of bioactive glass 45S5". Journal of Biomedical Materials Research, 30(4):509-514.

Filiaggi, M. J., Coombs, N.A. and Pilliar, R.M. (1991). "Characterisationof the interface in the plasma-sprayed HA coating/Ti-6Al-4V implant system". Journal of Biomedical Materials Research, 25(10):1211-1229.

Fleming, G., Dowling, A. & Addison, O. (2012). "The crushing truth about glass ionomer restoratives: Exposing the standard of the standard". Journal of Dentistry, 40(3):181-188.

Fletcher, J. P., Kirkpatrick, R.J., Howell, D. and Risbud, S.H. (1993). "^{31}P Magic-angle spinning nuclear magnetic resonance spectroscopy of calcium phosphate glasses". Journal of the Chemical Society, Faraday Transactions, 89(17):3297-3299.

Flora, N. J., Yonder, C.H., Jenkins, H.D.B (2004). "Lattice Energies of Apatites and the Estimation of $\Delta Hf°(PO_4^{3-}, g)$". Inorganic Chemistry, 43(7): 2340-2345.

Freeman, C. O., Brook, I.M., Johnson, A., Hatton, P.V., Hill, R.G. and Stanton, K.T. (2003). "Crystallisation modifies osteoconductivity in an apatite-mullite glass-ceramic". Journal of Materials Science: Materials in Medicine, 14(11):985-990.

Fujita, K., Nishiyama, N., Nemoto, K., Okada, T. and Ikemi, T. (2005). "Effect of base monomer's refractive index on curing depth and polymerization conversion of photo-cured resin composites". Dental Materials Journal, 24(3):403-408.

Gan, F. (1995). "Optical properties of fluoride glasses - a review". Journal of Non-Crystalline Solids, 184:9-20.

Gentleman, E., Fredholm, Y.C., Jell, G., Lotfibakhshaiesh, N., O'Donnell, M.D., Hill, R.G. and Stevens, M.M. (2010). "The effects of strontium-

substituted bioactive glasses on osteoblasts and osteoclasts in vitro". Biomaterials, 31(14): 3949-3956.

Goodridge, R. D., Wood, D.J., Ohtsuki, C. and Dalgarno, K.W. (2007). "Biological evaluation of an apatite-mullite glass-ceramic produced via selective laser sintering". Acta Biomaterialia, 3(2): 221-231.

Griffin, S.G. and Hill, R.G. (1999). Influence of glass composition on the properties of glass polyalkenoate cements. Part I: influence of aluminium to silicon ratio. Biomaterials, 20(17):1579-1586.

Griffin, S. G. and Hill, R.G. (2000a). Influence of glass composition on the properties of glass polyalkenoate cements. Part II: influence of phosphate content. Biomaterials, 21(4):399-403.

Griffin, S. G. and Hill, R.G. (2000b). Influence of glass composition on the properties of glass polyalkenoate cements. Part IV: influence of fluoride content. Biomaterials, 21(7):693-698.

Grossman, D.G. (1972). 'Machinable glass-ceramics based on tetrasilicic mica', Journal of American Ceramic Society, 55(9):446-449.

Hadis, M.A., Choong., N, Morrell A, Martin, R.A, Shelton, R.M, Palin, W.M. (2016). "Decreasing glass refractive index for development of light-curable bioactive composites". Dental Materials 32S:e21–e22.

Hadis, M.A., Tomlins, P.H., Shortall, A.C., Palin, W.M. (2010). Dynamic monitoring of refractive index change through photoactive resins. Dental Materials, 26(11):1106-1112.

Hench, L.L., Spilman, D.B., and Hench, J.W. (1988). Fluoride-containing Bioglass™ compositions, US Patent: 4775646. University of Florida.

Sanders., D.M., Pearson., W.B., Hench, L.L. (1974). "Quantitative Analysis of Glass Structure with the Use of Infrared Reflection Spectra". Applied Spectroscopy, 28(3):247-255.

Hill, R.G., Wood, D. and Thomas, M. (1993). "Trimethylsilylation analysis of the silicate structure of fluoro-alumino-silicate glasses and the structural role of fluoride". Journal of Materials Science, 1999;34(8):1767-1774.

Hill, R. and D. Wood (1995). "Apatite-mullite glass-ceramics". Journal of Materials Science: Materials in Medicine, 6(6):311-318.

Hill, R. G., Calver, A., Skinner, S., Stamboulis, A. and Law, R.V. (2006). "A MAS-NMR and Combined Rietveldt Study of Mixed Calcium/Strontium Fluorapatite Glass-Ceramics". Key Engineering Materials, 309:305-308.

Hill, R. G., Stamboulis A., and Law, R.V. (2006). "Characterisationof fluoride containing glasses by ^{19}F, ^{27}Al, ^{29}Si and ^{31}P MAS-NMR spectroscopy". Journal of Dentistry, 34(8):525-532.

Hill, R. G., Stamboulis, A., Law, R.V., Clifford, A., Towler, M.R., and Crowley, C. (2004). "The influence of strontium substitution in fluorapatite glasses and glass-ceramics". Journal of Non-Crystalline Solids, 336(3):223-229.

Hill, R. G., O'Donnell, M.D., Law, R.V., Karpukhina, N., Cochrane, B., and Tulyaganov, D.U. (2010). "The early stages of nucleation and crystallisation of an apatite glass-ceramic: Evidence for nano-scale crystallisation". Journal of Non-Crystalline Solids, 356(52-54):2935-2941.

Hill, R.G., Stamboulis, A. and Law, R. V. (2006a). "Characterisation of fluoride containing glasses by ^{19}F, ^{27}Al, ^{29}Si and ^{31}P MAS-NMR spectroscopy". Journal of Dentistry, 34(8):525-32.

Hill, R.G., Stamboulis, A. and Law, R. V. (2006b) Characterisation of fluoride containing glasses by ^{19}F, ^{27}Al, ^{29}Si and ^{31}P MAS-NMR spectroscopy. Journal of Dentistry, 34(8):525-32.

Hill, R.G., Calver, A., Stamboulis, A., and Bubb, N. (2007). "Real-time nucleation and crystallisation studies of a fluorapatite glass-ceramics using small-angle neutron scattering and neutron diffraction". Journal of the American Ceramic Society, 90(3):763-768.

Hill, R., A. Rafferty, P. Mooney and D. Wood (2000). "The influence of glass composition on nucleation crystallisation microstructure and properties of apatite-mullite glass-ceramics". Glass Science and Technology: Glastechnische Berichte, 73(1(C)):146-153.

Hill, R.G., Stamboulis, A., Law, R.V., Clifford, A., Towler, M., and Crowley, C. (2004). "The influence of strontium substitution in fluorapatite glasses and glass-ceramics". Journal of Non-Crystalline Solids, 336(3): 223-229.

Hill, R.G., Wood, D. and Thomas, M. (1999). "Trimethylsilylation analysis of the silicate structure of fluoro-alumino-silicate glasses and the structural role of fluoride". Journal of Materials Science, 34(8):1767-1774.

Hill, R.G., Patel, M., and Wood, D.J. (1991). "Preliminary Studies on Castable Apatite-Mullite Glass-Ceramics". 4th International Symposium on Ceramics in Medicine, London, Butterworth Heineman Ltd.

Höland, W., and Beall, G.H. (2012). Glass-ceramic technology. Hoboken, New Jersey Westerville, Ohio, Wiley; The American Ceramic Society.

Höland, W., and Rheinberger, V., (2008). Dental glass-ceramics. Bioceramics and their Clinical Applications. Cambridge, England, Woodhead Publishing Limited, p. 561.

Höland, W., Schweiger, M., Dittmer, M., and Ritzberger, C. (2015). "Radiopaque Strontium Fluoroapatite Glass-Ceramics". Frontiers in Bioengineering and Biotechnology, 3:149.

Höland, W., Rheinberger, V., Wegner, S., and Frank, M., (2000). "Needle-like apatite-leucite glass-ceramic as a base material for the veneering of metal restorations in dentistry". Journal of Materials Science Materials in Medicine,11(1):11-17.

Hopkins, R. H., Damon, D.H., Piotrowski, P., Walker, M.S. and Uphoff, J.H. (1971). "Thermal Properties of Synthetic Fluorapatite Crystals". Journal of Applied Physics, 42(1):272-275.

Huang, M., R. G. Hill and S. C. Rawlinson (2016). "Strontium (Sr) elicits odontogenic differentiation of human dental pulp stem cells (hDPSCs): A therapeutic role for Sr in dentine repair?" Acta Biomaterialia, 38:201-2011.

James, P. (1981). "Nucleation in glass forming systems - a review". American Ceramic Society Bulletin, 60(3):352-352.

Karageorgiou, V. and Kaplan D. (2005). "Porosity of 3D biomaterial scaffolds and osteogenesis". Biomaterials, 26(27): 5474-5491.

Karpukhina, N, Law, R.V. and Hill, R.G. (unpublished). The structure of fluor-phosph-alumino-silicate glasses. Manuscript in preparation.

Karpukhina, N, Law, R.V. and Hill, R.G. (2014). Crystallisation in oxide glasses – a tutorial review. Chemical Society Reviews, 2014(43):2174-2186.

Kendall, K. (1978). Complexities of compression failure. Proceedings of the Royal Society of London Series[a] Mathematical Physical and Engineering Sciences, 361(1705):245-263.

Khvostenko, D., Mitchell, J.C., Hilton, T.J., Ferracane J.L. and Kruzic, J.J. (2013). "Mechanical performance of novel bioactive glass containing dental restorative composites". Dental Materials, 29(11):1139-1148.

Kiczenski, T.J. and Stebbins, J.F. (2002). "Fluoride sites in calcium and barium oxyfluorides: ^{19}F NMR on crystalline model compounds and glasses". Journal of Non-Crystalline Solids, 306(2): 160-168.

Kirkpatrick, R. J. and R. K. Brow (1995). "Nuclear magnetic resonance investigation of the structures of phosphate and phosphate-containing glasses: a review". Solid State Nuclear Magnetic Resonance, 5(1):9-21.

Kitsugi, T., T. Yamamuro and T. Kokubo (1989). "Bonding behavior of a glass-ceramic containing apatite and wollastonite in segmental replacement of the rabbit tibia under load-bearing conditions". Journal of Bone and Joint Surgery-American Volume, 71A(2):264-272.

Kitsugi, T., T. Yamamuro and T. Kokubo (1990). "Analysis of A.W glass-ceramic surface by micro-beam X-ray-diffraction". Journal of Biomedical Materials Research, 24(2):259-273.

Kitsugi, T., Yamamuro, T., and Kokubo, T (1989). "Bonding behaviour of a glass-ceramic containing apatite and wollastonite in segmental replacement of the rabbit tibia under load-bearing conditions". Journal of Bone and Joint Surgery-American Volume, 71A(2):264-272.

Kokubo, T. (2008). Bioactive glass-ceramics. Bioceramics and their clinical applications. T. Kokubo. Cambridge, England, Woodhead Publishing Limited, p. 288-289.

Kokubo, T., Kushitani, H., Ohtsuki, C., Sakka, S., and Yamamuro, T.(1992). "Chemical-reaction of bioactive glass and glass-ceramics with a simulated body-fluid". Journal of Materials Science-Materials in Medicine, 3(2):79-83.

Kokubo, T., Kushitani, H., Sakka, S., Kitsugi, T. and Yamamuro, T. (1990). "Solutions able to reproduce in vivo surface-structure changes in bioactive glass-ceramic A-W". Journal of Biomedical Materials Research, 24(6):721-734.

Kokubo, T., Shigematsu, M., Nagashima, Y., Tashiro, M., Nakamura, T., Yamamuro, T and Higashi, S. (1982). "Apatite- and Wollastonite-Containg Glass-Ceramics for Prosthetic Application". Bulletin of the Institute for Chemical Research, Kyoto University, 60(3-4):260-268.

Kokubo, T., Ito, S., Shigematsu, M., Sakka., S. and Yamamuro, T. (1985). "Mechanical-properties of a new type of apatite-containing glass ceramic for prosthetic application". Journal of Materials Science, 20(6):2001-2004.

Kokubo, T., Ito, S., Shigematsu, M., Sanka, S., and Yamamuro, T. (1987). "Fatigue and life-time of bioactive glass-ceramic A-W containing apatite and wollastonite". Journal of Materials Science, 22(11):4067-4070.

Kokubo, T., Ito, S., Sakka, S., and Yamamuro, T., (1986). "Formation of a high-strength bioactive glass ceramic in the system MgO-CaO-SiO_2-P_2O_5". Journal of Materials Science, 21(2):536-540.

Kumar, V. and Gill, K.(2009). "Aluminium neurotoxicity: neurobehavioural and oxidative aspects". Archives of Toxicology, 83(11):965-978.

Kusumoto, H., Alolghaserni, S., Woodfine, B., Hill, R.G., Karpukhina N., and Law, R.V. (2016). "The effect of phosphate, fluoride, and soda content of the glass on the mechanical properties of the glass ionomer (polyalkenoate) cements". Journal of Non-Crystalline Solids, 449:94-99.

Lai, G., Li., M. Secondary caries. Contemporary approach to dental caries (2012). InTech, Shanghai, China, p. 403-414.

LeGeros, R.Z., Taheri M.H., Quirolgico, G.B. and LeGeros, J.P. (1980). "Formation and stability of apatites: Effects of some cationic substituents". 2nd International Congress on Phosphorus Compounds, Boston, Massachusetts, USA, IMPHOS (Paris): 89-103.

Lusvardi G., Malavasi G., Cortada M., Menabue L., Menziani M., Pedone, A., and Segre, U. (2008). Elucidation of the structural role of fluoride in potentially bioactive glasses by experimental and computational investigation. Journal of Physical Chemistry B, 112(40):12730-12739.

Lynch, E., Brauer, D. S., Karpukhina, N., Gillam, D. G. & Hill, R. G. (2012) Multi-component bioactive glasses of varying fluoride content for treating dentin hypersensitivity. Dental Materials, 28(2):168-78.

Malitson, I.H. (1963). "A Redetermination of Some Optical Properties of Calcium Fluoride." Applied Optics, 2(11):1103-1107.

Matsuya, S., Maeda, T. AND Ohta, M. (1996). "IR and NMR analyses of hardening and maturation of glass-ionomer cement." Journal of Dental Research, 75(12):1920-7.

Mazzaoui, S. A., M. F. Burrow, M. J. Tyas, S. G. Dashper, D. Eakins and E. C. Reynolds (2003). "Incorporation of casein phosphopeptide-amorphous calcium phosphate into a glass-ionomer cement". Journal of Dental Research, 82(11): 914-918.

McCabe, J., Watts, D., Wilson, H. and Worthington, H. (1990) An investigation of test-house variability in the mechanical testing of dental materials and the statistical treatment of results. Journal of Dentistry, 18(2):90-97.

McCubbin, F. and Nekvasil, H. (2008). "Maskelynite-hosted apatite in the Chassigny meteorite: Insights into late-stage magmatic volatile evolution in martian magmas". American Mineralogist, 93(4):676-684.

McCubbin, F., A. Steele, E. Hauri, H. Nekvasil, S. Yamashita and R. Hemley (2010). "Nominally hydrous magmatism on the Moon". Proceedings of the National Academy of Sciences of the United States of America, 107(25):11223-11228.

Mitsuhashi, A., Hanaoka, K. & Teranaka, T. (2003). "Fracture toughness of resin-modified glass ionomer restorative materials: effect of powder/liquid ratio and powder particle size reduction on fracture toughness". Dental Materials, 19(8):747-57.

Mneimne, M., Hill R.G., Bushby, AJ and Brauer, DS. (2011). "High phosphate content significantly increases apatite formation of fluoride-containing bioactive glasses". Acta Biomaterialia, 7(4):1827-1834.

Mohammed N, Lynch R. and Anderson P. (2014). "Effects of fluoride concentration on enamel demineralization kinetics *in vitro"*. Journal of Dentistry, 2014;42(5):613-618.

Montazerian, M. and Zanotto, E.D. (2016). "History and trends of bioactive glass-ceramics". Journal of Biomedical Materials Research A, 104(5):1231-1249.

Munhoz, T., Karpukhina, N., Hill, R. G., Law, R. V. and De Almeida, L. H. (2010). Setting of commercial glass ionomer cement Fuji IX by ^{27}Al and ^{19}F MAS-NMR. Journal of Dentistry, 38(4):325-30.

Munhoz, T., Karpukhina N., Hill R.G, Law, R.V. and De Almeida, L.H. (2010). "Setting of commercial glass ionomer cement Fuji IX by ^{27}Al and ^{19}F MAS-NMR". Journal of Dentistry, 38(4): 325-330.

Nakamura, T., Yamamuro, T., Higashi, S., Kokubo, T. and Itoo, S. (1985). "A new glass-ceramic for bone replacement: evaluation of its bonding to bone tissue". Journal of Biomedical Materials Research, 19(6):685-698.

Neo, M., Nakamura, T., Ohtsuki, C., Kokubo, T., and Yamamuro, T. (1993). "Apatite formation on three kinds of bioactive material at an early stage in vivo: a comparative study by transmission electron microscopy". Journal of Biomedical Materials Research, 27(8): 999-1006.

Ngo, H. C., Mount, G., McIntyre, J., Tuisuva., J. and Von Doussa, R.J. (2006). "Chemical exchange between glass-ionomer restorations and residual carious dentine in permanent molars: an *in vivo* study". Journal of Dentistry, 34(8):608-613.

O'Donnell., M, Watts, S., Law R.V. and Hill, R.G. (2008). "Effect of P_2O_5 content in two series of soda lime phosphosilicate glasses on structure and properties - Part II: Physical properties". Journal of Non-Crystalline Solids, 354:3561-3566.

O'Donnell, M., Karpukhina, N., Calver, A., Law, R.V., Bubb, N., Stamboulis A., and Hill, R.G. (2010). "Real time neutron diffraction and solid-state NMR of high strength apatite-mullite glass ceramic". Journal of Non-Crystalline Solids, 356(44-49):2693-2698.

O'Donnell, M., Candarlioglu, P., Miller, C., Gentleman, E., and Stevens, M. (2010). "Materials characterisation and cytotoxic assessment of strontium-substituted bioactive glasses for bone regeneration". Journal of Materials Chemistry, 20(40):8934-8941.

O'Donnell, M., Fredholm, Y., de Rouffignac A., and Hill, R.G. (2008). "Structural analysis of a series of strontium-substituted apatites". Acta Biomaterialia, 4(5):1455-1464.

Ohlmann, R. C., Steinbruegge, K.B. and Mazelsky, R. (1968). "Spectroscopic and Laser Characteristics of Neodymium-doped Calcium Fluorophosphate". Applied Optics, 7(5):905-914.

Orlovskii, V., Komlev V., and Barinov S. (2002). "Hydroxyapatite and hydroxyapatite-based ceramics". Inorganic Materials, 38(10):973-984.

Pan, H., Li, Z., Lam, W., Wong, J., Darvell, B., Luk, K., and Lu W. (2009). "Solubility of strontium-substituted apatite by solid titration". Acta Biomaterialia, 5(5):1678-1685.

Paul, A. (1982). Chemistry of glasses. London: Chapman and Hall.

Payne, S., Smith, L., Deloach, L., Kway, W., Tassano, J. and Krupke, W. (1994). "Laser, optical, and thermomechanical properties of Yb-doped fluorapatite". Journal of Quantum Electronics, 30(1):170-179.

Pinckney, L. R. and Dejneka, M.J. (1998). Transparent apatite glass-ceramics, Google Patents. WO1998043922A1.

Piper, W.W., Kravitz, L.C. and Swank, R.K. (1965). "Axially Symmetric Paramagnetic Color Centers in Fluorapatite". Physical Review, 138(6A):A1802-A1814.

Pires, R., Nunes, T.G., Abrahams, I., G. E. Hawkes, C. Morais, M. and Fernandez, C. (2004). "Stray-field imaging and multinuclear magnetic resonance spectroscopy studies on the setting of a commercial glass-ionomer cement". Journal of Materials Science: Materials in Medicine, 15(3):201-208.

Potin-Gautier, M., Dupuis V., Castetbon, A., and Moya, F. (1997). “Solubility and disintegration of a glass ionomer cement”. Chemical Speciation and Bioavailability, 9(3):95-99.

Prentice, L. H., Tyas, M. J. and Burrow, M. F. (2005) “The effect of particle size distribution on an experimental glass-ionomer cement”. Dental Materials, 21(6):505-10.

Priven, A. and Mazurin, O. (2003). ”Comparison of methods used for the calculation of density, refractive index and thermal expansion of oxide glasses”. Glass Technology, 44(4):156-166.

Rafferty, A., Clifford, A., Hill, R., Wood, D., Samuneva B. and Dimitrova-Lukacs, M. (2000a). "Influence of fluoride content in apatite-mullite glass-ceramics”. Journal of the American Ceramic Society, 83(11):2833-2838.

Rafferty, A., Hill R.G. and Wood, D. (2000b). “Amorphous phase separation of ionomer glasses” Journal of Materials Science, 35(15):3863-3869.

Rafferty, A., Hill, R.G. and Wood, D. (2003). “An investigation into the amorphous phase separation characteristics of an ionomer glass series and a sodium-boro-silicate glass system”. Journal of Materials Science, 38(11):2311-2319.

Ramsden, A. and James, P. (1984a). "The effects of amorphous phase-separation on crystal nucleation kinetics in $BaO\text{-}SiO_2$ glasses. 1. General survey”. Journal of Materials Science, 19(5): 1406-1419.

Ramsden, A. and James, P. (1984b). "The effects of amorphous phase-separation on crystal nucleation kinetics in $BaO\text{-}SiO_2$ glasses. 2. Isothermal heat-treatments at 700°C”. Journal of Materials Science, 19(9):2894-2908.

Randall, J. T., Rooksby, H. P. and Cooper, B. S. (1930). X-ray Diffraction and the Structure of Vitreous Solids - I. Zeitschrift für Kristallographie - Crystalline Materials, 75(1):196-214.

Ranu, H. S. (1987). "The thermal properties of human cortical bone: an in vitro study”. Engineering in Medicine, 16(3):175-176.

Rehman, I. and Bonfield., W. (1997). "Characterisationof hydroxyapatite and carbonated apatite by photo acoustic FTIR spectroscopy”. Journal of Materials Science-Materials in Medicine, 8(1): 1-4.

Reusche, E., Pilz, P., Oberascher, G., Lindner, B., Egensperger, R., Gloeckner, K., Trinka, E. and Iglseder, B. (2001). "Subacute fatal aluminum encephalopathy after reconstructive otoneurosurgery: A case report”. Human Pathology, 32(10):1136-1140.

Rodriguez, M., Felsenfeld, A.J. and Llach, F. (1990). "Aluminum administration in the rat separately affects the osteoblast and bone mineralization”. Journal of Bone Mineral Research, 5(1):59-67.

Rothwell, W. P., Waugh, J.S. and Yesinowski, J.P. (1980). "High-resolution variable-temperature phosphorus-31 NMR of solid calcium phosphates". Journal of the American Chemical Society, 102(8):2637-2643.

Sabareeswaran, A., Basu, B., Shenoy, S.J., Jaffer, Z., Saha, N., and Stamboulis, A. (2013). "Early osseointegration of a strontium containing glass ceramic in a rabbit model". Biomaterials, 34(37): 9278-9286.

Samuneva, B., Dimitrov, V., Kalimanova, S., Gattef, E. and Hill, R.G. (1998). "Crystallisation of gels in the apatite-mullite system". Journal of Sol-Gel Science and Technology, 13(1-3):951-956.

Saylor, C.P. (1995). "Accuracy of microscopical methods for determining refractive index by immersion". Journal of Research, 15(3):17.

Segall, B., Ludwig, G.W., Woodbury, H.H. and Johnson, P.D. (1962). "Electron spin resonance of a centre in calcium fluorophosphate". Physical Review, 128:76-79.

Shahid, S., Hassan, U., Billington, R. W., Hill, R. G. and Anderson, P. (2014) Glass ionomer cements: effect of strontium substitution on esthetics, radiopacity and fluoride release. Dental Materials, 30(3):308-13.

Shelby, J. E. (2005). Introduction to glass science and technology, 2nd ed. Edition. Cambridge: Royal Society of Chemistry.

Shortall, A. C., Palin, W.M. and Burtscher, P. (2008). "Refractive index mismatch and monomer reactivity influence composite curing depth". Journal of Dental Research, 87(1):84-88.

Siriphannon, P., Kameshima, Y., Yasumori, A., Okada, K., and Hayashi, S. (2000). "Influence of preparation conditions on the microstructure and bioactivity of alpha-CaSiO(3) ceramics: formation of hydroxyapatite in simulated body fluid". Journal of Biomedical Materials Research, 52(1):30-39.

Soulet, S., Carpena, J., Chaumont, J., Kaitasov, O., Ruault, M. and Krupa, J. (2001). "Simulation of the alpha-annealing effect in apatitic structures by He-ion irradiation: Influence of the silicate/phosphate ratio and of the OH(-)/F(-) substitution". Nuclear Instruments & Methods in Physics Research Section B-Beam Interactions With Materials and Atoms, 184(3):383-390.

Stamboulis, A., Law R.V. and Hill, R.G. (2004). Characterisationof commercial ionomer glasses using magic angle nuclear magnetic resonance (MAS-NMR). Biomaterials, 25(17):3907-3913.

Stamboulis, A., Hill, R.G. and Law, R.V. (2004a). Characterisationof the structure of calcium alumina-silicate and calcium fluoro-alumino-silicate glasses by magic angle spinning nuclear magnetic resonance (MAS-NMR). Journal of Non-Crystalline Solids, 333(1):101-107.

Stamboulis, A., Law, R.V. and Hill, R.G. (2004b). Characterisationof commercial ionomer glasses using magic angle nuclear magnetic resonance (MAS-NMR). Biomaterials, 25(17):3907-3913.

Stamboulis, A., Matsuya, S., Hill, R. G., Law, R. V., Udoh, K., Nakagawa, M. and Matsuya, Y. (2006). MAS-NMR spectroscopy studies in the setting reaction of glass ionomer cements. Journal of Dentistry, 34(8):574-81.

Stamboulis, A., Hill, R.G., Calver, A., Bubb, N., Manuel, P., Nakamura, T., Yamashita, K. and Neo, M. (2006). "Real time neutron diffraction studies of apatite glass ceramics". Bioceramics 18:309-312.

Stamboulis, A., R. Hill, R. Law, S. Matsuya, M. Barbosa, F. Monteiro, R. Correia and B. Leon (2004). "A MAS NMR study of the crystallisation process of apatite-mullite glass-ceramics". Bioceramics, 16(254-2):99-102.

Stanton K. and Hill R.G. (2000). The role of fluoride in the devitrification of $SiO_2{\cdot}Al_2O_3{\cdot}P_2O_5{\cdot}CaO{\cdot}CaF_2$ glasses. Journal of Materials Science, 35(8):1911-1916.

Stanton K.T. and Hill R.G. (2005). "Crystallisation in apatite-mullite glass–ceramics as a function of fluoride content". Journal of Crystal Growth, 275(1): e2061-e2068.

Stanton, K. T. (2000). The Effect of fluoride on microstructural development in apatite-mullite glass-ceramics. PhD thesis, University of Limerick.

Stanton, K. T. and Hill, R.G. (2005). "Crystallisation in apatite-mullite glass-ceramics as a function of fluoride content C3 - Journal of Crystal Growth". Proceedings of the 14th International Conference on Crystal Growth and the 12th International Conference on Vapor Growth and Epitaxy, 275(1-2):e2061-e2068.

Stanton, K. T., O'Flynn, K.P., Kiernan, S., Menuge, J., and Hill, R.G. (2010). "Spherulitic crystallisationcrystallisation of apatite-mullite glass-ceramics: Mechanisms of formation and implications for fracture properties". Journal of Non-Crystalline Solids 356(35-36):1802-1813.

Stanton, K., O'Flynn, K., Nakahara, S., Vanhumbeeck, J., Delucca, J., and Hooghan, B. (2009). "Study of the interfacial reactions between a bioactive apatite-mullite glass-ceramic coating and titanium substrates using high angle annular dark field transmission electron microscopy". Journal of Materials Science-Materials in Medicine, 20(4):851-857.

Stanton, K.T. and Hill R.G. (2005). "Crystallisation in apatite-mullite glass–ceramics as a function of fluoride content". Journal of Crystal Growth, 275(1):e2061-e2068.

Strnad, Z. (1992). "Role of the glass phase in bioactive glass-ceramics". Biomaterials, 13(5):317-321.

Tomozawa, M. (1972). "Liquid-phase separation and crystal nucleation in Li_2O-SiO_2 glasses". Physics and Chemistry of Glasses, 13(6):161.

Tulyaganov, D. U. (2000). "Phase equilibrium in the fluorapatite-anorthite-diopside system". Journal of the American Ceramic Society, 83(12):3141-3146.

Van Duinen, R., Davidson, C., De Gee, A. and Feilzer, A. (2004). "In situ transformation of glass-ionomer into an enamel-like material". American Journal of Dentistry, 17(4):223-227.

Verberckmoes, S., M. De Broe and P. D'Haese (2003). "Dose-dependent effects of strontium on osteoblast function and mineralization". Kidney International, 64(2):534-543.

Vogel, W. (1994) Glass chemistry, 2nd ed. Edition. Berlin;London:Springer-Verlag.

Vogel, W. and Gerth, K., (1962). Catalyzed crystallisation in glass. 63rd anniversary of the American Ceramic Society. Symposium on nucleation and crystallisation of glasses and melts. Reser, M.K. (edt). Toronto, Canada, American Ceramic Society, p. 11-22.

Vogel, W., Holand, W., Naumann, K., and Gummel, J. (1986). "Development of machineable bioactive glass-ceramics for medical uses". Journal of Non-Crystalline Solids, 80(1-3):34-51.

Wasson, E. A. & Nicholson, J. W. (1993) New aspects of the setting of glass-ionomer cements. Journal of Dental Research, 72(2):481-483.

Weber, W. (1993). "Alpha-decay-induced amorphization in complex silicate structures". Journal of the American Ceramic Society, 76(7):1729-1738.

Weber, W. J., Turcotte, R.P., Bunnell, L.R., Roberts, F.P. and Westsik, Jr. J.H. (1979). Radiation effects in vitreous and devitrified simulated waste glass. Ceramics in Nuclear Waste Management, p. 294-299.

White, T., Ferraris, C., Kim, J., Madhavi, S., Ferraris, G., and Merlino, S., (2005). "Apatite - An adaptive framework structure". Micro- and Mesoporous Mineral Phases, 57:307-401.

Wilson, A.D., Kent, B.E. (1971). "The glass-ionomer cement, a new translucent dental filling material". Journal of Applied Chemistry and Biotechnology, 21(11):313-313.

Wilson, A., Crisp, S., Prosser, H., Lewis, B. & Merson, S. (1980). "Aluminosilicate glasses for poly-electrolyte cements". Industrial & Engineering Chemistry Product Research and Development, 19(2):263-270.

Wilson, A., Hill, R., Warrens, C. & Lewis, B. (1989). "The influence of polyacid molecular-weight on some properties of glass-ionomer cements". Journal of Dental Research, 68(2):89-94.

Wood, D. and R. Hill (1991). "Glass ceramic approach to controlling the properties of a glass-ionomer bone cement". Biomaterials, 12(2):164-170.

Yang P, Yuan M, Zeigler D, Watkins S, Lee J, and C. Luscombe C. (2014). "Influence of fluoride substituents on the film dielectric constant and open-circuit voltage in organic photovoltaics". Journal of Materials Chemistry C, 2(17):3278-3284.

Zachariasen, W. H. (1932). “The Atomic Arrangement in Glass”. Journal of American Chemical Society, 54(10):3841–3851.

Zainuddin, N., Karpukhina, N., Hill, R.G., Law, R.V. (2009). "A long-term study on the setting reaction of glass ionomer cements by ^{27}Al MAS-NMR spectroscopy”. Dental Materials, 25(3):290-295.

Zainuddin, N., Karpukhina N., Law, R.V. and Hill, R.G. (2012). “Characterisationof a remineralizing Glass Carbomer® ionomer cement by MAS-NMR Spectroscopy”. Dental Materials, 28(10):1051-1058.

Zainuddin, N. (2009). "Structural and Setting reaction studies of Glass Polyalkenoate Cements by MAS-NMR Spectrocopy”. PhD thesis. London.

Zainuddin, N., Karpukhina, N., Hill, R. G. and Law, R. V. (2009). “A long-term study on the setting reaction of glass ionomer cements by ^{27}Al MAS-NMR spectroscopy”. Dental Materials, 25(3):290-295.

Zainuddin, N., Karpukhina, N., Hill, R.G. and Law, R.V. (2009). "A long-term study on the setting reaction of glass ionomer cements by ^{27}Al MAS-NMR spectroscopy”. Dental Materials, 25(3):290-295.

Zainuddin, N., Karpukhina, N., Law, R.V. and Hill, R.G. (2012). "Characterisation of a remineralising Glass Carbomer® ionomer cement by MAS-NMR spectroscopy”. Dental Materials, 28(10):1051-1058.

Zanotto, E. (2010). "A bright future for glass-ceramics”. American Ceramic Society Bulletin, 89(8): 19-27.

Zanotto, E., James, P., and Craievich, A. (1986). "The effects of amorphous phase-separation on crystal nucleation kinetics in BaO-SiO2 glasses .3. Isothermal treatments at 718°C to 760°C - small-angle X-ray-scattering results”. Journal of Materials Science, 21(9):3050-3064.

Zeng, Q. and Stebbins, J. (2000). “Fluoride sites in aluminosilicate glasses: High-resolution ^{19}F NMR results”. American Mineralogist, 85(5-6):863-867.

Zhang, S., Huang, J., Chen, Y., Gong, X., Lin, Y., Luo, Z. and Huang, Y. (2012). "Preparation and spectral properties of Nd^{3+}-doped transparent glass ceramic containing $Ca_5(PO_4)(3)F$ nanocrystals”. Journal of Non-Crystalline Solids, 358(20):2835-2840.

Zhang, S., Huang, J., Chen, Y., Gong, X., Lin, Y., Luo, Z. and Huang, Y. (2013a). "Site-selective excitation and emission of Eu^{3+}-doped transparent glass ceramic containing $Ca_5(PO_4)(_3)F$ nanocrystals”. Optical Materials Express 3(6):868-874.

Zhang, S., Huang, J., Chen, Y., Gong, X., Lin, Y., Luo, Z. and Huang, Y. (2013b). "Spectroscopic properties of Nd^{3+}-doped transparent glass ceramic containing $Sr_5(PO_4)(_3)F$ nanocrystals”. Journal of Non-Crystalline Solids, 366:35-41.

Zraikat, H., Palamara, J., Messer, H., Burrow, M., and Reynolds, E. (2011). "The incorporation of casein phosphopeptide-amorphous calcium phosphate into a glass ionomer cement". Dental Materials, 27(3):235-243.

APPENDIX A

Publications

frontiers in Materials

REVIEW
published: 09 January 2017
doi: 10.3389/fmats.2016.00059

Apatite Glass-Ceramics: A Review

Tomas Duminis, Saroash Shahid and Robert Graham Hill*

Unit of Dental Physical Sciences of the Centre for Oral Growth and Development, Institute of Dentistry, Barts and the London School of Medicine and Dentistry, Queen Mary University of London, London, UK

This article is a review of the published literature on apatite glass-ceramics (GCs). Topics covered include crystallization mechanisms of the various families of apatite GCs and an update on research and development on apatite GCs for applications in orthopedics, dentistry, optoelectronics, and nuclear waste management. Most apatite GCs crystallize through a homogenous nucleation and crystallization mechanism, which is aided by a prior liquid–liquid phase separation. Careful control of the base glass composition and heat-treatment conditions, which determine the nature and morphology of the crystal phases in the GC can produce GC materials with exceptional thermal, mechanical, optical, and biological properties. The GCs reviewed for orthopedic applications exhibit suitable mechanical properties and can chemically bond to bone and stimulate its regeneration. The most commercially successful apatite GCs are those developed for dental veneering. These materials exhibit excellent translucency and clinical esthetics and mimic the natural tooth mineral. Due to the ease of solid solution of the apatite lattice, rare earth doped apatite GCs are discussed for potential applications in optoelectronics and nuclear waste management. One of the drawbacks of the commercial apatite GCs used in orthopedics is the lack of resorbability; therefore, the review provides a direction for future research in the field.

Keywords: apatite, glass, glass-ceramic, biomaterial, fluorapatite, chlorapatite, nucleation and crystallization, orthopedic

OPEN ACCESS

Edited by:
Joachim Deubener, Clausthal University of Technology, Germany

Reviewed by:
Ana Candida Martins Rodrigues, Federal University of São Carlos, Brazil
Maziar Montazerian, Federal University of São Carlos, Brazil

****Correspondence:***
Tomas Duminis
t.duminis@qmul.ac.uk

Specialty section:
This article was submitted to Glass Science, a section of the journal Frontiers in Materials

Received: *18 June 2016*
Accepted: *15 December 2016*
Published: *09 January 2017*

Citation:
Duminis T, Shahid S and Hill RG (2017) Apatite Glass-Ceramics: A Review. Front. Mater. 3:59. doi: 10.3389/fmats.2016.00059

INTRODUCTION

Apatite is named after the Greek word "*apát*" meaning deceit because, in appearance, apatite is often mistaken for a number other minerals. Apatite has a chemical formula $Ca_5(PO_4)_3(F, Cl, OH)$. Due to an adaptive framework structure of apatite (White et al., 2005), its lattice can readily accommodate a number of ionic substitutions. Naturally occurring apatites are found in igneous, metamorphic, and sedimentary earth rocks and relatively recently, versions of fluor- and hydroxyapatite (HAp) were found on the surface of the Moon (McCubbin et al., 2010). Additionally, meteorites from the planet Mars, for example, Chassigny, which fell in provincial France in 1815, brought melt inclusions of Martian fluor- and chlorapatites (McCubbin and Nekvasil, 2008). Apatite is also the major inorganic component naturally found in the hard tissues of vertebrates; therefore, it has a profound biological and clinical significance.

Biological apatites have a chemical formula of $Ca_5(PO_4)_3(OH)$, with some degree of CO_3^{2-} substitution for PO_4^{3-}, F^- for OH^-, and Na^+ or Mg^{2+} for Ca^{2+} ions. Synthetic HAp has been used in various forms of health care, such as for bone replacement, dental cements, and dental porcelains. However, sintered porous or even dense HAp bone implants often fail due to poor mechanical properties that are inferior to the mechanical properties of the human bone (**Table 1**). Moreover, sintered blocks of

TABLE 1 | Mechanical properties of the glass-ceramics for orthopedic applications.

Material	Phase	Density (g/cm³)	Thermal expansion coefficient ($\times 10^{-6}$ K^{-1})	Compressive strength (MPa)	Flexural strenght (MPa)	Young's modulus (GPa)	Fracture toughness (MPa $\sqrt{m}$)	Reference
Cortical bone	Hydroxyapatite (HAp) + organic matrix	1.9	27.5 ± 3.9	133–295	35–283	7–20	5–7	An and Draughn (2000) Ranu (1987)
HA	HAp	3.16	10	120–150	60–120	35–120	0.8–1.2	Orlovskii et al. (2002)
A–W	Fluor/oxyapatite and wollastonite	3.07	8–10	1,080	215	118	2	Kokubo (2008)
Bioverit I	Apatite and fluorphlogopite	2.8	8–12	500	140–180	70–88	1.2–2.1	Höland and Beall (2012)
Bioverit II	Apatite and fluorphlogopite	2.5	8–12	450	90–140	70	1.2–1.8	Höland and Beall (2012)
Bioverit III	Fluorapatite (FAp) and aluminum phosphate	2.7–2.9	14–18	–	60–90	45	0.6	Höland and Beall (2012)
A–M	FAp and mullite	2.7–3.3	8–10	–	90–330	70–90	1.0–3.3	Ducheyne et al. (2011)

HAp require machining to shape to match the complex contours of the defect using expensive diamond tipped tools. A porous and bioactive 3D material may be highly desirable for bone regeneration because a porous material will allow osteoblasts to proliferate and integrate inside the 3D structure and enable vascularization of the newly formed bone, provided the porosity of the material is adequate. However, with the introduction of porosity into any bone substitute material or implant, mechanical properties are compromised as discussed by Karageorgiou and Kaplan (2005), rendering many of the porous bone substitute materials inappropriate for load-bearing applications.

Since the early 1970s, a number of melt-derived glass-ceramics have been developed that crystallize to apatite phases on controlled heat treatment. A glass-ceramic material can be cast into complex shapes by the "lost wax" casting route, which is usually a simple and cost-effective process. For illustration purposes, the reader is presented with an apatite–mullite glass-ceramic chess piece (**Figure 1**) produced by casting molten glass to shape by the "lost wax" method, which shows the complexity of shapes and surface detail that can be attained by this route. Machinable glass-ceramics (GCs), such as mica GCs discussed in this review can also be processed by computer-aided design/computer aided manufacturing (CAD/CAM).

FIGURE 1 | Apatite–mullite chess piece cast to shape by the lost wax method.

Apatite-containing GCs are highly biocompatible and can induce bone formation *in vivo* (Ducheyne et al., 2011). Therefore, apatite-based GCs are highly attractive for medical and dental applications. A bioactive material is defined as a material that exhibits a biological response at the interface once in contact with a biological tissue. A bioactive material may induce a biological response through its surface topography or by a controlled release of therapeutic ions. A number of bioactive apatite-containing glass-ceramics have been developed for orthopedic applications, and these can be categorized based on the type of secondary crystal phases present in the GC; apatite–wollastonite (A–W), commercially known as Cerabone®; apatite–fluoromica (A–FM), commercially known as Bioverit®; and apatite–mullite (A–M). Several apatite-containing GCs have also been developed for restorative dentistry applications for the fabrication of dental inlays, crowns, bridges, and veneers. These are namely apatite–leucite (A–L), commercially known as IPS d.SIGN®; and with apatite as the only phase, for example IPS e.max ZirPress® and IPS e.max Ceram®.

Apatite is a good host crystal phase for rare earth elements and exhibits low phonon energies (particularly FAp); therefore, apatite-containing glass-ceramics have also been investigated for potential applications in optoelectronics. Apatite phases are also

particularly attractive in nuclear waste immobilization, such as for the immobilization of Cl and Sr isotopes, where these radioactive elements can be readily incorporated into the apatite lattice.

A review on the history and trends of the bioactive glass-ceramics, including those that do not contain apatite phases has been recently published (Montazerian and Zanotto, 2016). The scope of this article is to review the fundamentals of the structure–property relationship and crystallization mechanisms of the various apatite glass-ceramics used in health care as well as those for potential applications in optoelectronics and nuclear waste management.

PRIOR LIQUID–LIQUID PHASE SEPARATION (LLPS)—PRECURSOR TO NUCLEATION AND CRYSTAL GROWTH

Liquid–liquid phase separation, also known as amorphous phase separation (APS), can occur in undercooled liquids either at or below the glass *liquidus* temperature. If LLPS occurs above the glass *liquidus* temperature, then such phase separation is termed stable immiscibility. On the other hand, if LLPS occurs below the *liquidus* state, such LLPS is termed metastable immiscibility. Undercooled liquids can undergo phase separation through spinodal decomposition or *via* nucleation and growth processes (binodal decomposition) (**Figure 2**).

Spinodal decomposition is a diffusion driven mechanism with no activation energy barrier. A system that undergoes spinodal decomposition is always unstable. In contrast, phase separation by nucleation and growth (in the binodal region) has a large free energy barrier and it is a metastable process involving an activation energy. Small angle neutron scattering (SANS) techniques can be used to study LLPS in both spinodally and binodally decomposed glasses. SANS scattering at lower q values correspond to larger phases, which can be attributed to a phase separation under the binodal region of the phase diagram, whereas neutrons scattered at higher q values correspond to a finer scale phase separation, which may be attributed to spinodally decomposed structures (Hill et al., 2007). Spinodal decomposition, unlike nucleation, generally results in sharp scattering maximum often referred to as a "spinodal ring" particularly during the early stages of phase separation. Spinodal decomposition is difficult to observe by microscopy techniques because of the diffuse interfaces between the phases. In contrast, nucleated amorphous phases can be readily observed by microscopy. Transmission electron microscopy (TEM) analysis shows (Hill and Wood, 1995) that LLPS *via* nucleation and growth results in sharp boundaries between the phases as observed in **Figure 3**.

Most of the glass-ceramics discussed in this review undergo a bulk nucleation and crystallization, which has been attributed to prior LLPS. Crystal nucleation may be aided by the composition of one of the phases being closer to the crystal phase than the parent glass composition. **Figure 3** shows a droplet-like phase that is rich in calcium and phosphorus that crystallizes to fluorapatite (FAp) (Hill and Wood, 1995). However, the A–W GC exhibits surface crystallization of both phases without the occurrence of prior LLPS (Kokubo et al., 1982).

There are two main ideas of how prior LLPS can influence the subsequent crystallization. Vogel and Gerth (1962) proposed that the effect of prior LLPS on glass crytsallization is due to the existence of interfaces in a phase-separated glass, which provide internal surfaces for heterogenous nucleation. However, Cahn (1969) and James (1981) suggested that if the composition of the LLPS phase is close to the composition of the subsequent crystal phase, the activation energy is lowered and subsequent homogenous crystallization is favored.

There are few studies on the importance of LLPS in regard to glass-ceramics, and it is worth briefly reviewing these studies. Ramsden and James (1984a,b) found that quenched $BaO–SiO_2$ glasses in which LLPS developed simultaneously with the nucleation of the crystals, the crystal nucleation rate increased with isothermal heat-treatment time. Ramsden and James (1984b)

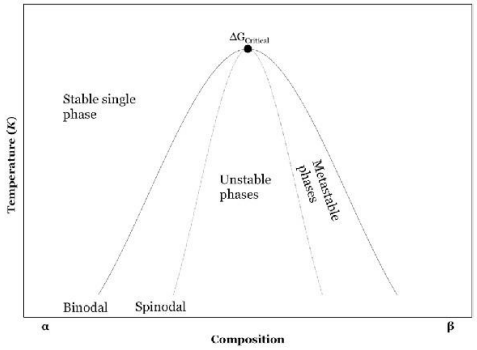

FIGURE 2 | Phase diagram of a binary system.

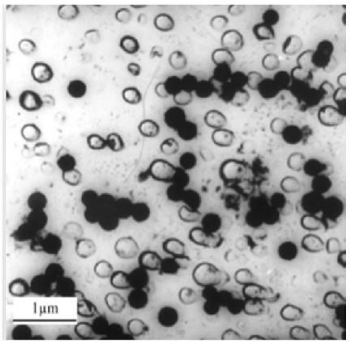

FIGURE 3 | Carbon replica transmission electron micrograph of a fluorapatite–mullite glass-ceramic showing evidence of droplet-like amorphous phase separation giving rise to hexagonal fluorapatite crystals (black zones) (Hill and Wood, 1995).

reported that the same system without prior LLPS did not show any increases in crystal nucleation rates. Thus, Ramsden and James (1984a,b) and later Zanotto et al. (1986) concluded that the predominant effect on crystal nucleation arises from the compositional changes brought about by phase separation. Although it has been shown that LLPS has a profound role in the formation of simple glass-ceramics, its effect in complex multicomponent systems, such as those with strong nucleants should not be generalized.

Tomozawa (1972) reported that lithium silicate glasses showed considerably increased crystal nucleation rates when the glass had undergone LLPS and proposed that the LLPS droplets consist of silica-depleted diffusion zones at their interfaces, therefore giving rise to sites for heterogenous nucleation.

The mechanism by which LLPS enhances subsequent crystallization depends on the composition of the glass and the composition of the crystalline phase. Apatite GC systems developed by Hill et al. (2004) bulk nucleate *via* prior amorphous separation, but can also crystallize through a surface mechanism. In simple glasses such as the lithium silicate glasses, LLPS enhances nucleation rate, by reducing the activation energy for nucleation. Although LLPS can enhance subsequent crystallization of a glass, based on the classical nucleation theory, the LLPS droplet diameter (D) should be larger than the critical radius (r^*) for crystal nucleation in order for nucleation to take place within the droplet phase. Therefore, fine scale LLPS can potentially suppress nucleation and subsequent crystallization.

In a study by Clifford et al. (2001a), it was found that base glasses in the A–M systems with a molar Ca to P ratio of 1.67 (glasses with an apatite stoichiometry) crystallize through an internal or bulk mechanism, and that base glasses with Ca to P ratios higher or lower than 1.67 crystallize through a surface mechanism. Interestingly, Clifford et al. (2001a) note that compositions with a molar Ca to P ratio above or below 1.67 can crystallize in bulk following an annealing hold for 1 h just above the glass transition temperature. Clifford et al. (2001a) study provides evidence that LLPS in the apatite–mullite system can be produced below the *liquidus* by nucleation and growth.

Rafferty et al. (2000b, 2003) used high temperature dynamic mechanical thermal analysis (DMTA) to show the presence of two mechanical loss peaks (tan δ) and two reductions in the storage modulus (E′) corresponding to two glass transition temperatures (**Figure 4**) for many of the A–M glass compositions providing evidence of an LLPS. On crystallization of FAp, only one glass transition temperature (T_g) was observed indicating that one of the two amorphous phases had crystallized to FAp.

Crystals or LLPS droplets in an undercooled liquid can undergo Ostwald ripening (OR) during a heat treatment. During an OR process, crystals or LLPS droplets can grow and produce larger LLPS droplets or crystals. Thermodynamically, OR is a favorable process because larger particles exhibit lower surface energy in contrast to smaller particles. Apatite crystal growth through OR process is observed in apatite glass-ceramics, such as reported by Höland et al. (2015). One of the key characteristics of an OR process is the reduction in the number of droplets/crystals and an increase in volume as a function of time, pressure or temperature.

Fluorapatite is part of the hexagonal group of crystals; therefore, it exhibits a kinetically favored growth in the crystallographic *c*-direction, which is seen in Höland et al. (2015)'s findings, whereby crystal length as a function of time due to OR process was more pronounced as opposed to crystal expansion at crystallographic *a*-direction. OR process can be used to produce a highly homogenous and mechanically superior microstructure of a GC.

BIOMEDICAL APPLICATIONS OF APATITE GLASS-CERAMICS

Orthopedics

Fluor/Oxyapatite–Wollastonite Glass-Ceramics

Kokubo et al. (1982) developed apatite–wollastonite (A–W) (β-$CaSiO_3$) system based on SiO_2–P_2O_5–CaO–MgO–CaF_2, also known by its commercial name Cerabone®. The β-wollastonite phase in the A–W system enhances mechanical performance of the glass-ceramic (**Table 1**). Kokubo et al. (1987) reported on the A–W GC ability to resist failure by fatigue. It was estimated that the life-time of an A–W GC, under a constant loading of 65 MPa in simulated body fluid is 10 years, compared to a sintered HAp, which under the same loading can sustain the loading before fracture for only 1 min. Both, apatite and β-wollastonite phases in the A–W system crystallize through a surface mechanism (Kokubo et al., 1982). As such, the A–W GC cannot be cast to shape by the "lost wax" technique and is processed through powder sintering route.

It was often claimed that the apatite phase in the A–W systems is FAp; however, Clifford and Hill (1996) noted that the A–W glasses are very deficient in fluorine content with regard to the FAp stoichiometry. Clifford and Hill (1996) further suggested that the apatite formed in A–W systems is therefore more likely to be a mixture of fluor- and oxyapatite. Based on the pioneering electron spin resonance (ESP) studies on fluor/oxyapatites, it has been long known that O^- can occupy F^- sites (Segall et al., 1962; Piper et al., 1965). Nonetheless, at present, the availability of high-resolution solid-state characterization techniques such as ^{17}O MAS-NMR coupled with dynamic nuclear polarization (DNP) and high field ^{19}F MAS-NMR could provide fast and accurate elucidation of oxygen and fluorine environments in the A–W GC; however, such work is yet to be published.

Calver et al. (2004) reported that modified Kokubo et al. (1982) A–W glass with higher metal fluoride content (AW3, **Table 2**) resulted in a completely changed apatite crystallization behavior. Calver et al. (2004) found that a base glass with the highest CaF_2 content favored volume FAp nucleation and crystallization. Calver et al. (2004) also found that A–W systems showed reduced T_g and FAp crystallization exotherms with increasing calcium fluoride content. Therefore, low calcium fluoride content in the original A–W system is actually suppressing crystallization of FAp. Filho et al. (1996) suggest that fully crystallized GCs, which are otherwise bioactive, will not exhibit any further bioactivity through the release of ions, such as Ca^{2+} and HPO_4^{2-}, once such ions take up higher energy coordination states in the apatite lattice. Therefore, from a bioactivity point of view, it may not always be

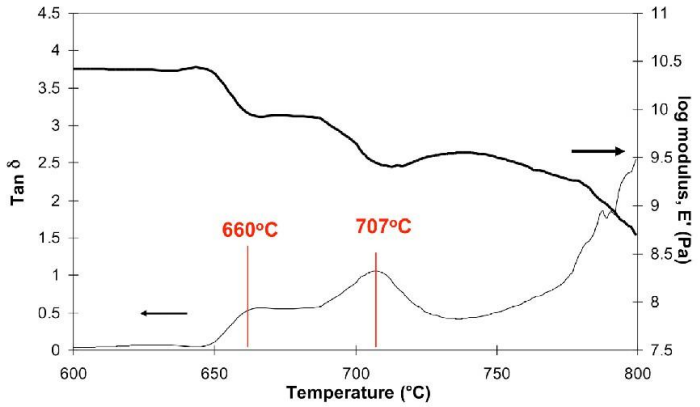

FIGURE 4 | Dynamic mechanical testing analysis (DMTA) of an A–M glass-ceramic showing two glass transitions, one at 660°C and second at 707°C and two decreases in modulus after Rafferty et al. (2000b) collected at a 5°C/min heating rate in a single frequency mode at 1 Hz.

TABLE 2 | A–W base glass compositions in mol% (Calver et al., 2004).

	SiO_2	P_2O_5	MgO	CaO	CaF_2
AW1	35.46	7.15	7.11	50.28	0
AW2	35.46	7.15	7.11	49.88	0.4
AW3	35.46	7.15	7.11	45.51	4.77

desirable to consume therapeutic ions for the formation of apatite within the glass matrix, as opposed to the release of such ions and subsequent formation of apatite on the surfaces of the material, that potentially lead to the formation of a strong and chemically stable implant–bone interface. Furthermore, the molar Ca to P ratio in a stoichiometric apatite crystal is 10 to 6 (1.67); therefore, GC systems containing a stoichiometric Ca to P ratio, or in other words, glass formulations with smaller compositional differences between the glass and the crystal phase preferentially crystallize in bulk, which is unfortunately not the case in the A–W system. On the other hand, the A–W system is inherently aluminum free; thus, risks associated with aluminum neurotoxicity, summarized by Kumar and Gill (2009) and reported by Reusche et al. (2001), are completely absent.

It could be argued as to why the original A–W system developed by Kokubo et al. (1982) contains magnesium and a non-stoichiometric Ca:P:F ratio that could otherwise aid bulk nucleation and crystallization of apatite phases. There is a considerable and long-standing proof, for example, as found by X-ray diffraction analyses of precipitated apatites by LeGeros et al. (1980), which demonstrates that the presence of Mg^{2+} ions in an aqueous solution cause a strain on the apatite structure causing it to collapse and, therefore, suppress its growth. In view of the biological apatite found in bone as opposed to tooth, Mg^{2+} ions alongside osteocalcine and proteoglycan proteins play a significant role in the development of a nanoscale apatite (Blumenthal et al., 1975), providing the bone tissue with a fine microstructure and the excellent properties that come with it. Therefore, on that basis, it could be argued that the A–W system is highly biomimetic in view of the elemental composition of the human bone.

In vivo animal studies on the implanted A–W glass-ceramic provide evidence for excellent osseointegration around the A–W implant and a chemical calcium phosphate-based interface (Kitsugi et al., 1989, 1990) between the implant and bone, with high bending and compressive strengths of 157 and 1060 MPa, respectively (Nakamura et al., 1985). Kokubo et al. (1990) found that A–W GC immersed in tris(hydroxymethyl)aminomethane (TRIS) buffer did not show bioactivity through the formation of apatite and these findings were contradictory to animal studies conducted previously, where the A–W GC was found to form a strong chemical interface with the living bone. Therefore, Kokubo et al. (1990) developed a simulated body fluid (SBF), an alternative immersion medium for *in vitro* assessment of bioactivity of the A–W GC. Kokubo et al. (1990) argued that TRIS buffer does not mimic the actual body environment because it is completely deficient in ions, such as Ca^{2+} and HPO_4^{2-} naturally found in the bodily fluids and, therefore, argued that the lack of apatite formation in TRIS buffer, as opposed to high bioactivity of the A–W GC in SBF, also supports the view that the apatite phase on the surfaces of the A–W GC forms by a chemical reaction between the A–W GC and the ions present in the body fluid. In view of this, it can be further postulated that apatite crystals within the A–W GC act as nuclei on which ions, such as Ca^{2+} and PO_4^{3-} in the solution nucleate and feed apatite formation until the eventual fusion between the apatite crystals in the A–W and the apatite in the living bone, whereby a chemical interface is formed.

Kokubo et al. (1992) reported that if aluminum is included in the A–W parent glass composition and then subsequently crystallized, the A–W GC does not show any bioactivity in SBF

as opposed to the same A–W material without aluminum. The addition of aluminum results in a more chemically stable residual glass phase, which reduces the release of Ca^{2+} and PO_4^{3-} ions, thereby affecting apatite formation (Strnad, 1992). Later, Blades et al. (1998) conducted *in vivo* animal study on aluminum-containing glass ionomer cements (GICs) as potential bone cements, where as low as 1 ppm of aluminum released was found to inhibit mineralization of the newly formed osteoid in rabbit bone. It is important to distinguish that the role of aluminum in Blades et al. (1998) study may be attributed to aluminum toxicity to bone-forming cells (Rodriguez et al., 1990) and direct inhibition of crystal growth as opposed to reduced bioactivity involving structural parameters of the residual glass phase, as proposed in Strnad (1992) study.

Good oseointegration through the formation of apatite on the implant surfaces (Neo et al., 1993) combined with good mechanical properties (Kokubo et al., 1985, 1986) perhaps explains why the A–W glass-ceramic has found promising applications in bone and vertebra replacement (Kokubo, 2008) and it is reported that over 50,000 successful bone implants have been made using the A–W glass-ceramic system (Zanotto, 2010). However, from a manufacturing point of view, a bulk crystallizing A–W material, such as proposed by Calver et al. (2004), could provide a more cost-effective material. *In vitro* and *in vivo* bioactivity of the modified A–W system developed by Calver et al. (2004) still needs to be established. The original A–W GC is currently manufactured by Nippon Electric Glass Co., Ltd. (Japan) (Montazerian and Zanotto, 2016).

Fluorapatite–Mica Glass-Ceramics

Grossman (1972) of Corning Glass Works, developed the first machinable mica glass-ceramic system, later marketed by Dentsply International under the name Dicor®. Dicor® was seen as a very significant development since the new GC material could be easily machined to shape without a critical failure. Machinability of the mica glass-ceramics is attributed to the eminent cleavage of the mica-type crystals as a result of anisotropic crystal growth. This facilitates crack propagation in the direction of cutting without causing a critical failure of the material.

Although mica glass-ceramics initially did not contain any apatite phases, Vogel et al. (1986) developed two GC systems (**Table 3**) with FAp and tri/tetrasilicic $Mg_3(AlSi_3O_{10}F_2)Na/K/Mg_3(Si_4O_{10}F_2)Na/K$ mica phases and an additional silica-free GC with apatite and aluminum phosphate phases.

Commercially available Bioverit I® and Bioverit II® systems crystallize to FAp and mica phases in bulk. Bioverit II® GC crystallizes to a smaller fraction of FAp, which can be explained by the very low P_2O_5 content in the composition (**Table 3**). Both systems have undergone prior APS into two droplet phases and a glassy matrix phase (Höland and Beall, 2012). One droplet phase is rich in apatite elements whereas the second droplet phase is closer to the mica composition. This may explain why both phases, apatite and mica, crystallize in bulk. Bioverit III is a silica-free phosphate glass that crystallizes to FAp and an aluminum phosphate ($AlPO_4$) (Höland and Beall, 2012); Bioverit III material exhibits lower mechanical properties (Höland and Beall, 2012); therefore, it has not been so extensively studied.

TABLE 3 | Examples of Bioverit® base glass composition in mol% (Höland and Vogel, 2013).

	Bioverit I	Bioverit II
SiO_2	29.44	44.12
Al_2O_3	9.04	17.47
P_2O_5	4.66	0.08
CaO	14.89	0.21
MgO	21.29	17.44
Na_2O	2.15	4.23
K_2O	3.57	3.10
TiO_2	–	–
F	14.96	13.17
Cl	–	0.17

Bioverit II contains a higher fraction of mica crystals. Therefore, Bioverit II GC exhibits better machinability but at the expense of lower mechanical properties than Bioverit I (**Table 1**). Based on ^{19}F MAS-NMR experiments of mica ceramics, it was demonstrated that the fluoride ion in mica systems exists mainly in Mg(n)-F type environments, with a chemical shift at about −174 ppm for Mg(3)-F (Fechtelkord et al., 2003). As of 2016, A–FM GCs, Bioverit I and II are currently manufactured by VITRON Spezialwerkstoffe GmbH (Germany).

Fluorapatite–Mullite Glass—Ceramics

Mullite is a rare naturally occurring aluminosilicate mineral. Mullite-reinforced matrices exhibit enhanced mechanical properties. FAp phases can act as nucleation and crystal growth sites for new apatite phases between the implant and living bone. Both crystal phases in the fluorapatite–mullite system show elongated needle-like microstructure and exceptional mechanical properties, particularly flexural strength and fracture toughness of up to 330 MPa and 3.3 MPa $\sqrt{m^2}$, respectively (**Table 1**). The A–M GC exhibits spherulitic crystallization, which enhances fracture toughness properties of the material (Stanton et al., 2010). The system nucleates in bulk; therefore, it is readily castable by the "lost wax" route.

The first melt-derived castable FAp ($Ca_5(PO_4)_3F$)—mullite ($Al_6Si_2O_{13}$) glass-ceramics were developed by Hill et al. (1991) and were based on the SiO_2–Al_2O_3–P_2O_5–CaO–CaF_2 system. Additionally, Samuneva et al. (1998) were also able to produce an A–M glass-ceramic by a sol–gel route, rather than a melt-quench route.

Hill et al. (1991) noted that base glasses with relatively low CaF_2 content (A–C, **Table 4**) surface crystallized to apatite and mullite phases upon heat treatment, whereas base glasses with metal fluoride content (D and E, **Table 4**) bulk crystallized to anorthite with only a small fraction of FAp. The work by Hill et al. (1991) and also subsequent work by Hill and Wood (1995); Clifford and Hill (1996); Hill et al. (2000); Rafferty et al. (2000a); Clifford et al. (2001a,b), and later by Stanton and Hill (2005) suggests that metal fluoride as well as phosphorus content in fluoro-phospho-aluminate systems will likely influence prior LLPS and will therefore determine whether the glass crystallizes *via* the homogenous bulk route (aided by the LLPS composition) or the heterogeneous surface route.

Stanton and Hill (2005) postulated that once crystallization of FAp crystal has begun, the surrounding glass becomes depleted in F, Ca, and P and moves closer to the mullite composition, whereupon, it crystallizes to mullite by the homogenous mechanism. Stamboulis et al. (2004) explained crystallization of FAp and mullite phases in the A–M system in even greater detail by analyzing heat-treated A–M samples with magic angle spinning-nuclear magnetic resonance (MAS-NMR) spectroscopy. Spectra from ^{27}Al MAS-NMR in **Figure 5** (left) show how aluminum resonance is relatively unchanged until the GC reaches second crystallization temperature (T_{p2}) whereupon it crystallizes to mullite. It can be observed from **Figure 5** (left) that a broad peak seen at around 50 ppm, assigned to Al(IV), remains unchanged even after FAp crystallization (T_{p1}). During second phase crystallization, an additional peak, at around 12 ppm, which is assigned to an Al(VI) in mullite is observed. Stamboulis et al. (2004) further explain that, during first and second crystallization processes, charge balancing cations for maintaining aluminum in a fourfold coordination state, Al(IV) are consumed during FAp formation; therefore, at higher temperatures, the lack of charge balancing cations to keep aluminum in a IV coordination state forces aluminum to take up higher coordination states, in this case, Al(VI). ^{19}F MAS-NMR spectra as shown in **Figure 5** (right) show how the fluorine environment changes with increasing heat-treatment temperature. The lowermost ^{19}F spectrum of the untreated LG120 glass in **Figure 5** (right) demonstrates two broad peaks at −90 and −150 ppm that can be attributed to the amorphous fluorine environments in the untreated glass, F–M(n) and Al–F–M(n) (Zeng and Stebbins, 2000). However, at T_{p1}, a sharp peak at around −103 ppm develops at the expense of F–Ca(n) peak, which is assigned to fluorine in a F–Ca(3) environment in FAp. At higher temperatures, such as T_{p2}, fluorine from Al–F–M(n) peak is also fully consumed and Stamboulis et al. (2004) further proposed that F–M(n) such as F–Ca(n) species preferentially charge balance the non-bridging oxygens in the phosphorus locality. It can be additionally postulated that such preference to balance the non-bridging oxygens in the phosphorus locality reduces kinetic energy barrier to FAp nucleation and crystal growth, since the local environment of Ca, P, and F in the glass is similar to that present in FAp.

Relatively recently, Stamboulis et al. (2006), Hill et al. (2007), and O'Donnell et al. (2010) conducted real-time SANS and neutron diffraction (ND) experiments on the A–M systems developed in the early 1990s. They postulated that amorphous glasses that form the A–M system may have undergone phase separation by spinodal decomposition during the casting process on a scale of 25–27 nm (Hill et al., 2007). Similarly, the same cast A–M system isothermally heat treated at 740°C and 750°C initially showed neutron scattering at higher q, which then moved to lower q with increasing temperatures where the scale of the LLPS corresponded to about 35 nm. This provides evidence that undercooled liquids can undergo LLPS by nucleation and growth, whereupon the chemical system can overcome the thermodynamic and kinetic energy barriers to nucleation and subsequent amorphous phase growth. It is suggested by Hill et al. (2007) that the A–M cast glass is initially phase-separated by spinodal decomposition, whereby rapid cooling creates a barrier to nucleation and growth. However, it may be argued that scattering at lower q in the as-cast glasses may be attributed to a finer LLPS by nucleation and growth. SANS experiments by Hill and coworkers provide evidence that finer scale phase separation in the apatite–mullite system increases in size as a function of temperature, which can be either attributed to the fact that the cast A–M system is initially spinodally decomposed and then undergoes LLPS by

TABLE 4 | A–M base glass compositions in mol% (Hill et al., 1991).

	SiO_2	Al_2O_3	P_2O_5	CaO	CaF_2
A	37.50	25.00	12.50	25.00	0.00
B	35.29	23.53	11.76	23.53	5.88
C	33.33	22.22	11.11	22.22	11.11
D	31.58	21.05	10.53	21.05	15.79
E	30.00	20.00	10.00	20.00	20.00

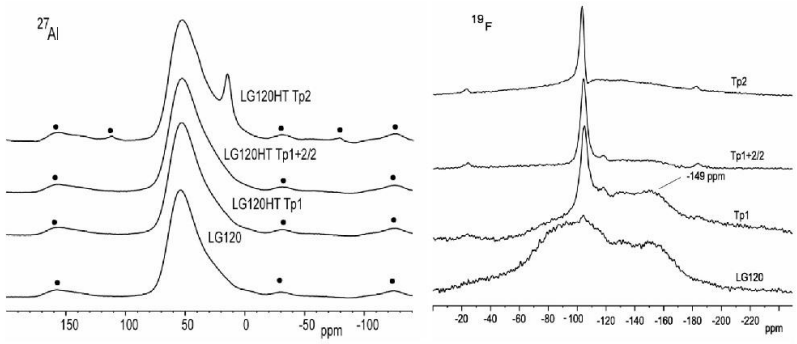

FIGURE 5 | ^{27}Al (left) and ^{19}F (right) MAS-NMR spectra of LG120 heat treated at different temperatures (Stamboulis et al., 2004).

nucleation and growth or more likely LLPS growth by an OR mechanism.

Further studies of an A–M glass-ceramic analyzed by heat treating an amorphous precursor glass up to 1,200°C with *in situ* TOF-ND (O'Donnell et al., 2010) explain the crystallization behavior of the A–M system in more detail. O'Donnell et al. (2010) reported that FAp and mullite crystallized on heating until 1,130°C followed by the partial dissolution of both phases at higher temperatures. It was also found that on the subsequent cooling of the A–M system, recrystallization occurred and additional new phases were produced, namely berlinite ($AlPO_4$) and cristobalite (SiO_2), which formed at around 1,025°C in addition to the FAp and mullite. This indicates that the subsequent cooling of the GC can produce additional crystal phases, which may be undesirable but can be avoided by introducing higher cooling rates to create an energy barrier to nucleation and growth of the undesirable crystal phases.

Stanton and Hill (2005) found that apatite phases in the A–M system grow as dendrites and spherulites. Generally, the microstructure of a GC is strongly influenced by the conditions of the heat-treatment of the parent glass, this namely includes duration, temperature, and cooling rate and whether or not the base glass compositions is doped with additional nucleants, for example, such as reported with niobium-doped FAp GCs by Denry et al. (2012). Mechanical properties, particularly fracture toughness of the A–M GC developed by Hill and coworkers, surpass mechanical properties of the alternative glass-ceramic systems discussed in this review.

In vivo animal studies conducted by Freeman et al. (2003) show that a fully crystallized A–M glass-ceramic osseointegrates with bone as shown in **Figure 6B**; however, its amorphous precursor base glass implant does not osseointegrate, which is evident from the fibrous tissue around the glass implant as shown in **Figure 6A** and the lack of implant/bone interfaces. Goodridge et al. (2007) report on both, *in vitro* and *in vivo* properties of the porous A–M glass ceramic system produced through selective laser sintering (SLS) method, using cast A–M and commercial A–W glass-ceramics as positive controls. In the 4 weeks study, Goodridge et al. (2007) reports that no sign of inflammation or adverse tissue reaction was observed around all the implants. Analyses of the implant–bone interfaces by scanning electron microscopy (SEM) showed evidence for bone ingrowth into the both porous materials, the A–M system produced through SLS method and the A–W sintered glass-ceramic. Although Goodridge et al. (2007) report that the laser sintered apatite–mullite system developed by Hill et al. (1991) does not form apatite in SBF, previous studies indicate that SBF studies are not adequate in the assessment of bioactivity of aluminum-containing GCs (Strnad, 1992).

Stanton et al. (2009) assessed the interfacial chemistry between the A–M system and a titanium alloy, for potential applications of the A–M system for orthopedic implant coatings. Stanton et al. (2009) enameled the A–M glass-ceramic to titanium by heat treatment and thereafter analyzed the interfacial reaction zone between the A–M glass-ceramic and the titanium alloy by high-angle annular dark field TEM (HAADF-TEM). Stanton et al. (2009) found that titanium diffused into the intermediate layer of the glass-ceramic and postulated that complex titanium silicides and titanium phosphides were formed based on the elemental analysis of the interfacial zones by energy dispersive X-rays (EDX), which produced characteristic photons for Ti, Si, and P elements, but not O elements. This study provides evidence that the A–M system can chemically adhere to titanium. This can be useful in overcoming the problem of coating detachment observed with micromechanical surface retention of plasma sprayed HAp coatings (Filiaggi et al., 1991). The A–M glass-ceramic coating may enhance osseointegration at the bone–implant interface and provide long-term stability of the A–M coated implants.

Wood and Hill (1991) produced cements from the A–M glass-ceramic ionomer-type systems with varying degrees of crystallinity for potential application as bone cements. Wood and Hill (1991) found that the degree of crystallinity of the A–M glass-ceramic can influence the properties of the cements, such as working and setting times of the cement pastes and the mechanical properties of the set cements.

Strontium-Substituted FAp Glass-Ceramics

Hill et al. (2004) developed strontium-substituted FAp glass-ceramics for potential orthopedic applications, in the system SiO_2–Al_2O_3–P_2O_5–CaO/SrO–CaF_2/SrF_2 (**Table 5**). Since strontium has a higher atomic number than calcium, strontium-substituted materials exhibit higher radiopacity, which enables the clinician to distinguish between the implant and bone on a radiograph.

Hill et al. (2004) observed that substituting strontium for calcium has little effect on the parent glass structure. However, the crystallization behavior of the glasses as a function of strontium content was markedly altered. Base glasses without any strontium exhibited complete bulk crystallization with the first crystallization temperature being independent of the particle size, whereas

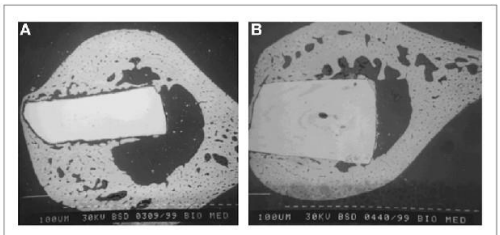

FIGURE 6 | Backscattered scanning electron micrographs of implanted LG120 base glass (A) and implanted LG120 glass-ceramic following subsequent crystallization to fluorapatite and mullite phases (B) (Freeman et al., 2003).

TABLE 5 | Strontium-substituted fluorapatite base glass compositions in mol% (Hill et al., 2004).

Glass code	SiO_2	Al_2O_3	P_2O_5	CaO	CaF_2	SrO	SrF_2
LG26	32.14	21.43	10.71	21.43	14.29	0.00	0.00
LG119	32.14	21.43	10.71	10.71	14.29	10.71	0.00
LG125	32.14	21.43	10.71	0.00	14.29	21.43	0.00
LG26Sr	32.14	21.43	10.71	0.00	0.00	21.43	14.29

glasses with strontium and no calcium exhibited predominantly surface nucleation. Glasses with equimolar proportions of calcium and strontium crystallized through bulk and surface. Hill et al. (2004) demonstrate that increasing strontium substitution hinders bulk crystallization of apatite, which is reflected in an increase in crystallization temperature, and promotion of surface nucleation of apatite at the expense of bulk nucleation, as evidenced by particle size dependence on the crystallization temperature of the FAp phases. Hill et al. (2004) also observed that equimolar strontium–calcium composition resulted in a glass with a reduced second exotherm associated with mullite crystallization. This can be attributed to an increased mobility of the glass network and a lower glass transition temperature, which produces a more dominant heterogenous crystallization effect. Such a reduction in crystallization temperature would suggest a new crystalline phase, and not simply a reduction in crystallization temperature Hill et al. (2004).

In another study, Hill et al. (2006) elucidated Ca and Sr sites in mixed FAp through ^{19}F MAS-NMR. Results showed the F to be present as F–Ca(3) in the all calcium glass and as F–Sr(3) in the all strontium glass. In the mixed glasses, fluorine was present as mixed sites: F–Ca(3), F–Ca(2)Sr, F–CaSr(2), and F–Sr(3). Ca had a higher tendency to occupy the F–M(3) sites than Sr, which may reflect the higher charge to size ratio of Ca^{2+} relative to Sr^{2+} and its greater affinity for F^- ions.

An *in vivo* animal study by Sabareeswaran et al. (2013) on a glass-ceramic that surface crystallized to a strontium FAp phase and a Sr-celsian phase (feldspar) as identified by XRD was found to be highly osteoconductive and biocompatible. X-ray microtomography (XMT) analyses of the synthetic–organic interfaces showed highly mineralized newly formed bone adjacent to the synthetic implant surface.

It is known that, at low concentrations, strontium can promote mineralization of bone (Verberckmoes et al., 2003). It is also known that strontium-containing bio-glasses show increased osteoblast proliferation and alkaline phosphatase activity (Gentleman et al., 2010). Therefore, it would be desirable to establish ion release (particularly Sr^{2+}) profile for the strontium FAp GC systems developed by Hill et al. (2004).

FAp and Chlorapatite Glass-Ceramics

Recently, Chen et al. (2014a,b) developed novel alkali-free FAp and chlorapatite (ClAp) glass-ceramics from bioactive glasses. Chen et al. (2014a) produced a series of bioactive glasses of varying metal fluoride content and found that bioactive glasses with high fluoride content crystallized to FAp and crystalline CaF_2 and SrF_2 on quenching. This demonstrates that metal fluoride content can determine crystallization window (T_x) between the glass transition (T_g) and the crystallization onset (T_{onset}). It is desirable to obtain initially amorphous base glass so that the crystallization of, say a FAp phase, can be controlled. Chen et al. (2014a) also found that the amorphous base glass powder without any fluoride content crystallized to a wollastonite phase through a surface mechanism. Additionally, all fluoride-containing glasses bulk crystallized to FAp *via* a homogenous nucleation mechanism.

Chen et al. (2014c) were able to develop novel bioactive chloroapatite, ClAp glass-ceramics in the system of SiO_2–P_2O_5–CaO–$CaCl_2$. It is known that ClAp completely converts to HAp in the presence of water (Elliott and Young, 1967), hence making ClAp glass-ceramics attractive for both, medical, and dental applications. Chen et al. (2014c) emphasize that ClAp is less stable than FAp. This is attributed to the chloride ion being larger than hydroxyl or fluoride ion. The fluoride ion is small enough to fit in the center of the Ca(II) triangle in the FAp lattice, whereas larger ions such as hydroxyl and chloride do not fit in the center of the Ca(II) triangle but are rather displaced above the plane of the Ca(II) triangle. The chloride ion is larger than hydroxyl ion, and therefore, it is displaced further away from the Ca(II) triangle. This intrinsic apatite lattice instability brought about by the chloride ion allows the rapid exchange for a smaller ion, such as a hydroxyl ion. On increasing the fluoride or chloride content in the bioactive glass systems, Chen et al. (2014b,c) found that there was an increasing tendency of the glasses to crystallize. The halogen-free glass surface crystallized to a pseudowollastonite (α-$CaSiO_3$) and an apatite, presumably an oxyapatite. Pseudowollastonite induces apatite formation in SBF (Siriphannon et al., 2000) and is highly resorbable *in vivo* (De Aza et al., 2000). ClAp phases in the Chen et al. (2014b) crystallized *via* the homogenous route, which from a material processing point of view is highly desirable. FAp is largely insoluble *in vivo* so ClAp GCs offer the potential for producing highly resorbable GC implants. Nonetheless, there is a need for further characterization of these ClAp GCs, including characterization of the *in vivo* activity and the relationships between the composition, heat-treatment, microstructure, and mechanical properties.

Dentistry

FAp–Leucite Glass-Ceramics

Höland et al. (1994) developed FAp-leucite ($KAlSi_2O_6$) (A–L) glass-ceramics in the SiO_2–Al_2O_3–Na_2O–K_2O–P_2O_5–F system, for potential application in restorative dentistry. Research led by Höland led to the development of the commercial A–L glass-ceramic IPS d.SIGN (Ivoclar Vivadent, Liechtenstein). Needle-like apatite phase in the A–L system crystallized through a homogenous crystallization mechanism, which is a likely indication of prior LLPS. Additionally, upon DSC analyses of the A–L system, Höland et al. (2000) observed a unique phenomenon; the A–L system exhibits two endothermic reactions, first at 565°C and second endothermic reaction at 634°C. Previously, the two endothermic reactions were assigned to a phase transformation into two amorphous phases; one glassy, silica-rich phase and a droplet-like phase rich in Ca and P elements. Höland et al. (2000) suggests that the second endothermic reaction at 634°C is a transformation to a crystal phase, namely a sodium–calcium orthophosphate ($NaCaPO_4$), which was confirmed by XRD analysis. Furthermore, Höland et al. (2000) observed another interesting phenomena; at higher temperatures (640°C), $NaCaPO_4$ crystals dissolved and recrystallized to a new crystal phase. However, this new crystal phase could not be matched to any known phases when checked against the International Center of Diffraction Data (ICDD) database. Additionally, Höland et al. (2000) found that once the new phase is formed, apatite crystallization proceeds at 700°C. Heat treatment of the A–L system at 700°C for 8 h does not result in a material with needle-like

microstructure; it requires additional heat treatment at 1,050°C for 2 h for the development of needle-like FAp crystals (Höland et al., 2000). This demonstrates that the thermal treatment of the base glass can strongly influence both, the appearance and other properties of the GC material.

Höland et al. (2000) suggest that the morphology of the needle-like apatite is comparable to that of the apatite in natural teeth; therefore, such needle-like FAp morphology imparts the GC restoration with exceptional esthetics. The A–L glass-ceramic exhibits good chemical durability, solubility of the GC being only at 60–70 μg/cm^2. Translucency of the A–L system varies between 5.8 and 10.4%, depending on the mode of processing. The A–L shows thermal expansion of 14.1–14.8 × 10^{-6} K^{-1}, which is close to that of titanium; therefore, the A–L glass-ceramic is highly suitable for direct sintering on metal abutments. Since 1998, there have been more than 60 million dental restorations performed using commercial IPS d.SIGN® A–L glass-ceramic (Höland and Rheinberger, 2008), making it the most commercially successful apatite glass-ceramic developed to date.

Strontium-Substituted A–L Glass-Ceramics

Höland et al. (2015) developed radiopaque strontium FAp (Sr-FAp) containing glass-ceramics (**Table 6**) for dental applications where Sr–FAp phase crystallized through homogenous mechanisms. Höland et al. (2015) were also able to obtain secondary and tertiary crystal phases, in addition to Sr–FAp, including leucite ($KAlSi_2O_6$), rubidium leucite ($RbSi_2O_6$), cesium pollucite ($CsAl_2S_2O_6$), and sodium strontium orthophpshate ($NaSrPO_4$). However, both leucite phases and pollucite phases showed surface crystallization. Höland et al. (2015) found that some of the base glasses that were rapidly quenched into water (to prevent crystallization) did not avoid crystallization completely. Based on XRD analyses of all parent glasses, Höland et al. (2015) found that all glasses, except reference glass No. 5, were nanocrystalline. XRD analyses of the base glasses No. 1 and No. 2 showed the presence of nanoscale $Sr_5(PO_4)_3F$, whereas base glasses No. 3 and 4 contained nanocrystalline phases of $NaSrPO_4$. Höland et al. (2015) also report that only two of the "as-quenched" base glasses were optically clear, namely, No. 1 and 5, as opposed to base glasses No. 2, 3, and 4, which were opalescent in the visible light. Höland et al. (2015) showed that Sr–FAp glass-ceramics are radiopaque; therefore, these dental GCs may become more clinically relevant once commercialized.

TABLE 6 | Strontium fluorapatite base glass compositions in mol% (Höland et al., 2015).

Glass code	1	2	3	4	5
SiO_2	58.7	59.4	60.4	61.1	66
Al_2O_3	9	9.1	9	9.1	8.5
Y_2O_3	3.1	2.2	0.1	0.1	–
La_2O_3	–	–	0.3	–	–
CaO	–	–	–	–	1.8
SrO	5.5	5.5	7.9	5.9	–
ZnO	–	–	–	–	1.3
Na_2O	10.1	10.2	8.4	10	8.9
K_2O	7.5	7.6	2.6	2.7	6.4
P_2O_5	1.8	1.8	1.8	1.7	0.2
F	2.4	2.3	2.6	2.4	3.2
Cs_2O	–	–	4.9	–	–
Rb_2O	–	–	–	4.8	–
ZrO_2	0.5	0.5	0.5	0.6	2.1
TiO_2	0.2	0.2	0.2	0.2	1.2
CeO_2	0.4	0.4	0.4	0.4	0.3
B_2O_3	0.3	0.3	0.4	0.2	0.1
Li_2O	0.5	0.5	0.5	0.8	–
Crystal phase	$Sr_5(PO_4)_3F$, $KAlSi_2O_6$	$Sr_5(PO_4)_3F$, $KAlSi_2O_6$, $NaSrPO_4$	$Sr_5(PO_4)_3F$, $CsAlSi_2O_6$, $NaSrPO_4$	$Sr_5(PO_4)_3F$, $RbAlSi_2O_6$, $NaSrPO_4$	$Ca_5(PO_4)_3F$

NANOSCALE APATITE GLASS-CERAMICS AND OPTOELECTRONICS

Glass-ceramics containing nanoscale phases of crystals are produced by carefully controlling heat treatments of the parent glasses, in which the nucleation rate is enhanced and the crystal growth rate is low. Crystal growth rates can be suppressed by keeping the crystal growth temperature close to T_g. The T_g of the residual glass phase increases as crystallization occurs. Crystallization of fluorine containing phases, such as FAp is particularly attractive here since a reduction in fluorine content in the residual glass phase results in a large increase in T_g. Alternatively, nanocrystalline phases in GCs can be obtained by developing parent glasses that phase-separate on a nanoscale, whereby subsequent crystal growth is limited by the boundaries of the LLPS domain, provided the parent glass does not overcome kinetic energy barrier to OR during heat treatment. Regardless of the application of the nano-GCs, the size and microstructure of apatite crystals are very important factors that determine whether a glass-ceramic is opaque or transparent after crystallization. Transparent GCs contain crystals smaller than the wavelength of light. Such nanoscale GCs are used for different applications, ranging from transparent zero thermal expansion coefficient cooking hobs, consumer electronics to laser amplifiers in optoelectronics. Transparency of the GC is highly desirable in these applications because light transmission through a transparent GC is highly efficient due to no or low internal light scattering.

Rare earth elements, such as those in the lanthanide group have special photon absorption and reemission properties. Under near-infrared excitation, rare earth elements can absorb low energy photons and reemit high energy photons (anti-Stokes emission). In contrast, quantum dots or organic dyes, on the other hand, are excited by high-energy photons but reemit low-energy photons (Stokes emission), which exhibit luminescence in the visible spectrum.

Glasses and glass-ceramics doped with rare earth elements exhibit special optical properties. Such glasses and glass-ceramics are used for applications in solid-state lasers, optical amplifiers, and display screens. Glasses doped with rare earth elements usually exhibit broader spectral bands and smaller absorption and reemission characteristics as compared to glass-ceramics, which are more efficient and show higher absorption and re-emission characteristic in addition to narrower spectral bands (Zhang et al., 2012, 2013a,b).

Furthermore, fluoride-containing crystals such as FAp are also known to have low phonon energies and low-dielectric loss, which is an attractive property in optoelectronics. Despite the commercial use of single crystal lasers based on apatites and the fact that apatite lattices are also very attractive for accommodating rare earth ions, there is limited number of publications on nanocrystalline apatite glass-ceramics since the first patent publication by Pinckney and Dejneka (1998).

Tulyaganov (2000) developed FAp ($Ca_5(PO_4)_3F$)–anorthite ($CaAl_2Si_2O_8$)–diopside ($CaMgSi_2O_6$) glass-ceramics in the system of SiO_2–Al_2O_3–P_2O_5–CaO–CaF_2–MgO (**Table 7**) for potential applications in optical amplifiers. In the above system, FAp crystallization was through a homogenous mechanism, whereas anorthite and diposide phases crystallized *via* a surface mechanism.

Hill et al. (2010) found evidence that FAp crystallization in the GC developed by Tulyaganov (2000) was on a nanoscale and self-limiting. Hill et al. (2010) provide evidence that FAp crystallization is self-limiting because the system exhibits LLPS on a nanoscale, i.e., the size of the phase-separated domain restricts subsequent crystal growth such that it cannot grow easily beyond the bounds of the LLPS. Hill et al. (2010) also argued that if the crystallization of the fluorine-containing crystal phase occurs close to the glass transition temperature and the crystallization process results in a significant increase in the glass transition temperature, the surrounding "glassy" phase will limit further crystal growth because of the increased glass transition temperature. Hill et al. (2010) proposed that metal fluoride content at or below the stoichiometry of the FAp crystal is one of the factors needed to obtain nanoscale phases of FAp in the GC studied. These results are explained in terms of an approach, which views glasses as being inorganic polymers where the presence of fluorine disrupts the glass network, and thereby reduces the energy barrier to homogeneous nucleation and crystallization of the FAp phases. Notably, Hill et al. (2010) also found some evidence that Mg can occupy Ca(II) sites of the FAp lattice, which was previously unknown in GCs. It is widely known that Mg^{2+} cations limit apatite crystal growth by blocking surface sites on the FAp crystal.

Doped single crystal FAp have been considered for potential applications in lasers (Ohlmann et al., 1968; Deloach et al., 1993, 1994). However, their poor thermomechanical properties (Hopkins et al., 1971; Payne et al., 1994) can result in beam distortion due to thermal distortion that produces refractive index variations within the crystal. Furthermore, production of single crystals of FAp is not only expensive but unlike a glass-ceramic route cannot be processed into fibers and complex shapes. Polycrystalline apatites generally result in an opaque material, which is undesirable for optoelectronics unless the crystals are nanoscale and less than the wavelength of light. Consequently, nanocrystalline FAp GCs are of particular interest.

Zhang et al. (2012, 2013a,b) developed Nd and Eu-doped visually transparent FAp glass-ceramics (**Table 8**) for potential applications in optical amplifiers. Nd and Eu ions are f-block elements and can exhibit high degree of up-conversion in appropriate crystal lattices; therefore, they are highly attractive dopants in rare earth accommodating lattices, such as the apatite. Zhang et al. (2012, 2013a,b) systems crystallize to FAp and mullite; therefore, careful control of the heat treatment is crucial to avoid the crystallization of the mullite phase.

The ZH1 Nd doped glass (**Table 8**), as compared to its undoped version, showed a markedly reduced FAp crystallization temperature, in contrast, ZH3, strontium version of the same parent glass (**Table 8**) did not show a reduction in crystallization temperature but rather a less pronounced area under the exotherm assigned to FAp. Furthermore, although Zhang et al. (2013b) systems contain strong nucleants, such as P_2O_5, comparing DSC traces of doped and undoped ZH3 versions, less pronounced FAp exotherms observed with Nd doped GC may be attributed to enhanced heterogenous nucleation mechanism, as opposed to reduced overall crystallization; however, such explanation would have to be confirmed by analyzing particle size dependence on the crystallization temperature. Notably, Zhang et al. (2012) system (ZH1, **Table 8**) could remain optically clear after 24-h heat treatment at 790°C. This indicates that Zhang et al. (2012) system has undergone LLPS on a nanoscale, which therefore restricts FAp growth beyond the LLPS domain. Additionally, the kinetic barrier to OR during heat treatment is, therefore, not overcome in Zhang et al. (2012, 2013a,b) systems, which prevents crystal growth into the light scattering dimensions.

Furthermore, SrFAp (Zhang et al., 2013b), as opposed to CaFAp (Zhang et al., 2012), GC was found to have a markedly reduced visible spectrum transmittance, which authors attributed to a lower volume fraction of SrFAp crystals ($12 \pm 2\%$) as opposed to volume fraction of CaFAp ($19 \pm 6\%$) in the alternative calcium-containing GC system. Additionally, Zhang et al. (2012) found that Nd-doped calcium FAp GC showed better absorption and emission properties as compared to a strontium FAp GC (Zhang et al., 2013b) and argued that better absorption and emission

TABLE 7 | Fluorapaite–anorthite–diposide base glass composition in mol%.

SiO_2	Al_2O_3	P_2O_5	CaO	CaF_2	MgO
34.7	11.1	5.4	37.2	1.8	9.7

TABLE 8 | Compositions of Nd and Eu doped base glasses in mol% (Zhang et al. (2012, 2013a,b)).

	SiO_2	Al_2O_3	P_2O_5	$CaCO_3$	$SrCO_3$	CaF_2	SrF_2	La_2O_3	$LiCO_3$	B_2O_3	ZrO_2	Nd_2O_3	Eu_2O_3
$Ca_5(PO_4)_3F:Nd^{3+}$ (ZH1)	29.4	18	12	20	0	18	0	0.3	0.5	0.3	0.5	1	0
$Ca_5(PO_4)_3F:Eu^{3+}$ (ZH2)	29.4	18	12	20	0	18	0	0.3	0.5	0.3	0.5	0	1
$Sr_5(PO_4)_3F:Nd^{3+}$ (ZH3)	29.4	18	12	0	20	0	18	0.3	0.5	0.3	0.5	1	0

properties of a calcium FAp GC may be attributed to a higher fraction of Nd ions being incorporated into the former crystal lattice. Therefore, Nd-doped calcium FAp GCs likely have an advantage over Nd-doped strontium FAp GCs.

Nonetheless, Zhang et al. (2012, 2013a,b) were able to closely match the refractive index between the glass matrix and the crystal phases for smooth photon transitions across the medium. Additionally, the crystals in the GCs are smaller than the excitation and emission wavelengths and, therefore, such crystals are outside of the light scattering dimensions that in turn produce an energy-efficient material for luminescence applications.

NUCLEAR WASTE IMMOBILIZATION

Currently, high-level radioactive waste (HLW) from nuclear fission products are fused at high temperatures (~1,250°C) with a borosilicate glass and subsequently stored in repositories. However, due to long half-life of α-emitting radioactive elements, these HLW can potentially only be stored for up to 300 years in these glass matrices. GC, on the other hand, can provide a useful alternative for nuclear waste immobilization because they will provide two barriers of containment: one being the host crystal phase(s) and second the amorphous glass matrix. Additionally, a devitrified material is more resistant to water due to a higher network connectivity of the residual glassy phase.

Weber et al. (1979) and Weber (1993) analyzed Cm-doped silicates with the apatite structure but found them to be poor nuclear waste hosts as they completely transformed into an amorphous state. This resulted in a volume expansion and microfracturing of the material.

It is quite important to point out that phosphate apatite, as opposed to other apatitic phases show better resistance to amorphization (due to nuclear decay) and better chemical stability. Soulet et al. (2001) demonstrated that phosphosilicate FAp ceramics exhibit increasing resistance to amorphization when SiO_4 is substituted by PO_4. Fang et al. (2014) also found that phosphate apatites exhibit superior chemical stability (under acetic acid challenge) when the atomic proportion of phosphorus replaced by silicon and sulfur did not exceed one-third.

At the Atomic Weapons Establishment (UK), Donald et al. (2007) developed novel calcium phosphate-based halogen-containing calcium apatite ceramics for a universal actinide- and halide-containing waste immobilization. In the preliminary study, Donald et al. (2007) produced four types of experimental halide-containing nuclear waste streams, in addition to a series of mainly sodium aluminum phosphate (NaAlP) glasses for subsequent encapsulation of the waste-hosting calcium phosphate ceramics. However, it is important to underline that apatite ceramics developed by Donald et al. (2007) require additional encapsulation in a durable glass matrix. Therefore, it may be argued that systems developed by Donald et al. (2007) are not traditional GCs; however, research led by Donald et al. (2007) is still ongoing. From a manufacturing point of view, developing a "traditional" apatite GC could possibly provide a more economical alternative. Nonetheless, apatite-containing glass-ceramics are potentially excellent candidates as nuclear waste hosts, which evident from studies on the apatite ceramic materials. Therefore, there is a great but challenging potential for new developments in this field.

CONCLUSION

The review provides an overview of the apatite glass-ceramics, their crystallization behavior, their remarkable properties, and commercial applications in the fields of medicine and dentistry, optoelectronics, and potential nuclear waste management.

The A–W glass-ceramic discussed in the review shows excellent osseointegration and exhibits clinically suitable mechanical properties, including fracture toughness and flexural strength. However, the failure of this system to bulk nucleate and a lack of bioresorbablity open up new challenging fronts for research and development to overcome these drawbacks. Data on the newly developed chlorapatite GCs suggest that these materials may provide the desired resorbability and osseointegration; however, further work is required in terms of their *in vivo* activity and structure–property relationship, including the microstructure and mechanical properties.

To date, the most commercially successful apatite glass-ceramics are those developed for dental veneering. These dental GCs exhibit low solubility, excellent translucency, and clinical esthetics, and are biomimetic in nature.

Current information in the literature suggests that apatite is potentially a good host phase for radioactive waste entrapment. Apatite glass-ceramics would be highly attractive for this application; however, a lack of publications in this area suggests that further studies are required.

The authors would like to conclude that apatite lattice inherently exhibits ease of solid solution whereby various ionic substitutions can take place. As such, its solid-state chemistry is of great interest in both, the fundamental as well as the applied research. Understanding derived from research in apatite-containing glass-ceramics continues to intrigue and convey new concepts in structural solid-state chemistry and the applied sciences discussed in this review with undoubtedly a great future potential.

AUTHOR CONTRIBUTIONS

TD produced the manuscript. SS and RH contributed to the critical revision and direction of the manuscript.

FUNDING

The authors would like to thank Cera Dynamics Limited, part of the James Kent Group and the Institute of Dentistry (Queen Mary University of London) for jointly funding TD.

REFERENCES

An, Y. H., and Draughn, R. A. (2000). *Mechanical Testing of Bone and the Bone-Implant Interface*. Boca Raton: CRC Press.

Blades, M., Moore, D., Revell, P., and Hill, R. (1998). *In vivo* skeletal response and biomechanical assessment of two novel polyalkenoate cements following femoral implantation in the female New Zealand White rabbit. *J. Mater. Sci. Mater. Med.* 9, 701–706. doi:10.1023/A:1008990516159

Blumenthal, N. C., Betts, F., and Posner, A. S. (1975). Effect of carbonate and biological macromolecules on formation and properties of hydroxyapatite. *Calcif. Tissue Res.* 18, 81–90. doi:10.1007/BF02546228

Cahn, J. W. (1969). The metastable liquidus and its effect on crystallization of glass. *J. Am. Ceram. Soc.* 52, 4. doi:10.1111/j.1151-2916.1969.tb11194.x

Calver, A., Hill, R. G., and Stamboulis, A. (2004). Influence of fluorine content on the crystallization behavior of apatite-wollastonite glass-ceramics. *J. Sci. Mater.* 39, 2601–2603. doi:10.1023/B:JMSC.0000020038.79675.0f

Chen, X., Brauer, D. S., Wilson, R. M., Hill, R. G., and Karpukhina, N. (2014a). Bioactivity of sodium free fluoride containing glasses and glass-ceramics. *Materials* 7, 5470–5487. doi:10.3390/ma7085470

Chen, X., Brauer, D. S., Wilson, R. M., Hill, R. G., and Karpukhina, N. (2014b). Novel alkali free bioactive fluorapatite glass ceramics. *J. Non Cryst. Solids* 402, 172–177. doi:10.1016/j.jnoncrysol.2014.05.025

Chen, X., Hill, R., and Karpukhina, N. (2014c). Chlorapatite glass-ceramics. *Int. J. Appl. Glass Sci.* 5, 207–216. doi:10.1111/ijag.12082

Clifford, A., and Hill, R. (1996). Apatite-mullite glass-ceramics. *J. Non Cryst. Solids* 196, 346–351. doi:10.1016/0022-3093(95)00611-7

Clifford, A., Hill, R., Towler, M., and Wood, D. (2001a). The crystallisation of glasses from the ternary CaF_2-$CaAl_2Si_2O_8$-P_2O_5 system. *J. Sci. Mater.* 36, 3955–3961. doi:10.1023/A:1017974306184

Clifford, A., Hill, R., Rafferty, A., Mooney, P., Wood, D., Samuneva, B., et al. (2001b). The influence of calcium to phosphate ratio on the nucleation and crystallization of apatite glass-ceramics. *J. Mater. Sci. Mater. Med.* 12, 461–469. doi:10.1023/A:1011213406951

De Aza, P. N., Luklinska, Z. B., Martinez, A., Anseau, M. R., Guitian, F., and De Aza, S. (2000). Morphological and structural study of pseudowollastonite implants in bone. *J. Microsc.* 197(Pt 1), 60–67. doi:10.1046/j.1365-2818.2000.00647.x

Deloach, L., Payne, S., Chase, L., Smith, L., Kway, W., and Krupke, W. (1993). Evaluation of absorption and emission properties of Yb-3 + doped crystals for laser applications. *IEEE J. Quant. Electron.* 29, 1179–1191. doi:10.1109/3.214504

Deloach, L., Payne, S., Smith, L., Kway, W., and Krupke, W. (1994). Laser and spectroscopic properties of Sr-5(PO4)(3)F-Yb. *J. Opt. Soc. Am. B* 11, 269–276. doi:10.1364/JOSAB.11.000269

Denry, I., Holloway, J., and Gupta, P. (2012). Effect of crystallization heat treatment on the microstructure of niobium-doped fluorapatite glass-ceramics. *J. Biomed. Mater. Res. B Appl. Biomater.* 100B, 1198–1205. doi:10.1002/jbm.b.32684

Donald, I., Metcalfe, B., Fong, S., Gerrard, L., Strachan, D., and Scheele, R. (2007). A glass-encapsulated calcium phosphate wasteform for the immobilization of actinide-, fluoride-, and chloride-containing radioactive wastes from the pyrochemical reprocessing of plutonium metal. *J. Nucl. Mater.* 361, 78–93. doi:10.1016/j.jnucmat.2006.11.011

Ducheyne, P., Healy, K. E., Grainger, D. W., Hutmacher, D. W., and Kirkpatrick, C. J. (2011). *Comprehensive Biomaterials*. Oxford: Elsevier.

Elliott, J. C., and Young, R. A. (1967). Conversion of single crystals of chlorapatite into single crystals of hydroxyapatite. *Nature* 214, 904–906.

Fang, Y., Ritter, C., and White, T. (2014). Crystal chemical characteristics of ellestadite-type apatite: implications for toxic metal immobilization. *Dalton Trans.* 43, 16031–16043. doi:10.1039/C4DT02088J

Fechtelkord, M., Behrens, H., Holtz, F., Fyfe, C., Groat, L., and Raudsepp, M. (2003). Influence of F content on the composition of Al-rich synthetic phlogopite: Part 1. New information on structure and phase-formation from Si-29, H-1, and F-19 MAS NMR spectroscopies. *Am. Mineral.* 88, 47–53. doi:10.2138/am-2003-0106

Filho, O. P., Latorre, G. P., and Hench, L. L. (1996). Effect of crystallization on apatite-layer formation of bioactive glass $45S_5$. *J. Biomed. Mater. Res.* 30, 509–514. doi:10.1002/(SICI)1097-4636(199604)30:4<509::AID-JBM9>3.0.CO;2-T

Filiaggi, M. J., Coombs, N. A., and Pilliar, R. M. (1991). Characterization of the interface in the plasma-sprayed HA coating/Ti-6Al-4V implant system. *J. Biomed. Mater. Res.* 25, 1211–1229. doi:10.1002/jbm.820251004

Freeman, C. O. I, Brook, M., Johnson, A., Hatton, P. V., Hill, R. G., and Stanton, K. T. (2003). Crystallization modifies osteoconductivity in an apatite-mullite glass-ceramic. *J. Mater. Sci. Mater. Med.* 14, 985–990. doi:10.1023/A:1026306901058

Gentleman, E., Fredholm, Y. C., Jell, G., Lotfibakhshaiesh, N., O'Donnell, M. D., Hill, R. G., et al. (2010). The effects of strontium-substituted bioactive glasses on osteoblasts and osteoclasts *in vitro*. *Biomaterials* 31, 3949–3956. doi:10.1016/j.biomaterials.2010.01.121

Goodridge, R. D., Wood, D. J., Ohtsuki, C., and Dalgarno, K. W. (2007). Biological evaluation of an apatite-mullite glass-ceramic produced via selective laser sintering. *Acta Biomater.* 3, 221–231. doi:10.1016/j.actbio.2006.10.005

Grossman, D. G. (1972). Machinable glass-ceramics based on tetrasilicic mica. *J. Am. Ceram. Soc.* 55, 446–449. doi:10.1111/j.1151-2916.1972.tb11337.x

Hill, R., Calver, A., Skinner, S., Stamboulis, A., Law, R., Nakamura, T., et al. (2006). A MAS-NMR and combined Rietveldt study of mixed calcium/strontium fluorapatite glass-ceramics. *Bioceramics* 18(Pts 1 and 2), 309–311:305–308. doi:10.4028/www.scientific.net/KEM.309-311.305

Hill, R., Calver, A., Stamboulis, A., and Bubb, N. (2007). Real-time nucleation and crystallization studies of a fluorapatite glass-ceramics using small-angle neutron scattering and neutron diffraction. *J. Am. Ceram. Soc.* 90, 763–768. doi:10.1111/j.1551-2916.2006.01474.x

Hill, R., Patel, M., and Wood, D. J. (1991). "Preliminary studies on castable apatite-mullite glass-ceramics," in *4th International Symposium on Ceramics in Medicine* (London: Butterworth Heineman Ltd.).

Hill, R., Rafferty, A., Mooney, P., and Wood, D. (2000). The influence of glass composition on nucleation crystallisation microstructure and properties of apatite-mullite glass-ceramics. *Glass Sci. Technol.* 73(1 Suppl. C), 146–153.

Hill, R., and Wood, D. (1995). Apatite-mullite glass-ceramics. *J. Mater. Sci. Mater. Med.* 6, 311–318.

Hill, R. G., O'Donnell, M. D., Law, R. V., Karpukhina, N., Cochrane, B., and Tulyaganov, D. U. (2010). The early stages of nucleation and crystallisation of an apatite glass-ceramic: evidence for nano-scale crystallisation. *J. Non Cryst. Solids* 356, 2935–2941. doi:10.1016/j.jnoncrysol.2010.05.102

Hill, R. G., Stamboulis, A., Law, R. V., Clifford, A., Towler, M. R., and Crowley, C. (2004). The influence of strontium substitution in fluorapatite glasses and glass-ceramics. *J. Non Cryst. Solids* 336, 223–229. doi:10.1016/j.jnoncrysol.2004.02.005

Höland, W., and Beall, G. H. (2012). *Glass-Ceramic Technology*. Hoboken, NJ; Westerville, OH: Wiley; The American Ceramic Society.

Höland, W., Frank, M., Schweiger, M., and Rheinberger, V. (1994). Development of translucent glass-ceramics for dental application. *Glastech. Ber. Glass Sci. Technol.* 67, 117–122.

Höland, W., and Rheinberger, V. (2008). "Dental glass-ceramics," in *Bioceramics and Their Clinical Applications*, ed. T. Kokubo (Cambridge, England: Woodhead Publishing Limited), 561.

Höland, W., Rheinberger, V., Wegner, S., and Frank, M. (2000). Needle-like apatite-leucite glass-ceramic as a base material for the veneering of metal restorations in dentistry. *J. Mater. Sci. Mater. Med.* 11, 11–17. doi:10.1023/A:1008977416834

Höland, W., Schweiger, M., Dittmer, M., and Ritzberger, C. (2015). Radiopaque strontium fluoroapatite glass-ceramics. *Front. Bioeng. Biotechnol.* 3:149. doi:10.3389/fbioe.2015.00149

Höland, W., and Vogel, W. (2013). "Machinable and phosphate glass-ceramics," in *Introduction to Bioceramics*, ed. L. L. Hench (London: Imperial College Press), 215–228.

Hopkins, R. H., Damon, D. H., Piotrowski, P., Walker, M. S., and Uphoff, J. H. (1971). Thermal properties of synthetic fluorapatite crystals. *J. Appl. Phys.* 42, 272–275. doi:10.1063/1.1659583

James, P. (1981). Nucleation in glass forming systems – a review. *J. Am. Ceram. Soc.* 60, 352–352.

Karageorgiou, V., and Kaplan, D. (2005). Porosity of 3D biomaterial scaffolds and osteogenesis. *Biomaterials* 26, 5474–5491. doi:10.1016/j.biomaterials.2005.02.002

Kitsugi, T., Yamamuro, T., and Kokubo, T. (1989). Bonding behavior of a glass-ceramic containing apatite and wollastonite in segmental replacement of the rabbit tibia under load-bearing conditions. *J. Bone Joint Surg. Am.* 71A, 264–272. doi:10.2106/00004623-198971020-00014

Kitsugi, T., Yamamuro, T., and Kokubo, T. (1990). Analysis of A.W glass-ceramic surface by micro-beam X-ray-diffraction. *J. Biomed. Mater. Res.* 24, 259–273. doi:10.1002/jbm.820240211

Kokubo, T. (2008). "Bioactive glass-ceramics," in *Bioceramics and Their Clinical Applications*, ed. T.Kokubo (Cambridge, England: Woodhead Publishing Limited), 288–289.

Kokubo, T., Ito, S., Sakka, S., and Yamamuro, T. (1986). Formation of a high-strength bioactive glass ceramic in the system MgO-CaO-SiO_2-P_2O_5. *J. Sci. Mater.* 21, 536–540. doi:10.1007/BF01145520

Kokubo, T., Ito, S., Shigematsu, M., Sakka, S., and Yamamuro, T. (1985). Mechanical-properties of a new type of apatite-containing glass ceramic for prosthetic application. *J. Sci. Mater.* 20, 2001–2004. doi:10.1007/BF01112282

Kokubo, T., Ito, S., Shigematsu, M., Sanka, S., and Yamamuro, T. (1987). Fatigue and life-time of bioactive glass-ceramic A-W containing apatite and wollastonite. *J. Sci. Mater.* 22, 4067–4070. doi:10.1007/BF01133359

Kokubo, T., Kushitani, H., Ohtsuki, C., Sakka, S., and Yamamuro, T. (1992). Chemical-reaction of bioactive glass and glass-ceramics with a simulated body-fluid. *J. Mater. Sci. Mater. Med.* 3, 79–83. doi:10.1007/BF00705272

Kokubo, T., Kushitani, H., Sakka, S., Kitsugi, T., and Yamamuro, T. (1990). Solutions able to reproduce *in vivo* surface-structure changes in bioactive glass-ceramic A-W. *J. Biomed. Mater. Res.* 24, 721–734. doi:10.1002/jbm.820240607

Kokubo, T., Shigematsu, M., Nagashima, Y., Tashiro, M., Nakamura, T., Yamamuro, T., et al. (1982). Apatite- and wollastonite-containg glass-ceramics for prosthetic application. *Bull. Inst. Chem. Res. Kyoto Univ.* 60, 260–268.

Kumar, V., and Gill, K. (2009). Aluminium neurotoxicity: neurobehavioural and oxidative aspects. *Arch. Toxicol.* 83, 965–978. doi:10.1007/s00204-009-0455-6

LeGeros, R. Z., Taheri, M. H., Quirolgico, G. B., and LeGeros, J. P. (1980). "Formation and stability of apatites: effects of some cationic substituents," in *2nd International Congress on Phosphorus Compounds* (Boston, MA: IMPHOS (Paris)), 89–103.

McCubbin, F., and Nekvasil, H. (2008). Maskelynite-hosted apatite in the Chassigny meteorite: Insights into late-stage magmatic volatile evolution in martian magmas. *Am. Mineral.* 93, 676–684. doi:10.2138/am.2008.2558

McCubbin, F., Steele, A., Hauri, E., Nekvasil, H., Yamashita, S., and Hemley, R. (2010). Nominally hydrous magmatism on the Moon. *Proc. Natl. Acad. Sci. U. S. A.* 107, 11223–11228. doi:10.1073/pnas.1006677107

Montazerian, M., and Zanotto, E. D. (2016). History and trends of bioactive glass-ceramics. *J. Biomed. Mater. Res. A.* 104, 1231–1249. doi:10.1002/jbm.a.35639

Nakamura, T., Yamamuro, T., Higashi, S., Kokubo, T., and Itoo, S. (1985). A new glass-ceramic for bone replacement: evaluation of its bonding to bone tissue. *J. Biomed. Mater. Res.* 19, 685–698. doi:10.1002/jbm.820190608

Neo, M., Nakamura, T., Ohtsuki, C., Kokubo, T., and Yamamuro, T. (1993). Apatite formation on three kinds of bioactive material at an early stage *in vivo*: a comparative study by transmission electron microscopy. *J. Biomed. Mater. Res.* 27, 999–1006. doi:10.1002/jbm.820270805

O'Donnell, M., Karpukhina, N., Calver, A., Law, R., Bubb, N., Stamboulis, A., et al. (2010). Real time neutron diffraction and solid state NMR of high strength apatite-mullite glass ceramic. *J. Non Cryst. Solids* 356, 2693–2698. doi:10.1016/j.jnoncrysol.2010.08.038

Ohlmann, R. C., Steinbruegge, K. B., and Mazelsky, R. (1968). Spectroscopic and laser characteristics of neodymium-doped calcium fluorophosphate. *Appl. Opt.* 7, 905–914. doi:10.1364/AO.7.000905

Orlovskii, V., Komlev, V., and Barinov, S. (2002). Hydroxyapatite and hydroxyapatite-based ceramics. *Inorg. Mater.* 38, 973–984. doi:10.1023/A:1014029514176

Payne, S., Smith, L., Deloach, L., Kway, W., Tassano, J., and Krupke, W. (1994). Laser, optical, and thermomechanical properties of Yb-doped fluorapatite. *IEEE J. Quant. Electron.* 30, 170–179. doi:10.1109/3.272077

Pinckney, L. R., and Dejneka, M. J. (1998). *Transparent Apatite Glass-Ceramics*. WIPO, WO 1998043922 A1.

Piper, W. W., Kravitz, L. C., and Swank, R. K. (1965). Axially symmetric paramagnetic color centers in fluorapatite. *Phys. Rev.* 138, A1802–A1814. doi:10.1103/PhysRev.138.A1802

Rafferty, A., Clifford, A., Hill, R., Wood, D., Samuneva, B., and Dimitrova-Lukacs, M. (2000a). Influence of fluorine content in apatite-mullite glass-ceramics. *J. Am. Ceram. Soc.* 83, 2833–2838. doi:10.1111/j.1151-2916.2000.tb01640.x

Rafferty, A., Hill, R., and Wood, D. (2000b). Amorphous phase separation of ionomer glasses. *J. Sci. Mater.* 35, 3863–3869. doi:10.1023/A:1004885531712

Rafferty, A., Hill, R., and Wood, D. (2003). An investigation into the amorphous phase separation characteristics of an ionomer glass series and a sodium-boro-silicate glass system. *J. Sci. Mater.* 38, 2311–2319. doi:10.1023/A:1026240525763

Ramsden, A., and James, P. (1984a). The effects of amorphous phase-separation on crystal nucleation kinetics in BaO-SiO2 glasses. 1. General survey. *J. Sci. Mater.* 19, 1406–1419. doi:10.1007/BF01026965

Ramsden, A., and James, P. (1984b). The effects of amorphous phase-separation on crystal nucleation kinetics in BaO-SiO2 glasses. 2. Isothermal heat-treatments at 700-degrees c. *J. Sci. Mater.* 19, 2894–2908. doi:10.1007/BF01026965

Ranu, H. S. (1987). The thermal properties of human cortical bone: an *in vitro* study. *Eng. Med.* 16, 175–176. doi:10.1243/EMED_JOUR_1987_016_036_02

Reusche, E., Pilz, P., Oberascher, G., Lindner, B., Egensperger, R., Gloeckner, K., et al. (2001). Subacute fatal aluminum encephalopathy after reconstructive otoneurosurgery: a case report. *Hum. Pathol.* 32, 1136–1140. doi:10.1053/hupa.2001.28251

Rodriguez, M., Felsenfeld, A. J., and Llach, F. (1990). Aluminum administration in the rat separately affects the osteoblast and bone mineralization. *J. Bone Miner. Res.* 5, 59–67. doi:10.1002/jbmr.5650050110

Sabareeswaran, A., Basu, B., Shenoy, S. J., Jaffer, Z., Saha, N., and Stamboulis, A. (2013). Early osseointegration of a strontium containing glass ceramic in a rabbit model. *Biomaterials* 34, 9278–9286. doi:10.1016/j.biomaterials.2013.08.070

Samuneva, B., Dimitrov, V., Kalimanova, S., Gattef, E., and Hill, R. (1998). Crystallization of gels in the apatite-mullite system. *J. Solgel Sci. Technol.* 13, 951–956. doi:10.1023/A:1008695812143

Segall, B., Ludwig, G. W., Woodbury, H. H., and Johnson, P. D. (1962). Electron spin resonance of a centre in calcium fluorophosphate. *Phys. Rev.* 128, 76–79. doi:10.1103/PhysRev.128.76

Siriphannon, P., Kameshima, Y., Yasumori, A., Okada, K., and Hayashi, S. (2000). Influence of preparation conditions on the microstructure and bioactivity of alpha-CaSiO(3) ceramics: formation of hydroxyapatite in simulated body fluid. *J. Biomed. Mater. Res.* 52, 30–39. doi:10.1002/1097-4636(200010)52:1<30::AID-JBM5>3.0.CO;2-Z

Soulet, S., Carpena, J., Chaumont, J., Kaitasov, O., Ruault, M., and Krupa, J. (2001). Simulation of the alpha-annealing effect in apatitic structures by He-ion irradiation: influence of the silicate/phosphate ratio and of the OH(-)/F(-) substitution. *Nucl. Instrum. Methods Phys. Res. B* 184, 383–390. doi:10.1016/S0168-583X(01)00764-9

Stamboulis, A., Hill, R., Calver, A., Bubb, N., Manuel, P., Nakamura, T., et al. (2006). Real time neutron diffraction studies of apatite glass ceramics. *Bioceramics* 18(Pts 1 and 2), 309–311:309–312. doi:10.4028/www.scientific.net/KEM.309-311.309

Stamboulis, A., Hill, R., Law, R., Matsuya, S., Barbosa, M., Monteiro, F., et al. (2004). A MAS NMR study of the crystallisation process of apatite-mullite glass-ceramics. *Bioceramics* 16, 254–252. doi:10.4028/www.scientific.net/KEM.254-256.99

Stanton, K., O'Flynn, K., Nakahara, S., Vanhumbeeck, J., Delucca, J., and Hooghan, B. (2009). Study of the interfacial reactions between a bioactive apatite-mullite glass-ceramic coating and titanium substrates using high angle annular dark field transmission electron microscopy. *J. Mater. Sci. Mater. Med.* 20, 851–857. doi:10.1007/s10856-008-3650-8

Stanton, K. T., and Hill, R. G. (2005). Crystallisation in apatite-mullite glass-ceramics as a function of fluorine content C3 – proceedings of the 14th international conference on crystal growth and the 12th international conference on vapor growth and epitaxy. *J. Cryst. Growth* 275, e2061–e2068. doi:10.1016/j.jcrysgro.2004.11.266

Stanton, K. T., O'Flynn, K. P., Kiernan, S., Menuge, J., and Hill, R. (2010). Spherulitic crystallization of apatite-mullite glass-ceramics: mechanisms of formation and implications for fracture properties. *J. Non-Cryst. Solids* 356, 1802–1813. doi:10.1016/j.jnoncrysol.2010.07.006

Strnad, Z. (1992). Role of the glass phase in bioactive glass-ceramics. *Biomaterials* 13, 317–321. doi:10.1016/0142-9612(92)90056-T

Tomozawa, M. (1972). Liquid-phase separation and crystal nucleation in Li_2O-SiO_2 glasses. *Phys. Chem. Glasses* 13, 161.

Tulyaganov, D. U. (2000). Phase equilibrium in the fluorapatite-anorthite-diopside system. *J. Am. Ceram. Soc.* 83, 3141–3146. doi:10.1111/j.1151-2916.2000.tb01695.x

Verberckmoes, S., De Broe, M., and D'Haese, P. (2003). Dose-dependent effects of strontium on osteoblast function and mineralization. *Kidney Int.* 64, 534–543. doi:10.1046/j.1523-1755.2003.00123.x

Vogel, W., and Gerth, K. (1962). "Catalyzed crystallization in glass," in *63rd Anniversary of the American Ceramic Society Symposium on Nucleation and Crystallization of Glasses and Melts*, ed. M. K. Reser (Toronto, Canada: American Ceramic Society), 11–22.

Vogel, W., Holand, W., Naumann, K., and Gummel, J. (1986). Development of machineable bioactive glass-ceramics for medical uses. *J. Non-Cryst. Solids* 80, 34–51.

Weber, W. (1993). Alpha-decay-induced amorphization in complex silicate structures. *J. Am. Ceram. Soc.* 76, 1729–1738. doi:10.1111/j.1151-2916.1993.tb06641.x

Weber, W. J., Turcotte, R. P., Bunnell, L. R., Roberts, F. P., and Westsik, J. H. Jr. (1979). "*Radiation Effects in Vitreous and Devitrified Simulated Waste Glass,*" in Ceramics in Nuclear Waste Management, eds T. D. Chikalla and J. E. Mendel (Virginia: National Technical Information Service, Springfield), 294–299.

White, T., Ferraris, C., Kim, J., Madhavi, S., Ferraris, G., and Merlino, S. (2005). Apatite – an adaptive framework structure. *Micro Mesoporous Mineral Phases* 57, 307–401. doi:10.2138/rmg.2005.57.10

Wood, D., and Hill, R. (1991). Glass ceramic approach to controlling the properties of a glass-ionomer bone cement. *Biomaterials* 12, 164–170. doi:10.1016/0142-9612(91)90195-G

Zanotto, E. (2010). A bright future for glass-ceramics. *Am. Ceram. Soc. Bull.* 89, 19–27.

Zanotto, E., James, P., and Craievich, A. (1986). The effects of amorphous phase-separation on crystal nucleation kinetics in $BaO\text{-}SiO_2$ glasses. 3. Isothermal treatments at 718°C to 760°C – small-angle X-ray-scattering results. *J. Sci. Mater.* 21, 3050–3064. doi:10.1007/BF00553336

Zeng, Q., and Stebbins, J. (2000). Fluoride sites in aluminosilicate glasses: high-resolution F-19 NMR results. *Am. Mineral.* 85, 863–867. doi:10.2138/am-2000-5-630

Zhang, S., Huang, J., Chen, Y., Gong, X., Lin, Y., Luo, Z., et al. (2012). Preparation and spectral properties of Nd3 + -doped transparent glass ceramic containing Ca-5(PO4)(3)F nanocrystals. *J. Non Cryst. Solids* 358, 2835–2840. doi:10.1016/j.jnoncrysol.2012.07.005

Zhang, S., Huang, J., Chen, Y., Gong, X., Lin, Y., Luo, Z., et al. (2013a). Site-selective excitation and emission of Eu3 + -doped transparent glass ceramic containing Ca-5(PO4)(3)F nanocrystals. *Opt. Mater. Express* 3, 868–874. doi:10.1364/OME.3.000868

Zhang, S., Huang, J., Chen, Y., Gong, X., Lin, Y., Luo, Z., et al. (2013b). Spectroscopic properties of Nd3 + -doped transparent glass ceramic containing Sr-5(PO4)(3)F nanocrystals. *J. Non Cryst. Solids* 366, 35–41. doi:10.1016/j.jnoncrysol.2013.01.048

Conflict of Interest Statement: The authors declare that the research was conducted in the absence of any commercial or financial relationships that could be construed as a potential conflict of interest.

DENTAL MATERIALS 34 (2018) e83–e88

Available online at www.sciencedirect.com

ScienceDirect

journal homepage: www.intl.elsevierhealth.com/journals/dema

Predicting refractive index of fluoride containing glasses for aesthetic dental restorations

Tomas Duminis, Saroash Shahid, Natalia G. Karpukhina, Robert G. Hill*

Centre for Oral Bioengineering, Institute of Dentistry, Queen Mary University of London, Mile End Road, London E1 4NS, United Kingdom

ARTICLE INFO

Article history:
Received 30 September 2017
Received in revised form
29 December 2017
Accepted 17 January 2018

Keywords:
Aesthetics
Glass ionomer cement
Dental composite
Fluoride
Refractive index
Translucency

ABSTRACT

Objective. Dental restoration aesthetics, particularly the translucency of modern dental restorative filling materials depends on the refractive index (RI) match between the different components in the material. In the case of dental composites (DC), the RI of the polymer must match the RI of the filler otherwise the material is optically opaque and has limited depth of cure. In the case of glass ionomer cements (GICs), the RI of the ion-leachable glass must match the RI of the polysalts to engineer a smart material with a tooth-like appearance. The RI of oxide glasses can be calculated by means of Appen factors. However, no Appen factors are available for the fluoride components in dental glasses. Therefore, the objective of this study is to empirically derive composition-specific Appen factors for the metal fluorides in complex multicomponent glasses for use in dentistry.

Methods. Two series of bioactive glasses and two series of ionomer-type glasses were produced for this study. Refractive indices of all glasses were then measured by the Becke Line technique. Thereafter, composition-specific factors for the metal fluorides were derived.

Results. It was found that increasing metal fluoride content reduces the RI of multicomponent dental glasses linearly. A series-specific Appen factors for the metal fluorides were successfully derived and allow RI calculation to within 0.005.

Significance. This paper proposes a modified Appen Model with composition-specific Appen factors for the metal fluorides for the development of dental restoratives with enhanced aesthetics and improved depth of cure of dental composites.

1. Introduction

The aesthetics, particularly the translucency is an important feature of dental restorations. In order to obtain a translucent glass ionomer cement (GIC) or a dental composite (DC) it is essential to match the refractive index of the glass to the polymer or the polysalt cement matrix to avoid light scattering at the interfaces. Light scattering at the interfaces results in an opaque material. In DCs, light scattering because of a RI mismatch between the resin and the glass filler causes light attenuation and strongly influences the depth of cure of the composite material [1]. Furthermore, in photoactive resin based composites RI mismatch between the resin and the filler increases light scattering, however the RI of the resin changes dynamically during the curing process [2]. This can either

* *Corresponding author.*
E-mail address: t.duminis@qmul.ac.uk (T. Duminis).
https://doi.org/10.1016/j.dental.2018.01.024

Table 1 – Appen factors for the various glass oxides [3].

Oxide	Appen factor
SiO_2	1.4585
Al_2O_3	1.52
P_2O_5	1.31
Na_2O	1.575
ZnO	1.71
K_2O	1.575
CaO	1.73
SrO	1.775

increase or decrease light scattering depending on the refractive index match, i.e. if the RI of the filler matches the RI of the uncured resin, then light scattering will increase as the material polymerizes and if the RI of the resin is lower, then as the material polymerizes, light scattering will decrease and so will the opacity and light transmission through the material. Optimum RI matching and careful design of the DCs may produce DC materials with considerably improved optical properties. The only alternative way to obtain a highly translucent cement is to have well dispersed nano-sized particles where the dimensions of the particles are smaller than the wavelength of the visible light. Such fine scale powder particles are particularly difficult to manufacture as they have a high tendency to aggregate once mixed essentially forming larger clusters to reduce their high surface energy. Furthermore, it is difficult and costly to produce such nano particles particularly from melt-derived glasses. It is notable that translucent glass-ceramics are also produced by matching the RI between the different components in these multiphasic materials i.e. crystal phase/s and the residual "glassy" phase.

In the case of fluoride free glasses the RI of the glass can be calculated within about 0.01 by the means of Appen factors [3], which are empirically derived factors calculated on the basis of previous measurements of RIs of oxide glasses. Appen factors have been successfully used to calculate not only RI but also thermal expansion coefficients [4]. The RI of an oxide glass can be calculated using the following equation:

$$n_d = \frac{\Sigma_{i=1}^{n} n_{d,i} C_i}{100} \quad (1)$$

where $n_{d,i}$ is the Appen factor (Table 1) for the respective oxide component and C_i is the mol% of the oxide component.

However, Appen factors for the metal fluorides are not available. Consequently, the refractive index of fluoride-containing glasses cannot be readily predicted. Fluoride components are known to reduce the RI of various glasses [5] and fluoride-containing glasses are attractive components for dental composites and particularly for GICs. The anticariogenic effects of fluoride have been long known [6]. Based on Scanning Electron Microradiography (SMR) *in vitro* studies, optimum fluoride concentrations under acidic conditions have also been proposed by Mohammed et al. [7].

However, despite the importance of RI it has rarely been measured for fluoride containing dental glasses there is only one peer reviewed article published in the literature. This article demonstrates how increasing CaF_2 content in bioactive glasses allows design of dental composite materials with improved optical properties, such as improved depth of cure and reduced light transmission [8]. Improved depth of cure of the DC will also result in increased longevity of the tooth restoration due to minimized shrinkage and increased polymerization.

Table 2 – Compositions of laboratory bioactive alkali phospho-silicate glasses (mol%) [10].

	SiO_2	P_2O_5	CaO	CaF_2	Na_2O
B2	36.41	6.04	24.74	4.53	28.28
C2	34.60	5.74	23.51	9.28	26.87
D2	32.95	5.47	22.38	13.62	25.59
E2	31.37	5.21	21.31	17.76	24.36
F2	28.40	4.71	19.29	25.54	22.06

The ability to model the role of metal fluorides on the RI of multicomponent glasses also allows the prediction of RI of fluorine-containing glass-ceramics (GCs) used in restorative dentistry, particularly GCs based on fluorapatite and fluormica phases. Since translucency is required for aesthetics, it is important to match the RI of the crystal phase to the residual glass phase. In these glass-ceramics, relatively large interlocking crystals are required to provide optimum strength and fracture toughness, as well as machinability in the case of mica glass-ceramics [9]. GCs containing nano-sized crystal phases would provide the desired aesthetics, however at the expense of mechanical properties and machinability. Therefore in summary it is necessary to develop a model by which RIs of fluoride-containing glasses can be predicted.

The objectives of this paper are to:

i) Measure the RI of two types of the fluoride-containing glasses used in glass (ionomer) cement formulations and as potential remineralising additives in various dental restorative materials.
ii) To develop Appen Factors for fluoride-containing glasses so that RIs of these glasses may be calculated which will allow the design of restoratives with improved translucency.

2. Materials and methods

2.1. *Glass synthesis*

Two series of bioactive glasses containing fluoride components were produced. These are given in Tables 2 and 3. The bioactivity of these two series of bioactive glasses was previously studied by Mneimne et al. [10] and Lynch et al. [11] respectively. In these glasses the metal fluorides were added to the composition rather than substituted for the metal oxide. All glasses were melted in platinum/rhodium 80/20 crucibles. Details of the synthesis conditions are given in the respective papers [10] and [11]. The first series of ionomer-type glasses (Table 4) are based on the series $4.5SiO_2 3Al_2O_3 1.5P_2O_5$(5-X)CaOX$CaF_2$. In this series of ion-leachable glasses CaO is substituted for CaF_2 on a molar basis. These glasses were synthesized using a method described earlier by Stanton and Hill [12]. A second series of high fluorine ionomer-type glasses (Table 5) were provided by Cera Dynamics Limited (Stoke-on-Trent, UK). These high fluorine glass samples were produced in a custom-built cold-top furnace to prevent fluorine volatilization. Full chemical analyses of the industrially manufactured

Table 3 – Compositions of multicomponent bioactive glasses in mol% [11].

	SiO_2	P_2O_5	CaO	CaF_2	SrO	SrF_2	Na_2O	K_2O	ZnO	$CaF_2 + SrF_2$
F0	44	5	15	0	15	0	10	10	1	0
F4	41.91	4.76	14.29	2.38	14.29	2.38	9.53	9.53	0.95	4.76
F13	38.01	4.32	12.96	6.81	12.96	6.81	8.64	8.64	0.86	13.62
F17	36.19	4.11	12.34	8.88	12.34	8.88	8.22	8.22	0.82	17.76
F25	32.76	3.72	11.17	12.77	11.17	12.77	7.45	7.45	0.74	25.54
F32	29.61	3.36	10.09	16.36	10.09	16.36	6.73	6.73	0.67	32.72

Table 4 – Compositions of model laboratory ionomer-type glasses in mol%.

	SiO_2	Al_2O_3	P_2O_5	CaO	CaF_2
LG99	32.14	21.43	10.71	14.29	21.43
LG95	32.14	21.43	10.71	20.00	15.71
LG134	32.14	21.43	10.71	25.00	10.71
LG115	32.14	21.43	10.71	28.57	7.14
LG116	32.14	21.43	10.71	35.71	0.00

Table 5 – Compositions of high fluorine ionomer-type glasses produced by Cera Dynamics Limited (mol%).

	SiO_2	Al_2O_3	P_2O_5	Na_2O	CaO	SrO	Fluorine
PF124	20.00	14.47	1.87	5.15	0.13	8.47	49.90
PF125	28.71	17.48	2.12	1.67	0.09	15.63	34.30
PF126	23.35	13.30	2.05	5.32	0.12	8.86	47.00
PF127	29.16	15.88	2.56	1.66	0.08	15.51	35.15
PF128	25.03	15.90	7.44	1.67	23.61	0.46	25.89
PF129	25.73	17.34	8.37	1.32	26.98	0.08	20.18
PF130	27.85	18.14	4.34	1.55	27.80	0.02	20.30
PF131	26.17	17.73	4.21	1.48	12.59	16.01	21.81

glasses was carried out by X-ray fluorescence. These glasses have much higher fluorine contents than the laboratory synthesized ionomer glasses whose compositions were designed to prevent fluorine loss as volatile silicon tetrafluoride [13].

2.2. *Measurement of RI*

Fluoride-containing glasses are prone to rapid crystallization [12] and fluoride loss on casting therefore as opposed to using Abbé refractometer refractive indices of the samples were measured by the Becke line test [14]. The refractive indices all fluoride-containing amorphous powdered glass samples were measured using polarized light microscopy by mounting the amorphous glass samples in suitable immersion liquids (Cargille, USA) and making observations of the Becke line. The immersion liquids have known refractive index values ranging from 1.45 to 1.70 with 0.01 intervals. Refractive index measurements were performed at room temperature (~20 °C) using the sodium D line. The microscope was calibrated prior to each measurement using a known RI glass sample. Digital images of the glass samples were captured using a digital camera (Q Imaging, Canada) affixed to the microscope and digitised by manufacturer's software.

2.3. *Appen factors*

First, Eq. (1) was used to calculate RIs of all glass samples. Since no Appen factors are available for the metal fluorides, the metal fluoride component contribution to the RI was underestimated. To compensate for this, multiple factors were tried for the respective metal fluoride (CaF_2/SrF_2) component until the calculated RI value matched to within 0.005 to experimentally derived RI value.

Table 6 – Empirically derived Appen factors.

	CaF_2	SrF_2	P_2O_5
[8]	1.42	–	–
[9]	1.45	1.47	–
LG	1.59	–	1.48

3. Results

All glasses used in the study were found to be amorphous by X-ray powder diffraction analyses. Fig. 1(a–c) shows the RI as a function of CaF_2, SrF_2 and F content for phospho-silicate bioactive glasses and alumino-silicate ionomer-type glasses. There is a linear decrease in RI with metal fluoride/elemental fluorine content. A comparison of the experimental and calculated RI values for Mneimne et al. [10] series of bioactive glasses shows a good correlation between the two (Fig. 1(a)). However, for more complex F series of bioactive glasses containing additional oxide components it can be observed that there is a slight deviation between the experimental and calculated values with Ca/SrF_2 contents (Fig. 1(b)). Fig. 1(c) shows the RI for a series of ionomer glasses based on $4.5SiO_2 3Al_2O_3 1.5P_2O_5 (5\text{-}X)CaO XCaF_2$. The RIs calculated using Appen factors agrees well with the experimentally determined RIs. Fig. 1(d) shows the RI as a function of F content for the industrially manufactured high fluorine (PF) series (Table 4) of glasses. In summary, there is a clear linear relationship between fluoride content (either as elemental F or as a metal fluoride) and refractive index of the glasses studied. Table 6 shows series-specific Appen factors derived from this study.

4. Discussion

Based on the experimentally derived RIs of the fluorine-containing glass samples, a linear ($R^2 = 0.98$) correlation between elemental fluorine/metal fluoride content and the refractive index of glasses is clearly observed. Generally, fluorine containing glasses have larger atomic spacings and therefore more disrupted structure. Larger spacing in the glass network results in the reduction in glass density and thus is attributed to lower refractive index. It has been long known that there is a linear correlation between density and refractive index in glasses [15]. However, many materials other than glasses do not exhibit this phenomenon. It may not be surprising that incorporation of fluoride lowers the dielectric constant of the glasses which is observed in other dielectric

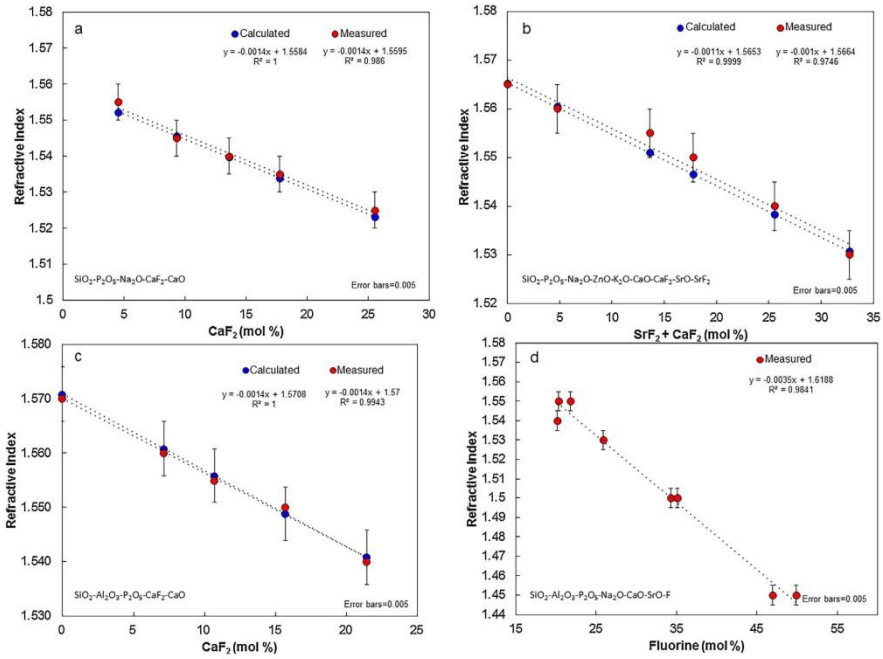

Fig. 1 – Refractive index and fluoride content (a – bioactive glasses described in [10]; b – bioactive glasses described in [11]; c – laboratory synthesised ionomer-type glasses; d – industrially synthesised ionomer-type glasses.

materials [16] and results in reduced polarizability and henceforth a reduction in refractive index.

For the first series of bioactive glasses developed by Mneimne et al. [10] calculated and measured RI values are matching within 0.005. In this series, it was found that CaF_2 contributes to the RI by a factor of 1.42, which is quite close to the RI of crystalline CaF_2, which at room temperature is 1.4338 [17]. It is notable that solid-state ^{19}F MAS-NMR studies of related glasses by Brauer et al. [18] have shown fluorine to be present as F-M(n) species where M is largely Ca with a small fraction of Na and n is close to four molecular dynamics simulations by Christie et al. [19] predict the formation of F-Ca(n) species. Thus in these glasses the fluorine exists in a fluorite like F-Ca(4) environment and it is therefore not surprising that the RI can be predicted based on a model assuming the presence of a fluorite-like environment. Furthermore, Brauer et al. [20] measured the density of CaF_2 containing bioactive glasses and showed the density could be predicted based on the assumption of fluorine existing in a CaF_2 like environment and using a density factor for crystalline CaF_2. It is worth noting that in the present glasses, as well as the ones studied by Brauer et al. [20] the CaF_2 was added to the glass rather than being substituted for CaO and in these glasses there is no change in the non-bridging oxygen content and the Q speciation of the silicon remains constant. In the original studies of Hench et al. [21] and more recently by Lusvardi et al. [22] CaF_2 was substituted for CaO which results in changes in the non-bridging oxygen content of the glass and the silicon speciation as well as potential loss of fluorine as silicon tetrafluoride during melting.

The calculations for the second series of bioactive glasses (Table 3) [11] with strontium and potassium components have also been performed by assuming the nominal proportions of CaF_2 and SrF_2 incorporated in the original glass composition. It was found that metal fluorides contribute to the RI by a factor of 1.45 (CaF_2) and 1.47 (SrF_2), which is higher than the factor for the first series. In the final melted glass composition the fluorine might be expected to form more F-Ca(n) species than F-Sr(n) species since Ca^{2+} has a slightly smaller ionic size than Sr^{2+} and this might be expected to favour F-Ca(n) speciation. In addition there is likely to be mixed F-Ca/Sr(n) and F-Na(n) sites where Na and Ca is more prevalent than Sr and this may an effect on the RI and hence may explain why the Appen factor for the metal fluoride component in this series is higher.

Appen factor for CaF_2 for the first series of aluminosilicate glasses (Table 4) was found to be 1.59, which is much higher when compared to the RI of crystalline CaF_2. In addition, it was also found that Appen factor for P_2O_5 is different from that published by Appen [3] and is around 1.48 for this series of glasses. This may be due to different phosphorus speciation in glass compositions containing aluminium and can be linked to several structural aspects [23].

Characterization by ^{19}F, ^{31}P, ^{29}Si and ^{27}Al MAS-NMR [24] indicate that the structure of ionomer type glasses is much

more complex than the fluoride containing bioactive glasses. The fluorine can exist as Al-F-Ca(n), as well as F-Ca(n) and the proportion of these two species changes with the glass composition [24]. The assumption of the glass consisting of a CaF_2 free glass plus CaF_2 like species in the calculation of the RI is only partially valid and neglects the presence of Al-F-Ca(n) species. In addition substituting CaF_2 for CaO may also reduce the non-bridging oxygen content of the glass, which will also influence the RI. In addition increasing fluorine content can cause the Al to move from Al(IV) to higher coordination states of V and VI.

Due to the complexity of the second series of high-fluorine ionomer-type glasses (Table 5) the data is expressed as measured RI as a function of elemental fluorine content. These compositions contain excessive amounts of fluorine and further structural characterization is ongoing. However, RIs that all within the compositional domain of this series of glasses can also be predicted based on the amount of elemental fluorine in mol% using equation for straight line expressed in Fig. 1(d).

Most commercial ionomer glasses also contain small amounts of sodium whereby it forms Al-F-Na(n) species in the glass in addition to Al-F-Ca(n) and F-Ca(n) species. Furthermore, many commercial glasses also contain strontium [23], which will result in Al-F-Sr(n) and F-Sr(n) speciation in addition to mixed species if calcium is included in the composition. In general the amount of sodium in ionomer glass compositions is typically less than 1% so the formation of Al-F-Na(n) species is not likely to have a large influence on the RI of ionomer-type glasses.

In regard to glass ionomer cements it is necessary that the RI of glass matches the RI of the polysalt matrix. This can be quite well facilitated in cement compositions where the initial difference between refractive index of the glass and the refractive index of the polyacid solution is lower.

5. Conclusions

The RI of fluoride containing bioactive glasses correlates linearly with metal fluoride content and the RI can also be predicted readily using Appen factors close to that of fluoride containing crystalline phases, such as CaF_2 as proposed in the study. The RIs of the more complex ionomer glasses also demonstrate a linear relationship with fluoride content. Nonetheless, the paper proposes a modified Appen Model with new composition-specific Appen factors for the metal fluorides for the development of highly translucent dental materials and improved depth of cure of dental composites. The present study also provides a very useful tool for the design of highly advanced restorative materials which can exhibit bioactivity alongside improved aesthetics and increased restoration longevity.

Acknowledgements

The authors would like to thank Cera Dynamics Limited, part of the James Kent Group and the Institute of Dentistry (Queen Mary University of London) for funding this project. The authors would also like to thank Dr Philip Frampton (Cera Dynamics Limited) for the high fluorine samples and XRF analyses. And finally, the corresponding author would also like to thank Dr Jamila Almuhamadi (Queen Mary University of London) for her explanation of the Becke line technique.

REFERENCES

[1] Shortall A, Palin W, Burtscher P. Refractive index mismatch and monomer reactivity influence composite curing depth. J Dent Res 2008;87:84–8.
[2] Hadis MA, Tomlins PH, Shortall AC, Palin WM. Dynamic monitoring of refractive index change through photoactive resins. Dent Mater 2010;26(11):1106–12.
[3] Appen AA. Khimiia stekla. Khimiia. Leningrad: Leningradskoe Otdnie; 1974. p. 310.
[4] O'Donnell M, Watts S, Law R, Hill RG. Effect of P_2O_5 content in two series of soda lime phosphosilicate glasses on structure and properties — Part II: physical properties. J Non-Cryst Solids 2008;354:3561–6.
[5] Gan F. Optical properties of fluoride glasses — a review. J Non-Cryst Solids 1995;184:9–20.
[6] Featherstone J. Prevention and reversal of dental caries: role of low level fluoride. Community Dent Oral Epidemiol 1999;27(1):31–40.
[7] Mohammed N, Lynch R, Anderson P. Effects of fluoride concentration on enamel demineralization kinetics in vitro. J Dent 2014;42(5):613–8.
[8] Hadis MA, Choong N, Morrell A, Martin RA, Shelton RM, Palin WM. Decreasing glass refractive index for development of light-curable bioactive composites. Dent Mater 2016;32S:e21–2.
[9] Höland W, Beall GH. Glass-Ceramic Technology. Second Edition Hoboken, NJ, USA: John Wiley & Sons, Inc.; 2012.
[10] Mneimne M, Hill RG, Bushby AJ, Brauer DS. High phosphate content significantly increases apatite formation of fluoride-containing bioactive glasses. Acta Biomater 2011;7(4):1827–34.
[11] Lynch E, Brauer D, Karpukhina N, Gillam D, Hill R. Multi-component bioactive glasses of varying fluoride content for treating dentin hypersensitivity. Dent Mater 2012;28(2):168–78.
[12] Stanton K, Hill R. The role of fluorine in the devitrification of $SiO_2{\cdot}Al_2O_3{\cdot}P_2O_5{\cdot}CaO{\cdot}CaF_2$ glasses. J Mater Sci 2000;35(8):1911–6.
[13] Hill R, Wood D, Thomas M. Trimethylsilylation analysis of the silicate structure of fluoro-alumino-silicate glasses and the structural role of fluorine. J Mater Sci 1999;34(8):1767–74.
[14] Saylor CP. Accuracy of microscopical methods for determining refractive index by immersion. J Res 1995;15(3):17.
[15] Bannister FA. A relation between the density and refractive index of silicate glasses, with application to the determination of imitation gemstones. Miner Mag 1931;22:136–54.
[16] Yang P, Yuan M, Zeigler D, Watkins S, Lee J, Luscombe C. Influence of fluorine substituents on the film dielectric constant and open-circuit voltage in organic photovoltaics. J Mater Chem C 2014;2(17):3278–84.
[17] Malitson IH. A redetermination of some optical properties of calcium fluoride. Appl Opt 1963;2(11):1103–7.
[18] Brauer D, Karpukhina N, Law R, Hill R. Structure of fluoride-containing bioactive glasses. J Mater Chem 2009;19(31):5629–36.
[19] Christie J, Pedone A, Menziani M, Tilocca A. Fluorine environment in bioactive glasses: ab initio molecular dynamics simulations. J Phys Chem B 2011;115(9):2038–45.

[20] Brauer D, Al-Noaman A, Hill R, Doweidar H. Density-structure correlations in fluoride-containing bioactive glasses. Mater Chem Phys 2011;130(1–2):121–5.
[21] Hench LL, Spilman DB, Hench JW. Fluoride-containing Bioglass™ compositions, 1988, Patent: US 4775646 A.
[22] Lusvardi G, Malavasi G, Cortada M, Menabue L, Menziani M, Pedone A, et al. Elucidation of the structural role of fluorine in potentially bioactive glasses by experimental and computational investigation. J Phys Chem B 2008;112(40):12730–9.
[23] Stamboulis A, Law R, Hill R. Characterisation of commercial ionomer glasses using magic angle nuclear magnetic resonance (MAS-NMR). Biomaterials 2004;25(17):3907–13.
[24] Zainuddin N, Karpukhina N, Law R, Hill R. Characterisation of a remineralising Glass Carbomer® ionomer cement by MAS-NMR spectroscopy. Dent Mater 2012;28(10):1051–8.

APPENDIX B

Poster Presentations

Cera Dynamics Ltd

in collaboration with Barts and The London School of Medicine and Dentistry

Refractive Index Matching for Superior Aesthetics

Translucency is an essential property of modern restoratives. In order to obtain an aesthetically superior product it is important to match the refractive index (RI) of the glass to the resin matrix.

In general the RI of glasses can be calculated using Appen factors; however, there are no Appen factors for fluoride-glasses.

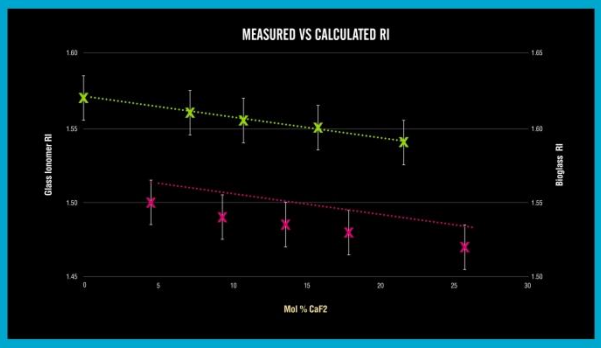

In this study we have measured the RI of a wide range of fluoride glasses. An empirical RI factor for amorphous fluorides was established. Cera Dynamics can use RI calculation to aid customers formulating aesthetically superior restoratives.

Tomas Duminis[1], Saroash Shahid[1], Robert Hill[1] & Phillip Frampton[2]

[1]Barts and the London School of Medicine and Dentistry, Queen Mary University of London, Mile End Road, London, E1 4NS United Kingdom

[2]Cera Dynamics Limited, Fountain Street, Stoke-on-Trent, ST4 2HB, United Kingdom

www.ceradynamics.com

Queen Mary University of London

Barts and The London School of Medicine and Dentistry

Development of novel fluorapatite glass-ceramics for use in biomimetic GICs

Tomas Duminis, Robert Hill, Natalia Karpukhina and Saroash Shahid

Centre for Oral Bioengineering, Institute of Dentistry, Barts and the London School of Medicine and Dentistry, Queen Mary University of London, Mile End Road, London E1 4NS, UK

Introduction

Fluorapatite (FAp) additives in glass ionomer cements (GICs) can be used to promote remineralisation [4]; however, due to light scattering at the interfaces between cement components they cause opacity and can result in a poorly translucent material (Figure 1(a)).

Some GIC glasses containing calcium, phosphorus and fluoride components can be developed into bioactive glass-ceramics (GCs) with FAp within the glass matrix [1]. If crystallites in the glass matrix are smaller than the wavelength of light, the material is translucent and aesthetic. It is known that if strontium is incorporated into the glass composition, the material can exhibit regenerative properties [2] and can also impart the material with diagnostic radiopacity [3]. The aim of this study is to develop novel ion-leachable strontium-substituted FAp nano-GCs for use in bioactive GICs.

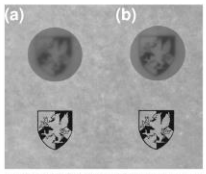

Figure 1: Disc (a) Refractive indices of cement components are not matching; DISC (b) Refractive indices of cement components are matching

Materials and Methods

A series of glasses of varying calcium substitution for strontium, based on the SiO_2-Al_2O_3-P_2O_5-CaO/SrO-CaF_2 system was synthesised by the melt-quench technique. To understand thermal properties, synthesised glasses were analysed by differential scanning calorimetry (DSC). Subsequently, all amorphous samples were pre-treated in bulk at the following temperatures: T_g (glass transition temperature), T_g+50°C, T_g+100°C and T_g+150°C for 1 hour. Pre-treated glasses were then processed into powder and analysed by ^{31}P and ^{19}F Magic Angle Spinning – Nuclear Magnetic Resonance (MAS-NMR.) scanning electron microscopy (SEM) and transmission electron microscopy (TEM).

Results and Discussion

DSC data presented in Figures 2(a) and 2(b) shows that increasing strontium content results in reduced homogenous crystallisation and a linear reduction in T_g.

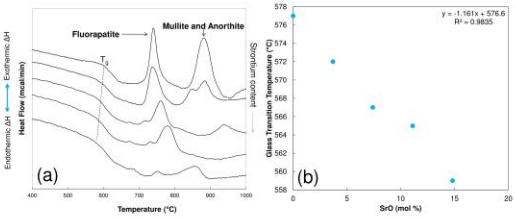

Figure 2: (a) DSC traces of glasses of varying strontium content showing reducing bulk FAp crystallisation with increasing strontium content (b) Reducing glass transition temperature as a function of strontium oxide content in the composition

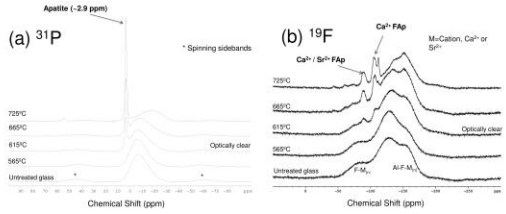

Figure 3: (a) ^{31}P MAS-NMR spectra of the samples treated at T_g, T_g+50°C, T_g+100°C and T_g+150°C (b) ^{19}F MAS-NMR of the samples treated at T_g (glass transition temperature), T_g+50°C, T_g+100°C and T_g+150°C

^{31}P MAS-NMR analysis of all treated samples shows a peak increasing in intensity with increasing temperature at approximately 2.9 ppm, which is assigned to fluoride ion in F-M(3) in FAp (Figure 3(a)). ^{19}F MAS-NMR analysis (Figure 3(b)) confirmed this to be in the form of acid-resistant FAp. Furthermore, ^{19}F MAS-NMR analysis showed that increasing Sr^{2+} in the nominal composition results in increased incorporation of Sr^{2+} into the apatite lattice during heat-treatment.

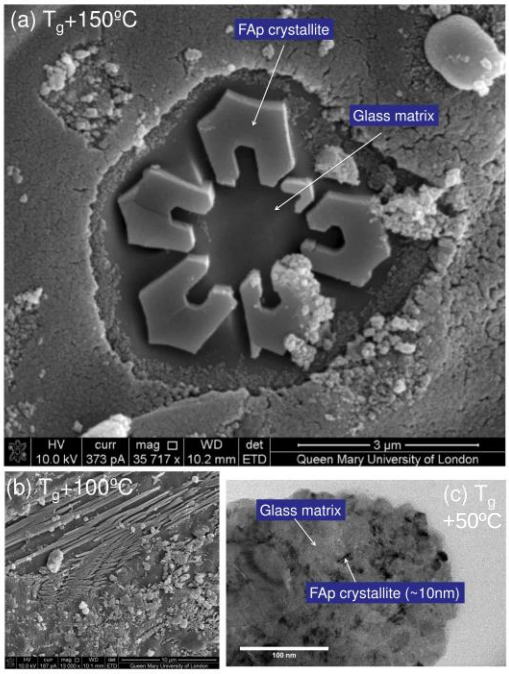

Figure 4: (a) SEM of a heat-treated GC sample showing microscale hexagonally shaped FAp crystallites within the amorphous matrix; (b) SEM of a GC showing needle-like fluorapatite microstructure and partially dendritic crystal growth; (c) TEM showing needle-like nanoscale (10-20nm) FAp crystallites within the amorphous glass matrix

SEM (Figures 4(a) and 4(b)) and TEM 4(c) of the heat-treated glasses show needle-like hexagonal FAp crystallites within the amorphous glass matrix. Lower heat-treatment temperatures produced optically clear nano-sized FAp GCs (Figure 4 (c)). Higher heat-treatment temperatures produced opaque GCs with crystallites on a microscale.

Conclusions

Nanoscale FAp GCs have been successfully developed for use in aesthetic GICs. Increasing strontium content in the developed compositions was found to promote surface crystallisation of FAp phases. Developed FAp GCs can be incorporated into GICs for improved remineralisation.

james kent GROUP

www.dentistry.qmul.ac.uk

References

1. Hill R, Stamboulis A, Law R, Clifford A, Towler M, Crowley C. The influence of strontium substitution in fluorapatite glasses and glass-ceramics. Journal of Non-Crystalline Solids. 2004;336(3):223-9.
2. Huang M, Hill RG, Rawlinson SC. Strontium (Sr) elicits odontogenic differentiation of human dental pulp stem cells (hDPSCs): A therapeutic role for Sr in dentine repair? Acta Biomater. 2016.
3. Shahid S, Hassan U, Billington RW, Hill RG, Anderson P. Glass ionomer cements: effect of strontium substitution on esthetics, radiopacity and fluoride release. Dent Mater. 2014;30(3):308-13.
4. Van Dijmen RN, Davidson CL, De Gee AJ, Feilzer AJ. In situ transformation of glass-ionomer into an enamel-like material. Am J Dent. 2004;17(4):225-7.

APPENDIX C

Conference Abstracts

1

Conference: British Society for Oral and Dental Research Annual Meeting (Sept. 14-16, 2015)

Title: **Modified Appen Model for Developing Restoratives with Enhanced Clinical Aesthetics**

Presentation type: Oral

Authors: Tomas Duminis, Saroash Shahid, Philip Frampton and Robert Hill

Objectives: Acid-degradable and inert glasses containing CaF_2 and SrF_2 are widely used as fillers in aesthetic dental restorative materials. Aesthetically superior polyalkenoate cements and dental composites are produced by matching the refractive index (RI) of the glass to the resin or the polysalt matrix to avoid light scattering at the interfaces. RIs of glasses can be calculated by the means of Appen factors. However, there were no Appen factors for amorphous metal fluorides published to date. Hence, the objective of this study was to empirically derive Appen factors for amorphous Calcium and Strontium fluorides. **Methods**: Several series of acid-degradable fluoroaluminosilicate glasses of varying metal fluoride content were selected for this study. The Appen equation was used to estimate RIs of glasses by using previously published RIs for the crystalline metal fluorides, in addition to Appen factors for the glass oxides. RIs of glasses were measured by the Becke line technique. Fragments of coarse glass samples were dispersed in mineral oils of varying RI (1.45-1.55) and observed under a phase contrast microscope until RI match was found. Subsequently, once experimental RIs of glasses became available, Appen factors for amorphous CaF_2 and SrF_2 were derived. **Results**: Empirical Appen factors for the amorphous metal fluorides were found to be higher than those for the crystalline metal fluorides. It was also found that the RIs of glasses reduced linearly (R^2=0.98) with increasing fluoride content. **Conclusions**: Empirical Appen factors have been successfully derived for the amorphous metal fluorides that enable accurate RI estimation of fluoride-containing glasses for the development of dental restoratives with enhanced clinical aesthetics.

2

Conference: IADR General Session (June 22-25, 2016) (Seoul, Republic of Korea)
June 22-25, 2016 - Seoul, Republic of Korea

Title: **Novel Strontium-substituted Fluorapatite Glass-ceramics for Remineralising Glass Ionomer Cements**

Presentation type: Poster

Authors: Tomas Duminis, Saroash Shahid and Robert Hill

Objectives: Although fluorapatite (FAp) additives in glass ionomer cement (GIC) may act as nuclei for the remineralisation of tooth, they affect the aesthetics of the material. Upon controlled heat-treatment GIC glasses which contain strontium as a radiopacifier can nano-crystallise to produce glass-ceramics (GC) with FAp within the glass matrix. Such glasses will be beneficial for enhancing the remineralising potential of GICs without affecting the aesthetics. The aim of this study is to develop novel strontium-substituted GCs for use in GICs. **Methods**: A series of glasses of varying strontium substitution for calcium, based on the SiO_2-Al_2O_3-P_2O_5-CaO/SrO-CaF_2 system was produced by the melt-quench route. For heat-induced apatite crystallisation all glasses were subjected to a heat-treatment regime at the following temperatures Tg, Tg+50°C, Tg+100°C and Tg+150°C for 1 hour. Glasses were then analysed by HT-DSC, multinuclear MAS-NMR, XRD, ATR-FTIR and SEM before and after heat-treatment to assess apatite crystallisation. **Results**: HT-DSC data suggests that increasing strontium content results in reduced volume crystallisation and a linear reduction in Tg. ^{31}P MAS-NMR analysis of the glasses showed presence of apatite after heat treatment. ^{19}F MAS-NMR analysis confirmed this be in the form of fluorapatite. Increasing heat-treatment temperature resulted in increased apatite crystallisation. SEM of heat-treated glasses showed needle-like fluorapatite crystals within the amorphous glass matrix. **Conclusions**: Fluorapatite containing glasses have been successfully developed for use in GICs. Increasing strontium content in the above systems was found to have a profound effect on the crystallisation behaviour of the glasses. Crystalline phase in the developed apatite containing glasses was identified to be a mixed strontium/calcium fluorapatite phase.

APPENDIX D

X-ray fluorescence analysis

INORGANIC ANALYSIS REPORT

UKAS TESTING
0013

Queen Mary University of London - Dental Physical Sciences
Francis Bancroft Building
RM 2.20.1 Second Floor
Mile End Road
London
E1 4NS

ceram
Queens Road, Penkhull, Stoke-on-Trent, Staffordshire, ST4 7LQ, UK

tel: (customer enquiries) +44 (0)1782 764428
tel: (switchboard) +44 (0)1782 764444
fax: +44 (0)1782 412331
email: enquiries@ceram.com
web: www.ceram.com

FAO: Mr Saroash Shahid

Report of Tests on: Fluoroaluminosilicate Glass 4
Your Reference: RIVA
Ceram Reference: (134252)-17299
Date Reported: 23-Aug-2013 **Order Number:** 9270312
Date Logged: 16-Aug-2013 **Date(s) of Test(s):** 21-Aug-2013 **to** 23-Aug-2013

XRF Analysis

Methods C15, C201 based on BSEN ISO 12677:2011

Result(s)		Units	
Sample Basis			Dried 110 deg C
Silicon Dioxide	SiO_2	%	30.87
Titanium Dioxide	TiO_2	%	<0.01
Aluminium Oxide	Al_2O_3	%	26.88
Iron (III) Oxide	Fe_2O_3	%	0.03
Calcium Oxide	CaO	%	0.16
Magnesium Oxide	MgO	%	0.02
Potassium Oxide	K_2O	%	0.01
Sodium Oxide	Na_2O	%	2.16
Phosphorus Pentoxide	P_2O_5	%	4.35
Chromium (III) Oxide	Cr_2O_3	%	<0.01
Manganese (II,III) Oxide	Mn_3O_4	%	<0.01
Zirconium Oxide	ZrO_2	%	0.02
Hafnium (IV) Oxide	HfO_2	%	<0.01
Lead Oxide	PbO	%	<0.02
Zinc Oxide	ZnO	%	0.03
Barium Oxide	BaO	%	0.16
Strontium (II) Oxide	SrO	%	22.02
Tin (IV) Oxide	SnO_2	%	<0.01
Copper Oxide	CuO	%	0.04
Boric Oxide (by ICP)	B_2O_3	%	0.09
Lithium Oxide (by ICP)	Li_2O	%	<0.01
Fluorine	F	%	7.80
Oxygen Equivalent Fluorine	OEF	%	-3.28
Loss on Ignition		%	7.80
Loss on Ignition Temperature		°C	500
Total		%	99.16
Sulphur Trioxide	SO_3	%	<0.05
UKAS Accredited			Yes

The sulphur trioxide may not be a total sulphur figure but is the sulphur remaining after LOI and fusion. Results are quoted to 2 decimal places but are accurate to 3 significant figures or the number of figures given, whichever is the lesser.

Opinions and interpretations expressed herein are outside the scope of UKAS Accreditation.

End of Test Report

Mrs Sharon Mansfield
Author

INORGANIC ANALYSIS REPORT

UKAS TESTING
0013

Queen Mary University of London - Dental Physical Sciences
Francis Bancroft Building
RM 2.20.1 Second Floor
Mile End Road
London
E1 4NS

ceram
Queens Road, Penkhull, Stoke-on-Trent, Staffordshire, ST4 7LQ, UK

tel: (customer enquiries) +44 (0)1782 764428
tel: (switchboard) +44 (0)1782 764444
fax: +44 (0)1782 412331
email: enquiries@ceram.com
web: www.ceram.com

FAO: Mr Saroash Shahid

Report of Tests on: Fluoroaluminosilicate Glass 5
Your Reference: IONOFIL
Ceram Reference: (134252)-17300
Date Reported: 23-Aug-2013 **Order Number:** 9270312
Date Logged: 16-Aug-2013 **Date(s) of Test(s):** 21-Aug-2013 **to** 23-Aug-2013

XRF Analysis

Methods C15, C201 based on BSEN ISO 12677:2011

Result(s)		Units	
Sample Basis			Dried 110 deg C
Silicon Dioxide	SiO_2	%	30.02
Titanium Dioxide	TiO_2	%	0.06
Aluminium Oxide	Al_2O_3	%	22.85
Iron (III) Oxide	Fe_2O_3	%	0.06
Calcium Oxide	CaO	%	0.19
Magnesium Oxide	MgO	%	<0.02
Potassium Oxide	K_2O	%	1.52
Sodium Oxide	Na_2O	%	1.28
Phosphorus Pentoxide	P_2O_5	%	4.26
Chromium (III) Oxide	Cr_2O_3	%	<0.01
Manganese (II,III) Oxide	Mn_3O_4	%	<0.01
Zirconium Oxide	ZrO_2	%	<0.02
Hafnium (IV) Oxide	HfO_2	%	<0.01
Lead Oxide	PbO	%	<0.02
Zinc Oxide	ZnO	%	<0.01
Barium Oxide	BaO	%	0.09
Strontium (II) Oxide	SrO	%	20.44
Tin (IV) Oxide	SnO_2	%	<0.01
Copper Oxide	CuO	%	0.02
Boric Oxide (by ICP)	B_2O_3	%	1.84
Lithium Oxide (by ICP)	Li_2O	%	<0.01
Fluorine	F	%	7.43
Oxygen Equivalent Fluorine	OEF	%	-3.13
Loss on Ignition		%	12.23
Loss on Ignition Temperature		°C	500
Total		%	99.16
Sulphur Trioxide	SO_3	%	<0.05
UKAS Accredited			Yes

The sulphur trioxide may not be a total sulphur figure but is the sulphur remaining after LOI and fusion. Results are quoted to 2 decimal places but are accurate to 3 significant figures or the number of figures given, whichever is the lesser.

Opinions and interpretations expressed herein are outside the scope of UKAS Accreditation.

End of Test Report

Mrs Sharon Mansfield
Author

INORGANIC ANALYSIS REPORT

UKAS TESTING
0013

Queen Mary University of London - Dental Physical Sciences
Francis Bancroft Building
RM 2.20.1 Second Floor
Mile End Road
London
E1 4NS

ceram
Queens Road, Penkhull, Stoke-on-Trent, Staffordshire, ST4 7LQ, UK

tel: (customer enquiries) +44 (0)1782 764428
tel: (switchboard) +44 (0)1782 764444
fax: +44 (0)1782 412331
email: enquiries@ceram.com
web: www.ceram.com

FAO: Mr Saroash Shahid

Report of Tests on: Fluoroaluminosilicate Glass 1
Your Reference: KETAC FIL
Ceram Reference: (134253)-17302
Date Reported: 23-Aug-2013 **Order Number:** 9270219
Date Logged: 16-Aug-2013 **Date(s) of Test(s):** 21-Aug-2013 **to** 23-Aug-2013

XRF Analysis

Methods C15, C201 based on BSEN ISO 12677:2011

Result(s)		Units	
Sample Basis			Dried 110 deg C
Silicon Dioxide	SiO_2	%	28.40
Titanium Dioxide	TiO_2	%	<0.01
Aluminium Oxide	Al_2O_3	%	26.85
Iron (III) Oxide	Fe_2O_3	%	0.02
Calcium Oxide	CaO	%	0.08
Magnesium Oxide	MgO	%	<0.02
Potassium Oxide	K_2O	%	0.02
Sodium Oxide	Na_2O	%	3.64
Phosphorus Pentoxide	P_2O_5	%	6.01
Chromium (III) Oxide	Cr_2O_3	%	<0.01
Manganese (II,III) Oxide	Mn_3O_4	%	<0.01
Zirconium Oxide	ZrO_2	%	<0.02
Hafnium (IV) Oxide	HfO_2	%	<0.01
Lead Oxide	PbO	%	<0.02
Zinc Oxide	ZnO	%	<0.01
Barium Oxide	BaO	%	0.09
Strontium (II) Oxide	SrO	%	21.86
Tin (IV) Oxide	SnO_2	%	<0.01
Copper Oxide	CuO	%	<0.01
Boric Oxide (by ICP)	B_2O_3	%	<0.05
Lithium Oxide (by ICP)	Li_2O	%	<0.01
Fluorine	F	%	10.80
Oxygen Equivalent Fluorine	OEF	%	-4.55
Lanthanum (III) Oxide	La_2O_3	%	6.59
Loss on Ignition		%	0.35
Loss on Ignition Temperature		°C	500
Total		%	100.16
Sulphur Trioxide	SO_3	%	<0.05
UKAS Accredited			Yes

The sulphur trioxide may not be a total sulphur figure but is the sulphur remaining after LOI and fusion. Results are quoted to 2 decimal places but are accurate to 3 significant figures or the number of figures given, whichever is the lesser.

Opinions and interpretations expressed herein are outside the scope of UKAS Accreditation.

End of Test Report

Mrs Sharon Mansfield
Author

INORGANIC ANALYSIS REPORT

UKAS TESTING
0013

Queen Mary University of London - Dental Physical Sciences
Francis Bancroft Building
RM 2.20.1 Second Floor
Mile End Road
London
E1 4NS

ceram
Queens Road, Penkhull, Stoke-on-Trent, Staffordshire, ST4 7LQ, UK

tel: (customer enquiries) +44 (0)1782 764428
tel: (switchboard) +44 (0)1782 764444
fax: +44 (0)1782 412331
email: enquiries@ceram.com
web: www.ceram.com

FAO: Mr Saroash Shahid

Report of Tests on: Fluoroaluminosilicate Glass 2
Your Reference: CHEMFIL ROCK
Ceram Reference: (134253)-17303
Date Reported: 23-Aug-2013 **Order Number:** 9270219
Date Logged: 16-Aug-2013 **Date(s) of Test(s):** 21-Aug-2013 **to** 23-Aug-2013

XRF Analysis

Methods C15, C201 based on BSEN ISO 12677:2011

Result(s)		Units	
Sample Basis			Dried 110 deg C
Silicon Dioxide	SiO_2	%	20.34
Titanium Dioxide	TiO_2	%	0.01
Aluminium Oxide	Al_2O_3	%	20.67
Iron (III) Oxide	Fe_2O_3	%	0.03
Calcium Oxide	CaO	%	4.98
Magnesium Oxide	MgO	%	<0.02
Potassium Oxide	K_2O	%	0.05
Sodium Oxide	Na_2O	%	0.58
Phosphorus Pentoxide	P_2O_5	%	14.21
Chromium (III) Oxide	Cr_2O_3	%	<0.01
Manganese (II,III) Oxide	Mn_3O_4	%	<0.01
Zirconium Oxide	ZrO_2	%	0.07
Hafnium (IV) Oxide	HfO_2	%	0.01
Lead Oxide	PbO	%	<0.02
Zinc Oxide	ZnO	%	12.64
Barium Oxide	BaO	%	0.48
Strontium (II) Oxide	SrO	%	11.60
Tin (IV) Oxide	SnO_2	%	<0.01
Copper Oxide	CuO	%	<0.01
Boric Oxide (by ICP)	B_2O_3	%	0.45
Lithium Oxide (by ICP)	Li_2O	%	0.25
Fluorine	F	%	3.70
Oxygen Equivalent Fluorine	OEF	%	-1.56
Loss on Ignition		%	11.49
Loss on Ignition Temperature		°C	500
Total		%	100.00
Sulphur Trioxide	SO_3	%	<0.05
UKAS Accredited			Yes

The sulphur trioxide may not be a total sulphur figure but is the sulphur remaining after LOI and fusion. Results are quoted to 2 decimal places but are accurate to 3 significant figures or the number of figures given, whichever is the lesser.

Opinions and interpretations expressed herein are outside the scope of UKAS Accreditation.

End of Test Report

Mrs Sharon Mansfield
Author

INORGANIC ANALYSIS REPORT

Queen Mary University of London - Dental Physical Sciences
Francis Bancroft Building
RM 2.20.1 Second Floor
Mile End Road
London
E1 4NS

ceram
Queens Road, Penkhull, Stoke-on-Trent, Staffordshire, ST4 7LQ, UK
tel: (customer enquiries) +44 (0)1782 764428
tel: (switchboard) +44 (0)1782 764444
fax: +44 (0)1782 412331
email: enquiries@ceram.com
web: www.ceram.com

UKAS TESTING 0013

FAO: Mr Saroash Shahid

Report of Tests on: Fluoroaluminosilicate Glass 3
Your Reference: CHEMFIL SUPERIOR
Ceram Reference: (134253)-17304
Date Reported: 23-Aug-2013 **Order Number:** 9270219
Date Logged: 16-Aug-2013 **Date(s) of Test(s):** 21-Aug-2013 **to** 23-Aug-2013

XRF Analysis

Methods C15, C201 based on BSEN ISO 12677:2011

Result(s)		Units	
Sample Basis			Dried 110 deg C
Silicon Dioxide	SiO_2	%	23.82
Titanium Dioxide	TiO_2	%	<0.01
Aluminium Oxide	Al_2O_3	%	26.18
Iron (III) Oxide	Fe_2O_3	%	0.02
Calcium Oxide	CaO	%	8.82
Magnesium Oxide	MgO	%	0.03
Potassium Oxide	K_2O	%	0.02
Sodium Oxide	Na_2O	%	8.26
Phosphorus Pentoxide	P_2O_5	%	8.09
Chromium (III) Oxide	Cr_2O_3	%	<0.01
Manganese (II,III) Oxide	Mn_3O_4	%	<0.01
Zirconium Oxide	ZrO_2	%	<0.02
Hafnium (IV) Oxide	HfO_2	%	<0.01
Lead Oxide	PbO	%	<0.02
Zinc Oxide	ZnO	%	<0.01
Barium Oxide	BaO	%	<0.01
Strontium (II) Oxide	SrO	%	0.03
Tin (IV) Oxide	SnO_2	%	<0.01
Copper Oxide	CuO	%	<0.01
Boric Oxide (by ICP)	B_2O_3	%	<0.05
Lithium Oxide (by ICP)	Li_2O	%	<0.01
Fluorine	F	%	12.20
Oxygen Equivalent Fluorine	OEF	%	-5.14
Loss on Ignition		%	17.08
Loss on Ignition Temperature		°C	500
Total		%	99.42
Sulphur Trioxide	SO_3	%	0.08
UKAS Accredited			Yes

The sulphur trioxide may not be a total sulphur figure but is the sulphur remaining after LOI and fusion. Results are quoted to 2 decimal places but are accurate to 3 significant figures or the number of figures given, whichever is the lesser.

Opinions and interpretations expressed herein are outside the scope of UKAS Accreditation.

End of Test Report

Mrs Sharon Mansfield
Author

INORGANIC ANALYSIS REPORT

LUCIDEON
insight creating advantage

UKAS TESTING
0013

James Kent (Ceramic Materials) Limited
Fountain Street
Fenton
Stoke on Trent
Staffs
ST4 2HB

FAO: Christopher Jackson

Report of Tests on: CJ219 (QMTD7)
Your Reference: 1890
Lucideon Reference: (155334)-30545
Date Reported: 07-Dec-2015 **Order Number:** 8069
Date Logged: 02-Dec-2015 **Date(s) of Test(s):** 03-Dec-2015 **to** 07-Dec-2015

XRF Analysis

Methods C201 based on BSEN ISO 12677:2011

Result(s)		Units	
Sample Basis			Dried 110 deg C
Silicon Dioxide	SiO_2	%	25.81
Titanium Dioxide	TiO_2	%	<0.01
Aluminium Oxide	Al_2O_3	%	26.08
Iron (III) Oxide	Fe_2O_3	%	0.02
Calcium Oxide	CaO	%	20.58
Magnesium Oxide	MgO	%	0.07
Potassium Oxide	K_2O	%	0.01
Sodium Oxide	Na_2O	%	3.15
Phosphorus Pentoxide	P_2O_5	%	15.02
Chromium (III) Oxide	Cr_2O_3	%	<0.01
Manganese (II,III) Oxide	Mn_3O_4	%	<0.01
Zirconium Oxide	ZrO_2	%	0.83
Hafnium (IV) Oxide	HfO_2	%	0.02
Lead Oxide	PbO	%	<0.02
Zinc Oxide	ZnO	%	0.08
Barium Oxide	BaO	%	<0.01
Strontium (II) Oxide	SrO	%	<0.01
Tin (IV) Oxide	SnO_2	%	<0.01
Copper Oxide	CuO	%	<0.01
Fluorine	F	%	12.10
Oxygen Equivalent Fluorine	OEF	%	-5.08
Loss on Ignition		%	0.07
Loss on Ignition Temperature		°C	500
Total		%	98.74
Sulphur Trioxide	SO_3	%	<0.05
UKAS Accredited			Yes

The sulphur trioxide may not be a total sulphur figure but is the sulphur remaining after LOI and fusion. Results are quoted to 2 decimal places but are accurate to 3 significant figures or the number of figures given, whichever is the lesser.

Opinions and interpretations expressed herein are outside the scope of UKAS Accreditation.

End of Test Report

Mrs Sharon Mansfield
Author

Lucideon Limited
Queens Road, Penkhull
Stoke-on-Trent
Staffordshire ST4 7LQ

T +44 (0)1782 764428
enquiries@lucideon.com
www.lucideon.com

INORGANIC ANALYSIS REPORT

LUCIDEON
insight creating advantage

UKAS TESTING
0013

James Kent (Ceramic Materials) Limited
Fountain Street
Fenton
Stoke on Trent
Staffs
ST4 2HB

FAO: Christopher Jackson

Report of Tests on: CJ220 (QMTD8)

Your Reference: 1891

Lucideon Reference: (155334)-30546

Date Reported: 07-Dec-2015 **Order Number:** 8069

Date Logged: 02-Dec-2015 **Date(s) of Test(s):** 03-Dec-2015 **to** 07-Dec-2015

XRF Analysis

Methods C201 based on BSEN ISO 12677:2011

Result(s)		**Units**	
Sample Basis			Dried 110 deg C
Silicon Dioxide	SiO_2	%	20.36
Titanium Dioxide	TiO_2	%	0.01
Aluminium Oxide	Al_2O_3	%	23.42
Iron (III) Oxide	Fe_2O_3	%	0.02
Calcium Oxide	CaO	%	11.27
Magnesium Oxide	MgO	%	0.04
Potassium Oxide	K_2O	%	0.01
Sodium Oxide	Na_2O	%	2.30
Phosphorus Pentoxide	P_2O_5	%	15.81
Chromium (III) Oxide	Cr_2O_3	%	<0.01
Manganese (II,III) Oxide	Mn_3O_4	%	<0.01
Zirconium Oxide	ZrO_2	%	0.96
Hafnium (IV) Oxide	HfO_2	%	0.02
Lead Oxide	PbO	%	<0.02
Zinc Oxide	ZnO	%	0.50
Barium Oxide	BaO	%	0.15
Strontium (II) Oxide	SrO	%	17.89
Tin (IV) Oxide	SnO_2	%	<0.01
Copper Oxide	CuO	%	<0.01
Fluorine	F	%	12.60
Oxygen Equivalent Fluorine	OEF	%	-5.32
Loss on Ignition		%	0.05
Loss on Ignition Temperature		°C	500
Total		%	100.13
Sulphur Trioxide	SO_3	%	<0.05
UKAS Accredited			Yes

The sulphur trioxide may not be a total sulphur figure but is the sulphur remaining after LOI and fusion. Results are quoted to 2 decimal places but are accurate to 3 significant figures or the number of figures given, whichever is the lesser.

Opinions and interpretations expressed herein are outside the scope of UKAS Accreditation.

End of Test Report

Mrs Sharon Mansfield
Author

Lucideon Limited
Queens Road, Penkhull
Stoke-on-Trent
Staffordshire ST4 7LQ

T +44 (0)1782 764428
enquiries@lucideon.com
www.lucideon.com

INORGANIC ANALYSIS REPORT

LUCIDEON
insight creating advantage

UKAS TESTING
0013

James Kent (Ceramic Materials) Limited
Fountain Street
Fenton
Stoke on Trent
Staffs
ST4 2HB

FAO: Christopher Jackson

Report of Tests on: CJ221 (QMTD9)
Your Reference: 1892
Lucideon Reference: (155334)-30547
Date Reported: 07-Dec-2015 **Order Number:** 8069
Date Logged: 02-Dec-2015 **Date(s) of Test(s):** 03-Dec-2015 **to** 07-Dec-2015

XRF Analysis

Methods C201 based on BSEN ISO 12677:2011

Result(s)		Units	
Sample Basis			Dried 110 deg C
Silicon Dioxide	SiO_2	%	18.23
Titanium Dioxide	TiO_2	%	<0.01
Aluminium Oxide	Al_2O_3	%	21.84
Iron (III) Oxide	Fe_2O_3	%	0.02
Calcium Oxide	CaO	%	0.33
Magnesium Oxide	MgO	%	<0.02
Potassium Oxide	K_2O	%	<0.01
Sodium Oxide	Na_2O	%	2.04
Phosphorus Pentoxide	P_2O_5	%	15.09
Chromium (III) Oxide	Cr_2O_3	%	<0.01
Manganese (II,III) Oxide	Mn_3O_4	%	<0.01
Zirconium Oxide	ZrO_2	%	0.83
Hafnium (IV) Oxide	HfO_2	%	0.02
Lead Oxide	PbO	%	<0.02
Zinc Oxide	ZnO	%	0.26
Barium Oxide	BaO	%	0.30
Strontium (II) Oxide	SrO	%	33.61
Tin (IV) Oxide	SnO_2	%	<0.01
Copper Oxide	CuO	%	<0.01
Fluorine	F	%	11.50
Oxygen Equivalent Fluorine	OEF	%	-4.84
Loss on Ignition		%	0.04
Loss on Ignition Temperature		°C	500
Total		%	99.26
Sulphur Trioxide	SO_3	%	0.07
UKAS Accredited			Yes

The sulphur trioxide may not be a total sulphur figure but is the sulphur remaining after LOI and fusion. Results are quoted to 2 decimal places but are accurate to 3 significant figures or the number of figures given, whichever is the lesser.

Opinions and interpretations expressed herein are outside the scope of UKAS Accreditation.

End of Test Report

Mrs Sharon Mansfield
Author

Lucideon Limited
Queens Road, Penkhull
Stoke-on-Trent
Staffordshire ST4 7LQ

T +44 (0)1782 764428
enquiries@lucideon.com
www.lucideon.com